The Dissertation Committee for Murat Kadir Deliomeroglu Certifies that this is the approved version of the following dissertation:

Formylated Dipyrromethane Based Phosphate Derivatives Receptors

Committee:

Jonathan L. Sessler, Supervisor

Eric V. Anslyn

Guangbin Dong

Jennifer S. Brodbelt

Walter L. Fast

Formylated Dipyrromethane Based Phosphate Derivatives Receptors

by

Murat Kadir Deliomeroglu, B.S.

Dissertation

Presented to the Faculty of the Graduate School of

The University of Texas at Austin

in Partial Fulfillment

of the Requirements

for the Degree of

Doctor of Philosophy

The University of Texas at Austin

May 2016

Scientia Dux Vitae Certissimus

Acknowledgements

First and foremost I would like to thank my supervisor Dr. Jonathan Sessler for his generosity and trust in my abilities.

I would also like to thank all members of Sessler group, past and present, for their help, support, and friendship, especially Dr. Christian Preihs, Dr. Nathan Bill, Dr. Eric Silver, Dr. Dani Lyons, Dr. Gregory Thiabaud, Ren-Tsung Wu, Dr. Gabriela Vargas-Zuniga, Yerim Yeon, Dr. Dong Sub Kim.

I would like to thank the UT staff, Dr. Vincent M. Lynch for patiently collecting the X-ray diffraction data and refining them, Steve Sorey for running various 2D NMR experiments, Dr. Ian Riddington for running MS analyses.

I also thank those who have played great roles in making me love chemistry, Dr. Hakan Usta and Dr. Metin Balcı.

I also would like to thank my college friends who pursued similar career routes as me, Şeyma Ekiz, Özden Çelikbilek, Esra Eroğlu, Dr. Esra Korkut Altınok, Dr. Çağatay Dengiz. Thank you for your friendship and support throughout my life journey.

I would also like to thank Brian Dillon for his constant support and bringing joy and happiness to my life.

Last but not least, I would like to thank my parents Ahmet and Vesile Deliömeroğlu and my brother Turan Deliömeroğlu for their support, and unconditional love.

Formylated Dipyrromethane Based

Phosphate Derivatives Receptors

Publication No._____

Murat Kadir Deliomeroglu, Ph.D.

The University of Texas at Austin, 2016

Supervisor: Jonathan L. Sessler

Anions are key components in many biological and industrial processes. They play crucial roles in both health and the environment. In many cases, it is important to control the concentration of anions or their removal in order to mediate their deleterious effects. Therefore, recognition of anions is of interest to researchers. However, the recognition of many anions remains challenging due to their relative large size-to-charge ratios, diverse geometries, and higher energies of solvation. This doctoral Dissertation summarizes the author's effort to design, synthesize, and study various receptors that were intended to overcome those challenges. In Chapter 1, a brief introduction to anion binding chemistry is provided with a particular focus on phosphate anion recognition. The common defining feature of the receptors reviewed is the pyrrole ring. The new structures are often designed *via* modification of known macrocyclic molecules. In

Chapter 2, structural modifications of a Schiff-base receptor (2,6-diamidopyridine dipyrromethane) and incorporation of that modified receptor into polymeric materials are discussed. These polymeric materials were studied for their anion binding properties in methylene chloride and tested for their ability to extract dihydrogenphosphate from water. In Chapter 3, a series of four-fold formylated bisdipyrromethane (tetrakis(1*H*-pyrrole-2-carbaldehyde)) receptors is reported. The anion binding properties of these receptors were studied with dihydrogenphosphate along with other possibly competitive anions (*e.g.*, chloride and hydrogensulfate). Data to support the contention that the receptors undergo conformational reorganization in order to accommodate the bound oxoanions both in chloroform solution and in the solid state are also provided. In Chapter 4, an electroactive analogue of the systems, discussed in Chapter 3, along with a new binding-site-enriched analogue are presented. These analogues exploit the binding characteristics of the tetrakis(1*H*-pyrrole-2-carbaldehyde) series. Taken in concert the findings detailed in these Chapters are expected to lead to a greater understanding of phosphate binding in the case of formylated dipyrromethane based anion receptors.

Table of Contents

List of Tables

List of Figures

List of Schemes

List of Common Abbreviations

2D	Two-dimensional
bisDPM	Bisdipyrromethane
bs	Broad singlet in NMR
bt	Broad triplet in NMR
C[4]P	Calix[4]pyrrole
calcd	Calculated
CCDC	Cambridge Crystallographic Data Centre
CI	Chemical ionization
Cp	Cyclopentadienyl
DCM	Dichloromethane
DI	Deionized
DMF	Dimethylformamide
DMSO	Dimethyl sulfoxide
DPM	Dipyrromethane
EBPR	Enhanced biological phosphate removal
EPI	Epichlorohydrin
ESI	Electrospray ionization
ESRD	End-stage renal disease
EtOAc	Ethyl acetate
equiv	Equivalent
FES	Flame emission spectroscopy
GPC	Gel permeation chromatography
HOESY	Heteronuclear nuclear Overhauser effect spectroscopy

HRMS	High-resolution mass spectrometry
ITC	Isothermal titration calorimetry
nd	not determined
NMR	Nuclear Magnetic Resonance
NOESY	Nuclear Overhauser effect spectroscopy
NS	Not studied
PBP	Phosphate binding protein
PDB	Protein data bank
PDI	Polydispersity index
$PhPO_3H$	Phenylphosphonic
pMMA	poly(methyl methacrylate)
poly-P	Polyphosphate
s	Singlet (in NMR spectrum)
SEM	2-(Trimethylsilyl)ethoxymethyl
TBA^+	Tetrabutylammonium cation
TEA	Triethylamine
TFA	Trifluoroacetic acid
TMA^+	Tetramethylammonium cation
TMS	Trimethylsilane
THF	Tetrahydrofuran
TLC	Thin-layer chromatography
TFA	Trifluoroacetic acid
trisDPM	Tris(dipyrromethane)
UV-Vis	Ultraviolet and visible

1. Introduction to Anion Binding Chemistry

Supramolecular chemistry is chemistry beyond the molecule. Some of the early examples in this field come from Pedersen, Lehn, and Cram in late 1960s.[1–3] Pedersen prepared salt-polyether complexes in which various cations were bound *via* ion-dipole interactions involving the lone pairs of the polyether oxygen atoms.[1] After the birth of this new field, increasing emphasis was placed on the recognition of transition metals, organic cations, neutral species, and anionic species.[4] Recognition of a guest may be studied by measuring changes in one or more defining properties of a host (*e.g.*, light absorption, the nuclear magnetic resonance (NMR) chemical shift, solubility, conductance, chemical reactivity, etc.) as a function of the ligand concentration.[5] In this context, one defines a molecular complex as a non-covalently-bound species of definite substrate-to-ligand stoichiometry that is formed in a reversible equilibrium process in solution.

A large number of acyclic and cyclic compounds have been used to coordinate metal cations and have been evaluated for their ability to recognize these and other positively charged guests, including alkylammonium cations. Some of this work dates back to the days of Werner, an early Nobel Prize winner. Overtime, the importance of anions in biological systems became increasingly recognized. As a result, in recent years, attention has been paid to design and construct anion receptors.[6]

Anion receptors, the main focus of this Dissertation, are species that interact specifically with anions. Anions play essential roles in many biological processes. They are also of critical interest in the areas of synthetic and industrial chemistry.[6] They are prevalent in many enzymatic active sites and are among the most pervasive of known pollutants. Among the most widespread anionic pollutants are phosphate and nitrate that

arise from an overuse of agricultural fertilizers. They lead directly to eutrophication of lakes and waterways.[7] In coastal areas, occurrences of dead zones, which are caused by eutrophication, have increased from 10 documented cases in 1960 to 405 documented cases in 2008.[8]

Anion concentration imbalances are also of medical relevance and, indeed are associated with several conditions. Hyperphosphatemia is a disturbance in electrolyte levels that results from abnormally high concentrations of phosphate in human serum. It affects nearly all patients suffering from end-stage renal disease (ESRD).[9] Unfortunately, 70% of individuals with ESRD are unable to process this accumulated excess phosphate through hemodialysis; as a result, these patients often suffer from deleterious symptoms, including soft tissue calcification, cardiovascular complications, and even death.[10]

Development of molecular constructs capable of binding anions efficiently, especially phosphate in its various protonated forms, is of critical interest as it may provide a first step towards solving various problems related to anion detection, extraction, removal, and separation.[11,12] To date, a number of recognition motifs have been exploited to achieve anion recognition, including coulombic interactions, hydrogen bonding, halogen bonding, and anion-π interactions.[13–17] A brief history of the development of these recognition motifs now follows.

1.1. History of Synthetic Anion Binding Receptors

In 1949, Walker discussed the relatively insoluble behavior of the carboxylic acid salts of amidines.[18] The complementary nature of the cation (amidines) and anion (acetates, benzoates) led Walker to suggest that complex formation might occur even in the solution state. In 1954, Tanford investigated the association of the acetate with the

ammonium and guanidinium cations.[19] Tanford was particularly interested in these complexes because he appreciated that the interactions between guanidinium and carboxylate ions could be playing a key role in protein chemistry.[20]

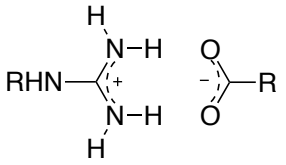

1.1

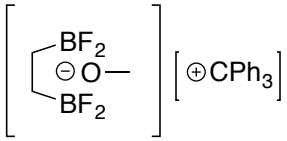

1.2

Although it was concluded that association between the ions in complex **1.1** together was weak, it became clear that non-covalent interactions involving anions were possible. One early example involved the chelated complex (**1.2**) between the methoxide anion and a bidentate boron Lewis acid.[21]

More than a decade later, Park and Simmons reported encapsulation of halide ions by macrobicyclic amines.[22] On the basis of ^{1}H NMR spectroscopic analyses, it was concluded that the *out,out*-1,11-diazabicyclo[9,9,9]nonacosane bis(hydrochloride) (**1.3**) converts to the *in,in*-isomer (**1.4**) upon the addition of trifluoroacetic acid (TFA) (*cf.* Scheme 1.1). A second equilibrium between **1.4** and **1.5** becomes established more slowly, over the course of several days, as inferred from the emergence of a third signal in the ^{1}H NMR spectrum. The equilibrium could be driven in the forward direction by adding chloride (Cl^-) salts and by heating. This caused the signals of **1.5** to sharpen. Crystallographic support that a Cl^- anion occupied the central cavity of the *in,in*- isomer was also mentioned.[22]

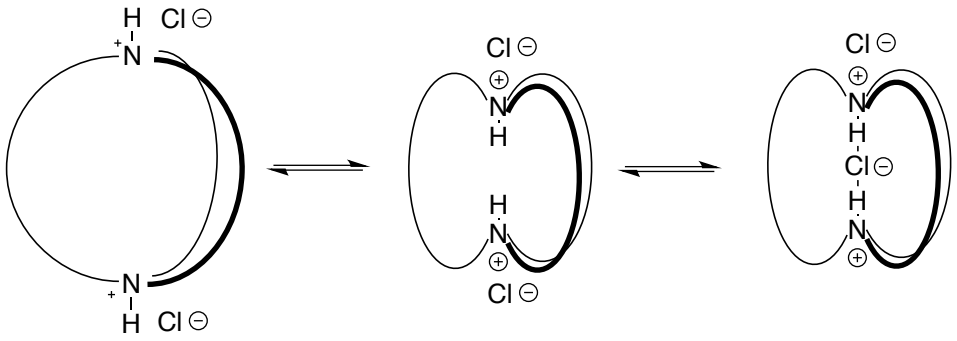

1.3 **1.4** **1.5**

Scheme 1.1: Schematic representation of equilibriums converting from *out,out-* isomer (**1.3**) to *in, in-* isomer (**1.4**) and diffusion of Cl^- ion into the cavity of *in,in-* isomer (**1.5**).

Following the study reported by Park and Simmons, many researchers began focusing on the problem of anion recognition. Many known interactions have been studied in this context. In general, interactions that may be used to drive complex formation between two molecules include:

- Electrostatic interactions (*e.g.*, dipole-dipole interactions)
- Polarization interactions (*e.g.*, dipole-induced dipole interactions)
- Exchange repulsion (repulsion of overlapping short-range electron distributions)
- Charge transfer (from HOMO to LUMO, for example)
- Higher order interactions

Morokuma[23] has discussed these various interactions and typical contributions to complex formation in his paper " Why Do Molecules Interact? The Origin of Electron Donor-Acceptor Complexes, Hydrogen Bonding, and Proton Affinity."

Each of the main bonding motifs (*e.g.*, classically defined hydrogen bonding, CH hydrogen bonding, coulombic attractions, anion-π interactions) is composed of a unique combination of the interactions listed above. One example of very strong hydrogen

bonding is the complex $H_3N\cdots HF$ with stabilizing electrostatic (-25.6 kcal/mol), charge-transfer (-4.1 kcal/mol), and polarization component (-2.0 kcal/mol), as well as a destabilizing exchange repulsion contribution (16.0 kcal/mol).[23] While each of these five components contributes to the total interaction energy, there is an indication that very strong hydrogen bonding is primarily electrostatic.

Since this Dissertation is about formylated-dipyrromethane based structures as phosphate anion receptors, a brief introduction is given here that details 1) anion binding in the content of pyrrole-based anion receptors and 2) phosphate receptors and sensors.

1.2. Brief Review of Pyrrole-Based Anion Receptors

The chemistry of pyrrole-based anion recognition dates to 1990. At that time, Sessler and coworkers serendipitously found[15] the presence of electron density in the center of the pentapyrrolic macrocycle during an X-ray diffraction analysis of what was assumed to be the bis HPF_6 salt of sapphyrin **1.6**.[15] What was found was that a fluoride ion (F^-) was bound in the sapphyrin core, giving rise to the observed X-ray scattering. The aromatic 22-π-electron sapphyrin (**1.6**) system has a core size of roughly 5.5 Å diameter, and its core is big enough to bind a fluoride ion (F^-) with strong hydrogen bonding interactions. In comparison, an 18-π-electron porphyrin system does not bind a F^- ion, since the *trans* nitrogen distances are too short (about 4 Å).[15] The fully protonated sapphyrin, acting as an F^- receptor, was the first example of a rapidly increasing class of a pyrrole-based anion receptor.

Subsequent to the 1990 discovery of the anion binding properties of sapphyrin research with pyrroles as anion receptors began to diverge. Two general directions emerged. One direction was focused on understanding the fundamentals more deeply by

considering structurally simpler pyrrole-based systems, whereas the other direction was toward the development of more advanced and complex receptor systems that could potentially target anions other than F^-.

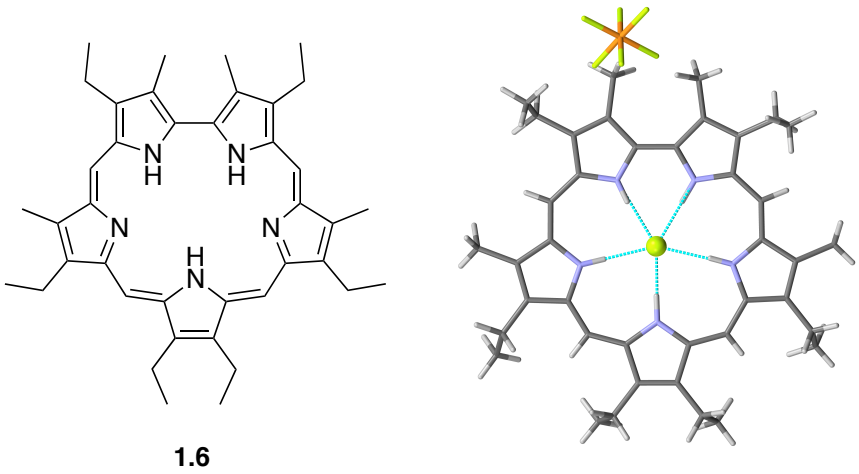

1.6

Figure 1.1: Structure of a Sapphyrin **1.6** and X-ray crystal structure of the doubly protonated **1.6** ([**1.6** + 2H]$^{2+}$) showing the bound F^- ion. Also shown is the hexafluorophosphate counter anion. This structure was originally reported by Sessler *et al.*[15] and was redrawn using data from the Cambridge Crystallographic Data Centre (CCDC) (CCDC number 1184078).

In 1992, The second example of a protonated macrocyclic poly-pyrrole system, namely rosarin (**1.7**) was prepared.[24] X-ray diffraction analysis showed that this triply protonated non-planar system, [**1.7**+3H]$^{3+}$, bound two Cl^- anions in its core in solid state.[24]

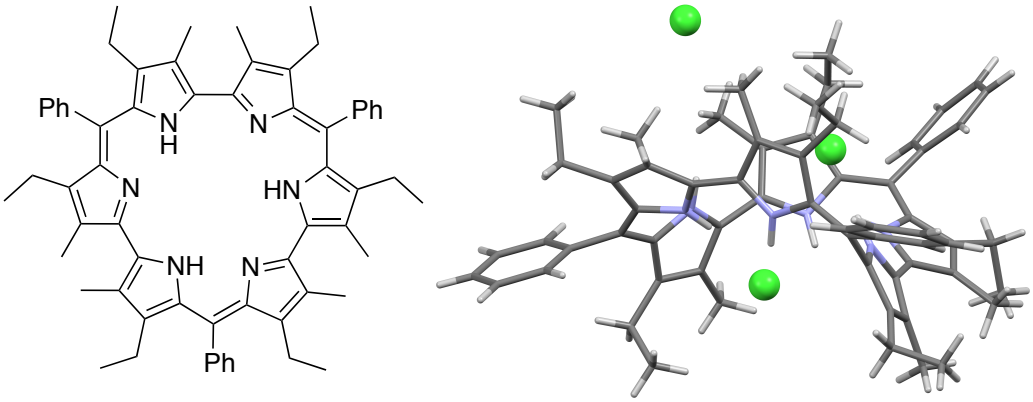

1.7

Figure 1.2: Structure of a rosarin **1.7** and X-ray crystal structure of the triply protonated **1.7** ([**1.7** + 3H]$^{3+}$) with three Cl^- counter anion. This structure was originally reported by Sessler *et al*.,[24] and was redrawn using data from the CCDC (CCDC number 1190538).

An example of an effort toward simpler structures was presented by Sessler and coworkers in 1994.[25] This study involved the first structurally characterized linear hexapyrrin **1.8**, which was obtained by the acid catalyzed condensation of diformylbipyrrole with a bis-α-free bipyrrole. The resultant product had direct resemblance to prodigiosins (a three pyrrole-containing natural oligomer, *e.g*., **1.9**). The linear hexapyrrin system **1.8** can be thought as an α,α'-linked prodigiosin dimer containing not one, but two potential Cl^- anion binding clefts. The crystal structure of hexapyrrin bis HCl salt showed that two bound Cl^- anions were tethered to the flat diprotonated hexapyrrin *via* two sets of three hydrogen bonds thereby providing direct structural conformation for the mode of binding presumed to be operative in prodigiosin and its analogues.[25] Prodigiosins, a set of naturally occurring, open-chain pyrrolylopyrromethene-type oligopyrroles, have been proposed to affect the into-cell transport of HCl and studied as potential antineoplastic and immunosuppressive agents.[26]

Interestingly, the suggestion that protonated prodigiosin can act as a Cl^- receptor and carrier came after Sessler's work on **1.8** was published.

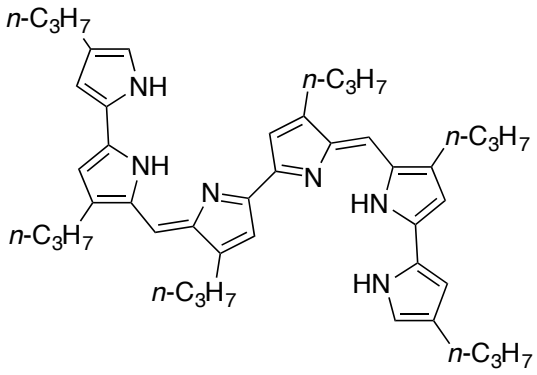

1.8

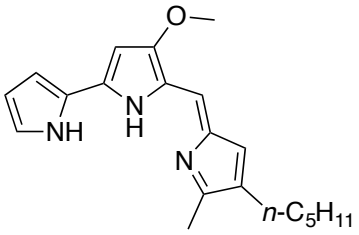

1.9

In 1996, Gale and Sessler[27] reported the anion binding properties of a class of pyrrolic macrocycles called porphyrinogens that were first synthesized by Baeyer[28] in 1886. These macrocycles were renamed as calix[4]pyrroles (C[4]P) to stress the analogy to calixarenes. Porphyrinogens (or C[4]Ps) are macrocyclic compounds consisting of four pyrrole rings linked at the α-positions *via* sp^3-hybridized carbon atoms. Porphyrinogens with hydrogen atoms at the *meso*-position are prone to oxidize into the corresponding porphyrins. On the other hand, fully *meso*-substituted porphyrinogens were claimed to be not only stable crystalline materials but also readily obtainable. The report by Gale and Sessler included anion binding studies of two C[4]P derivatives, octamethyl C[4]P (**1.10**) and tetraspirocyclohexyl C[4]P (**1.10'**), with halides in solution and in solid state (*cf.* Figure 1.3).

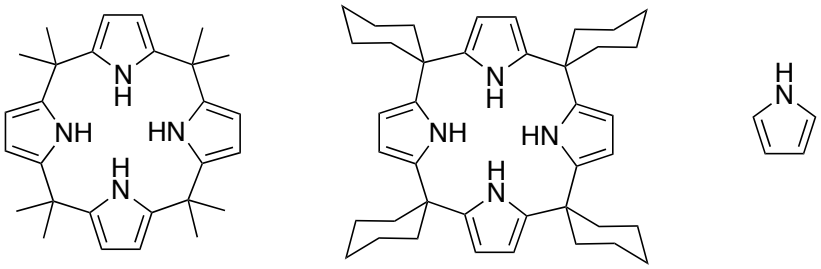

1.10 **1.10'** **1.11**

Since then, considerable attention has been paid to C[4]Ps as anion receptors and increasing effort has been devoted to enhancing the binding affinity and selectivity for specific anions.[27,29,30] Chapter 3 presents studies that show an improvement in the recognition of tetrahedral anions by new constructs prepared from the same building blocks as C[4]P but possessing very different structural forms.

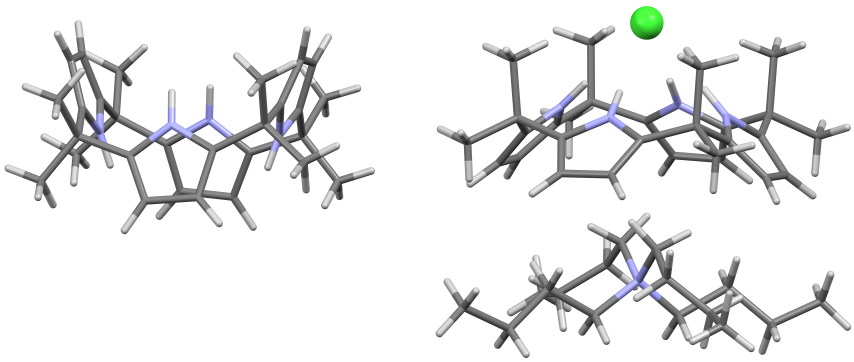

Figure 1.3: X-ray crystal structures of octamethyl C[4]P **1.10** free in 1,3-alternate conformation (left) and **1.10** co-crystallized with TBACl in the cone conformation (right). These structures were originally reported by Gale *et al*.,[27] and were redrawn using data from the CCDC (CCDC numbers 1288397 and 1269267, respectively).

In 2001, Gale *et al*. reported that pyrrole (**1.11**) itself could act as an anion receptor.[31] In this report, tetramethylammonium (TMA^+) Cl^- was recrystallized from pyrrole to provide a co-crystal wherein two pyrrole molecules interact with a single Cl^- anion. The pyrrole·Cl^- complex in question was characterized crystallographically (*cf*.

Figure 1.4). Comparison to the C[4]P·Cl^- complexes showed marked similarities (Table 1.1), both in the interaction distances and in the angles between the adjacent pyrrole donors.[31]

	N-H···Cl distance in Å	Dihedral angle of coordinating pyrroles
1.10·Cl^- (C[4]P)[27]	3.264 – 3.331	60.36°
1.11·Cl^- (pyrrole)[31]	3.241	61.73°

Table 1.1: Comparison of selected crystallographic values for **1.10**·Cl^- and **1.11**·Cl^- complexes.

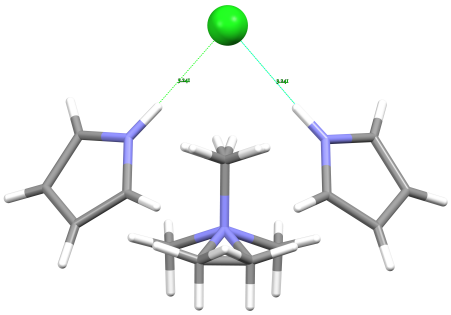

Figure 1.4: X-ray crystal structure of the complex[31] formed between TMACl and pyrrole (**1.11**). The two N-H···Cl distances are equal at 3.24 Å while TMA^+ cation is disordered. This structure was redrawn using data from the CCDC (CCDC number 173101).

Cyclo[8]pyrrole **1.12** is another protonated expanded porphyrin system that complexed with an anionic guest by binding it within its cavity.[32] Macrocyclic **1.12** was obtained by a highly efficient one-step synthesis, based on the use of $FeCl_3$ as the oxidant and readily accessible α,α'-unsubstituted bipyrrole as the only organic precursor. The

doubly protonated cyclo[8]pyrrole derivative, [**1.12** + 2H]$^{2+}$, was shown to host a sulfate counter ion (SO_4^{2-}) in its cavity (Figure 1.5).

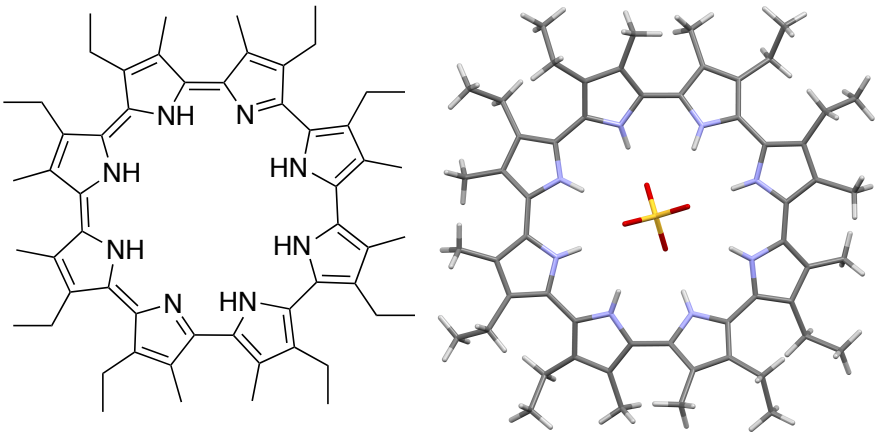

1.12

Figure 1.5: Structure of a cyclo[8]pyrrole **1.12** and X-ray crystal structure of the doubly protonated form ([**1.12** + 2H]$^{2+}$) showing the bound sulfate counter anion. A half molecule of CH_3OH is omitted for clarity. This structure was originally reported by Sessler *et al*.[32] and was redrawn using data from the CCDC (CCDC number 176189).

Ballester *et al*., have contributed to anion recognition by exploring anion-π interactions since 2002.[33–36] Many $\alpha,\alpha,\alpha,\alpha$-*meso*-tetraaryl-C[4]P derivatives (**1.13**–**1.15**) were prepared by this group and studied in solution and in the solid state. Physical organic chemical studies were employed to quantify the proposed anion-π interactions.[34] Based on the upfield chemical shift of the arene signals observed *via* ^{1}H NMR spectroscopy, as well as X-ray crystallographic studies, it was concluded that the Cl^-–arene interactions observed in these complexes were established exclusively *via* the π-aromatic system. Quantitative Hammett free-energy relationships, derived from a library of derivatives with varying R groups (**1.13**–**1.15**), were presented in support of the conclusion that the inferred Cl^--π interactions are dominated by electrostatic effects.

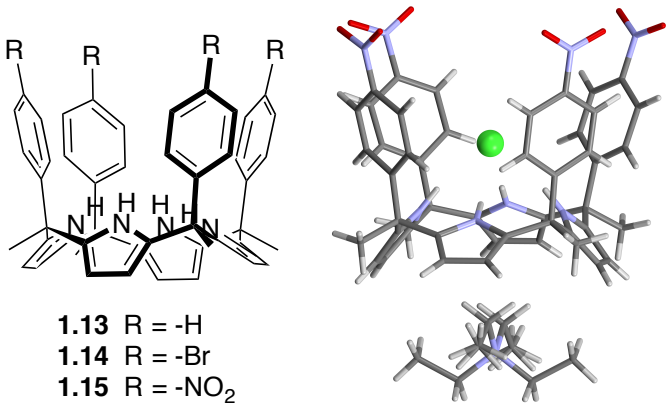

Figure 1.6: Chemical structures of three *α,α,α,α-meso*-tetraaryl-C[4]P derivatives **1.13**–**1.15** and X-ray crystal structure of **1.15** with TEACl.[34] This structure was originally reported by Ballester *et al*.,[34] and was redrawn using data from the CCDC (CCDC number 677142).

Acyclic oligopyrrole receptors have been suggested to be versatile because of their enhanced conformational flexibility. However, the number of such alternatives to the calixpyrrole receptors is still limited. Maeda *et al*. studied the anion recognition properties of boron-appended dipyrrolyldiketones (*e.g*., **1.16**).[37–40] Compound **1.16** containing fluorine atoms in the *β*-positions of the pyrrole rings was shown to be an efficient anion receptor by UV-Vis and fluorescence spectroscopic changes, especially for acetate anion (as TBA^+ salt) in CH_2Cl_2. Scheme 1.2 illustrates the proposed conformational change of **1.16** upon binding a halide ion.

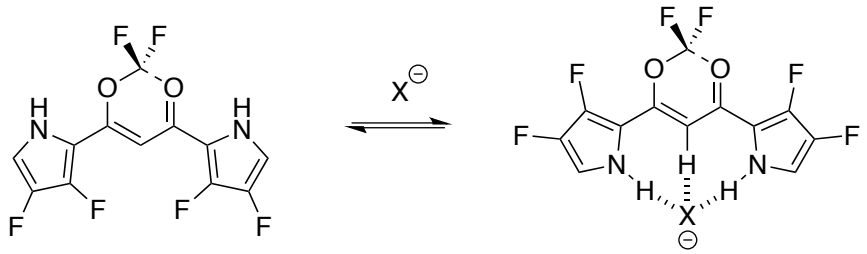

1.16 **1.16'**

Scheme 1.2: Schematic representation of the conformational changes associated with halide binding by **1.16** as proposed by Maeda and coworkers.[40]

In 2014, Ghosh *et al*. reported an *o*-phenylenevinylene-bridged tetrapyrrolic macrocycle (**1.17**) that was obtained by means of a Horner–Wadsworth–Emmons reaction between benzylbisphosphonate and 2-(trimethylsilyl)ethoxymethyl (SEM)-protected diformylpyrrole, followed by deprotection of the SEM groups.[41] This "conformationally flexible" tetrapyrrole can be considered as an expanded C[4]P. It was found to act as a receptor for the Cl^- and Br^- anions in THF-d_8. However, it was found to undergo deprotonation upon exposure to F^-.[41]

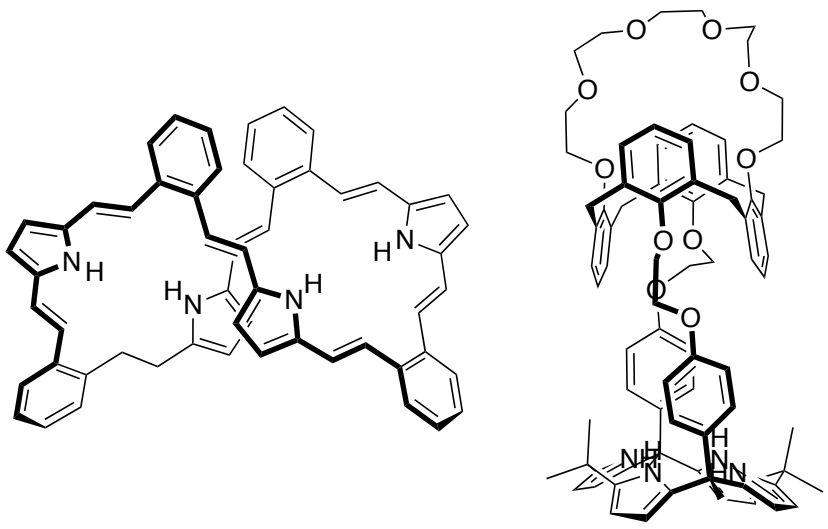

1.17 **1.18**

Kim et al. published a series of C[4]P-based ion pair receptors.[42–44] Receptor **1.18** containing both cation- and anion-recognition sites was shown to complex ion pairs (*i.e.*, salts) both in solution and in the solid state. This class of receptors is made up a C[4]P capped with a crown ether-strapped calix[4]arene. The 1:1 **1.18**·CsF complex was shown to be stable despite the large distance between anionic and cationic constituents of the bound ion pair. In this system, hydrogen bonding and coulombic interactions involving cation-π interactions are thought to lead to the observed binding. Kim *et al.*, also prepared slightly modified derivatives in order to elucidate the binding mode and to effect anion extraction.

1.3. PHOSPHATE RECEPTORS AND SENSORS

After the discovery of F^- anion in the core of a sapphyrin macrocycle, subsequent studies provided support for the contention that sapphyrin also interacts with other anions, including $H_2PO_4^-$.[45,46] Crystallographic data and ^{31}P NMR spectroscopic studies were used to understand the binding interactions with phosphate derivatives. It was concluded that doubly protonated and positively charged sapphyrin, [**1.19**+2H]$^{2+}$, interacts with monobasic phosphoric acid, $H_2PO_4^-$ to form a 1:1 salt with the second $H_2PO_4^-$ present in the salt not interacting directly with the macrocycle (Figure 1.7). The simple observation of coprecipitation of sapphyrin **1.20** with a double-stranded DNA from an aqueous solution led Sessler, Iverson, and co-workers to study the interaction of sapphyrins with DNA and other phosphate derivatives.[45]

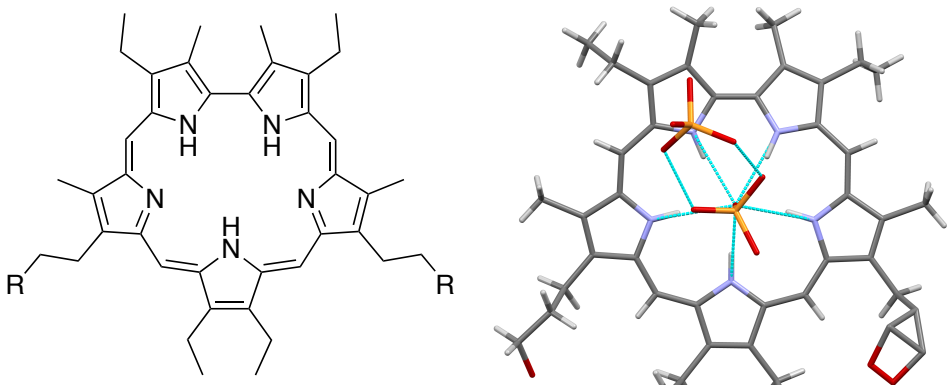

1.19 R = CH_2OH
1.20 R = $CON(CH_2CH_2OH)_2$

Figure 1.7: Structure of sapphyrins **1.19** and **1.20** and X-ray crystal structure of the doubly protonated **1.19** ([**1.19** + 2H]$^{2+}$) with two $H_2PO_4^-$ ions, one "sitting atop" of the central cavity. The structure was originally reported by Sessler *et al.*,[46] and was redrawn using data from the CCDC (CCDC number 1315691).

In 2003, Anslyn and co-workers reported C_{3v}-symmetric tripodal receptors which recognize tetrahedral oxyanions.[47] Receptor **1.21** was reported to have the highest affinity for HPO_4^{2-} in water containing 2% (v/v) CH_3OH among all known anion binding agents. The binding isotherm obtained from UV-Vis spectroscopic analysis was indicative of a 1:1 binding with a K_a of 2.5 x 10^4 M^{-1} at pH = 7.4 (5 mM HEPES). It was concluded that the shape, size, and charge of receptor **1.21** led to the observed high affinity and selectivity for HPO_4^{2-} relative to other anions (*e.g.*, SO_4^{2-}, NO_3^-, Cl^-) that were included in the study.

Although pH effects were discussed in the paper, there are two points that were not well clarified in the eyes of the present author. First, the protonation state of the bound phosphate derivative was not well defined in the report. Moreover, it was not clear whether pH was taken into account in calculating the binding affinity of **1.21** with HPO_4^{2-}. At pH = 7.4, only 61% of the total phosphate concentration is expected to exist in the

form of HPO_4^{2-}.[48] The second point that needs clarification involves the protonation state of the receptor **1.21**. All three free amine groups were assumed to be protonated based on a general pKa comparison to an ammonium ion (pKa approximately 10). However, this assumption was not tested.

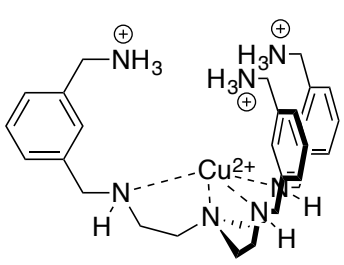

1.21

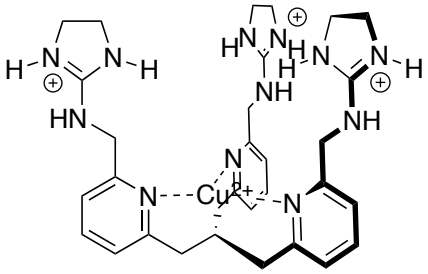

1.22

Later in the same year, Tobey *et al*. presented a receptor system, **1.22**, that proved useful for phosphate sensing in saliva samples.[49] Receptor **1.22** was used in an indicator-displacement assay made up from **1.22** and a colored organic molecule, 5(6)-carboxyfluorescein (**1.23**). Sensing was achieved by monitoring the colorimetric response induced by an analyte-driven change in the microenvironment of the dye **1.23**.

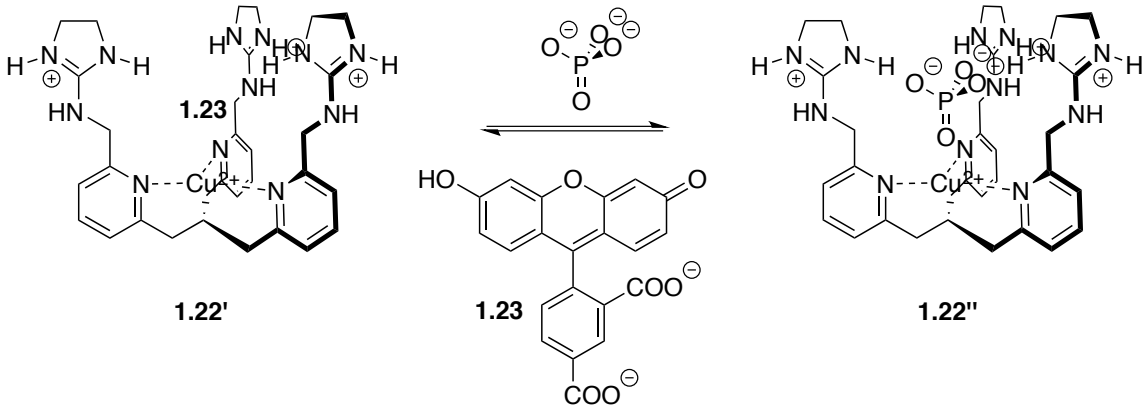

1.22' **1.23** **1.22''**

Figure 1.8: Schematic representation of the indicator (**1.23**) displacement assay used by Anslyn and coworkers to quantify phosphate concentrations in saliva.[49]

A 2,6-diamidopyridinedipyrromethane hybrid macrocycle (**1.24**) has been reported[50] to show a high selectivity for $H_2PO_4^-$ and HSO_4^- relative to NO_3^- in acetonitrile (CH_3CN) as inferred from solution phase UV-Vis spectrophotometric titrations. This finding by Sessler and co-workers led them to suggest[51] that **1.25** or related systems might find use in nuclear waste remediation applications requiring the selective removal of HSO_4^- from NO_3^--rich waste mixtures.

It was concluded that **1.24** binds $H_2PO_4^-$ as a 1:2 (**1.24**:$H_2PO_4^-$) complex.[50] This was attributed to the existence of two binding sites of **1.24** for this particular anion, $H_2PO_4^-$. The inherent flexibility of **1.24**, especially within the DPM subunit, was thought to allow the NH hydrogen bond donors in the receptor to orient in such a way that multiple, disparate NH-anion interactions are possible.

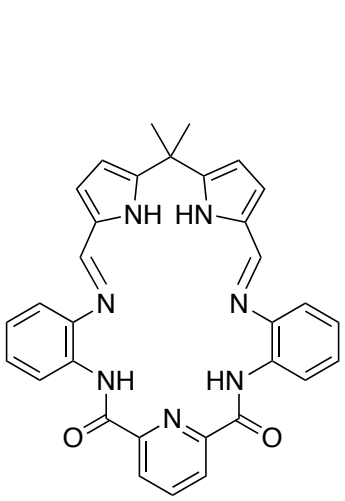

1.24

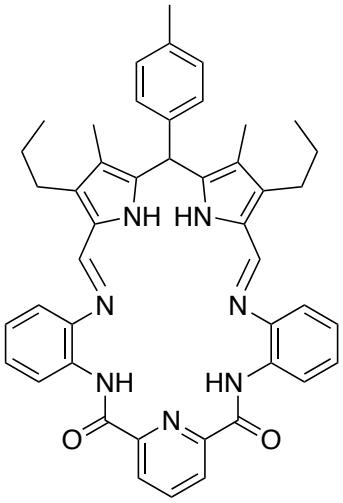

1.25

Cyclic polyamines have been extensively studied and their structures have been tailored for the recognition of inorganic phosphate. The actual recognition takes advantage of a combination of intermolecular forces, namely hydrogen bonding and coulombic interactions. Some examples of cyclic polyamine receptors are provided below. A detailed review can be found in the literature.[52] One protonated polyaza-

cryptand ligand (**1.26**) was studied for size- and temperature-dependent encapsulation of tetrahedral ClO_4^- and $H_2PO_4^-$ anions.[53] Another example of cyclic polyamines is compound **1.27**.[54] It was synthesized from three equivalents of dialdehyde and two equivalents of the constituent triamine (which is a precursor of **1.26)** to form a Schiff-base cage like-structure. The Schiff-base cage was then reduced to give **1.27**. The amide analogue **1.26** (obtained from diacyldichloride starting material instead of a dialdehyde) was reported to be selective for nitrate.[55] Receptor **1.27** was shown by X-ray structural analyses to form anion complexes with both nitrate and tetrahedral oxyanions sulfate and phosphate.

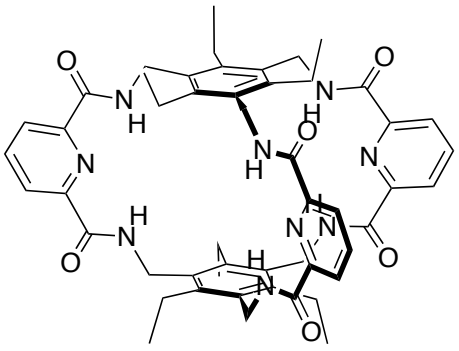

1.26

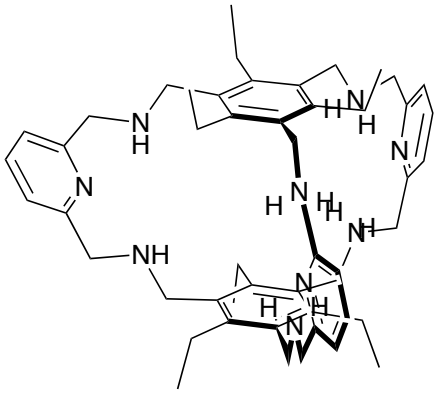

1.27

A dicationic C[4]P system (**1.28**) was studied as a pyrophosphate sensing[56] using a version of the indicator-displacement assay that was defined[49] earlier in this section.

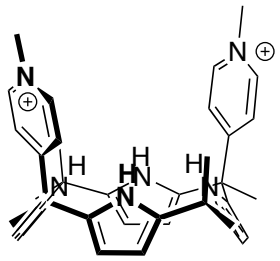

1.28

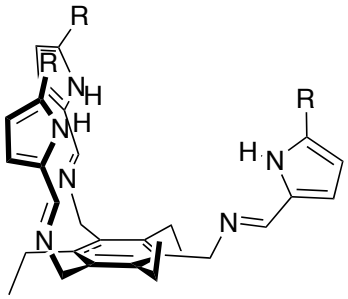

1.29 R = H

1.30 R = 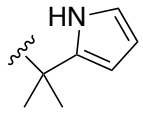

In 2012, Sessler and coworkers reported two tripodal receptors based on pyrrole- and DPM-functionalized derivatives of a sterically geared precursor, 1,3,5-tris(aminomethyl)-2,4,6-triethylbenzene.[57] These systems display high affinity and selectivity for tetrahedral anionic guests as inferred from solution phase isothermal titration calorimetric (ITC) analyses carried out in CH_3CN, as well as solid state single crystal X-ray diffraction analyses. Both receptors (**1.29** and **1.30**) were constructed from the well-known tripodal core, a subunit that confers a high degree of preorganization within receptors built up from it.

In 2013, Cai *et al*. published a pyrrole-based triazolium-phane, **1.31**, with pyrrole NH and cationic CH donor groups as a receptor that functions in polar media for tetrahedral oxyanions.[58] Macrocyclic receptor **1.31** is positively charged and was prepared *via* the tetraalkylation of a macrocycle originally prepared by click chemistry using the non-coordinating counter anion BF_4^-. The prepared salt displays a high selectivity for tetrahedral oxyanions, such as HSO_4^-, $H_2PO_4^-$, and $HP_2O_7^{3-}$, over spherical and trigonal planar anions in mixed polar organic-aqueous media. The selectivity for tetrahedral oxyanions is lost in CH_3CN. Both experimental and theoretical results from the study provided support for the seemingly counterintuitive conclusion that, in CH_3OH,

triazolium $(CH)^+$–anion interactions are energetically less important than neutral aromatic CH–anion interactions.

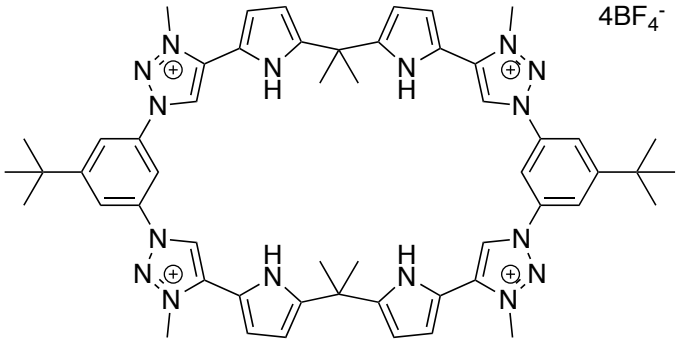

1.31

Very recently, Lin and coworkers reported a multi-functional mechanically interlocked switchable [2]rotaxane, **1.32**.[59] The system was synthesized by means of a CuAAC click reaction and consists of two molecular stations and rotaxane arms that are terminated with boron-dipyrromethane (BODIPY) fluorophores. The dumbell-shaped BODIPY-based "axel" displays an on-off-on fluorescence bahviorur and thus functions as an acid-base controllable molecular switch. This switching has its origins the supramolecular energy transfer between the macrocycle and BODIPY stoppers. The underlying photoinduced electron transfer process could be driven not only by the addition of acid-base but also *via* the addition of the $H_2PO_4^-$ anion. Rotaxane **1.32**, both as is and without the macrocycle threaded, was reported to display fluorescence quenching selectively in the presence of $H_2PO_4^-$.

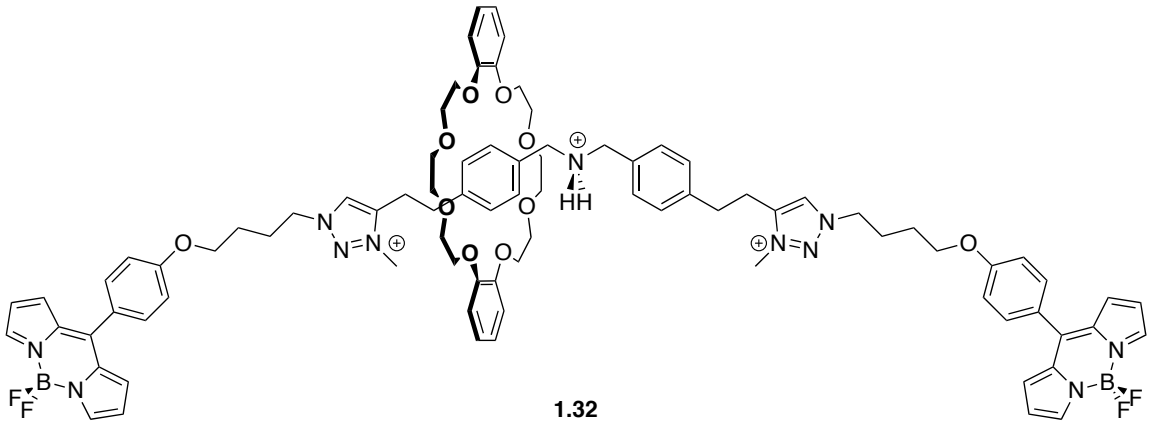

1.32

In this Chapter, we have tried to provide some background information about anion receptors, more specifically pyrrole-based systems and phosphate binding motifs. This has been illustrated with examples taken from the literature. Our contributions in these areas will be presented in Chapters 2, 3, and 4.

1.4. REFERENCES

1. Pedersen, C. J. Cyclic Polyethers and Their Complexes with Metal Slats. *J. Am. Chem. Soc.* **1967**, *89* (26), 7017–7036.
2. Dietrich, B.; Lehn, J. M.; Sauvage, J. P. Les Cryptates. *Tetrahedron Lett.* **1969**, *10* (34), 2889–2892.
3. Cram, D. J.; Cram, J. M. Host-Guest Chemistry. *Science* **1974**, *183* (4127), 803–809.
4. Bowman-James, K.; Bianchi, A.; Garcia-Espana, E. *Anion Coordination Chemistry*; Wiley-VCH Verlag & Co. KGaA: Weinheim, 2012.
5. Connors, K. A. *Binding Constants: The Measurement of Molecular Complex Stability*; John Wiley & Sons: New York, 1987.
6. Sessler, J. L.; Gale, P. A.; Cho, W.-S. *Anion Receptor Chemistry*; The Royal Society of Chemistry: Cambridge, U.K., 2006.
7. Carpenter, S. R.; Caraco, N. F.; Correll, D. L.; Howarth, R. W.; Sharpley, A. N.; Smith, V. H. Nonpoint Pollution of Surfaces Waters with Phosphorus and Nitrogen. *Ecol. Appl.* **1991**, *8* (3), 559–568.

8. Selman, M.; Greenhalgh, S. Eutrophication : Sources and Drivers of Nutrients Pollution. *WRI Policy Note* **2009**, (2), 1–8.

9. Gutzwiller, J.-P.; Schneditz, D.; Huber, A. R.; Schindler, C.; Gutzwiller, F.; Zehnder, C. E. Estimating Phosphate Removal in Haemodialysis: An Additional Tool to Quantify Dialysis Dose. *Nephrol. Dial. Transplant.* **2002**, *17* (6), 1037–1044.

10. Qunibi, W. Y. Consequences of Hyperphosphatemia in Patients with End-Stage Renal Disease (ESRD). *Kidney Int. Suppl.* **2004**, *66* (90), S8–S12.

11. Hirsch, A. K. H.; Fischer, F. R.; Diederich, F. Phosphate Recognition in Structural Biology. *Angew. Chem. Int. Ed.* **2007**, *46* (3), 338–352.

12. Zhang, Y.; Desmidt, E.; Van Looveren, A.; Pinoy, L.; Meesschaert, B.; Van Der Bruggen, B. Phosphate Separation and Recovery from Wastewater by Novel Electrodialysis. *Environ. Sci. Technol.* **2013**, *47* (11), 5888–5895.

13. Gale, P. A. Anion and Ion-Pair Receptor Chemistry: Highlights from 2000 and 2001. *Coord. Chem. Rev.* **2003**, *240*, 191–221.

14. Tobey, S. L.; Anslyn, E. V. Energetics of Phosphate Binding to Ammonium and Guanidinium Containing Metallo-Receptors in Water. *J. Am. Chem. Soc.* **2003**, *125* (48), 14807–14815.

15. Sessler, J. L.; Cyr, M. J.; Lynch, V.; McGhee, E.; Ibers, J. A. Synthetic and Structural Studies of Sapphyrin, a 22-π-electron Pentapyrrolic "Expanded Porphyrin." *J. Am. Chem. Soc.* **1990**, *112* (7), 2810–2813.

16. Cavallo, G.; Metrangolo, P.; Pilati, T.; Resnati, G.; Sansotera, M.; Terraneo, G. Halogen Bonding: A General Route in Anion Recognition and Coordination. *Chem. Soc. Rev.* **2010**, *39* (10), 3772–3783.

17. Gamez, P.; Mooibroek, T. J.; Teat, S. J.; Reedijk, J. Anion Binding Involving Pi-Acidic Heteroaromatic Rings. *Acc. Chem. Res.* **2007**, *40* (6), 435–444.

18. Walker, J. Some Observations on Salts of Amidines and Related Compounds. *J. Chem. Soc.* **1949**, (0), 1996–2002.

19. Tanford, C. The Association of Acetate with Ammonium and Guanidinium Ions. *J. Am. Chem. Soc.* **1954**, *76* (3), 945.

20. Tanford, C. Preparation and Properties of Serum and Plasma Proteins. XXIII. Hydrogen Ion Equilibria in Native and Modified Human Serum Albumins. *J. Am. Chem. Soc.* **1950**, *72* (1), 441–451.

21. Shriver, D. F.; Biallas, M. J. Observation of the Chelate Effect with a Bidentate Lewis Acid, $F_2BCH_2CH_2BF_2$. *J. Am. Chem. Soc.* **1967**, *89* (5), 1078–1081.

22. Park, C. H.; Simmons, H. E. Macrobicyclic Amines. III. Encapsulation of Halide Ions by In,in-1,(k + 2)-Diazabicyclo[k.l.m.]alkane Ammonium Ions. *J. Am. Chem. Soc.* **1968**, *90* (9), 2431–2432.

23. Morokuma, K. Why Do Molecules Interact? The Origin of Electron Donor-Acceptor Complexes, Hydrogen Bonding and Proton Affinity. *Acc. Chem. Res.* **1977**, *10* (8), 294–300.

24. Sessler, J. L.; Weghorn, S. J.; Morishima, T.; Rosingana, M.; Lynch, V.; Lee, V. Rosarin: A New, Easily Prepared Hexapyrrolic Expanded Porphyrin. *J. Am. Chem. Soc.* **1992**, *114* (14), 8306–8307.

25. Sessler, J. L.; Weghorn, S. J.; Lynch, V.; Fransson, K. 5,15,25-Tris-nor-Hexapyrrin: The First Structurally Characterized Linear Hexapyrrin. *J. Chem. Soc. Chem. Commun.* **1994**, *169* (11), 1289.

26. Ohkuma, S.; Sato, T.; Okamoto, M.; Matsuya, H.; Arai, K.; Kataoka, T.; Nagai, K.; Wasserman, H. H. Prodigiosins Uncouple Lysosomal Vacuolar-Type ATPase through Promotion of H^+/Cl^- Symport. *Biochem. J.* **1998**, *334* (3), 731–741.

27. Gale, P. A.; Sessler, J. L.; Kral, V.; Lynch, V. Calix[4]pyrroles: Old yet New Anion-Binding Agents. *J. Am. Chem. Soc.* **1996**, *118* (21), 5140–5141.

28. Baeyer, A. Ueber Ein Condensationsproduct von Pyrrol Mit Aceton. *Berichte der Dtsch. Chem. Gesellschaft* **1886**, *19* (2), 2184–2185.

29. Allen, W. E.; Gale, P. A.; Brown, C. T.; Lynch, V. M.; Sessler, J. L. Binding of Neutral Substrates by Calix[4]pyrroles. *J. Am. Chem. Soc.* **1996**, *118* (49), 12471–12472.

30. Gale, P. A.; Sessler, J. L.; Král, V. Calixpyrroles. *Chem. Commun.* **1998**, (1), 1–8.

31. Coles, S. J.; Gale, P. A.; Hursthouse, M. B. The First Example of an Anion-Pyrrole Complex. *CrystEngComm* **2001**, *3* (53), 259–261.

32. Seidel, D.; Lynch, V.; Sessler, J. L. Cyclo[8]pyrrole: A Simple-to-Make Expanded Porphyrin with No Meso Bridges. *Angew. Chem. Int. Ed.* **2002**, *41* (8), 1422–1425.

33. Quiñonero, D.; Garau, C.; Rotger, C.; Frontera, A.; Ballester, P.; Costa, A.; Deyà, P. M. Anion-π Interactions: Do They Exist? *Angew. Chem. Int. Ed.* **2002**, *41* (18), 3389–3392.

34. Gil-Ramírez, G.; Escudero-Adán, E. C.; Benet-Buchholz, J.; Ballester, P. Quantitative Evaluation of Anion-π Interactions in Solution. *Angew. Chem. Int. Ed.* **2008**, *47* (22), 4114–4118.

35. Ballester, P. Anion Binding in Covalent and Self-Assembled Molecular Capsules. *Chem. Soc. Rev.* **2010**, *39* (10), 3810–3830.

36. Adriaenssens, L.; Estarellas, C.; Vargas Jentzsch, A.; Martinez Belmonte, M.; Matile, S.; Ballester, P. Quantification of Nitrate-Pi Interactions and Selective Transport of Nitrate Using calix[4]pyrroles with Two Aromatic Walls. *J. Am. Chem. Soc.* **2013**, *135* (22), 8324–8330.

37. Maeda, H.; Kusunose, Y. Dipyrrolyldiketone Difluoroboron Complexes: Novel Anion Sensors with C-H···X- Interactions. *Chem. Eur. J.* **2005**, *11* (19), 5661–5666.

38. Maeda, H.; Ito, Y. BF2 Complex of Fluorinated Dipyrrolyldiketone: A New Class of Efficient Receptor for Acetate Anions. *Inorg. Chem.* **2006**, *45* (20), 8205–8210.

39. Maeda, H.; Ito, Y.; Kusunose, Y.; Nakanishi, T. Di-Pyrrolyl-Pyrazoles: Anion Receptors in Protonated Form and Efficient Building Blocks for Organized Structures. *J. Org. Chem.* **2007**, *72* (7), 2612–2616.

40. Maeda, H.; Bando, Y. Recent Progress in Research on Anion-Responsive Pyrrole-Based π-Conjugated Acyclic Molecules. *Chem. Commun.* **2013**, *49* (39), 4110–4113.

41. Ghosh, S. K.; Ishida, M.; Li, J.; Cha, W.-Y.; Lynch, V. M.; Kim, D.; Sessler, J. L. Synthesis and Anion Binding Studies of o-Phenylenevinylene-Bridged Tetrapyrrolic Macrocycle as an Expanded Analogue of calix[4]pyrrole. *Chem. Commun.* **2014**, *50* (28), 3753–3756.

42. Sessler, J. L.; Kim, S. K.; Gross, D. E.; Lee, C. H.; Kim, J. S.; Lynch, V. M. Crown-6-calix[4]arene-Capped calix[4]pyrrole: An Ion-Pair Receptor for Solvent-Separated CsF Ions. *J. Am. Chem. Soc.* **2008**, *130* (39), 13162–13166.

43. Kim, S. K.; Sessler, J. L.; Gross, D. E.; Lee, C.-H.; Kim, J. S.; Lynch, V. M.; Delmau, L. H.; Hay, B. P. A calix[4]arene Strapped calix[4]pyrrole: An Ion-Pair Receptor Displaying Three Different Cesium Cation Recognition Modes. *J. Am. Chem. Soc.* **2010**, *132* (16), 5827–5836.

44. Kim, S. K.; Sessler, J. L. Calix[4]pyrrole-Based Ion Pair Receptors. *Acc. Chem. Res.* **2014**, *47*, 2525–2536.

45. Iverson, B. L.; Shreder, K.; Král, V.; Sessler, J. L. Phosphate Recognition by Sapphyrin. A New Approach to DNA Binding. *J. Am. Chem. Soc.* **1993**, *115* (16), 11022–11023.

46. Král, V.; Furuta, H.; Shreder, K.; Lynch, V.; Sessler, J. L. Protonated Sapphyrins. Highly Effective Phosphate Receptors. *J. Am. Chem. Soc.* **1996**, *118*, 1595–1607.

47. Tobey, S. L.; Jones, B. D.; Anslyn, E. V. C3v Symmetric Receptors Show High Selectivity and High Affinity for Phosphate. *J. Am. Chem. Soc.* **2003**, *125* (14), 4026–4027.

48. Bjerrum, J. *Stability Constants of Metal-Ion Complexes, with Solubility Products of Inorganic Substances: Inorganic Ligands*; Special publication; Chemical Society: London, 1958.

49. Tobey, S. L.; Anslyn, E. V. Determination of Inorganic Phosphate in Serum and Saliva Using a Synthetic Receptor. *Org. Lett.* **2003**, *5* (12), 2029–2031.

50. Sessler, J. L.; Katayev, E.; Pantos, G. D.; Ustynyuk, Y. A. Synthesis and Study of a New Diamidodipyrromethane Macrocycle. An Anion Receptor with a High Sulfate-to-Nitrate Binding Selectivity. *Chem. Commun.* **2004**, (11), 1276–1277.

51. Sessler, J. L.; Katayev, E.; Dan Pantos, G.; Scherbakov, P.; Reshetova, M. D.; Khrustalev, V. N.; Lynch, V. M.; Ustynyuk, Y. A. Fine Tuning the Anion Binding Properties of 2,6-Diamidopyridine Dipyrromethane Hybrid Macrocycles. *J. Am. Chem. Soc.* **2005**, *127* (32), 11442–11446.

52. Bazzicalupi, C.; Bencini, A.; Lippolis, V. Tailoring Cyclic Polyamines for Inorganic/organic Phosphate Binding. *Chem. Soc. Rev.* **2010**, *39* (10), 3709–3728.

53. Yang, L.-Z.; Li, Y.; Jiang, L.; Feng, X.-L.; Lu, T.-B. Size and Temperature Dependent Encapsulation of Tetrahedral Anions by a Protonated Cryptand Host. *CrystEngComm* **2009**, (11), 2375–2380.

54. Mateus, P.; Delgado, R.; Brandão, P.; Félix, V. Polyaza Cryptand Receptor Selective for Dihydrogen Phosphate. *J. Org. Chem.* **2009**, *74* (22), 8638–8646.

55. Bisson, A. P.; Lynch, V. M.; Monahan, M.-K. C.; Anslyn, E. V. Recognition of Anions through NH-Pi Hydrogen Bonds in a Bicyclic Cyclophane- Selectivity for Nitrate. *Angew. Chem. Int. Ed. English* **1997**, *36* (21), 2340–2342.

56. Sokkalingam, P.; Kim, D. S.; Hwang, H.; Sessler, J. L.; Lee, C.-H. A Dicationic calix[4]pyrrole Derivative and Its Use for the Selective Recognition and Displacement-Based Sensing of Pyrophosphate. *Chem. Sci.* **2012**, *3*, 1819.

57. Bill, N. L.; Kim, D.-S.; Kim, S. K.; Park, J. S.; Lynch, V. M.; Young, N. J.; Hay, B. P.; Yang, Y.; Anslyn, E. V.; Sessler, J. L. Oxoanion Recognition by Benzene-Based Tripodal Pyrrolic Receptors. *Supramol. Chem.* **2012**, *24* (1), 72–76.

58. Cai, J.; Hay, B. P.; Young, N. J.; Yang, X.; Sessler, J. L. A Pyrrole-Based Triazolium-Phane with NH and Cationic CH Donor Groups as a Receptor for Tetrahedral Oxyanions That Functions in Polar Media. *Chem. Sci.* **2013**, *4* (4), 1560–1567.

59. Arumugaperumal, R.; Srinivasadesikan, V.; Ramakrishnam Raju, M. V.; Lin, M.-C.; Shukla, T.; Singh, R.; Lin, H.-C. Acid/Base and $H_2PO_4^-$ Controllable High-Contrast Optical Molecular Switches with a Novel BODIPY Functionalized [2]Rotaxane. *ACS Appl. Mater. Interfaces* **2015**, *7* (48), 26491–26503.

2. Schiff-base Appended Polymers for Phosphate Removal

The remediation of phosphate-contaminated water bodies and the effective treatment of hyperphosphatemia are two big challenges in which phosphate recognition could play a useful role. Chapter 1 presents synthetic organic receptors that achieve phosphate recognition. In this chapter, we briefly introduce the state of the art in phosphate removal. Next, we present findings from synthetic and phosphate extraction studies that involve polymeric materials with pendent Schiff-base macrocycles designed to function as phosphate anion receptors.

2.1. Challenges in Anion Extraction

In Chapter 1, some of the challenges associated with anion recognition were outlined. These derive in part from the larger size of anions relative to their isoelectronic cations, the diverse geometries that anions often display, and the higher energies of solvation that must typically be overcome.[1]

Anions are generally larger than cations. Therefore, larger hosts are required for recognition of anions.[2] A F^- anion has a radius of 1.2–1.4 Å.[3] A porphyrin system with *trans*-nitrogen distances[4] of about 4 Å is too small to bind F^- ions. However, an early solid state study involving the sapphyrin-F^- complex ((**1.6**+2H)$^{2+}$·F^-) revealed[4] a F^- ion in the pentapyrrolic core of the sapphyrin (Figure 2.1). Sapphyrin **1.6** has a core size of roughly 5.5 Å in diameter and therefore, its core is large enough to accommodate a bound F^- anion.

Figure 2.1 shows two macrocyclic systems, sapphyrin and cyclo[8]pyrrole, each with an anionic guest in its central cavity. In this Figure, the sapphyrin-F^- complex (**1.6**+2H)$^{2+}$·F^-) is shown on the left, while the cyclo[8]pyrrole-H_2SO_4 salt (**1.12** +

2H]$^{2+}$·SO_4^{2-}) is shown on the right. While a size comparison of differently shaped anions such as F^- versus SO_4^{2-} is difficult, the sulfur (S) oxygen (O) bond distance[5] of about 1.5 Å in SO_4^{2-} is such that a tetrahedral SO_4^{2-} is bigger than a spherical F^-. As can be seen in Figure 2.1, a SO_4^{2-} anion was hosted in octapyrrolic macrocycle **1.12**, which has a larger cavity diameter of roughly 7.5–7.7 Å.[6]

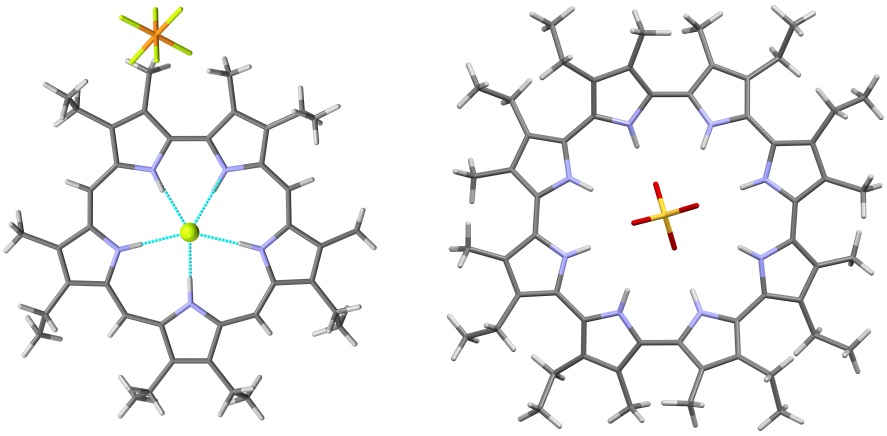

Figure 2.1: Single crystal structures of the sapphyrin-F^- complex (**1.6**+2H)$^{2+}$·F^-) to the left and the cyclo[8]pyrrole-H_2SO_4 salt (**1.12** + 2H]$^{2+}$·SO_4^{2-}) to the right. These structures were originally reported by Sessler *et al.*[4,6] and were redrawn using data from the CCDC (CCDC numbers 1184078 and 176189, respectively).

Targeting anions with tetrahedral geometry is likely to require not only larger hosts but also appropriately shaped binding sites for selective recognition. Consistent with this thinking is the fact that there are more tripodal or cage-like synthetic receptors for phosphate recognition than planar cyclic systems, as noted in Chapter 1.

Another hurdle associated with anion binding is that certain anions, including tetrahedral oxoanions such as $H_2PO_4^-$ and HSO_4^-, are susceptible to proton transfer.[7] The receptor itself can undergo deprotonation as one manifestation of this problem. For

example, Gale *et al*. reported unusual titration profiles obtained upon introduction of electron withdrawing groups on his previously reported systems. Detailed solution and solid state studies revealed that an increase in the acidity of pyrrolic hydrogens, as a result of the structural modifications, led to deprotonation by basic anions such as F^-, $H_2PO_4^-$, and benzoate.[8]

In polar media, including water, anion recognition is rendered further challenging both because of solvation (e.g. ΔG_h = -300 kJ/mol for NO_3^- and ΔG_h = -465 kJ/mol for $H_2PO_4^-$, where ΔG_h = Gibbs free energy change of hydration)[9] and competitive hydrogen bond donation associated with the solvent shell.[10] Gabbaï and coworkers have been successful in meeting this challenge. They described[11] the synthesis of a cationic Lewis acidic borane which forms a highly stable zwitterionic ammonium/fluoroborate complex by a C-H···F-B hydrogen bond in aqueous media. They also demonstrated the use of a cationic borane receptor for the extraction of F^- from water.[11] The same group recently employed a neutral bidentate Lewis acid system containing two antimony(V) centers to "squeeze out" the F^- ions from water, overcoming the hydration barrier.[12] However, to our knowledge, there is no reported artificial receptor capable of extracting $H_2PO_4^-$ out of water into an organic phase even though it has the exact same hydration enthalpy value as F^-.[9]

2.2. Current State of Art for Phosphate Removal

In 1997, crystallographic data was presented for a phosphate residing in the pocket of a phosphate-binding protein (PBP) from *E. coli* bacteria (Figure 2.2).[13] This periplasmic PBP is involved in the highly selective uptake and active transport of phosphate into bacteria cells. The binding site of PBP is located in a deep pocket far from

the protein surface. In this deep pocket, phosphate is bound in a fully dehydrated form and is completely and efficiently shielded from the solvent. The binding pocket of the PBP provides for twelve stabilizing hydrogen bonding interactions. These have their origin surrounding amino acid residues, namely residues Thr10, Phe11, Ser38, Gly140, Thr141, and the side chains of residues Ser38, Arg135 (2 hydrogen bonds), Ser139, Thr141. Also involved is a negatively charged carboxylate group from Asp56 that is thought to be specifically dedicated to the binding of a protonated form of phosphate. Presumably, as a result of these highly oriented bonds, PBP is unable to bind sulfate.

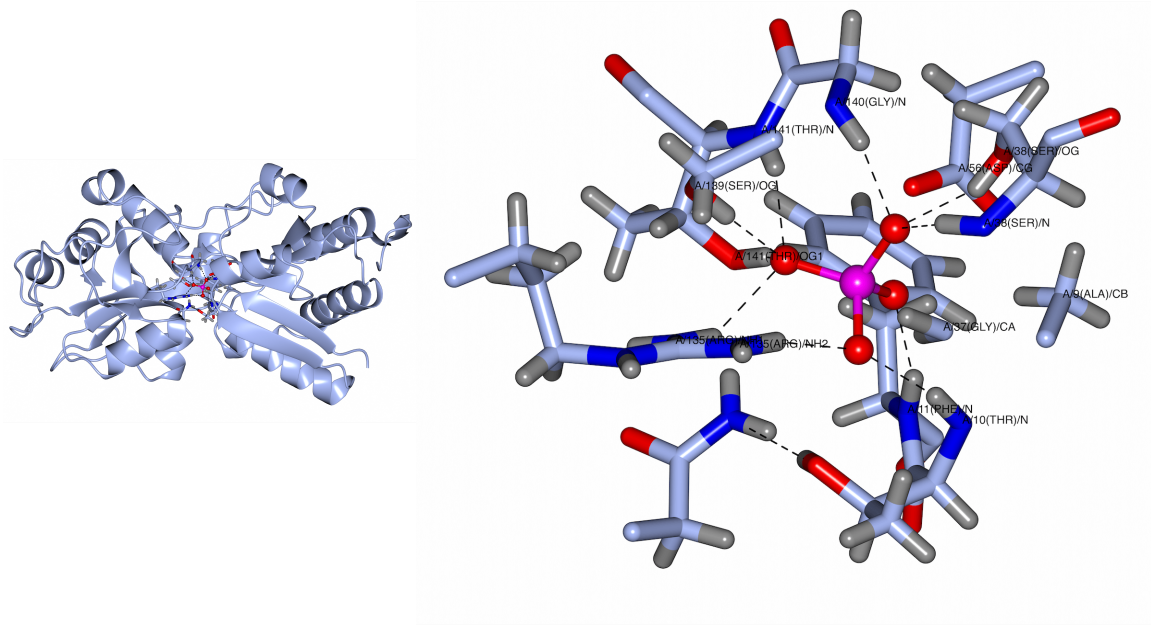

Figure 2.2: X-ray crystal structure of *E. Coli* phosphate-binding protein (PBP) (left) and the binding site of the PBP (right). This structure was originally reported by Quiocho and coworkers[13] and was redrawn using the program QtMG using data from the protein data bank (PDB) (PDB code: 1IXH, 0.98 Å resolution).

This protein structure is presented as an example of naturally occurring phosphate recognition and transport (essentially, extraction) in nature. Some structural elements that

researchers may use to guide their own receptor designs include the complex three-dimensional structure of the PBP, the presence of cooperative attractive interactions, the presence of repulsive interactions for the sake of selectivity, and the absence of solvent in the bound form.

Although the PBP shown above is a great example of effective phosphate binding found in nature, it is unlikely this protein will see application in the area of wastewater remediation due to its rather high cost. However, some biological methods are used in wastewater processing. One of these, called "enhanced biological phosphate removal" (EBPR), involves storage of phosphate as polyphosphates (poly-P) in the forms of biomass.

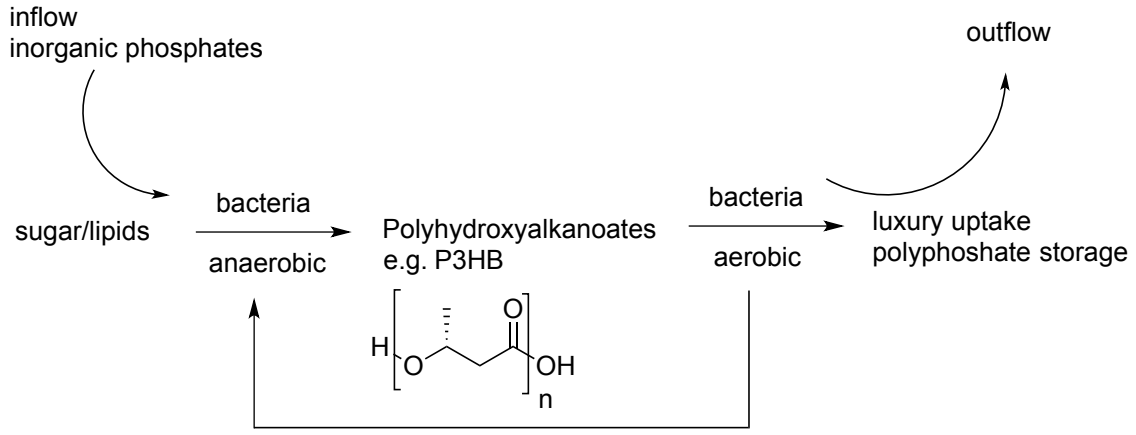

Scheme 2.1: Basic concept of the anaerobic-aerobic process known as enhanced biological phosphate removal (EBPR).

The underlying mechanism, known as "luxury uptake",[14] involves circulation of activated sludge through anaerobic and aerobic phases, with the wastewater added during the anaerobic phase.[15] By means of the alternating anaerobic-aerobic cycles microorganisms accumulate phosphate in the form of poly-P (Scheme 2.1). Efficient

phosphate removal is achieved by the physical removal of the microorganisms.[16] This method is well established in its engineering but little-studied in terms of its microbiology.[17] Although EBPR is suitable for treating industrial wastewater and polluted waterways, and has the potential to reduce the impact of eutrophication, it is not a viable approach phosphate removal in applications, such as hyperphosphatemia, that require biocompatibility with human subjects.

As noted earlier, patients with end-stage renal disease (ESRD) suffer from elevated phosphate concentrations in their serum as explained in Chapter 1.[18] This condition known as hyperphosphatemia. The current methods for treating hyperphosphatemia are three-hour long daily dialysis session,[19] dietary restrictions, consumption of hard cations or Sevelamer (a cross-linked poly(allylamine) (PAA), *e.g.*, Renagel®).

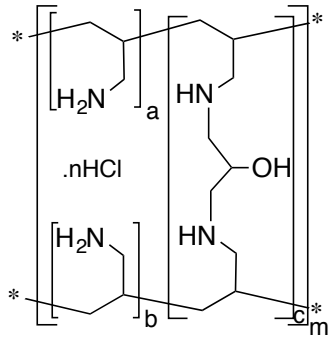

Renagel

a+b=9, c=1
n=0.4 (40% protonated)

Oral administration of cross-linked PAA serves to control the concentration of phosphorus available for absorption in the gastrointestinal track. This polymer is not selective for phosphate and it also binds chloride. Rather high ingested doses are thus needed. Adverse effects are also seen sometimes in patients undergoing such therapy. We

thus believe there remains a need for biologically compatible materials capable of binding phosphate under conditions associated with the treatment of hyperphosphatemia.

2.3. Schiff-base Macrocycle Appended Polymeric Material for Phosphate Extraction

Schiff-base macrocycles **1.24** and **1.25**, reviewed in Chapter 1, were chosen as models for the development of polymeric materials containing pendent 2,6-diamidopyridine dipyrromethane receptors for the purpose of phosphate extraction from aqueous media. The structural modification needed to attach the 2,6-diamidopyridine dipyrromethane systems to polymeric material is discussed in the following section.

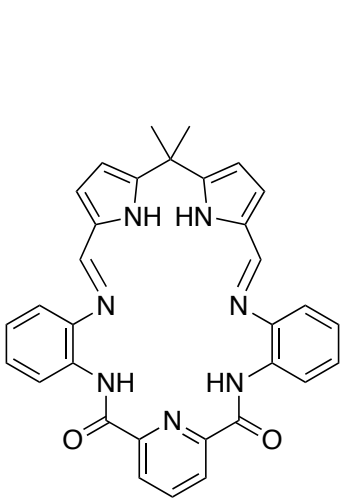

1.24

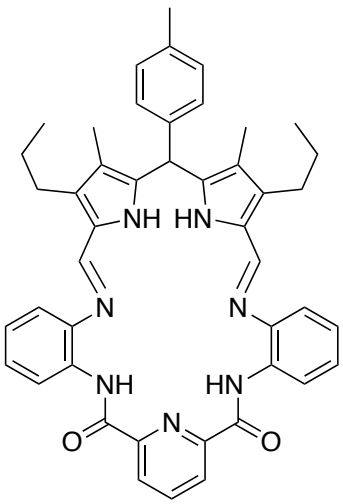

1.25

Polymeric materials with pendent phosphate receptors were proposed based on a prior study wherein polymers with pendent C[4]P anion receptors were used to extract halide anion salts from aqueous phases. In that study, Aydogan and Sessler used a *meso*-functionalized C[4]P system as pendent receptors on a poly-(methyl methacrylate) (pMMA) backbone to obtain the co-polymer **2.1**.[20] This co-polymer was shown to be

capable of extracting TBACl and TBAF salts from aqueous media into CH_2Cl_2, whereas the control compounds **1.10** (octamethyl C[4]P) and **2.4** (pMMA without the receptor pendants) were not effective.

Aydogan and Sessler improved their first generation C[4]P-pMMA material (**2.1**) by creating a co-polymer (**2.2**) that also contained a pendent cation-binding receptor (benzo-15-crown-5, **2.5**).[21] Co-polymer **2.2**, containing both pendent anion and cation receptors, was found capable of extracting halide salts from water as ion-pairs, namely KF and KCl, into an organic phase. The anion extraction could be followed visually observed by using a cationic dye with a Cl^- counter anion (**2.6**). This colored agent was shown to be carried from the aqueous solution into the organic phase (CH_2Cl_2) by the polymer **2.2**. This was not true for any control systems, including monomer **1.10**, crown ether **2.5**, or the monofunctionalized polymer **2.1**, and pMMA **2.3**.[21] The extraction events were also monitored by various analytical methods, *e.g.*, ^1H and ^{19}F NMR spectroscopy and flame emission spectroscopy (FES).

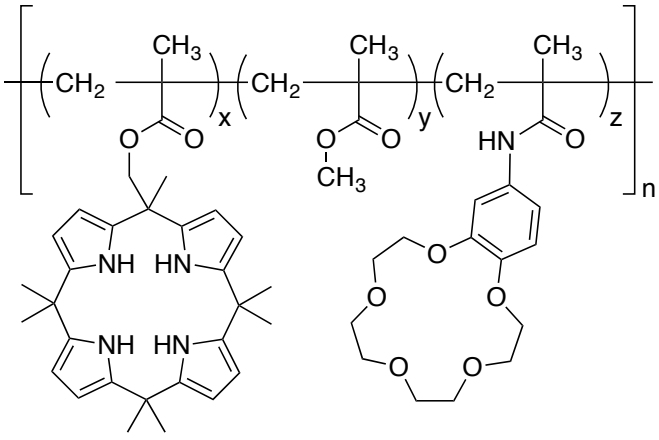

2.1: x = 1, y = 14, z = 0; M_n = 90 kDa
2.2: x = 1, y = 14, z = 0.8; M_n = 57 kDa
2.3: x = 0, y = 12, z = 1; M_n = 33 kDa
2.4: x = 0, y = 1, z = 0; M_n = 40 kDa

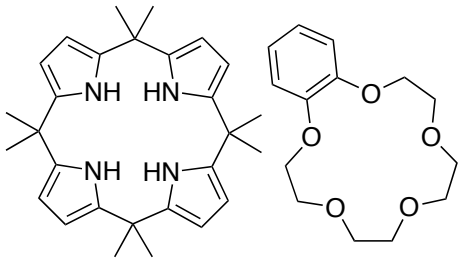

1.10 **2.5**

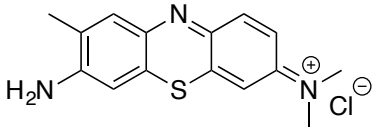

2.6

2.4. Results and Discussion

2.4.1. Syntheses and Structures

Two new Schiff-base macrocycles, **2.15a** and **2.15b**, were constructed by cyclization of the dialdehydes **2.9a** and **2.9b** with diamine **2.14** *via* diimine formation (Scheme 2.2). The dialdehydes **2.9a** and **2.9b** and the diamine **2.14** were prepared according to literature procedures.[22,23] All structures were characterized by ^{1}H and ^{13}C NMR spectroscopy and high-resolution mass spectrometry (HRMS). ^{1}H NMR spectroscopy was used to monitor the formation of imine bonds in the final step. Imine bond formation was confirmed by absence of a signal at 9.4 ppm (the resonance frequency for the aldehyde CH proton of **2.9b**) and the presence of a signal at 8.3 ppm ascribed to the imine CH proton (*cf*. Figure 2.3). Figure 2.4 shows the X-ray crystal structures of two precursors **2.9b** and **2.14** and the two Schiff-base macrocycles **2.15a** and **2.15b**.

While macrocycle **2.15a** was designed as a control compound, macrocycle **2.15b** was designed to serve as a precursor that would allow attachment of the Schiff-base macrocyclic framework to a polymeric support. In other words, it was expected that macrocycle **2.15b** would allow access to polymeric materials with pendent Schiff-base receptors.

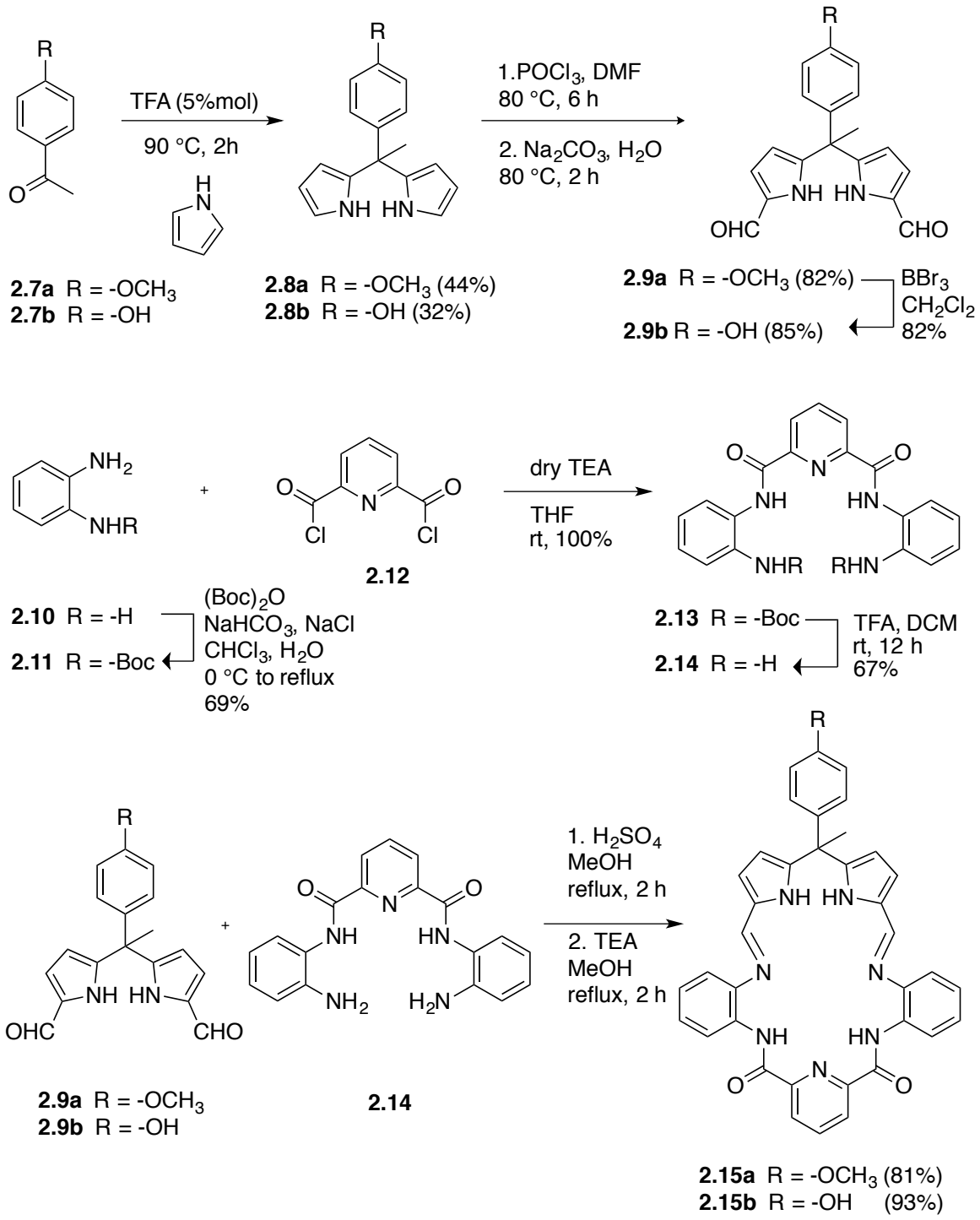

Scheme 2.2: The synthesis of Schiff-base macrocycles **2.15a** and **2.15b**.

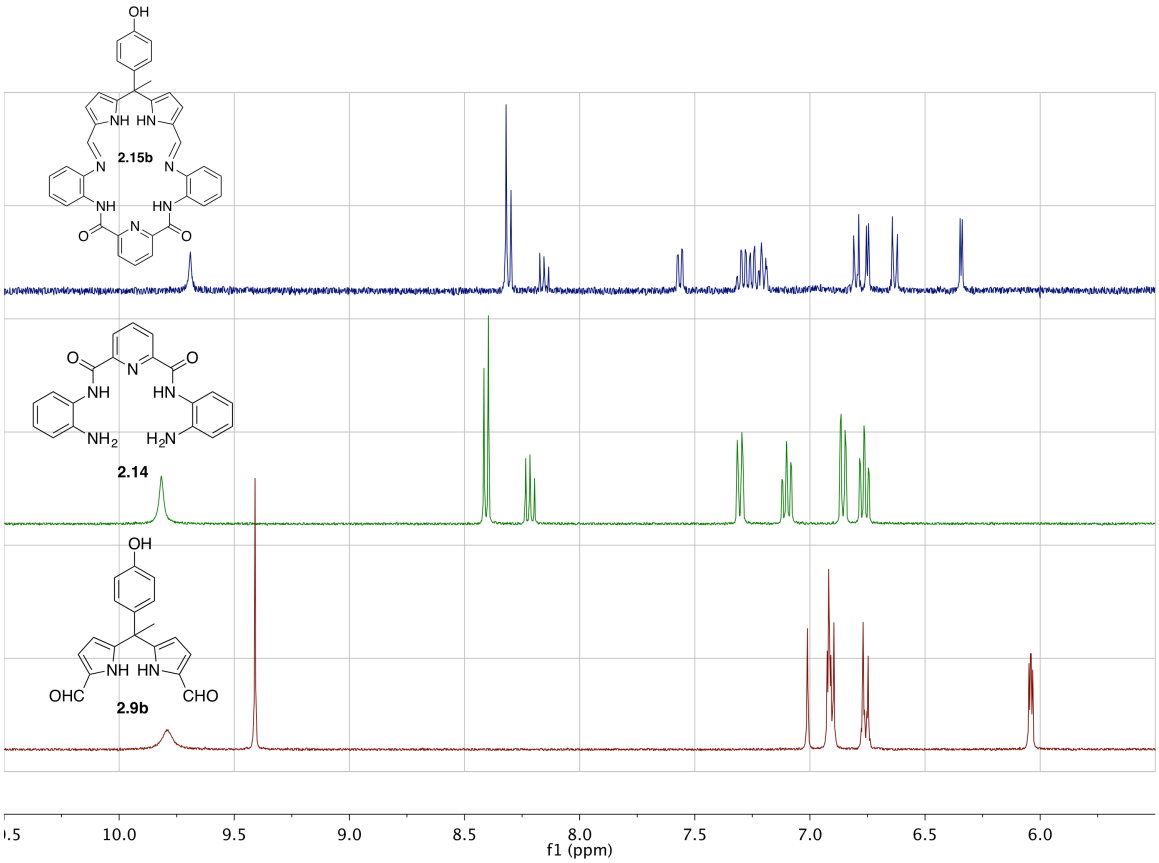

Figure 2.3: Stacked partial ^{1}H NMR spectra of **2.9b** (bottom), **2.14** (middle), and **2.15b** (top) in CD_3CN.

Solid state structural studies were carried out using single crystals of **2.15a** co-crystallized with CH_3OH and **2.15b** co-crystallized with DMF. Both structures revealed similar conformations in which the aryl moiety of the DPM subunit (originating from **2.9b**) and the pyridine moiety (originating from **2.14**) are in *cis* positions relative to the *o*-phenylene rings. Based on the conformational similarity between the single crystal structures of **2.15a** and **2.15b**, it was inferred that the methyl group did not have a substantial impact on the conformation of the macrocyclic framework. This lack of difference was considered to augur well for the use of macrocycles functionalized in the phenolic position as precursors for polymer formation.

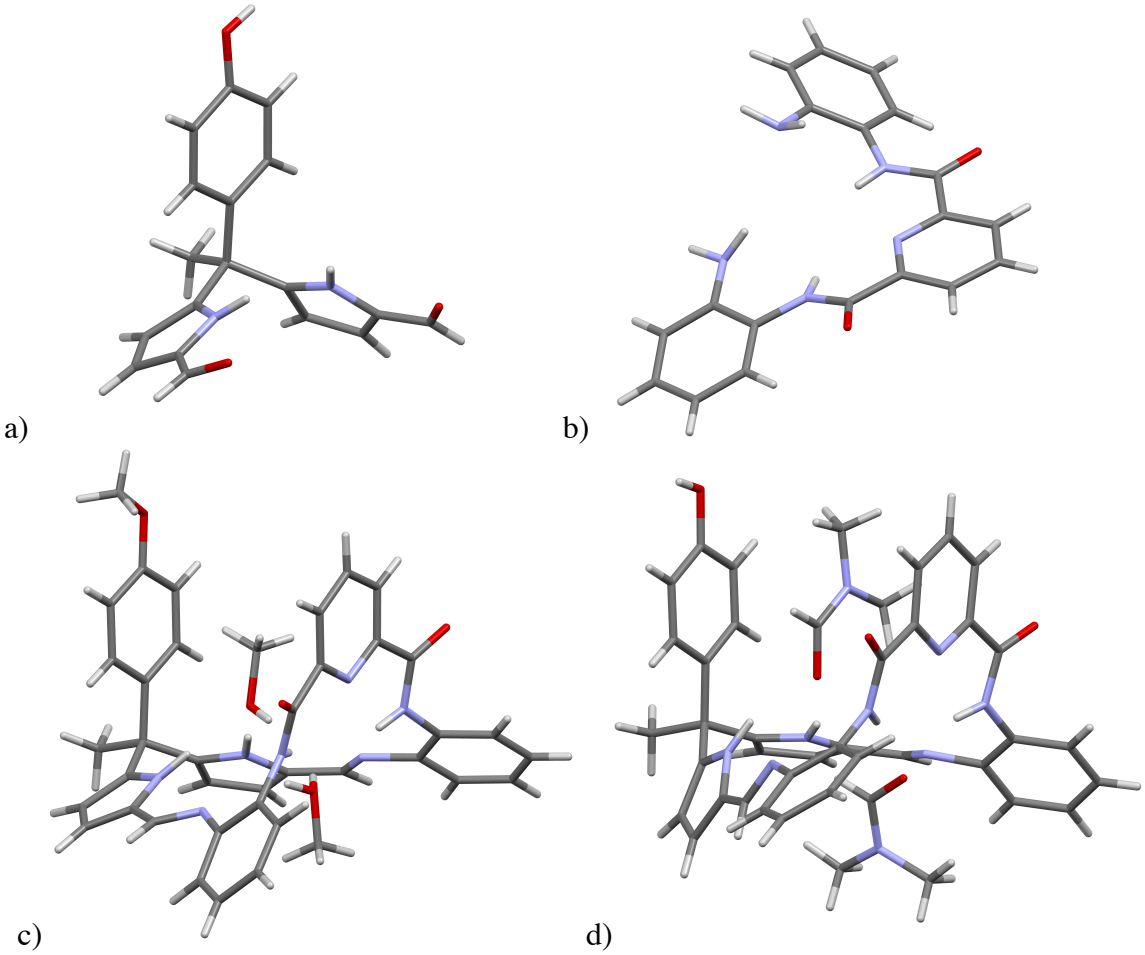

Figure 2.4: Single crystal structures of a) **2.9b**, b) **2.14**, c) **2.15a**·2CH_3OH, and d) **2.15b**·2 DMF.

It is also instructuve to compare the conformations of these two new Schiff-base macrocycles (**2.15a** and **2.15b**) with those of similar macrocycles reported previously, namely **1.24**[22] and **1.25**.[24] Reported modeling studies[24] showed that the free ligands **1.24** and **1.25** could exist in two different conformations. In the case of **1.25**, the tolyl and pyridine fragments were calculated to adopt either in *trans* or *cis* positions relative to the *o*-phenylene rings. However, single crystal structures of both **2.15a** and **2.15b** revealed a

cis-like conformation. The contrast was thought to arise from two structural differences in the DPM subunits. Compound **1.25** has a tolyl ring, a hydrogen atom, and two fully β-substituted pyrrole rings in the *meso*-position,[24] whereas the new system **2.15b** has an aryl ring, a methyl group, and two β-free pyrrole rings.

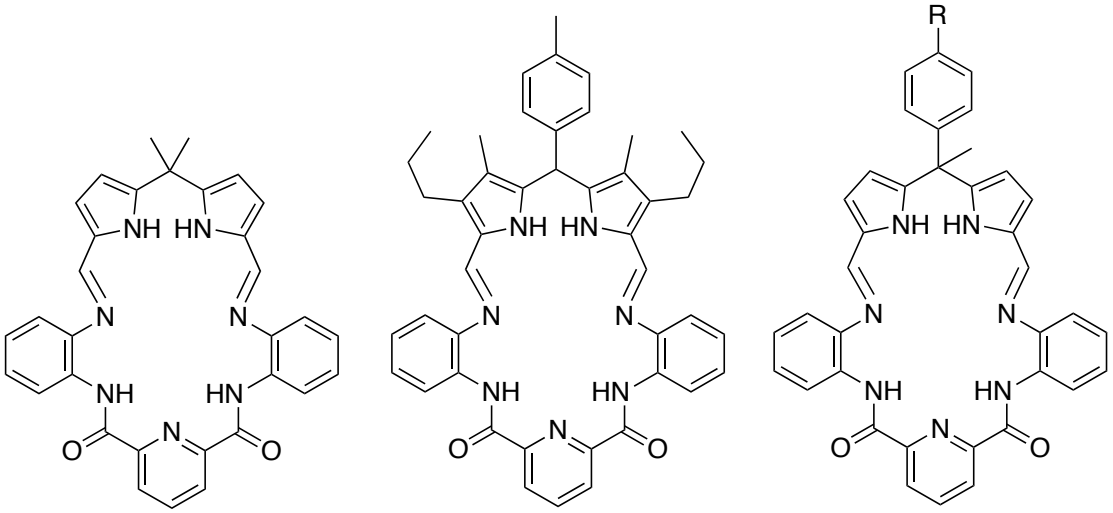

1.24 **1.25** **2.15a** R = -OCH_3 **2.15b** R = -OH

It is likely that these structural differences, particularly those involving the *meso*-positions and the β-substituents of the pyrrole rings, are reflected in the actual conformations observed for macrocycles **1.24**, **1.25, 2.15a**, and **2.15b**.

2.4.2. Anion binding studies of 2.15a and 2.15b

It was considered possible that the anion binding affinities could emerge because of these inferred structural differences. The anion binding affinities of the new systems, **2.15a** and **2.15b**, were thus tested.

Figure 2.5 shows partial ^{1}H NMR spectra of **2.15a** recorded in CD_2Cl_2 in the presence of varying molar equivalents of $TBAH_2PO_4$. Major changes observed in the

chemical shifts of the pyrrole NH signal and the imine CH signal (*cf*. Figure 2.5). Saturation behavior in signal shifts is observed at approximately 2.5 molar equivalents of $TBAH_2PO_4$.

For quantification of the binding affinities, UV-Vis spectroscopic studies, in which receptor **2.15a** was titrated with $TBAH_2PO_4$ and $TBAHSO_4$ in CH_2Cl_2, were conducted. Experimental details and spectra are presented in Section 2.6.2 (page 66). Table 2.1 shows the binding affinities obtained from the titration studies, as well as the affinities previously reported for **1.24**[22] and **1.25**[24] in CH_3CN.

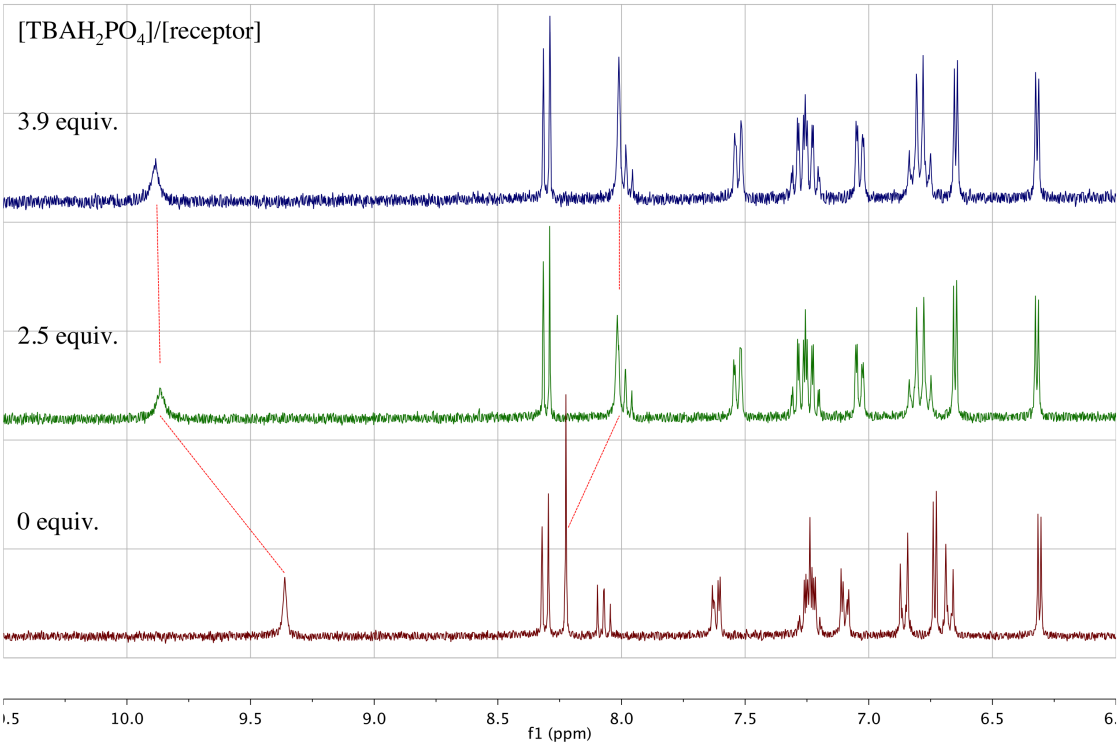

Figure 2.5: Stacked partial ^{1}H NMR spectra of **2.15a** in CD_2Cl_2 at varying molar ratio of $TBAH_2PO_4$.

Anion	**2.15a**[a]	**2.15b**[b]	**1.24**[b,c]	**1.25**[b,d]
$H_2PO_4^-$	(2.1 ± 0.3) x 10^5	1.7 x 10^5	K_1 = 3.4 x 10^5	(2.9 ± 0.2) x 10^4
			K_2 = 2.6 x 10^4	
HSO_4^-	(1.2 ± 0.2) x 10^4	nd	(6.4 ± 0.3) x 10^4	(1.1 ± 0.2) x 10^5

[a] in CH_2Cl_2, [b] in CH_3CN, [c] reported in reference-22, [d] in reported in reference-24, nd: not determined.

Table 2.1: Binding affinity constants (in M^{-1}) for **2.15a**, **2.15b**, **1.24**, and **1.25** with TBA^+ salts of oxyanions by UV-Vis spectroscopy in specified solvents.

From the binding affinity constants listed in Table 2.1, the order of anion selectivity of **2.15a** for the oxyanions $H_2PO_4^-$ and HSO_4^- in CH_2Cl_2 is the same as that of the receptor **1.24** in CH_3CN. However, the $H_2PO_4^-$ binding stoichiometries of the two systems (**2.15a** and **1.24**) differ. A 1:2 binding stoichiometry for $H_2PO_4^-$ was reported for **1.24**. Formation of **1.24**·$2H_2PO_4^-$ complex was supported[22] by a competition study in which a solution of **1.24** containing 10 molar equivalents of HSO_4^- was titrated with $H_2PO_4^-$.[22] Spectral changes from that study were interpreted in terms of that **1.24** having a second binding site for $H_2PO_4^-$ that was effective for complexation even in the presence of 10 molar equivalents of HSO_4^-.[22]

Receptor **2.15a**, on the other hand, displayed a 1:1 binding stoichiometry for $H_2PO_4^-$ anion in CH_2Cl_2. The isosbestic point observed* at 327 nm in the UV-Vis spectral titration is most easily interpreted in terms of two absorbing species at this wavelength (namely, the free receptor **2.15a** and the bound form of the receptor, **2.15a**·$H_2PO_4^-$) that are interconverting between one another. A Job plot obtained from the same experiment (*cf.* Figure 2.14) likewise proved a 1:1 binding stoichiometry. Additionally, the data

* The total concentration of the receptor species was held constant throughout the titration of **2.15a** with $TBAH_2PO_4$.

obtained from UV-Vis spectra could be fit well to a 1:1 binding isotherm (*cf*. Figure 2.15). Based on these observations, we conclude that receptor **2.15a** has high affinity and selectivity for $H_2PO_4^-$ anion and binds this target with a 1:1 binding stoichiometry in organic media (*i.e*., CH_2Cl_2).

Among the receptors listed in Table 2.1, **1.25** displays the greatest affinity for HSO_4^-. This was explained by the "frozen" conformation of **1.25** that results from the fact that substituting the β-positions of the pyrrole units are substituted and a tolyl group is present on one of these "*meso*-like" positions of the DPM subunit.

One of the most substantial differences between the two new receptors, **2.15a** and **2.15b**, was their relative solubilities. In fact, derivative **2.15b**, the putative precursor for polymeric materials, displayed low solubility in organic solvents (*e.g*., CH_2Cl_2, $CHCl_3$, CH_3OH, CH_3CN), whereas **2.15a** was freely soluble at the mM level in typical halogenated solvents. This low solubility precluded quantitative analyses in the case of **2.15b** in CH_2Cl_2. It could be studied in CH_3CN, the same conditions under which **1.24** and **1.25** were studied. The affinity constant of **2.15b** for $H_2PO_4^-$ was determined (K_a = 1.7 x 10^5 M^{-1} *via* UV-Vis spectroscopy and K_a = 1.6 x 10^5 M^{-1} *via* ITC) proved competitive with those of previous receptors. Although it was proposed that structure **2.15b** will be modified by further substitution at the phenolic position, it was gratifying that the core macrocycle proved effective for $H_2PO_4^-$ binding.

2.4.3. Synthesis of Polymeric Material with Pendent Schiff-base Macrocycles

In order to obtain polymeric materials containing pendent Schiff-base macrocycles, two general synthetic approaches were considered. The first approach involves attachment of DPM subunits to a polymer backbone (or to a polymerizable

moiety) before formation of the Schiff-base macrocycle (Scheme 2.3). The second approach involves attachment of pre-formed Schiff-base systems (*e.g.*, **2.15b**) to a polymer backbone (or to a polymerizable moiety) (Scheme 2.4).

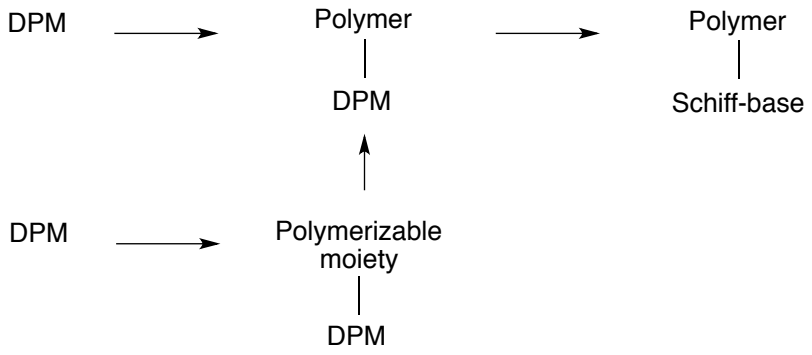

Scheme 2.3: The first synthetic approach that was considered for the synthesis of polymeric materials containing Schiff-base macrocyclic pendants. It starts from DPM precursors.

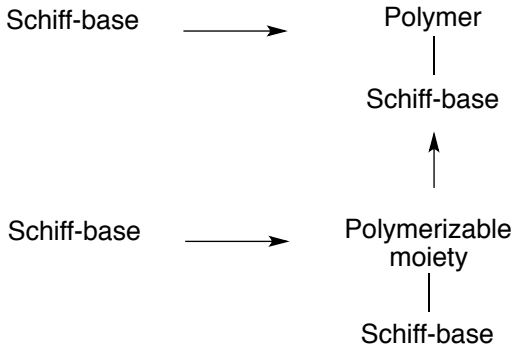

Scheme 2.4: The second synthetic approach considered for the synthesis of polymeric materials containing Schiff-base macrocyclic pendants. This approach relies on the use of precursors containing the preformed macrocycle.

The approach involving the attachment of a preformed functionalized Schiff-base to a functionalized polymer backbone was considered. The functionalized Schiff-base **2.15b**, prepared in 93% yield (see Experimental Section 2.6.1, page 55), was attached to

the commercially available functionalized-polystyrene **2.16** (poly(vinylbenzyl chloride), 60/40 mixture of 3- and 4- isomers) under S_N2 reaction conditions (Scheme 2.5).

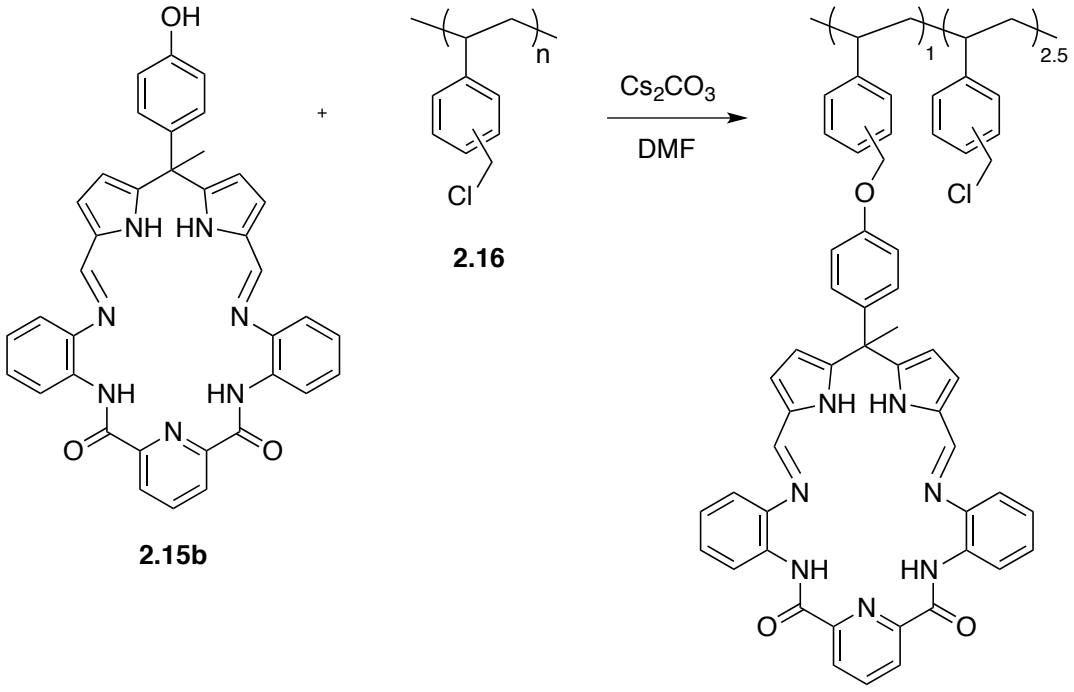

Scheme 2.5: Preparation of the polymer **2.17** by post-polymerization modification of commercially available functionalized polystyrene **2.16** with **2.15b**.

As inferred from integration of the ^{1}H NMR spectrum (the ratio of the signal at 9.5 ppm to those at 9–5.5 ppm), it was concluded that the new polymeric material **2.17** bears one pendent Schiff-base macrocycle for every 3.5 phenyl groups present on the styrene backbone (*cf*. Figure 2.6). In other words, the reaction between equimolar amounts of **2.15b** and **2.16** yielded about 30% substitution of **2.16** with **2.15b**. The net result is a co-polymer **2.17** bearing pendent Schiff-base macrocycles (Scheme 2.5). Co-polymer **2.17** proved appreciably soluble in $CHCl_3$. It could thus be used for liquid-liquid and solid-liquid extraction studies as detailed in the next section.

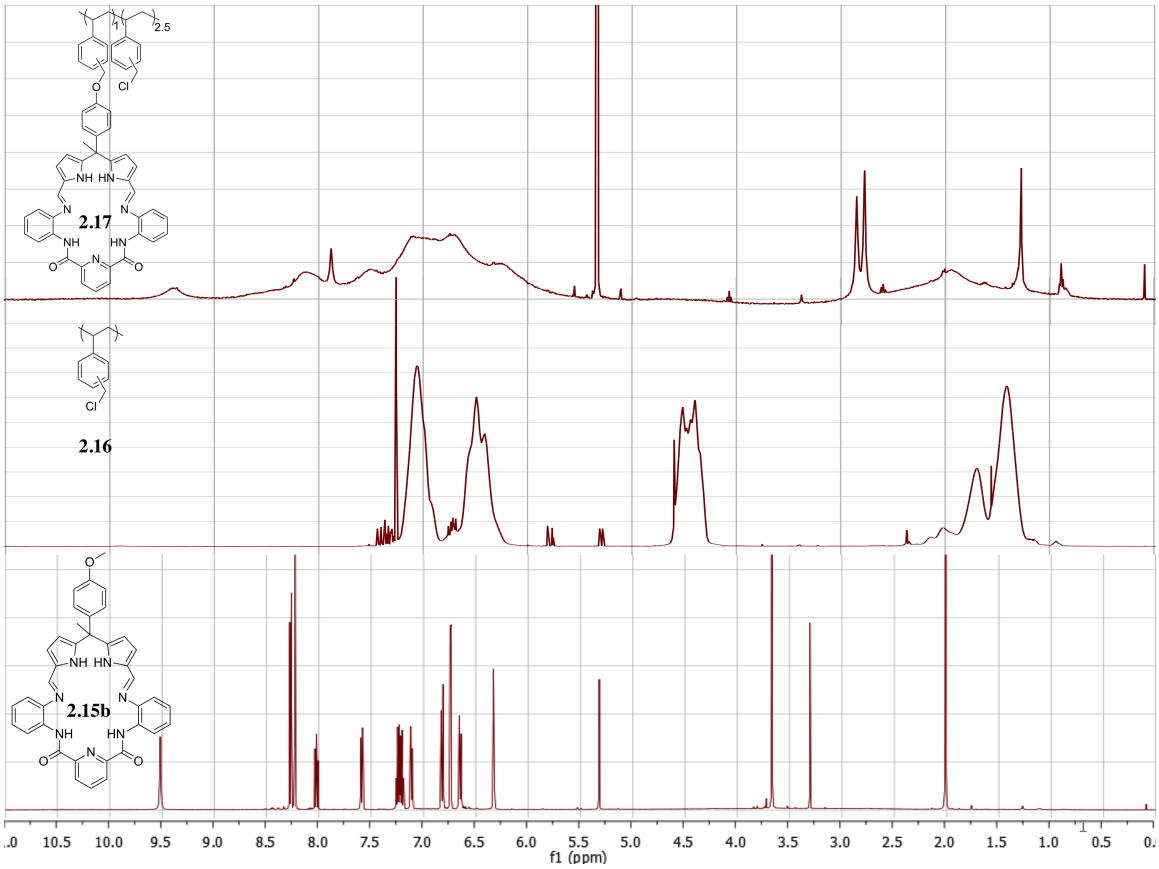

Figure 2.6: ^{1}H NMR spectra of **2.15a** in CD_2Cl_2 (bottom), commercially available functionalized polystyrene **2.16** in $CDCl_3$ (middle), and co-polymer product **2.17** in CD_2Cl_2 (top).

2.4.4. Anion Binding Studies of Co-polymer 2.17 in $CHCl_3$ *via* UV-Vis Spectroscopy

UV-Vis spectroscopy was used to confirm the presence of the pendent Schiff-base macrocycles in the case of co-polymer **2.17**. Polymer **2.16**, lacking absorbance features in the 300–400 nm spectral range, reacted with compound **2.15b**, which is insoluble in $CHCl_3$. The product, assumed to be co-polymer **2.17**, proved soluble in $CHCl_3$.

Moreover, it displayed UV-Vis spectral features between 300 and 400 nm in $CHCl_3$ that are characteristic of a Schiff-base macrocycle such as **2.15b** (*cf*. Figure 2.7a).

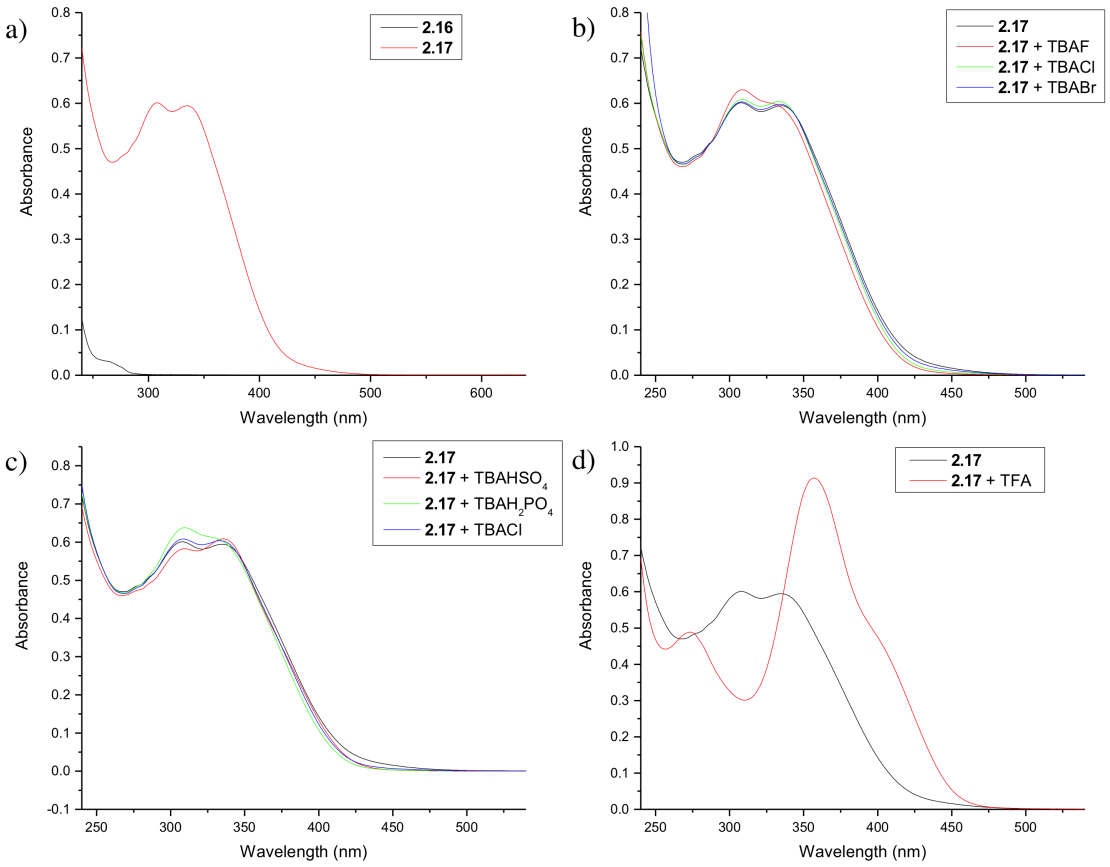

Figure 2.7: UV-Vis spectral changes observed in $CHCl_3$ under conditions where a) the polymer **2.16** (7.5 mg/L) and co-polymer **2.17** (18.6 mg/L), b) addition of various TBA^+ halide salts into solutions of **2.17**, c) addition of various TBA^+ anion salts into solutions of **2.17**, d) addition of TFA into a solution of **2.17**.

Solutions of **2.17** in $CHCl_3$ were screened for spectral changes when treated with various TBA^+ anion salts. Among the halide anions, F^- induced the biggest spectral change (Figure 2.7b). The spectrum of **2.17** that resulted upon exposure to $TBAH_2PO_4$ was similar to those produced when **2.15a** was treated with $H_2PO_4^-$ (*cf*. Figure 2.7c and Figure 2.13). On the other hand, the addition of $TBAHSO_4$ addition caused a spectral

change in **2.17** that differed from what was observed when **2.15a** was exposed to the same salt (Figure 2.7c). The effect of TFA on the spectrum of **2.17** in $CHCl_3$ was also tested. The spectral change (Figure 2.7d) was attributed to protonation of the two imine groups present in the Schiff-base macrocycle framework.

2.4.5. Extraction Studies with Co-polymer 2.17

Copolymer **2.17** was tested for its ability to extract $H_2PO_4^-$ anion salts using two experimental techniques. The first of this involves a liquid-liquid extraction. In this case, a solution of co-polymer **2.17** in $CDCl_3$ was layered with a solution of $TBAH_2PO_4$ in D_2O (Figure 2.8). After shaking[†] and separating the phases, changes in the $H_2PO_4^-$ anion concentration in both phases were quantified *via* ^{31}P NMR spectroscopy using $PhPO_3H$ (in D_2O) and $TBAPF_6$ (in $CDCl_3$) as the internal standards.

Figure 2.8: Graphical presentation of the liquid-liquid extraction approach used to test co-polymer 2.17 as a possible phosphate anion extractant (using TBA^+ as the anion source). Left: $H_2PO_4^-$ solution in D_2O, Right: Biphasic mixture obtained by adding a solution of co-polymer **2.17** in $CDCl_3$ to the solution on the left.

In the second method, a solid-liquid extraction, solid co-polymer **2.17** was added into a solution of $TBAH_2PO_4$ in CD_3OD (or in D_2O in a separate experiment). After

[†] Shaking a biphasic mixture co-polymer **2.17** in $CDCl_3$ and $TBAH_2PO_4$ in D_2O causes gelation as discussed later in this Section. Gelation occurs in bottom layer (i.e., $CDCl_3$). A photo of formed gel is shown in Figure 2.11.

shaking and separating solution phase, the change in the $H_2PO_4^-$ anion concentration in CD_3OD was quantified *via* ^{31}P NMR spectroscopy using $PhPO_3H$ as the internal standard. The results are summarized in Table 2.2.

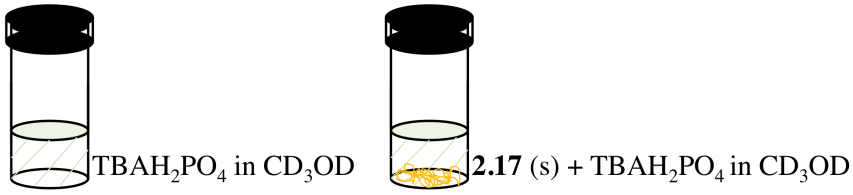

Figure 2.9: Graphical presentation of solid-liquid extraction approach used to test co-polymer 2.17 as a possible phosphate anion extractant (using TBA^+ as the anion source). Left: $H_2PO_4^-$ solution in CD_3OD, Right: Biphasic mixture obtained by adding solid co-polymer **2.17** into the solution on the left.

Extraction type	Source solvent	Extractant solvent	% change ($[H_2PO_4^-]$)	
	$[H_2PO_4^-]$ [a], V	[**2.17**], V	in source	in extractant
Liquid-liquid	D_2O	$CDCl_3$		
	50 mM, 1.0 mL	10 mg/1.0 mL	+13%	0%
Solid-liquid	CD_3OD	Solid **2.17**		
	20 mM, 1.5 mL	10 mg	-6%	-
	50 mM, 1.5 mL	10 mg	+4%	-
Solid-liquid	D_2O	Solid **2.17**		
	50 mM, 1.0 mL	11 mg	+6%	-

[a] $TBAH_2PO_4$ was used as the $H_2PO_4^-$ source. V stands for volume. % changes were quantified by using internal standard ($PhPO_3H$ or $TBAPF_6$) *via* ^{31}P NMR spectroscopy.

Table 2.2: Results of extraction studies conducted with co-polymer **2.17** as a putative extractant.

The results summarized in Table 2.2 proved hard to interpret. The common result among four entries was an increase in the concentration of $H_2PO_4^-$ in the source phase (i.e., stock $H_2PO_4^-$ solution that is tested for extraction). Although removal of $H_2PO_4^-$ from its original source phase was the desired outcome, the unexpected increase in $H_2PO_4^-$ concentration in the source can be explained by the removal of water from the $H_2PO_4^-$ source phase, leading to a more concentrated $H_2PO_4^-$ solution.

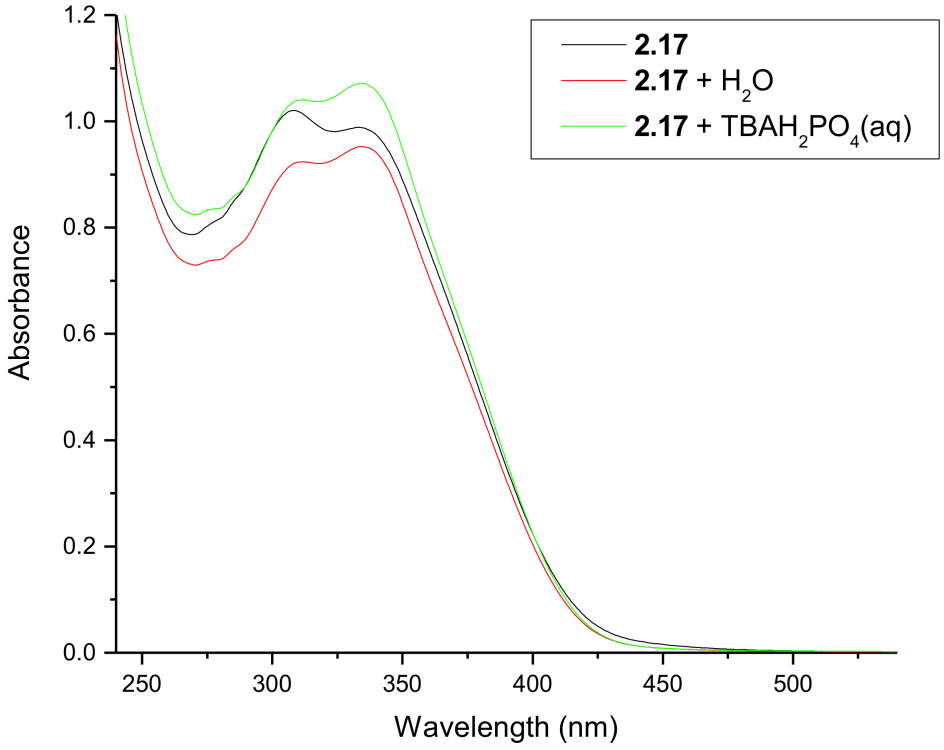

Figure 2.10: UV-Vis spectra of **2.17** (25 mg/L) in $CHCl_3$ (black), **2.17** in $CHCl_3$ after vigorous shaking with deionized (DI) water (red), and **2.17** in $CHCl_3$ after shaking with aqueous $TBAH_2PO_4$ solution (green).

Figure 2.10 shows the UV-Vis spectra of **2.17** in $CHCl_3$ before exposing to water, after shaking with water, and after shaking with aqueous $TBAH_2PO_4$ solution. The major spectral change was the change observed in the relative intensity of the two maxima of the co-polymer **2.17** after contacting with water, independent of the $H_2PO_4^-$ content.

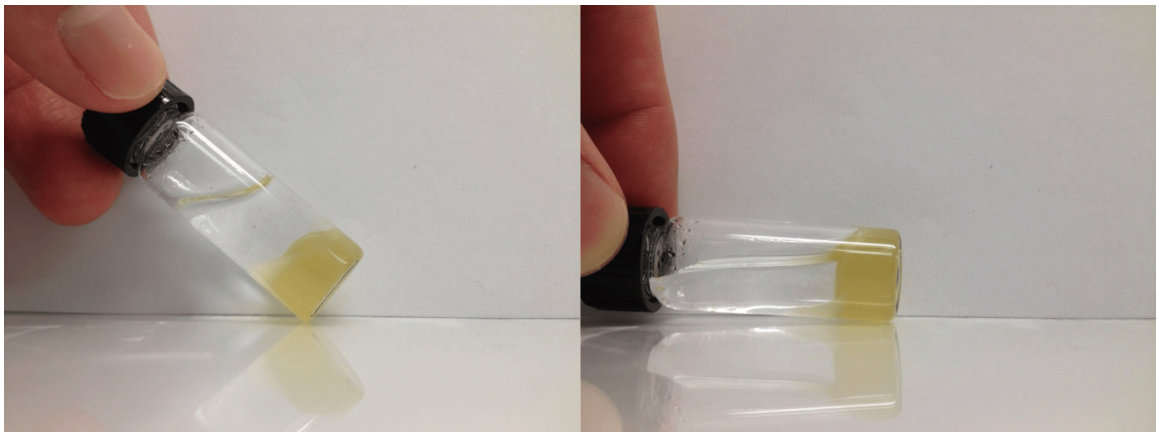

Figure 2.11: Photos of gel formed during the extraction study with the co-polymer **2.17**. Bottom layer was initially a solution of the co-polymer **2.17** in $CHCl_3$ and top layer is aqueous solution.

During the liquid-liquid extraction study conducted with **2.17**, gelation behavior regardless of the content of the aqueous solutions was observed. On the basis of this observedgelation behavior and the UV-Vis spectral changes seen when **2.17** in $CHCl_3$ is brought into contact with water, we propose that this polymeric material can absorb water. Removing water from the aqueous phase under conditions of liquid-liquid would serve to increase the effective $TBAH_2PO_4$ concentration in that source phase, thus accounting for the results in Table 2.2.

Although gelation behavior is not observed in solid-liquid extractions using **2.17** as extractant, these studies served to the same cause, an increase in the effective $TBAH_2PO_4$ concentration in that source phases (D_2O, and CD_3OD)

2.4.6. Synthesis of Cross-linked Polymeric Material with Pendent Schiff-base Macrocycles

Since the attachment of **2.15b** to **2.16** to obtain co-polymer **2.17** using substitution chemistry (*vide supra*) worked well, various other modifications in the phenolic position of **2.15b** were tested. Macrocycle **2.15b** was regioselectively substituted in its phenolic position with a polymerizable styrene unit, a clickable propargyl group, and a cross-linker, epichlorohydrin (EPI), to give **2.15c**, **2.15d**, and **2.15e**, respectively (Scheme 2.6).

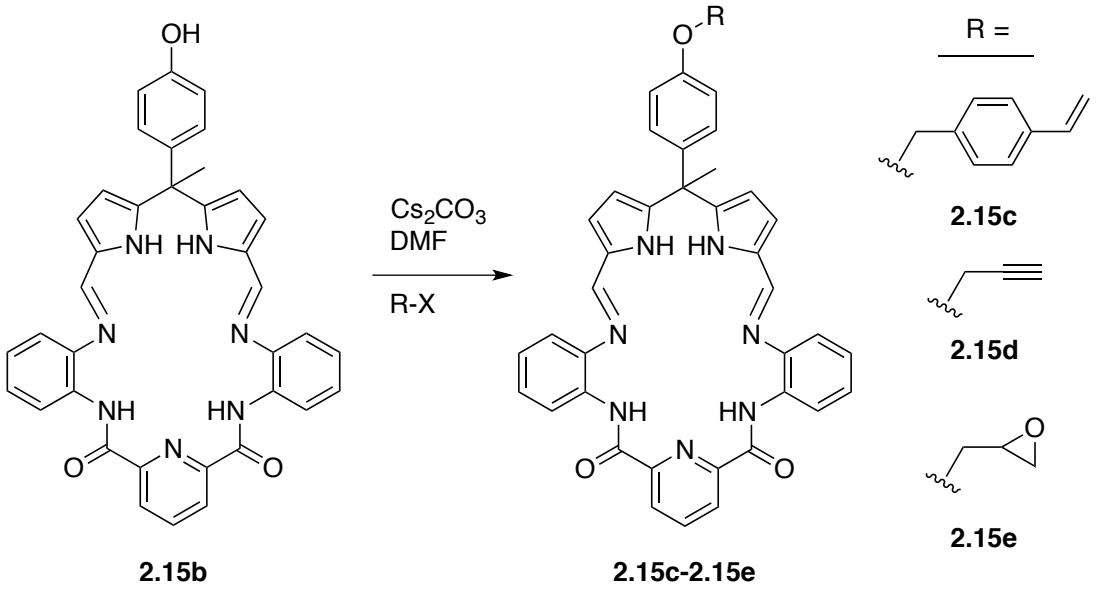

Scheme 2.6: Syntheses of **2.15c**–**2.15e** by nucleophilic substitution.

In order to incorporate the new macrocyclic framework into a cross-linked PAA network, the synthetic route shown in Scheme 2.7 was followed. The control system (**2.21**), an EPI (**2.19**) cross-linked PAA, was prepared along with a pendent Schiff-base containing derivative, **2.22**. Both hydrogels were prepared *via* an aqueous reaction of a 20% w/v solution of linear PAA·HCl chains and EPI, which served as the crosslinking agent.[25] The commercially available PAA·HCl (Alfa Aesar) used in the synthesis of the

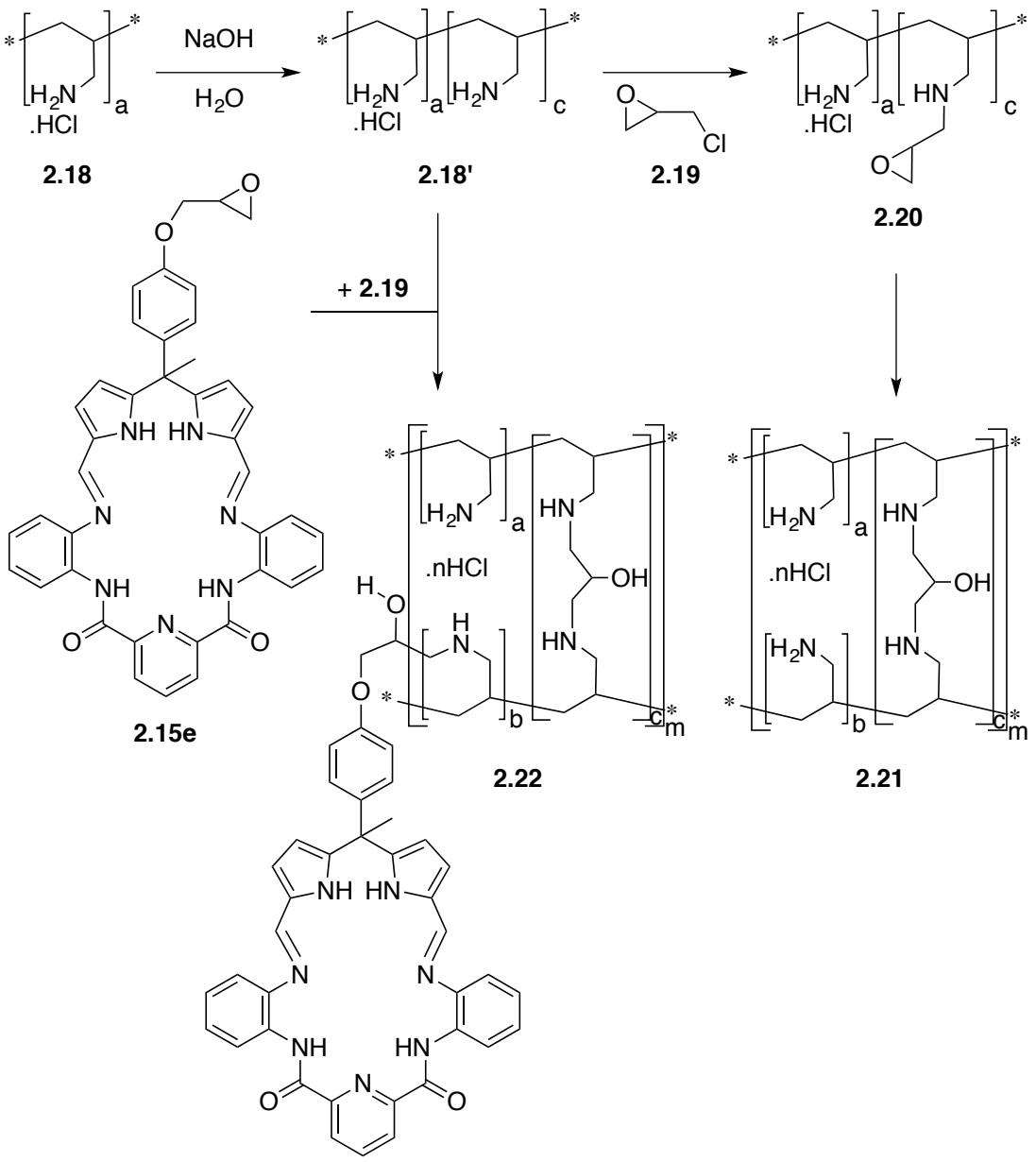

Scheme 2.7: Synthetic route for preparation of a cross-linked polymeric material with pendent Schiff-base macrocycles (**2.22**). Also shown is a synthesis of a control system without the pendants (**2.21**).

gels had molecular weights of 120000-200000 g/mol. Before crosslinking the polymer chains, a fraction of the HCl groups of PAA·HCl was neutralized by adding NaOH

solution. This provides free NH_2 sites for the subsequent EPI cross-linking reaction. For the synthesis of **2.22**, Schiff-base **2.15e** was added along with EPI in the cross-linking step. Two insoluble systems, **2.21** and **2.22**, resulted. Both were tested as possible $H_2PO_4^-$ extractants using a solid-liquid extraction approach.

2.4.7. Extraction Studies with 2.22

Figure 2.12 shows three ^{31}P NMR spectra arising from the solid-liquid extraction

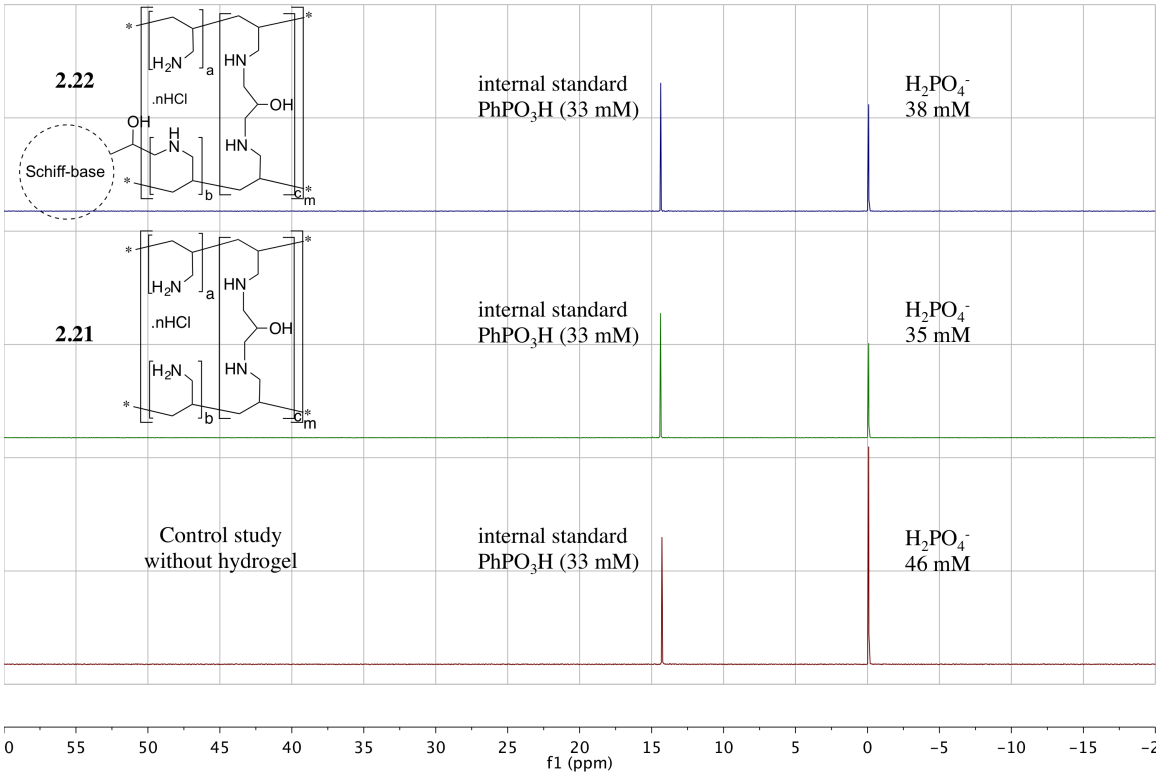

Figure 2.12: Stacked partial ^{31}P NMR spectra (in D_2O) of a stock KH_2PO_4 solution (46 mM) containing phenylphosphonic acid ($PhPO_3H$, 33 mM) as the internal standard (bottom), the stock KH_2PO_4 solution (1.0 mL) after treatment with cross-linked PAA **2.21** (15 mg) containing a $PhPO_3H$ (33 mM) internal standard (middle), and the stock KH_2PO_4 solution (1.0 mL) after treatment with Schiff-base appended cross-linked PAA **2.22** (15 mg) containing a $PhPO_3H$ (33 mM) internal standard (top).

studies in which **2.21** and **2.22** were used in conjunction with KH_2PO_4. The bottom spectrum is of a stock KH_2PO_4 solution (46 mM) in D_2O containing phenylphosphonic acid ($PhPO_3H$, 33 mM) as the internal standard.

The spectrum in the middle is of the KH_2PO_4 (1.0 mL) aliquot after it had been treated with control cross-linked PAA **2.21** (15 mg). A decrease in $H_2PO_4^-$ concentration from 46 mM to 35 mM was observed. The top spectrum is of a separate KH_2PO_4 (1.0 mL) aliquot after having been treated with Schiff-base appended cross-linked PAA **2.22** (15 mg). A decrease in $H_2PO_4^-$ concentration from 46 mM to 38 mM was observed. On this basis, it was concluded that the functionalized solid hydrogel **2.22** (15 mg) was less effective at extracting $H_2PO_4^-$ than the same amount of solid hydrogel **2.21**. This discrepancy can be explained by the increased molecular weight of binding sites in **2.22** due to the presence of heavy Schiff-base units.

2.5. CONCLUSIONS

A new functionalized Schiff-base macrocyclic framework, which relies on a formylated-DPM as a precursor, was prepared. Control compound **2.15a**, bearing this new framework, was studied for its anion binding properties in CH_2Cl_2. It was concluded that **2.15a** displays higher affinity for $H_2PO_4^-$ than it does for HSO_4^- in CH_2Cl_2. In this solvent, the $H_2PO_4^-$ anion is bound with a binding stoichiometry 1:1 (**2.15a**: $H_2PO_4^-$). Covalent attachment of the new framework to a polymeric backbone was achieved using derivative **2.15b**. It was shown that **2.15b** could be attached to many different systems *via* substitutions involving the phenolic position of **2.15b**. In this way, derivatives **2.15c**–**2.15e** were prepared. The co-polymer **2.17**, also obtained *via* a substitution reaction, was studied for its anion binding potential in $CHCl_3$ *via* UV-Vis spectroscopy and for its

extraction ability. Little change in the feature of co-polymer **2.17** was seen in $CHCl_3$ with all anions tested, including the common halides, $H_2PO_4^-$ and HSO_4^- (all as their TBA^+ salts). Under conditions of liquid-liquid extraction, co-polymer **2.17** forms gels, independent of whether an anion is present in the aqueous phase. Extraction studies did not reveal a reduction in the $H_2PO_4^-$ concentration in the aqueous solution when 2.17 was tested as an extractant.

A hydrogel containing pendent Schiff-base macrocycles (**2.22**) was also prepared. In hydrogel **2.22**, pendent Schiff-bases were covalently attached to a PAA backbone by adding a mixture of **2.15e** and EPI during the cross-linking step. Solid-liquid extraction studies revealed that **2.22** is less efficient for KH_2PO_4 extraction than the control hydrogel **2.21**. presumably due to large molecular weight of pendent receptor (Schiff-base, **2.15e**) in **2.22**.

The bottom line for this project is that a tremendous amount of synthetic effort was invested. Unfortunately, although some synthetic challenges were overcome, no improvement over existing systems was achieved. In light of this development, we directed our efforts to understanding the contribution the core DPM subunit to $H_2PO_4^-$ binding. The ensuing Chapters present the results of these efforts.

2.6. EXPERIMENTAL

All solvents and chemicals were purchased from Aldrich, TCI, Acros, or Alfa Aesar unless otherwise noted. Pyrrole was distilled at 80 °C under reduced pressure (100 mbar) prior to use. Other solvents and reagents were used without further purification. The NMR spectra were referenced to residual solvent proton peaks. The NMR solvents were purchased from Cambridge Isotope Laboratories. Chemical ionization (CI) and electrospray ionization

(ESI) mass spectra were recorded on a VG ZAB-2E instrument and a VG AutoSpec apparatus, respectively. Thin-layer chromatography (TLC) analyses were carried out using silica gel (200 mm) glass-backed sheets obtained from Sorbent Technologies. Column chromatography was performed on Sorbent Technologies silica gel 60 O (40–63 mm). For all micro-calorimetric titrations was used a MicroCal VP-ITC instrument.

2.6.1. Synthesis and Characterization

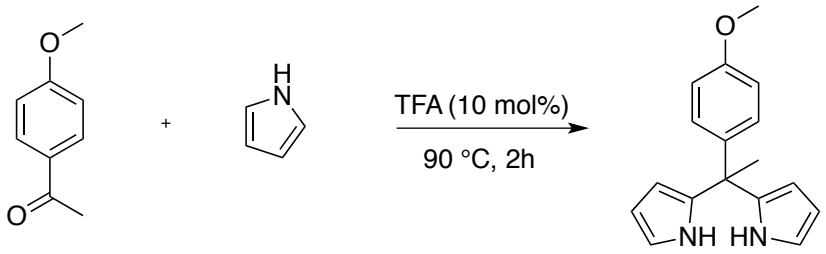

2.7a **1.11** (25 equiv) **2.8a** (44%)

2,2'-(1-(4-Methoxyphenyl)ethane-1,1-diyl)bis(1*H*-pyrrole) (**2.8a**): This intermediate was prepared using a slightly modified procedure first reported by Lindsey *et al*.[26] Briefly, in a 500 mL round bottom flask, 4'-methoxyacetophenone (**2.7a**) (8.0 g, 53.3 mmol, 1 equiv.) was added to freshly distilled pyrrole (100.0 g, 1490.3 mmol, 25 equiv.). TFA (650 mg, 5.7 mmol, 10 mol%) was then added to the reaction mixture. This caused a color change from colorless to pale yellow. The resulting solution was stirred at 90 °C for 2 h. Unreacted pyrrole[‡] and TFA were removed at 80 °C under reduced pressure (100 mbar). The resulting dark green oil was dried *in vacuo* overnight to give a brown solid. This product, **2.8a** (R_f = 0.8[§]), was separated from non-reacted starting material **2.71** (R_f = 0.7) by column chromatography (silica gel, CH_2Cl_2). This gave

[‡] 86 g of pyrrole was recovered.
[§] TLC plates were stained by I_2 to aid visualization.

compound **2.8a** in purified from as a white-solid (6.3 g, 44% yield). ^{1}H NMR (300 MHz, $CDCl_3$) δ 7.76 (bs, 2H, NH), 7.03 (d, 2H), 6.81 (d, 2H), 5.96 (m, 2H), 6.64 (m, 2H), 6.17 (m, 2H, pyrrole CH), 3.78 (s, 3H), 2.02 (s, 3H) ppm. ^{13}C NMR (125 MHz, $CDCl_3$) δ 158.1, 139.4, 137.7, 128.4, 116.8, 113.3, 108.1, 106.1, 55.2, 44.0, 28.9 ppm. HRMS (CI+) *m/z* for $C_{17}H_{18}N_2O$ $[M]^+$ calcd 266.1419, found 266.1418.

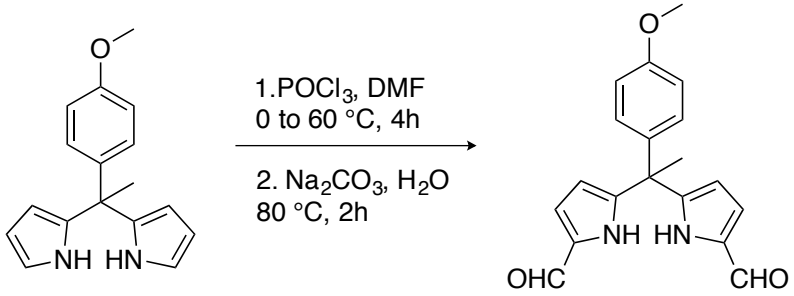

2.8a **2.9a**

5,5'-(1-(4-Methoxyphenyl)ethane-1,1-diyl)bis(1*H*-pyrrole-2-carbaldehyde) (**2.9a**): A slightly modified literature procedure[22] was employed. Briefly, a solution of **2.8a** (6.3 g, 23.7 mmol, 1 equiv.) in DMF (25 ml, 350 mmol, 15 equiv.) was cooled to 0 °C in an external ice bath. To the solution, phosphoryl chloride ($POCl_3$) (21.7 g, 142 mmol, 6 equiv.) was added dropwise *via* an addition funnel. A color change from colorless to orange was observed during the addition. The mixture was stirred at 0 °C for 1 h. The solution was then heated to 60 °C and stirred for 3 h. The solution was allowed to cool to room temperature and then to 0 °C in an ice bath. Aqueous Na_2CO_3 (52 g in 100 ml) was added slowly until a pH of 10 was reached. The solution was then stirred at 80 °C for 2 h. The solution was allowed to cool to room temperature. This gave a mixture containing insoluble solid material. This reaction mixture was extracted with EtOAc. The resulting organic phase was dried over anhydrous sodium sulfate (Na_2SO_4) before being subjected to column chromatography (silica gel, CH_2Cl_2:EtOAc (5:4)). Product **2.9a** (R_f = 0.8) was

obtained as a white solid (6.3 g, 82%) after collecting the appropriate fractions and precipitating by treating with hexanes. ^{1}H NMR (400 MHz, $CDCl_3$) δ 10.46 (bs, 2H), 9.26 (s, 2H), 7.00 (d, 2H), 6.89 (m, 2H), 6.82 (d, 2H), 6.14 (m, 2H), 3.81 (s, 3H), 2.11 (s, 3H) ppm. ^{13}C NMR (125 MHz, $CDCl_3$) δ 178.78, 158.48, 146.50, 136.91, 132.58, 128.20, 121.77, 113.68, 110.29, 55.14, 44.86, 28.50 ppm. FTIR: 3268, 1667, 1651, 1614, 1481, 1434, 1410, 1266, 1216, 1200, 1177, 1045, 1021, 788, 760 cm^{-1}. HRMS (ESI+) *m/z* for $C_{19}H_{18}N_2O_3$ $[M+H]^+$ calcd 323.13170, found 323.13902.

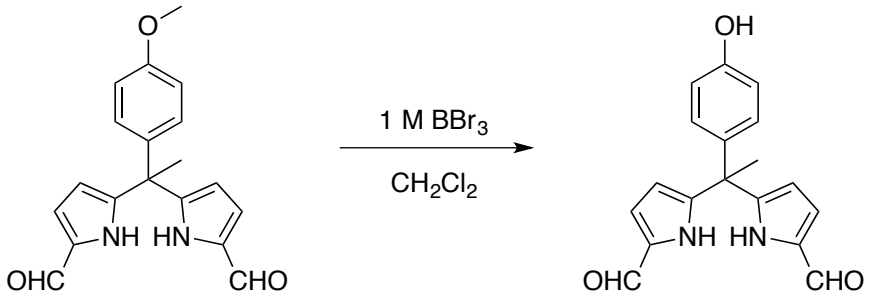

2.9a **2.9b**

In a 500 ml Shlenck flask flushed with argon, formyl-methoxy-dipyrromethaned (1.53 g, 4.75 mmol, 1 equiv.) was dissolved in dry, degassed, CH_2Cl_2 (60 ml). The solution was cooled to 0 °C using an ice bath, and a 1 M boron tribromide (BBr_3) solution in CH_2Cl_2 (2.97 g, 12.0 mmol) was added slowly *via* syringe. The resulting solution was stirred at 0 °C for 2 h. The solution was then warmed to room temperature and stirred for an additional 2 h. The precipitation of an orange solid was observed immediately upon BBr_3 addition. To this mixture, 100 ml of water was added. Stirring was then continued for another 2 h. The mixture was extracted with EtOAc, giving a dark red solution. This red solution was dried over Na_2SO_4 and the volatiles removed by means of a rotary evaporation. The product was purified by column chromatography over silica gel using

a mixture of CH_2Cl_2 and EtOAc (3:1) as the eluent. Due to the poor solubility of the crude, the column was loaded using silica gel, the crude product supported on. The product **2.9b** was isolated as an off-white solid (1.2 g, 82.1%). ^{1}H NMR (400 MHz, 1% CD_3OD in $CDCl_3$) 2.04 (s, 3H, meso-CH_3), 6.12 (m, 2H, pyrrole CH), 6.73 (d, 2H, Ar H), 6.85 (d, 2H, Ar H), 6.90 (m, 2H, Ar H), 9.30 (s, 2H, formyl protons), 10.23 (br s, 2H, pyrrole NH). ^{13}C NMR (100 MHz, CD_3OD) δ 179.54, 156.41, 147.34, 136.43, 133.24, 133.19, 128.37, 115.03, 110.71, 45.15, 27.32 ppm. FTIR: 3284, 3208, 1630, 1482, 1435, 1318, 1295, 1201, 1172, 1052, 785, 771, 698.

Alternatively, **2.9b** could be prepared by the following reaction sequence:

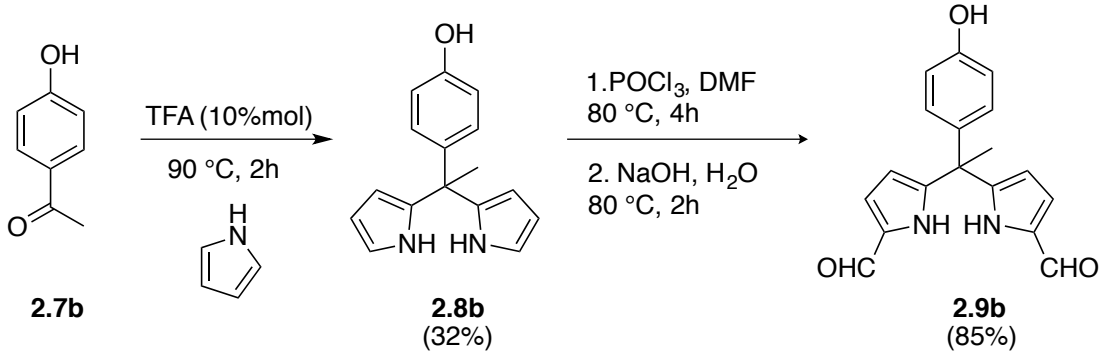

2.7b **2.8b** (32%) **2.9b** (85%)

For the synthesis of **2.8b**, a procedure identical to that used to prepare **2.8a** (*vide supra*) was used, albeit starting with **2.7b**. For the synthesis of **2.9b**, a procedure identical to that used to prepare **2.9a** (*vide supra*) was used, albeit starting with **2.8b**.

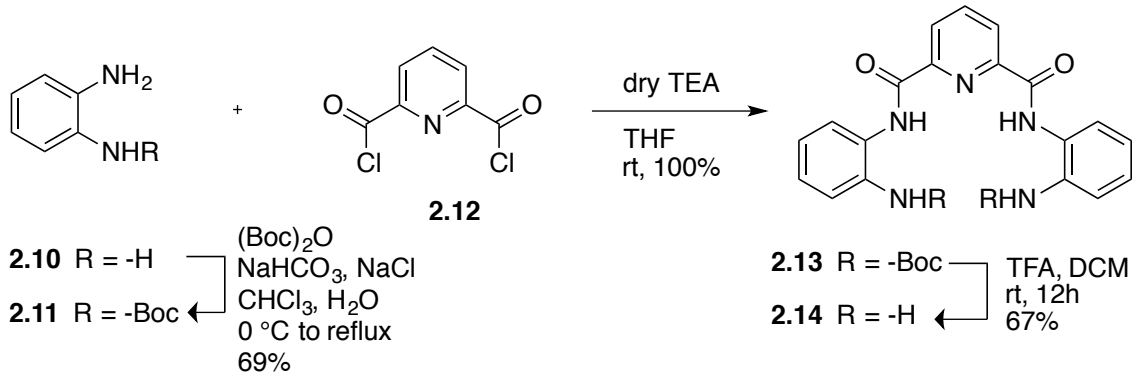

The mono-protected form (**2.11**) of *o*-phenylenediamine (**2.10**) is a known compound.[27] The same procedure used to obtain **2.11**. Briefly, o-phenylenediamine (5 g, 46.3mmol) was dissolved in 200 ml $CHCl_3$. A 100 ml aqueous solution containing 2.33 g of sodium bicarbonate (27.78 mmol) and 2.77 g of sodium chloride (47.4 mmol) was prepared. These solutions were combined in a 500 ml round bottom flask and cooled in an ice-bath. Di-*tert*-butylpyrocarbonate (10.33 g, 47.4 mmol) was dissolved in 100 ml $CHCl_3$ and added slowly to the reaction mixture cooled in an external ice-bath. The resulting mixture was stirred in an ice-bath for 30 minutes. The reaction vessel was first heated to room temperature and then heated at reflux (73.6 ^{0}C) for 12 h. The reaction mixture was left standing and phase separation was observed. The aqueous phase was extracted with $CHCl_3$ (2x 50 ml). Combined organic extracts were dried over anhydrous sodium sulfate. Solvent was removed under reduced pressure. The resulting solids were re-dissolved in a 3:1 mixture of CH_2Cl_2 and EtOAc. The resulting solution was subjected to column chromatography (silica gel) using a 3:1 mixture of CH_2Cl_2 and EtOAc as the eluent. The doubly protected side product elutes first with (R_f = 0.92), followed by mono-protected, desired product (**2.11**) (R_f = 0.8). After removal of the solvent, this desired product was obtained as a white solid (6.64 g, 67%).

Bis(2-aminophenyl)pyridine-2,6-dicarboxamide (**2.13**) was synthesized using the procedure reported by the Sessler group.[24] Compound **2.11** (6.64 g, 32 mmol) was dissolved in 30 ml dry tetrahydrofuran (THF). To this solution, 4.45 ml of dry triethylamine (TEA) was added under Ar. The resulting solution was placed in a water-bath and 2,6-pyridine-dicarboxylic acid chloride (**2.12**) (3.26 g, 16 mmol, 0.5 equiv.) in dry THF (40 ml) was added. The ensuing mixture was stirred for 4 h. It was then filtered to remove insoluble by products. After removal of solvent under reduced pressure, the reaction product was passed through a very short column eluting with CH_2Cl_2. This

procedure was used to remove a material that did not migrate under conditions of TLC analysis.

N^2,N^6-Bis(2-aminophenyl)pyridine-2,6-dicarboxamide (**2.14**): Compound **2.13** (6.37 g, 12 mmol) in CH_2Cl_2 (100 ml) was placed in a water-bath. TFA (19 ml) was added slowly to this solution. The resulting mixture was stirred for 3.5 h. TLC analysis (CH_2Cl_2:EtOAc 3:1) revealed conversion of material that moved at the solvent front spot to one that did not move. To neutralize the TFA, an aqueous solution of NaOH (10.77 g, 300 mL DI water) was added slowly to the reaction mixture with vigorous stirring in an external ice-bath. In order to ensure that all TFA was neutralized, the pH of the aqueous solution checked. The desired pH value of 10 was reached. After separating the phases, organic phase was dried over anhydrous Na_2SO_4. Volatiles were removed and dried *in vacuo* to give yellow crystalline product (**2.14**) (2.7 g, 60%).

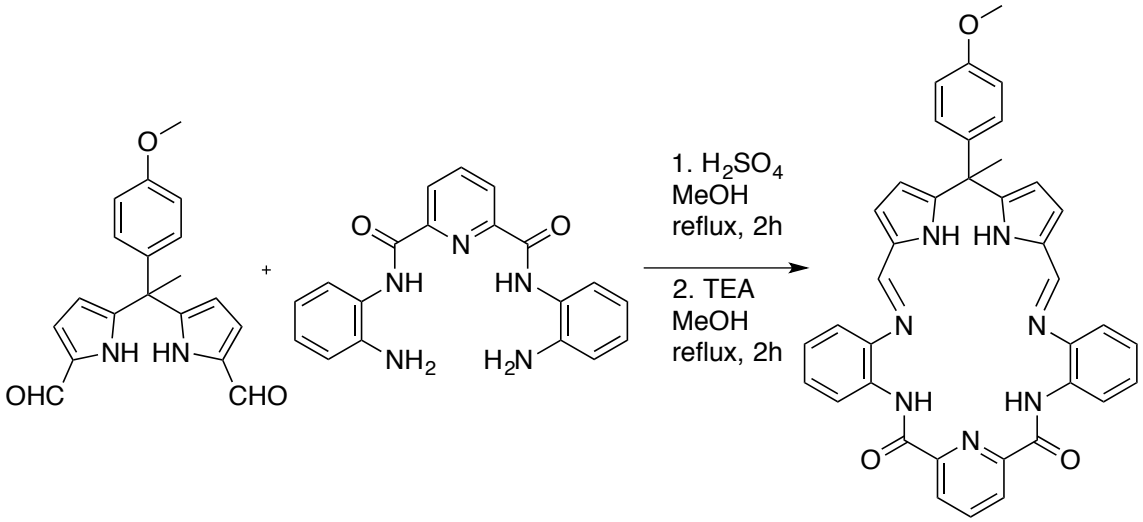

2.9a **2.14** **2.15a** (81%)

(4*E*,13*E*)-2-(4-Methoxyphenyl)-2-methyl-1^1*H*,3^1*H*-5,7,11,13-tetraaza-9(2,6)-pyridina-1,3(2,5)-dipyrrola-6,12(1,2)-dibenzenacyclotetradecaphane-4,13-diene-8,10-

dione (**2.15a**): In a 50 ml round bottom flask, **2.9a** (46.4 mg, 0.144 mmol, 1 equiv.) and **2.14** (50 mg, 0.144 mmol) were dissolved in dry methanol (20 ml). Concentrated H_2SO_4 (16.9 μL, 0.317 mmol, 2.2 equiv.) was then added using a syringe. The resulting solution was heated at reflux under argon for 15 min. The volatiles were removed under reduced pressure. The resulting residue was washed with $CHCl_3$ to give a salt-like orangish-brown solid. This crystalline solid was redissolved in CH_3OH. An excess of TEA (0.1 ml) was added to this solution. The resulting mixture was heated at reflux for 15 min then was cooled to room temperature. The product was collected in the form of a light pink precipitate, which was washed with cold methanol to yield the free-base macrocycle. ^{1}H NMR (500 MHz, CD_2Cl_2) δ ^{1}H NMR (500 MHz, CD_2Cl_2) δ 9.52 (bs, 2H), 8.27 (d, 2H, *J* = 7.8 Hz), 8.23 (s, 2H), 8.02 (t, 1H, *J* = 7.9 Hz), 7.59 (dd, 2H, *J* = 7.8 Hz, *J* = 1.7 Hz), 7.24 (dt, 2H *J* = 7.4 Hz, *J* = 1.6 Hz), 7.20 (dt, 2H, *J* = 7.4 Hz, *J* = 1.6 Hz), 7.11 (dd, 2H, *J* = 7.8 Hz, *J* = 1.7 Hz), 6.82 (d, 2H, *J* = 8.8 Hz), 6.74 (d, 2H, *J* = 3.8 Hz), 6.65 (d, 2H, *J* = 8.8 Hz), 6.33 (d, 2H, *J* = 3.8 Hz), 3.67 (s, 3H), 2.01 (s, 3H) ppm. ^{13}C NMR (126 MHz, CD_2Cl_2) δ 163.95, 159.12, 151.61, 150.41, 146.24, 143.66, 139.44, 138.70, 131.25, 131.03, 128.64, 127.65, 127.23, 126.38, 125.98, 119.61, 119.36, 114.26, 109.71, 55.68, 45.38, 29.51 ppm. HRMS (ESI+) *m/z* for $C_{38}H_{32}N_7O_3$ $[M]^+$ calcd 634.25565, found 634.25611.

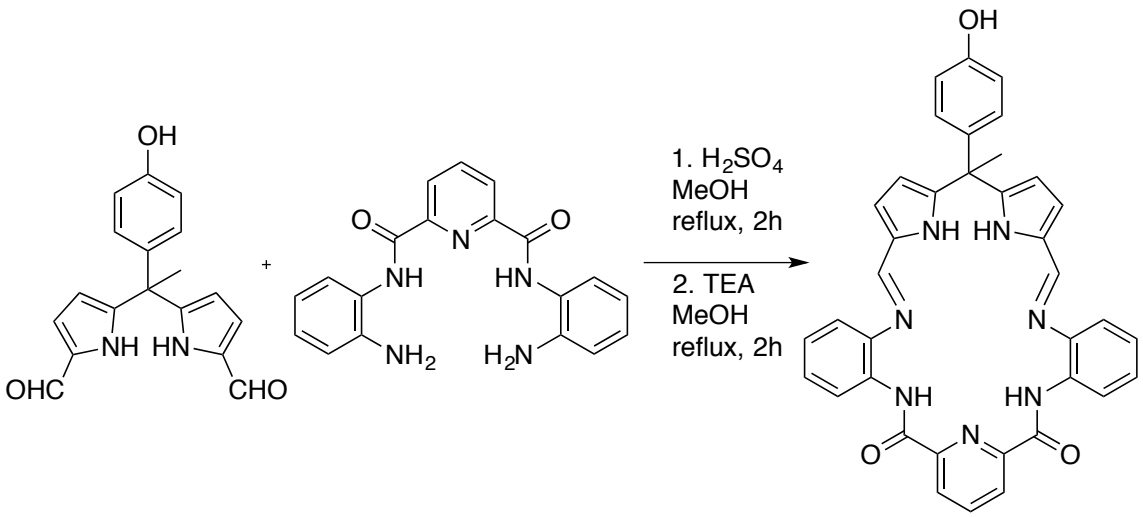

2.9b **2.14** **2.15b** (93%)

(4E,13E)-2-(4-Hydroxyphenyl)-2-methyl-11H,31H-5,7,11,13-tetraaza-9(2,6)-pyridina-1,3(2,5)-dipyrrola-6,12(1,2)-dibenzenacyclotetradecaphane-4,13-diene-8,10-dione (**2.15b**): The procedure reported for the formation of other Schiff-base macrocycles was used, albeit with **2.9b** and **2.14** as the starting materials.[24] In a 100 ml round bottom flask, compound **2.9b** (352 mg, 1.1 mmol) and compound **2.14** (347 mg, 0.98 mmol) were dissolved in distilled methanol (60 ml). H_2SO_4 conc. (115 μL, 2.1 mmol) was then added dropwise using a syringe. The resulting solution was heated at reflux under argon for 15 min. The solution was cooled to room temperature and an excess of TEA was added *via* syringe. The solution was stirred at room temperature for 15 min. The product was collected in the form of a very pale yellow precipitate and washed with cold methanol to yield 490 mg of macrocycle **2.15b** (93% yield). ^{1}H NMR (400 MHz, DMSO-d_6) δ 10.99 (bs, 2H), 10.33 (s, 2H), 9.26 (s, 1H), 8.14–8.16 (m, 3H), 8.05 (s, 2H), 7.35 (d, 2H), 7.26 (t, 2H), 7.16 (t, 2H), 7.04 (d, 2H), 6.57–6.59 (m, 6H), 6.12 (d, 2H), 1.88 (s, 3H) ppm. ^{13}C NMR (150 MHz, DMSO-d_6) δ 163.20, 155.79, 151.53, 149.20, 149.02, 142.83, 139.29, 137.74, 130.66, 129.37, 128.12, 127.62, 127.33, 124.91, 124.44, 119.81, 117.31,

114.73, 108.67, 44.22, 29.65 ppm. HRMS (ESI+) *m/z* for $C_{37}H_{29}N_7O_3$ $[M+H]^+$ calcd 620.24063, found 620.24046.

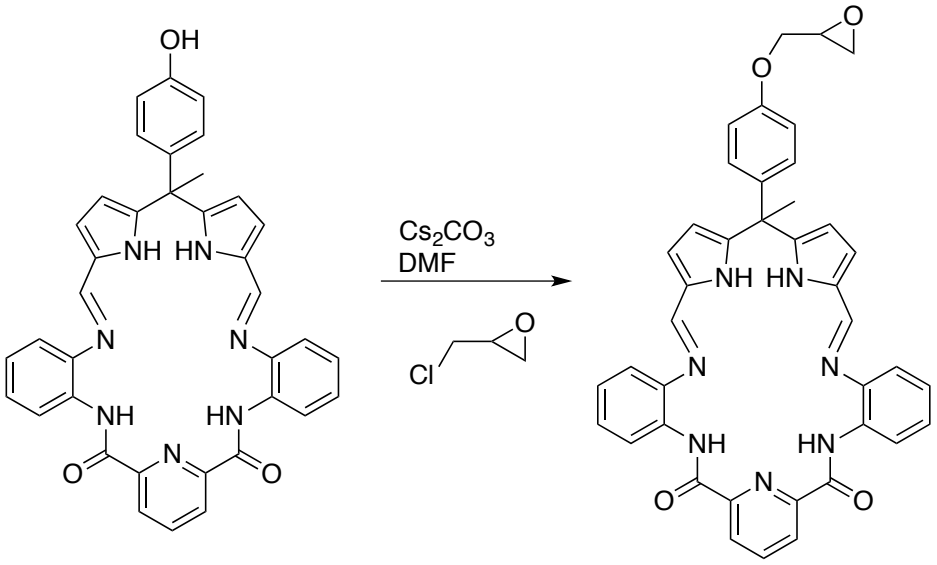

2.15b **2.19** **2.15e**

A similar substitution procedure used to obtain co-polymer **2.17** was used, albeit compounds **2.15b** and **2.19** as starting materials. The product **2.15e** is stable enough to characterize but not to store on bench top. ^{1}H NMR (400 MHz, $CDCl_3$) δ 9.51 (bs, 2H), 8.23 (d, *J* = 7.8 Hz, 2H), 8.19 (s, 2H), 7.91 (t, *J* = 7.8 Hz, 1H), 7.59 (dt, *J* = 7.2 Hz, *J* = 2.0 Hz, 2H), 7.17 (m, 4H), 7.04 (dd, *J* = 7.2 Hz, *J* = 2.0 Hz, 2H), 6.80 (d, *J* = 8.9 Hz, 2H), 6.68 (d, *J* = 3.7 Hz, 2H), 6.63 (d, *J* = 8.8 Hz, 2H), 6.29 (d, *J* = 3.7 Hz, 2H), 4.08 (dd, *J* = 11.0 Hz, *J* = 3.0 Hz, 1H), 3.76 (dd, *J* = 11.0 Hz, *J* = 5.8 Hz, 1H), 3.22 (m, 1H), 2.81 (t, *J* = 4.9 Hz, 1H), 2.64 (dd, *J* = 4.9 Hz, *J* = 2.7 Hz, 1H), 2.0 (s, 3H) ppm. ^{13}C NMR (101 MHz, $CDCl_3$) δ 163.48, 157.22, 150.73, 149.67, 149.65, 142.68, 138.90, 138.62, 130.56, 128.12, 127.05, 126.46, 125.88, 125.59, 125.56, 118.77, 118.63, 114.36, 109.21, 68.67, 50.02, 36.52, 31.25, 29.28 ppm. HRMS (ESI^+) calcd for $C_{40}H_{33}N_7O_4$ $[M+H]^+$ 676.26670, found 676.26750.

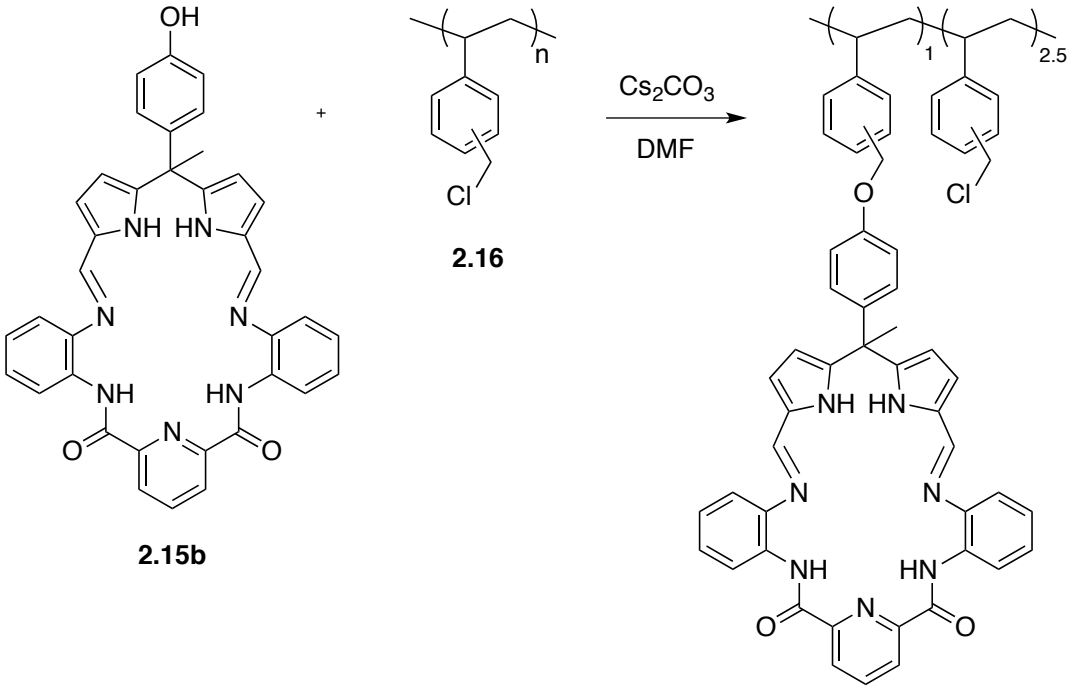

Co-polymer **2.17**: To a solution of **2.15b** (340 mg, 0.55 mmol) in DMF (5 mL), were added Cs_2CO_3 (185 mg, 0.56 mmol) and CsBr (2 mg). The resultant mixture was stirred for 15 minutes at room temperature. A solution of polymer **2.16** (85 mg, 0.55 mmol Cl) was then added. The mixture was heated to 80 °C for 12 h. The reaction mixture was then allowed to cool to room temperature. Before being sparged into CH_3OH, the insoluble were collected by filtration. The filtrate was precipitated in CH_3OH (200 mL). The precipitate that resulted was filtered and dried *in vauo*. The solid obtained was dissolved in CH_2Cl_2 and insoluble inorganics and non-reacted **2.15b** were removed by filtration. CH_2Cl_2 was removed under reduced pressure. Compound **2.17** was solidified with CH_3OH and dried *in vacuo* to give a light yellow powder (210 mg).

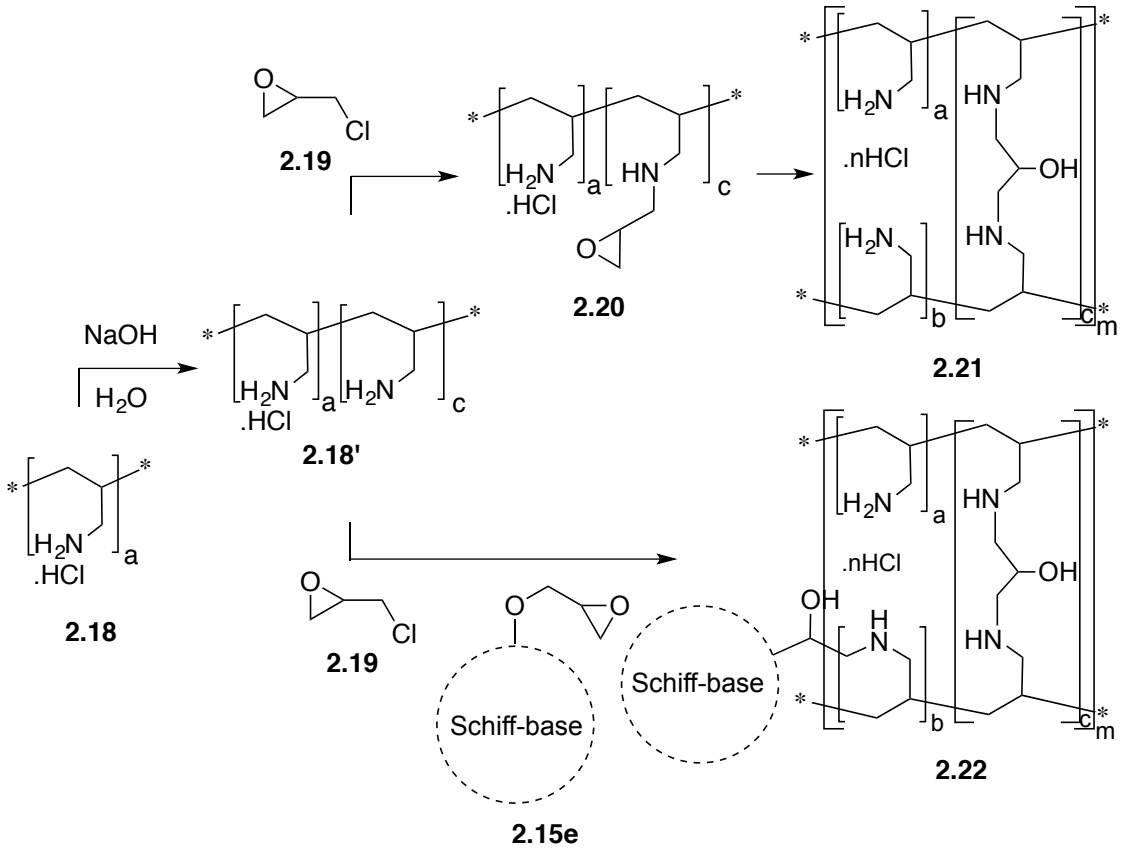

Randomly cross-linked PAA·HCl (**2.21**) and the randomly cross-linked PAA·HCl derivative with Schiff-base pendants (**2.22**) were prepared as follows: A 20% w/v solution of PAA·HCl (160 mg, 0.8 ml) was mixed with a 10 M solution of NaOH (68 mg) until the exotherm subsided and the reaction vessel cooled down to room temperature. This mixture was split into two equal parts. To one, the cross-linker (EPI, **2.19**) (40 mg) was added. To the other one, precursor **2.15e** (49 mg) along with EPI (**2.19**) (40 mg) was added. Both mixtures formed gels within an hour. The dried gel slabs were ground into small pieces for use in solid-liquid extraction studies.

2.6.2. UV-Vis Spectroscopic Studies

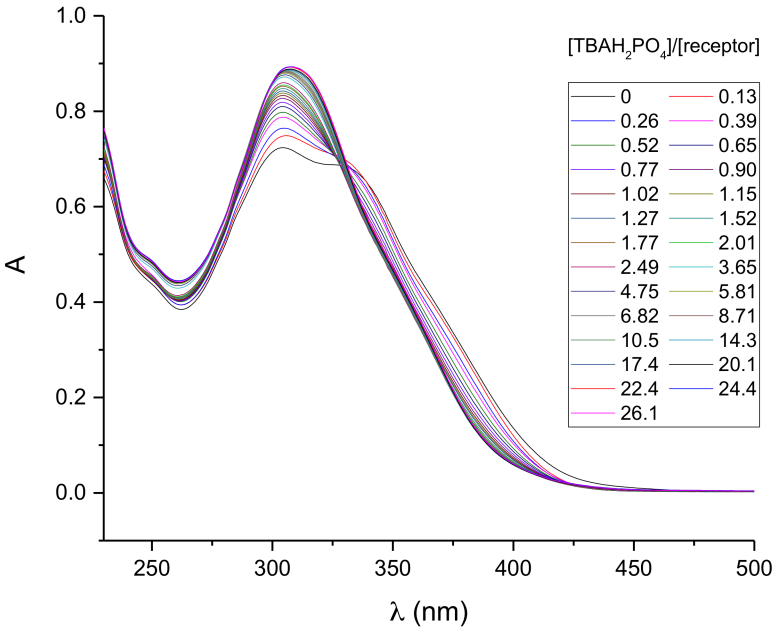

Figure 2.13: Stacked UV-Vis spectra corresponding to the titration of **2.15a** (2.43 x 10^{-5} M) with $TBAH_2PO_4$ (1.27 x 10^{-3} M) in CH_2Cl_2.

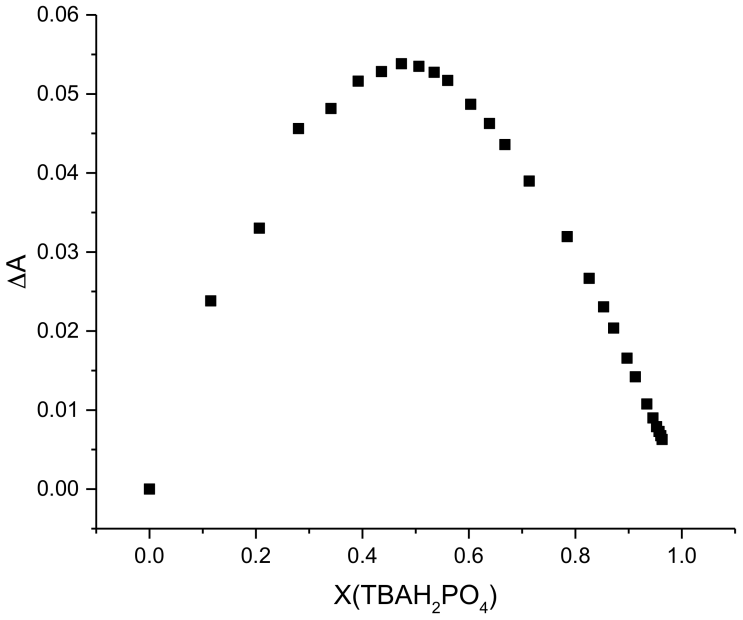

Figure 2.14: Job plot for **2.15a** binding with $TBAH_2PO_4$ derived using the spectra shown in Figure 2.13 at 306.7 nm. The observed maximum near a 0.5 mole fraction supports a value of 1:1 binding stoichiometry.

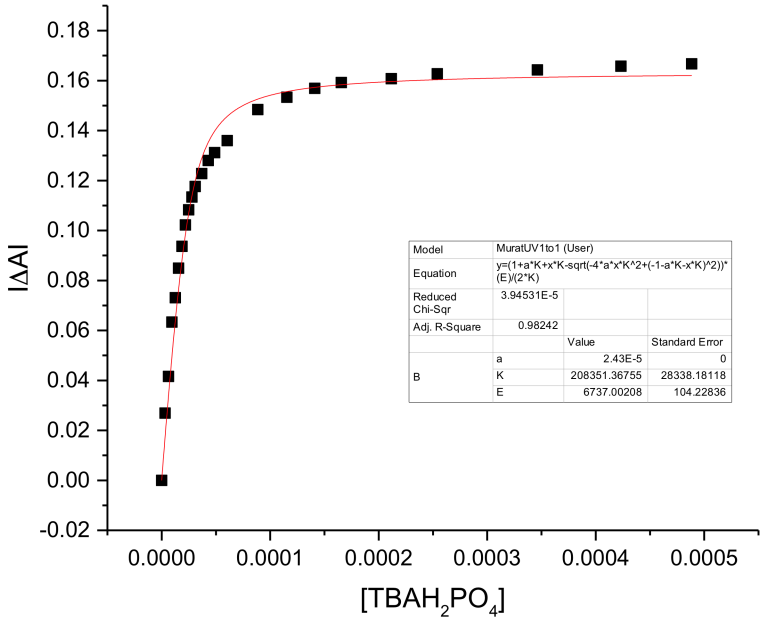

Figure 2.15: Binding curve and 1:1 fit generated from the titration data shown in Figure 2.13 using the spectral changes at 306.7 nm. $K_a = (2.1 \pm 0.3) \times 10^5\ M^{-1}$.

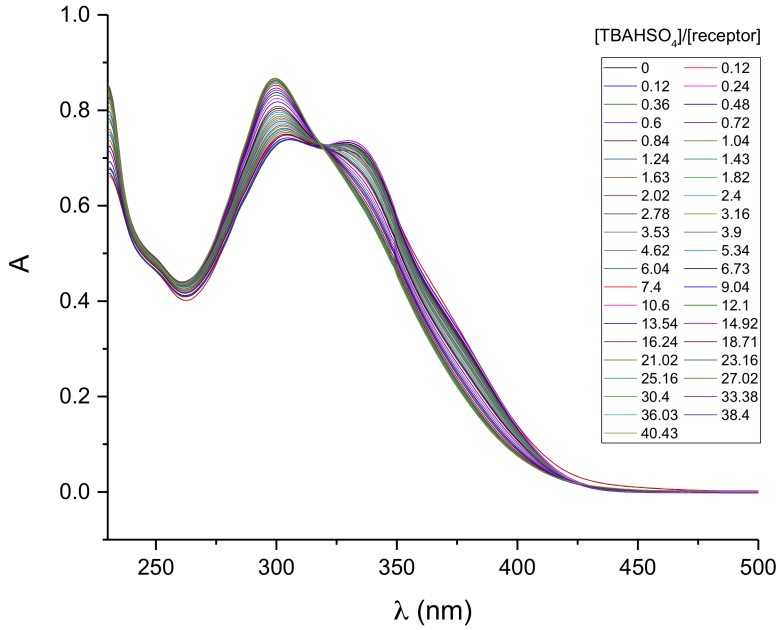

Figure 2.16: Stacked UV-Vis spectra corresponding to the titration of **2.15a** (2.43×10^{-5} M) with $TBAHSO_4$ (1.97×10^{-3} M) in CH_2Cl_2.

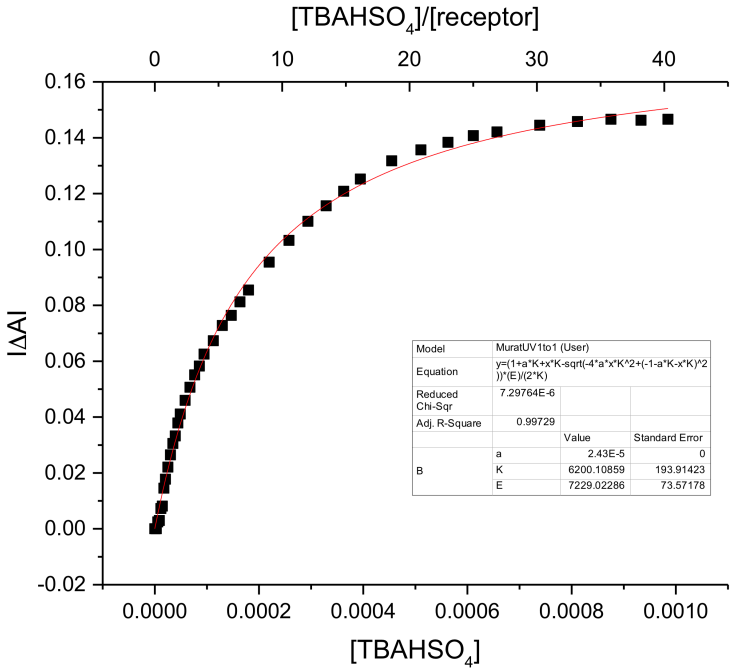

Figure 2.17: Binding curve and 1:1 fit generated from the titration data shown in Figure 2.16 using the spectral changes at 300 nm. $K_a = (1.2 \pm 0.2) \times 10^4\ M^{-1}$.

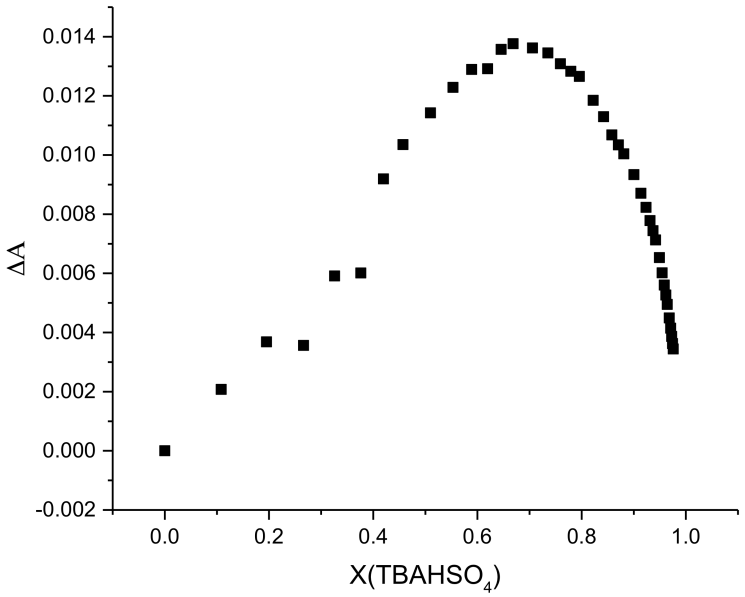

Figure 2.18: Job plot for **2.15a** binding with $TBAHSO_4$ derived from the spectral data shown in Figure 2.16 at 300 nm. The maximum at a mole fraction of about 0.67 is consistent with a 1:2 (**2.15a**:$TBAHSO_4$) binding stoichiometry.

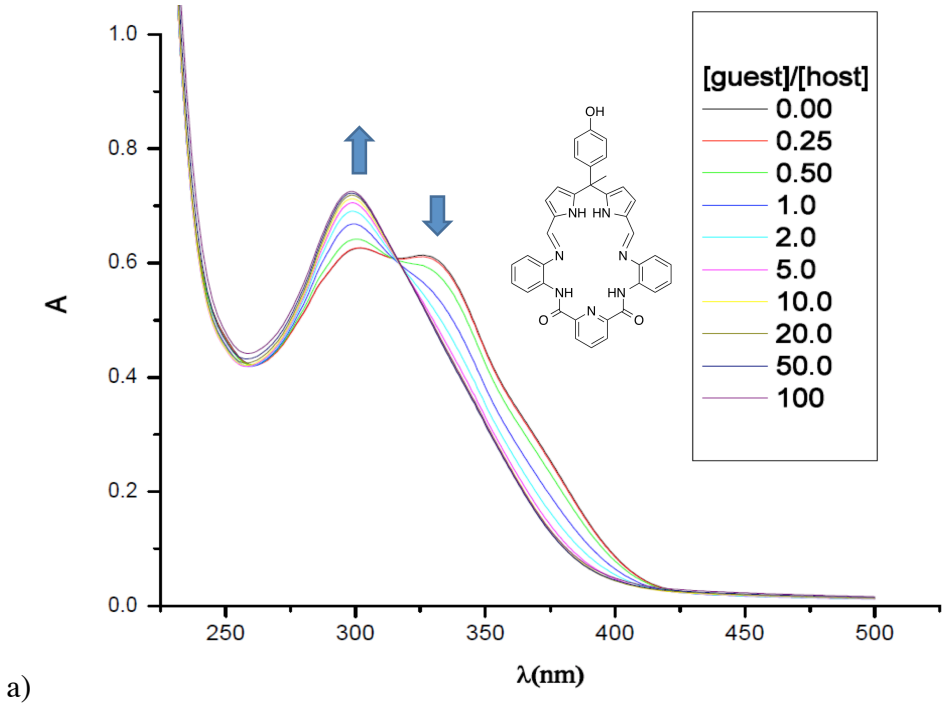

a)

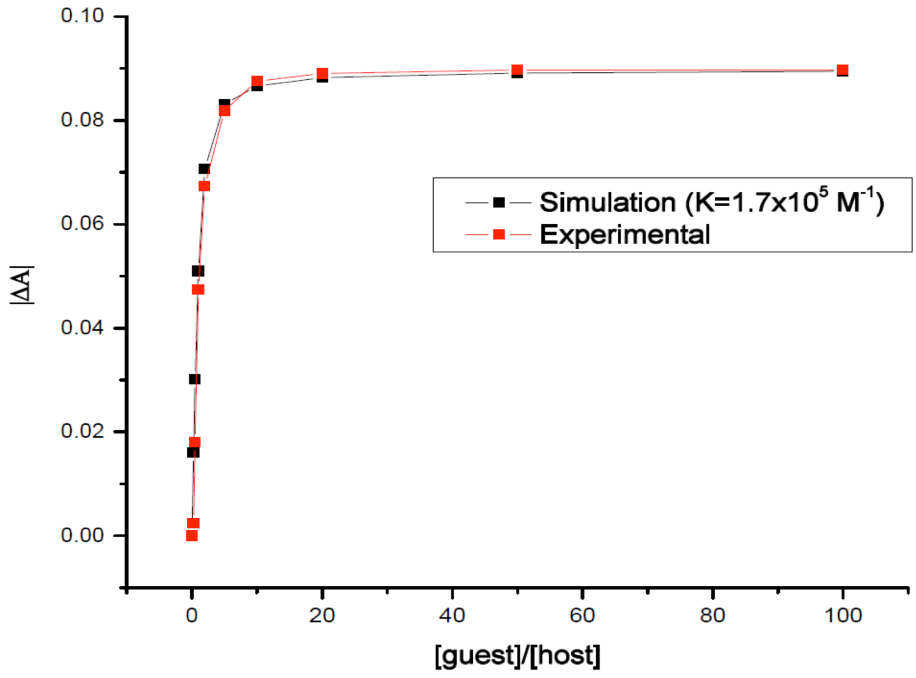

b)

Figure 2.19: a) Stacked UV-Vis spectra for the titration of **2.15b** (1.8 x10^{-5} M) with $TBAH_2PO_4$ in CH_3CN. Binding curve derived from the spectral changes observed in (a) at 326 nm. b) Also shown is a 1:1 (**2.15b**: $TBAH_2PO_4$) simulation with association constant K_a = 1.7 x 10^5 M^{-1}.

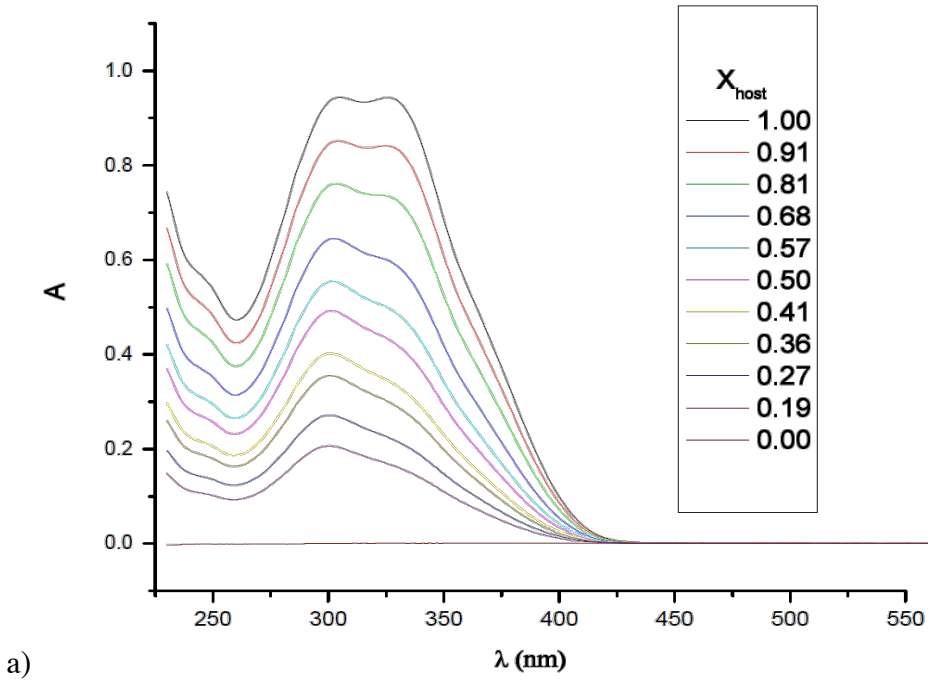

a)

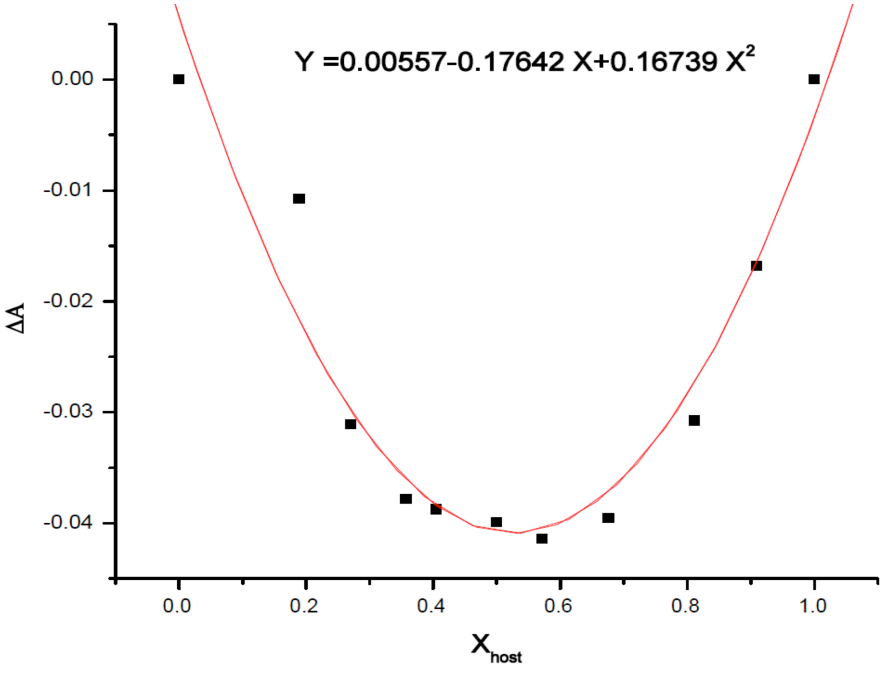

b)

Figure 2.20: a) Stacked UV-Vis spectra corresponding to Job plot of **2.15b** with $TBAH_2PO_4$ in CH_3CN. The d ecrease in absorbance at 326 nm is plotted against [**2.15b**]+[$TBAH_2PO_4$] = 2.28 x 10^{-5} M at each point and X_{host} = [**2.15b**]/([**2.15b**]+[$TBAH_2PO_4$]). The minimum, dy/dx = 0 was seen when X_{host} = 0.53, as would be expected for 1:1 binding.

2.6.3. Isothermal Titration Calorimetric Studies

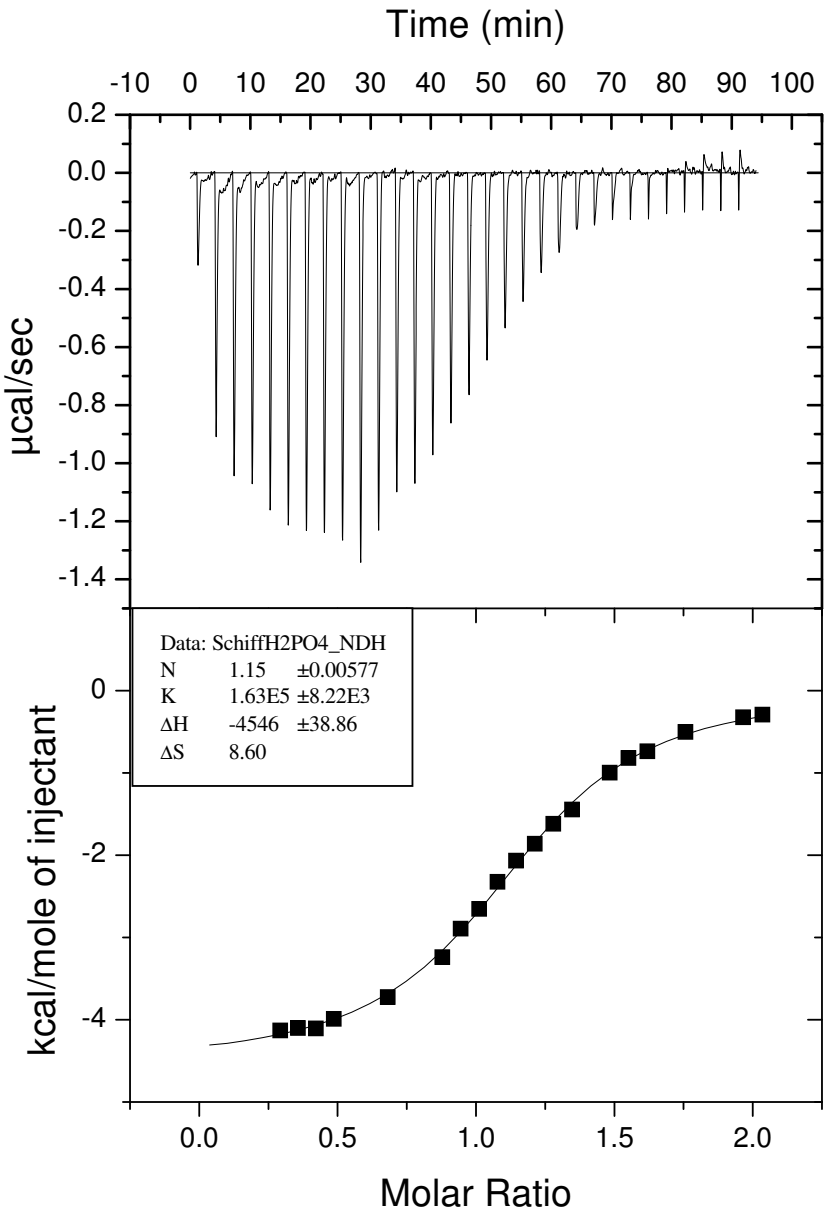

Figure 2.21: ITC titration of **2.15b** (1 x 10^{-4} M) with $TBAH_2PO_4$ (2 x 10^{-3} M) in dry CH_3CN. The calculated binding constant for a 1:1 binding is K_a = (1.63 ± 0.08) x 10^5 M^{-1}.

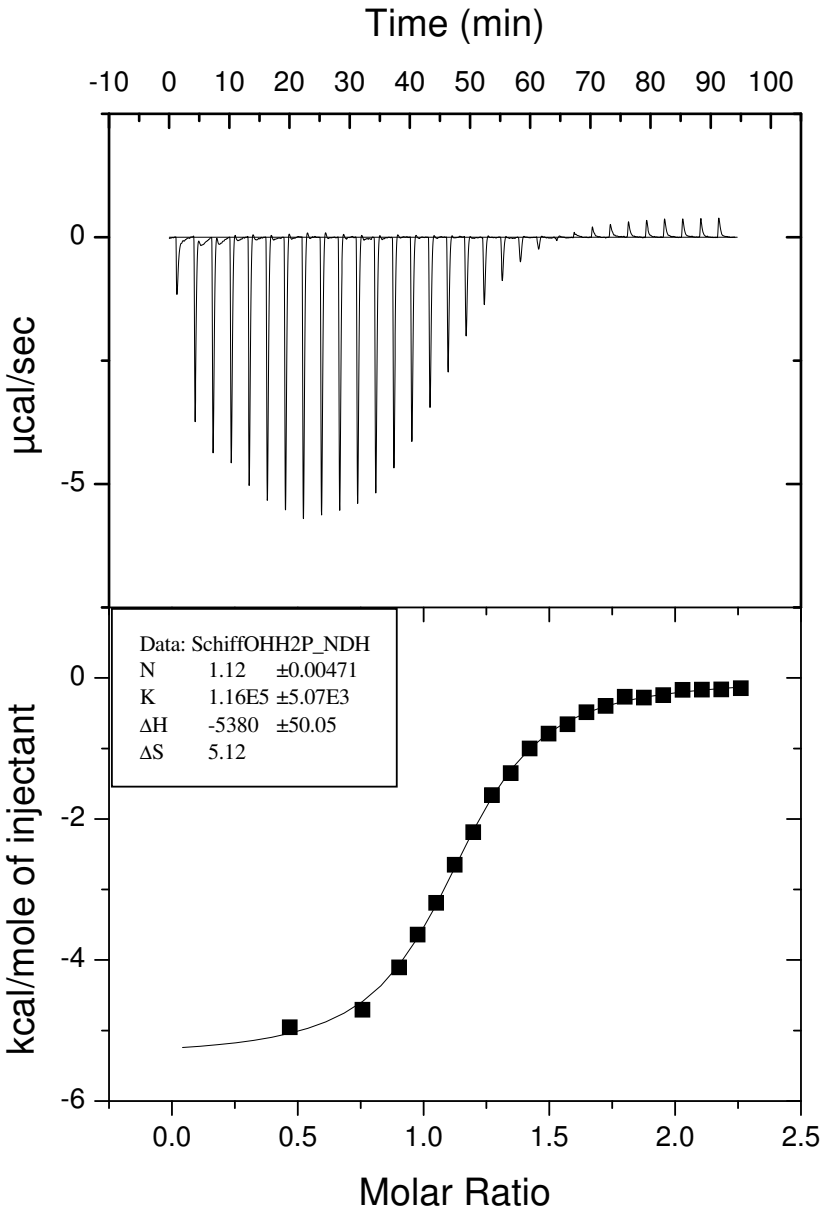

Figure 2.22: ITC titration of **2.15b** (3 x 10^{-4} M) with $TBAH_2PO_4$ (6 x 10^{-3} M) in dry CH_3CN. The calculated binding constant for a 1:1 binding is K_a = (1.16 ± 0.05) x 10^5 M^{-1}.

2.7. REFERENCES

1. Sessler, J. L.; Gale, P. A.; Cho, W.-S. *Anion Receptor Chemistry*; The Royal Society of Chemistry: Cambridge, U.K., 2006.
2. Steed, J. W.; Turner, D. R.; Wallace, K. *Core Concepts in Supramolecular Chemistry and Nanochemistry*; Wiley, Hoboken, NJ, 2007.
3. Rashin, A. a.; Honig, B. Reevaluation of the Born Model of Ion Hydration. *J. Phys. Chem.* **1985**, *89* (26), 5588–5593.
4. Sessler, J. L.; Cyr, M. J.; Lynch, V.; McGhee, E.; Ibers, J. A. Synthetic and Structural Studies of Sapphyrin, a 22-π-Electron Pentapyrrolic "Expanded Porphyrin." *J. Am. Chem. Soc.* **1990**, *112* (7), 2810–2813.
5. Katayev, E. A.; Boev, N. V.; Khrustalev, V. N.; Ustynyuk, Y. A.; Tananaev, I. G.; Sessler, J. L. Bipyrrole- and Dipyrromethane-Based Amido-Imine Hybrid Macrocycles. New Receptors for Oxoanions. *J. Org. Chem.* **2007**, *72* (8), 2886–2896.
6. Seidel, D.; Lynch, V.; Sessler, J. L. Cyclo[8]pyrrole: A Simple-to-Make Expanded Porphyrin with No Meso Bridges. *Angew. Chem. Int. Ed.* **2002**, *41* (8), 1422–1425.
7. Jeffrey, G. A. *An Introduction to Hydrogen Bonding (Topics in Physical Chemistry)*, Oxford University Press, 1997.
8. Camiolo, S.; Gale, P. A.; Hursthouse, M. B.; Light, M. E.; Shi, A. J. Solution and Solid-State Studies of 3,4-Dichloro-2,5-Diamidopyrroles: Formation of an Unusual Anionic Narcissistic Dimer. *Chem. Commun.* **2002**, *3* (7), 758–759.
9. Marcus, Y. Thermodynamics of Solvation of Ions. *J. Chem. Soc. Faraday Trans.* **1991**, *87* (18), 2995–2999.
10. Schmidtchen, F. P.; Berger, M. Artificial Organic Host Molecules for Anions. *Chem. Rev.* **1997**, *97* (5), 1609–1646.
11. Chiu, C. W.; Gabbaï, F. P. Fluoride Ion Capture from Water with a Cationic Borane. *J. Am. Chem. Soc.* **2006**, *128* (44), 14248–14249.
12. Hirai, M.; Gabbaï, F. P. Squeezing Fluoride out of Water with a Neutral Bidentate Antimony(V) Lewis Acid. *Angew. Chem. Int. Ed.* **2015**, *54* (4), 1205–1209.
13. Wang, Z.; Luecke, H.; Yao, N.; Quiocho, F. A. A Low Energy Short Hydrogen Bond in Very High Resolution Structures of Protein Receptor--Phosphate Complexes. *Nat. Struct. Biol.* **1997**, *4* (7), 519–522.
14. Levin, G. V.; Shapiro, J. Metabolic Uptake of Phosphorus by Wastewater Organisms. *Water Environ. Fed.* **1965**, *37* (6), 800–821.

15. Barnard, J. L. Biological Nutrient Removal without the Addition of Chemicals. *Water Res*. **1975**, *9* (5-6), 485–490.

16. Mino, T.; Van Loosdrecht, M. C. M.; Heijnen, J. J. Microbiology and Biochemistry of the Enhanced Biological Phosphate Removal Process. *Water Res*. **1998**, *32* (11), 3193–3207.

17. Mino, T. Microbial Selection of Polyphosphate-Accumulating Bacteria in Activated Sludge Wastewater Treatment Processes for Enhanced Biological Phosphate Removal. *Biochemistry. (Mosc)*. **2000**, *65* (3), 341–348.

18. Goldsmith, D. R.; Scott, L. J.; Cvetkovi, R. S.; Plosker, G. L.; Bihl, G.; Kidney, W.; West, S.; Africa, S.; Bommer, J. Sevelamer Hydrochloride A Review of Its Use for Hyperphosphataemia in Patients with End-Stage Renal Disease on Haemodialysis. *Drugs* **2008**, *68* (1), 85–104.

19. Ayus, J. C.; Achinger, S. G.; Mizani, M. R.; Chertow, G. M.; Furmaga, W.; Lee, S.; Rodriguez, F. Phosphorus Balance and Mineral Metabolism with 3 H Daily Hemodialysis. *Kidney Int*. **2007**, *71* (4), 336–342.

20. Aydogan, A.; Coady, D. J.; Lynch, V. M.; Akar, A.; Marquez, M.; Bielawski, C. W.; Sessler, J. L. Poly(methyl Methacrylate)s with Pendant Calixpyrroles: Polymeric Extractants for Halide Anion Salts. *Chem. Commun*. **2008**, (12), 1455–1457.

21. Aydogan, A.; Coady, D. J.; Kim, S. K.; Akar, A.; Bielawski, C. W.; Marquez, M.; Sessler, J. L. Poly(methyl Methacrylate)s with Pendant Calixpyrroles and Crown Ethers: Polymeric Extractants for Potassium Halides. *Angew. Chem. Int. Ed*. **2008**, *47* (50), 9648–9652.

22. Sessler, J. L.; Katayev, E.; Pantos, G. D.; Ustynyuk, Y. A. Synthesis and Study of a New Diamidodipyrromethane Macrocycle. An Anion Receptor with a High Sulfate-to-Nitrate Binding Selectivity. *Chem. Commun*. **2004**, 11, 1276–1277.

23. Lee, C. H.; Na, H. K.; Yoon, D. W.; Won, D. H.; Cho, W. S.; Lynch, V. M.; Shevchuk, S. V.; Sessler, J. L. Single Side Strapping: A New Approach to Fine Tuning the Anion Recognition Properties of calix[4]pyrroles. *J. Am. Chem. Soc*. **2003**, *125* (24), 7301–7306.

24. Sessler, J. L.; Katayev, E.; Dan Pantos, G.; Scherbakov, P.; Reshetova, M. D.; Khrustalev, V. N.; Lynch, V. M.; Ustynyuk, Y. A. Fine Tuning the Anion Binding Properties of 2,6-Diamidopyridine Dipyrromethane Hybrid Macrocycles. *J. Am. Chem. Soc*. **2005**, *127* (32), 11442–11446.

25. Kioussis, D. R.; Smith, D. F.; Kofinas, P. Ammonium Perchlorate-Binding Poly(allylamine Hydrochloride) Hydrogels for Wastewater Remediation. *J. Appl. Polym. Sci*. **2001**, *80* (11), 2073–2083.

26. Lee, C.-H.; S. Lindsey, J. One-Flask Synthesis of Meso-Substituted Dipyrromethanes and Their Application in the Synthesis of Trans-Substituted Porphyrin Building Blocks. *Tetrahedron* **1994**, *50* (39), 11427–11440.

27. Varghese, S.; Senanayake, T.; Murray-Stewart, T.; Doering, K.; Fraser, A.; Casero, R. A.; Woster, P. M. Polyaminohydroxamic Acids and Polyaminobenzamides as Isoform Selective Histone Deacetylase Inhibitors. *J. Med. Chem.* **2008**, *51* (8), 2447–2456.

3. Formylated Bisdipyrromethane Receptors

Reproduced in part from:

Deliomeroglu, M. K.; Lynch, V. M.; Sessler, J. L.

Conformationally switchable non-cyclic tetrapyrrole receptors: Synthesis of tetrakis(1*H*-pyrrole-2-carbaldehyde) derivatives and their anion binding properties

Chemical Communications, **2014**, *50* (80), 11863–11866

3.1. Dipyrromethane-based Receptors

Calix[4]pyrrole (C[4]P) is a non-conjugated macrocyclic system. It was first synthesized by Baeyer in 1886.[1] C[4]P consists of four pyrrole rings and four sp^3 hybridized *meso*-carbon atoms in an alternating pattern. In 1996, Gale *et al*. reported[2] anion binding studies of two C[4]P derivatives, namely octamethylcalix[4]pyrrole (**1.10**) and tetraspirocyclohexylcalix[4]pyrrole (**1.10'**), as mentioned in Chapter 1.

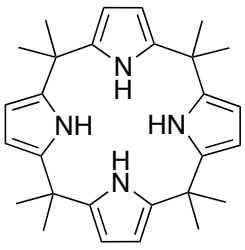

1.10

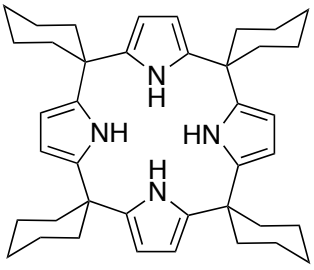

1.10'

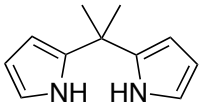

3.1

These two systems (**1.10** and **1.10'**) were found to bind the F^- and Cl^- anions well in halogenated solvents (*e.g.*, CH_2Cl_2), along with their counter cations in certain instances.[3,4] However, they did not bind the $H_2PO_4^-$ anion well.[2] The main research goal

underlying this Chapter was to test acyclic bisdipyrromethane (bisDPM)-based C[4]P analogues for $H_2PO_4^-$ anion recognition.

In C[4]P, halide anion binding induces conformational change from a limiting 1,3-alternate conformation (the free form) to a cone conformation (halide-bonded form) (*cf*. Figure 1.3). This structural switching allows the formation of four NH—anion hydrogen bonds in the case of F^-.[2] Under most analytical conditions (*e.g*., ^1H NMR spectroscopy, isothermal titration calorimetry, etc.), C[4]P proved less effective as a receptor for larger anions, including the $H_2PO_4^-$.[2]

With a given C[4]P system, each *meso*-carbon with two neighboring pyrrole rings can be considered as a dipyrromethane (DPM) subunit. The simplest DPM building block of C[4]P **1.10** is 2,2'-(propane-2,2-diyl)bis(1*H*-pyrrole), **3.1** (*vide supra*). This acyclic structure was not an effective halide ion receptor according to Cho *et al*..[5] In the case of F^- and Cl^- anion salts studied in CD_2Cl_2, compound **1.10** displayed association constants that were >2x greater than those recorded for the corresponding acyclic building block, dipyrromethane (DPM) **3.1** (*cf*. Table 3.1).

	Anions[a]					
Receptor	F^- [b]	Cl^-	Br^-	I^-	$H_2PO_4^-$	HSO_4^-
1.10[2]	1.7×10^4	3.5×10^2	1.0×10^1	$< 10^1$	9.7×10^1	$< 10^1$
3.1[5]	2.1×10^3	1.1×10^2	1.9×10^1	$< 10^1$	3.1×10^3	$< 10^1$

[a] All salts were used as TBA^+ salts. [b] TBAF was used as commercially available trihydrate.

Table 3.1: Association constants of **1.10** and **3.1** with selected anions in CD_2Cl_2 at 298 K.[2,5]

This difference in association constants was ascribed to the greater pre-organization of the cyclic system, as well as to the increased number of pyrrolic NH hydrogen bond donors provided by **1.10** compared to **3.1**. On the other hand, compound **3.1** displayed a higher affinity toward $H_2PO_4^-$ (as its tetra-*n*-butylammonium (TBA^+) salt) than did **1.10** in CD_2Cl_2. While this apparent difference was not studied in detail, it might reflect the fact that the $H_2PO_4^-$ anion is too large to be hosted efficiently within the NH-rich C[4]P pseudo cavity. In contrast, the presumably greater flexibility of **3.1** might allow it to form more favorable interactions with $H_2PO_4^-$ and other oxoanions as compared to **1.10**.[5] While untested, this hypothesis provides an incentive to create and study new DPM-based anion receptors. A goal of this effort would be to create improved phosphate anion receptors that are also easier to prepare than C[4]P. In this chapter we focus on DPM receptors that have been formylated in their so-called α-pyrrolic positions.

In synthetic work reported in 2003, aimed at producing a C[4]P-texaphyrin chimera,[6] the α-pyrrolic positions of **3.1** were subjected to formylation to obtain diformyl-DPM **3.2** (Figure 3.1). The anion binding properties of **3.2** with TBAF were studied by ITC in CH_3CN and *via* X-ray crystallography in the solid state.[7] Despite the observation that F^- anion may be bound in the solid state, as inferred from an unpublished[**] crystal structure (*cf*. Figure 3.1), it was concluded that **3.2** was not an effective anion receptor.

[**] Unpublished result from Dr. Michael Huggins' post-doctoral study at the University of Texas at Austin (2007).

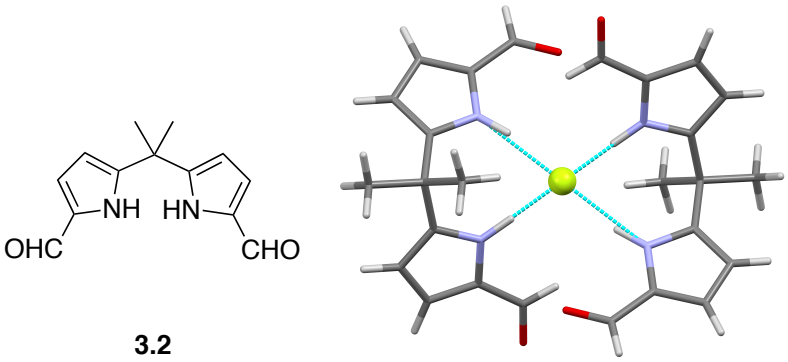

3.2

Figure 3.1: Left: Structure of diformyl-DPM (**3.2**) and Right: Single crystal structure of the 2:1 $(\mathbf{3.2})_2$·TBAF complex. The TBA^+ counter cation is omitted for clarity. This structure was not reported but redrawn using data from the CCDC (CCDC number 186152).

On the other hand, we have found[8] that the bisdipyrromethane (bisDPM) structures (**3.3a**–**3.5a**) and their formylated derivatives (**3.3b**–**3.5b**) are effective and somewhat selective receptors for the TBA^+ salts of $H_2PO_4^-$ and hydrogenpyrophosphate ($HP_2O_7^{3-}$) in $CHCl_3$, as inferred from NMR and UV-Vis spectroscopic and X-ray diffraction analyses. The syntheses, structural characterization, and anion binding properties of a series of tetrakis(1*H*-pyrrole-2-carbaldehyde) receptors, consisting of **3.3b**–**3.5b**, are discussed in this Chapter.

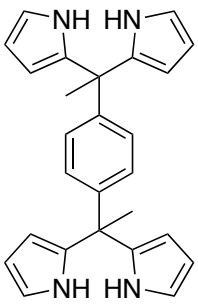

3.3a

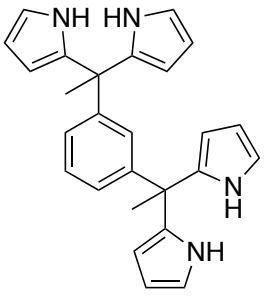

3.4a

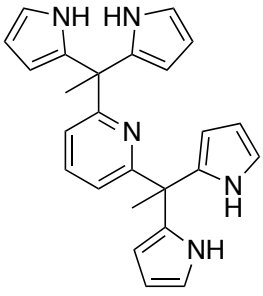

3.5a

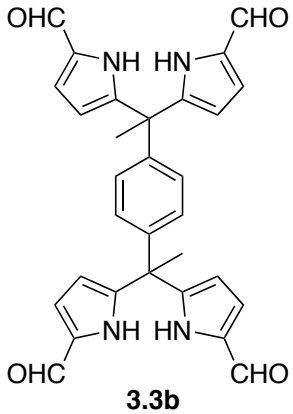

3.3b

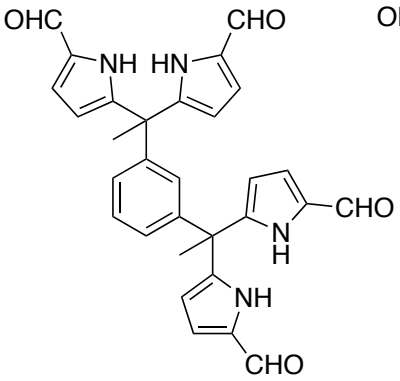

3.4b

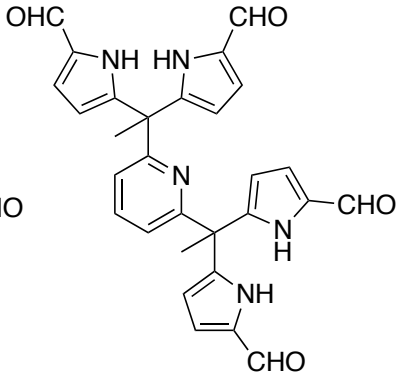

3.5b

3.2. BISDIPYRROMETHANE SYSTEMS IN THE LITERATURE

In the previous section, the goal of using DPM-based systems as $H_2PO_4^-$ anion receptors was highlighted. There are several methods reported in the literature for the synthesis of DPMs. Lindsey *et al*., developed[9] the so-called "one-flask" synthetic method for *meso*-substituted DPMs, which he and others appreciated as being key precursors for the syntheses of asymmetric porphyrins and porphyrinogens (*i.e*., C[4]P). The method that was developed for aldehydes was also used for terephthalaldehyde, a dialdehyde, to make the bisDPM **3.6**.[9] Such bisDPM constructs were used as precursors for dimeric porphyrins[10] or internally bridged expanded porphyrin[11] systems.

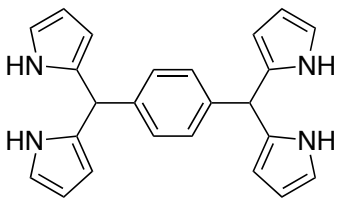

3.6

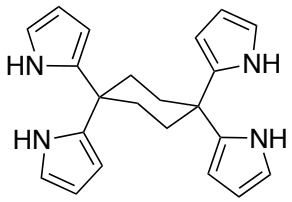

3.7

In another report, a diketone, 1.4-cyclohexadione, was used to obtain the bisDPM derivative (**3.7**) in high yield.[12] Although these two bisDPM structures, **3.6** and **3.7**, were readily obtained from their relative dicarbonyl compounds, Panda and coworkers found[13]

that only one of two adjacent carbonyl groups reacted with pyrrole under similar acid catalyzed conditions (Scheme 3.1).

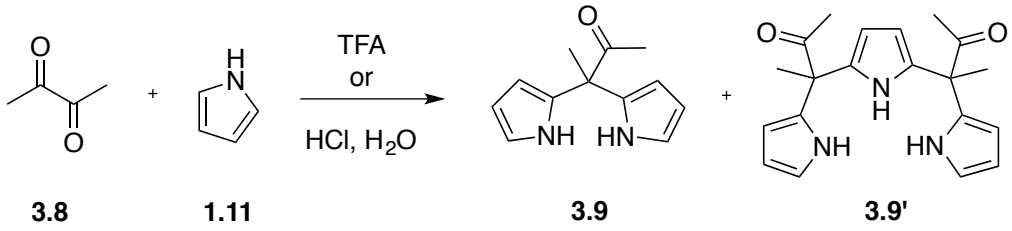

Scheme 3.1: Reaction of an adjacent diketone (**3.8**) with pyrrole (**1.11**).[13]

To investigate a flexible alkyl-chain-linked bisDPM, diketone **3.10** was used as a starting material. Instead of the expected bisDPM structure **3.11**, a ring annulated product 2,3-dihydro-1*H*-pyrrolizine **3.12** was obtained (Scheme 3.2). This result is consistent with what Panda and coworkers reported.[14,15] In addition to **3.12**, various annulation products (**3.12'** and **3.12''**) were detected by ^{1}H NMR and by MS analyses (Scheme 3.2).

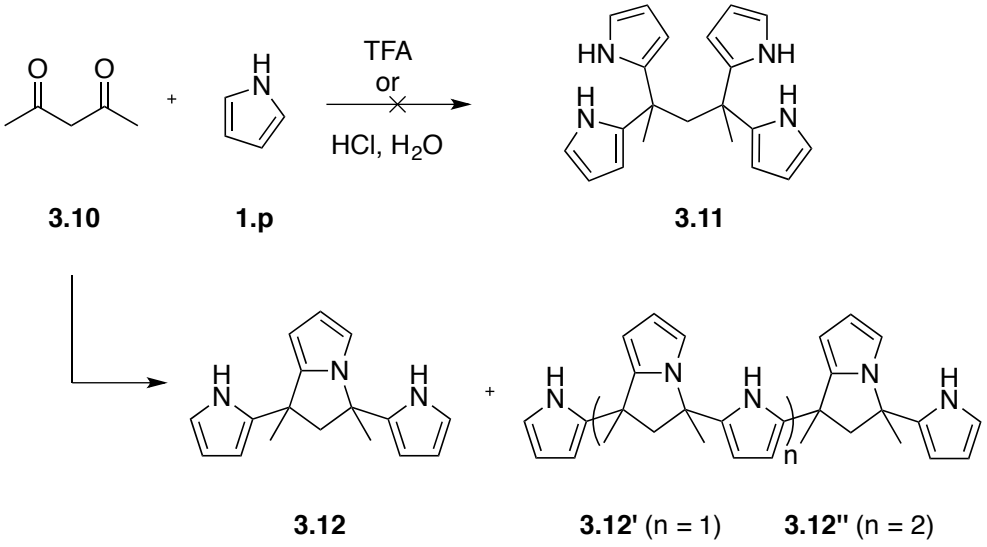

Scheme 3.2: Reaction of 2,4-pentadione (**3.10**) with pyrrole to produce 2,3-dihydro-1*H*-pyrrolizine (**3.12**) and further propagated derivatives (**3.12'** and **3.12''**).

3.3. Results and Discussion

3.3.1. Synthesis and Characterization

Using bisDPM synthetic methods similar to those reported, we prepared a series of new receptors.[8] The first set of these receptors, specifically the tetrakis(1*H*-pyrrole-2-carbaldehyde) compounds **3.3b**, **3.4b**, and **3.5b**, is covered in this Chapter. As detailed below, the precursors to these receptors (**3.3a**, **3.4a**, and **3.5a**) are open-chain analogues of C[4]P in that all three contain four pyrrole rings. They may be prepared in one step from commercially available materials. As detailed below, four-fold formylation of the bisDPM derivatives tunes their electronics and conformation to create systems that display high affinities for the $H_2PO_4^-$ and $HP_2O_7^{3-}$ anions in $CHCl_3$.

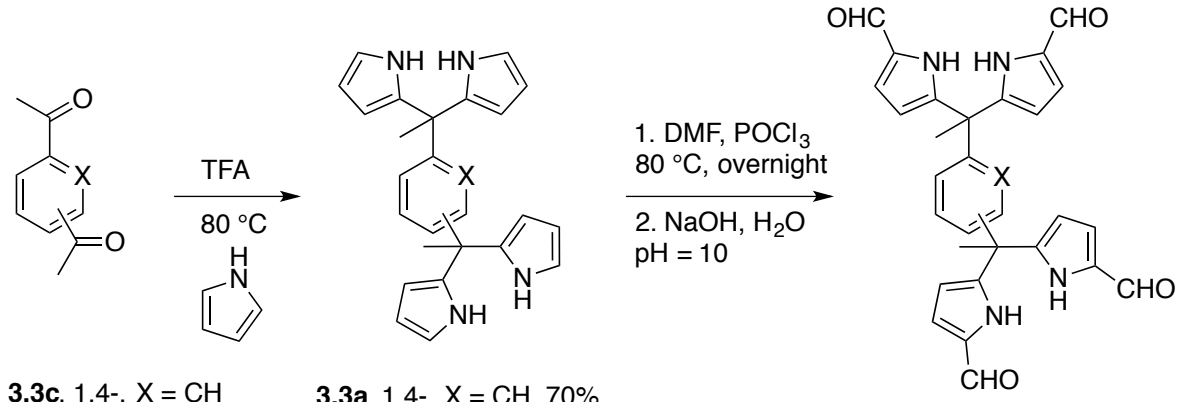

Scheme 3.3: Syntheses of compounds **3.3b**–**3.5b**.

As shown in Scheme 3.3, compounds **3.3b**–**3.5b** were synthesized in high yields from diketones (**3.3c**–**3.5c**) precursors that have two carbonyl groups bridged by rigid but free-to-rotate linkers. The requisite bisDPM intermediates, **3.3a**–**3.5a**, were obtained *via*

the electrophilic aromatic substitution of pyrrole by various aromatic diketones. The yields for **3.3a** and **3.5a** were better than those for typical simple DPMs.[9] This finding is ascribed to the fact that products **3.3a** and **3.5a** precipitate from the reaction solution (pyrrole serves as solvent) under the reaction conditions (see Experimental Section of this Chapter). The bisDPMs **3.3a**–**3.5a** were then formylated by the Vilsmeier–Haack reaction to produce **3.3b**–**3.5b** in relatively high yields (>80%). Purification of **3.3b** and **3.4b** was carried out by recrystallization from hot dimethylformamide (DMF) at 80 °C. The molecular structures were fully characterized by ^{1}H NMR and ^{13}C NMR spectroscopy, HRMS, and, in the case of **3.3b** and **3.4b**, single crystal X-ray diffraction analyses. The compound **3.3b** co-crystallized from DMF (*cf*. Figure 3.2) and from DMSO (CCDC-1012698) as **3.3b**·2DMF and **3.3b**·2DMSO, respectively.

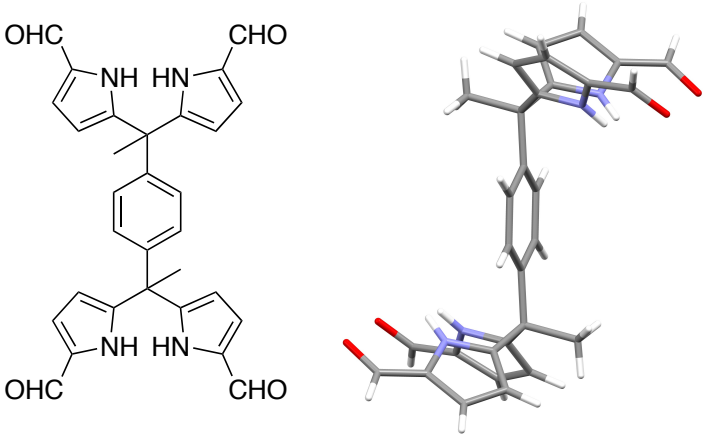

3.3b

Figure 3.2: Left: Structure of **3.3b** and Right: Single crystal structure of **3.3b**. Two DMF molecules are omitted for clarity. (CCDC number 1012698).

Similarly, a co-crystal of **3.4b**·2DMF was also obtained and structurally characterized (Figure 3.3). Two formylated-DPM subunits of both **3.3b** and **3.4b**, interacting with two DMF molecules, stabilize *trans*-like conformations. For the *meta*-

derivative, **3.4b**, the *trans*-like conformation leads to conformational isomerism in the solid state. Figure 3.3 shows only one of the atropisomers. All other synthetic details and procedures for the receptors can be found in the Experimental Section of this Chapter (page 109).

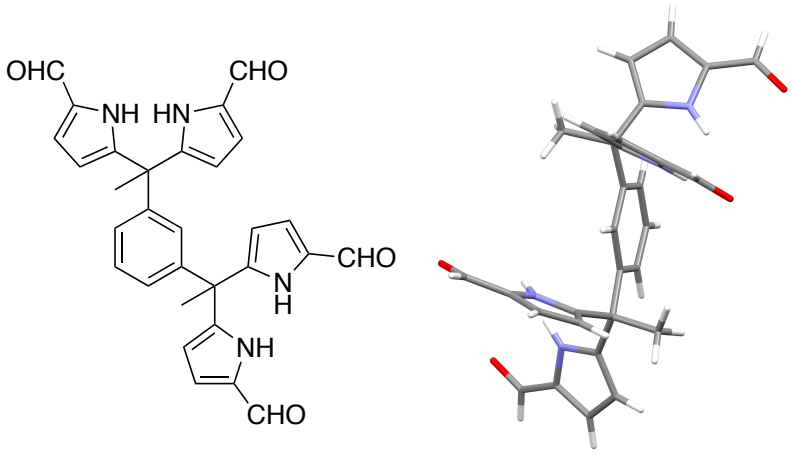

3.4b

Figure 3.3: Left: Structure of **3.4b** and Right: Single crystal structure of **3.4b**. The other major conformation and two DMF molecules are omitted for clarity. (CCDC number 1012700).

3.3.2. Anion Binding Studies

3.3.2.1. Solubility Inferred from Visual Changes

Receptors **3.3b** and **3.4b** were purified by crystallization from DMF, and isolated as co-crystals with DMF. In an effort to study the anion binding of **3.3b** under conditions involving minimal competition[††], the DMF was removed from samples of **3.3b**·2DMF by sonicating the crystals in $CHCl_3$. The DMF-free form of **3.3b** displayed noticeably lower solubility in $CHCl_3$. Treatment of turbid mixtures of **3.3b** with approximately 1.2 molar equivalents of the TBA^+ salts of various test anions ($H_2PO_4^-$, $HP_2O_7^{3-}$, HSO_4^-, $C_6H_5CO_2^-$,

[††] Solvent effects are discussed later, in the section entitled "Solution State Studies via ^{1}H NMR Spectroscopy" and in Chapter 4.

Cl^-, and NO_3^-) allowed for visual differentiation between the various anion salts (Figure 3.4). While the vials containing $TBAH_2PO_4$ and $(TBA)_3HP_2O_7$ became transparent, the vials containing other salts remained turbid.

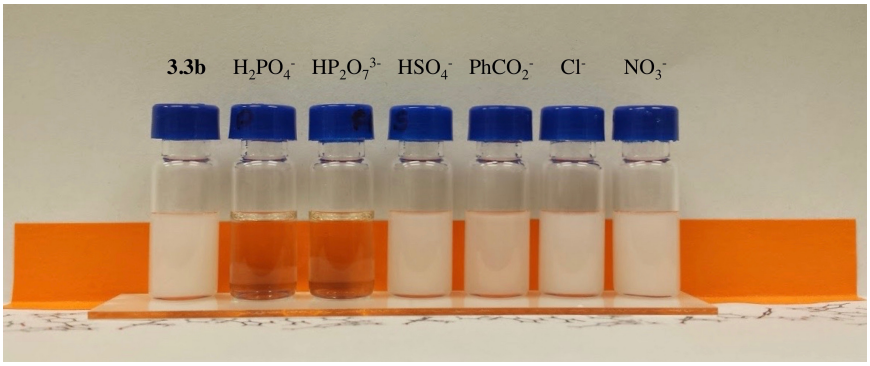

Figure 3.4: The photo of turbid mixtures of **3.3b** in $CHCl_3$ containing no added salt, 1.2 equiv. of $TBAH_2PO_4$, $(TBA)_3HP_2O_7$, $TBAHSO_4$, $TBAC_6H_5CO_2$, TBACl, and $TBANO_3$, respectively, from left to right. Note that an orange background is used to aid in visualization.

3.3.2.2. Gaseous State Studies Involving Mass Spectrometry

Mass spectrometric (MS) analyses provided evidence that receptor **3.3b** would interact with the $H_2PO_4^-$ anion in the gas phase. In these studies, an equimolar mixture of **3.3b** and $TBAH_2PO_4$ in $CHCl_3$ was directly injected into the MS instrument without passing the species through a separation column. Two ionization methods, negative ion atmospheric pressure chemical ionization (Ni-APCI) and electrospray ionization in negative mode (ESI^-), were used. Proton abstraction and anion adduction are active mechanisms in Ni-APCI.[16] The low resolution Ni-APCI MS analysis revealed a signal at *m/z* 505.2 corresponding to [**3.3b**-H]$^-$ and another signal at *m/z* 541.2 ascribable to the dihydrate ([**3.3b**-H]$^-\cdot 2H_2O$). Another signal can be observed at *m/z* 603.2 which, on the basis of a high-resolution MS analysis with ≤1.15 ppm error was assigned to [**3.3b**$\cdot H_2PO_4^-$] (*cf.* Figure 3.5).

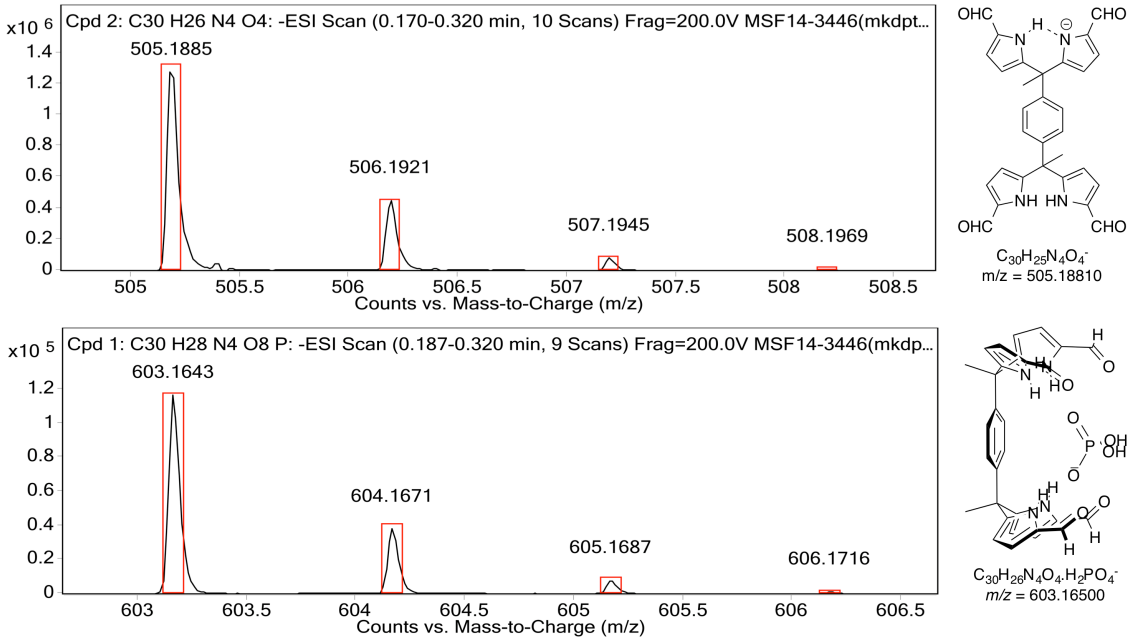

Figure 3.5: High-resolution mass spectra (electrospray ionization in negative mode) of **3.3b** (top) and of an equimolar mixture of **3.3b** and $TBAH_2PO_4$ in $CHCl_3$ (bottom).

3.3.2.3. Solid State Studies Involving X-ray Diffraction

Further insights into the binding modes of the receptors **3.3b** and **3.4b** came from single crystal X-ray diffraction analyses.[17] Diffraction-grade single crystals of the pyrophosphate complex **3.3b**·$(TBA)_2H_2P_2O_7$ were obtained by layering a solution of **3.3b**·$H_2P_2O_7^{2-}$ in CH_2Cl_2 with *n*-pentane. The complex **3.3b**·$H_2P_2O_7^{2-}$ in CH_2Cl_2 was prepared by treating **3.3b** with $(TBA)_3HP_2O_7$. This served to improve the net solubility by converting the poorly soluble receptor (*vide supra*; page 84) into the corresponding pyrophosphate complex. In the solid state, a 2:2 complex, [**3.3b**·$H_2P_2O_7^{2-}$]$_2$ is seen (*cf.* Figure 3.6). The overall complex consists of a hydrogen-bonded dimer that lies across a crystallographic inversion center.

The protonation state of the bound pyrophosphate in the complex [**3.3b**·$H_2P_2O_7^{2-}$]$_2$ was deduced from the presence of two TBA^+ counter cations per pyrophosphate dianion.

The $H_2P_2O_7^{2-}$ anion lies parallel to the π-surface of the bridging benzene ring. Both diformyl-DPM arms are oriented such that four hydrogen bonds between the diformyl-DPM units in **3.3b** and the bound $H_2P_2O_7^{2-}$ are favored. The N-H···O distances between the NH protons of **3.3b** and the O atoms of $H_2P_2O_7^{2-}$ range from 2.648 to 2.690 Å, separations that are short compared to typical N-H···O distances.[18,19] Each bound $H_2P_2O_7^{2-}$ interacts with another $H_2P_2O_7^{2-}$ anion forming a hydrogen bonded dimer. In the dimer, four protons are shared between eight oxygen atoms. The observed O···O distances of 2.508–2.518 Å are within the range expected for this type of proton bridged O-H···O interaction.[19,20]

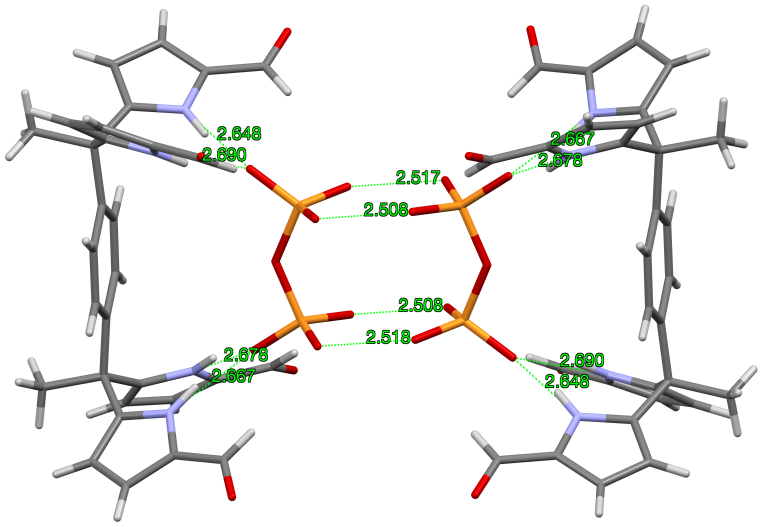

Figure 3.6: Single crystal structure of the 2:2 complex [**3.3b**·$H_2P_2O_7^{2-}$]$_2$ viewed from the side relative to the bridging benzene rings. Two TBA^+ counter cations and the disordered CH_2Cl_2 solvent molecules per pyrophosphate are omitted for clarity (CCDC number 1444559).

Diffraction grade single crystals of the complex **3.4b**·$TBAH_2PO_4$ were obtained in a similar way. The resulting structure is shown in Figure 3.7. There is no evidence of dimerization in this case. The lack of dimerization is ascribed to the relatively tight

binding between the TBA^+ counter cation and the bound $H_2PO_4^-$ guest, which precludes further inter-complex interactions. In the solid state, complex **3.4b**·$H_2PO_4^-$ displays the same conformation for the diformyl-DPM units as observed in **3.3b**·$H_2P_2O_7^{2-}$. The four N-H···O distances that characterize the interaction between the NH protons of **3.4b** and the O atoms of $H_2PO_4^-$ range from 2.704 to 2.760 Å, whereas the two O-H···O distances associated with this interaction are 2.681 and 2.726 Å, respectively.

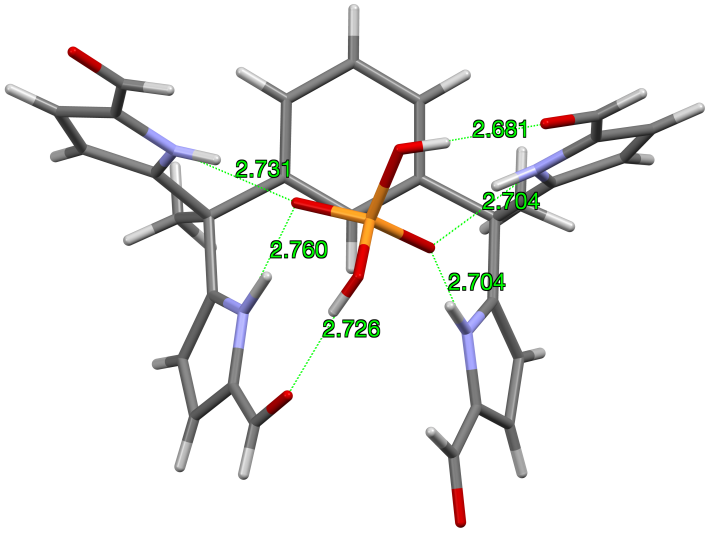

Figure 3.7: Single crystal structure of the 1:1 complex **3.4b**·$H_2PO_4^-$ viewed from the top of the bound $H_2PO_4^-$ molecular ion. One TBA^+ counter cation is associated with each complex. One TBA^+ and one $CHCl_3$ solvent molecule are omitted for clarity (CCDC number 1444560).

3.3.2.4. Solution State Studies via UV-Vis Spectroscopy

UV-Vis spectroscopy was used to characterize the formylated derivatives (**3.3b**–**3.5b**) in $CHCl_3$. These receptors are characterized by μM solubilities amenable to UV-

Vis spectral analyses. Figure 3.8 displays the absorption spectra of several key compounds, namely **3.3a–c**, **3.3b**·$H_2PO_4^-$, and the control compound **3.13** in $CHCl_3$.

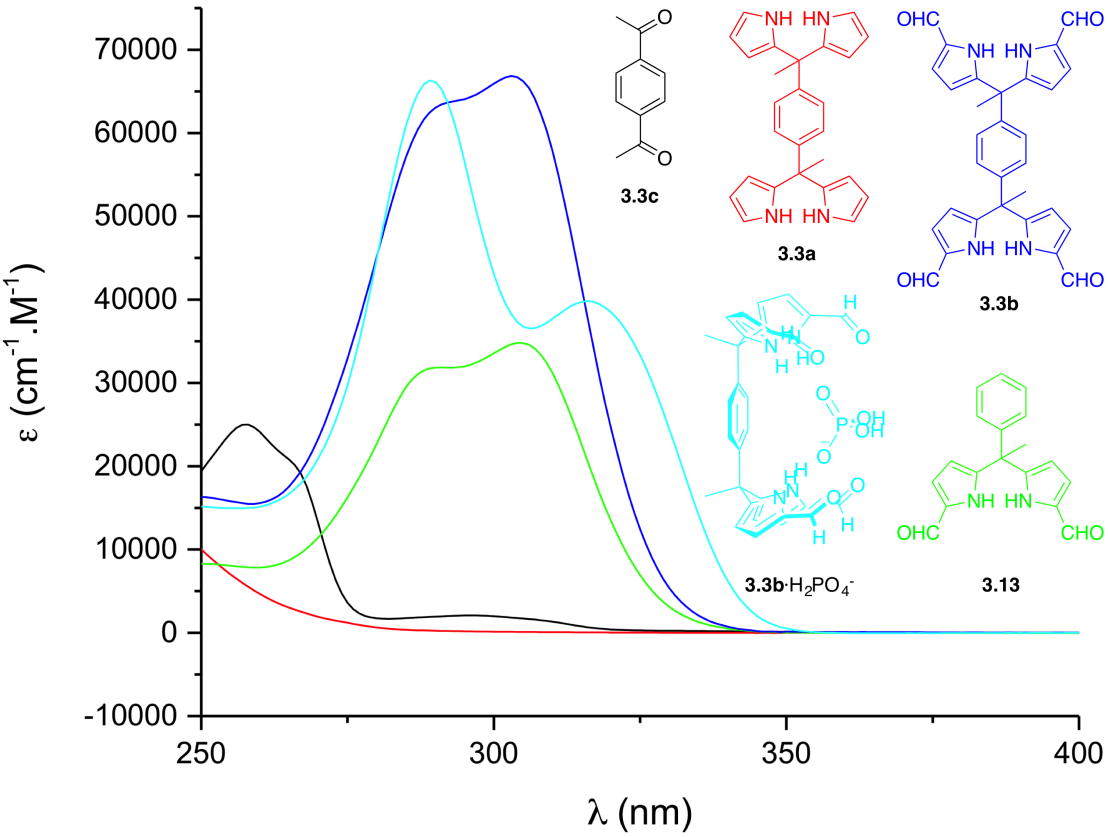

Figure 3.8: UV-Vis spectra recorded in $CHCl_3$. Black **3.3c**, red **3.3a**, dark blue **3.3b**, light blue **3.3b** determined in the presence of one molar equivalent of $TBAH_2PO_4$. The green trace corresponds to the control compound **3.13**.

The available UV-Vis wavelength range in $CHCl_3$ is ≥250 nm since the solvent $CHCl_3$ absorbs very strongly at wavelengths of <250 nm. Therefore, not all compounds of interest could be studied *via* UV-Vis spectroscopy. For instance, in $CHCl_3$ **3.3a** does not have a Soret band between 250–800 nm, whereas the formylated derivative **3.3b** has a clear Soret band in the 275 and 325 nm spectral region.

In an effort to quantify the anion selectivities, titration studies were performed. In these studies, the anion-induced changes (if any) were monitored by UV-Vis spectroscopy under conditions where compound **3.3b** is fully soluble. Compound **3.3b** (*ca*. 10 mM) was first titrated with $TBAH_2PO_4$ in dry $CHCl_3$, keeping the total concentration of **3.3b** constant throughout the study. A significant change in the absorption spectrum of **3.3b** was observed with saturation occurring after the addition of approximately one equivalent of $TBAH_2PO_4$ (*cf*. Figure 3.9). Two isosbestic points, at 293 and 315 nm, respectively, were seen. This is taken as evidence that only two absorbing species, namely the free host (**3.3b**) and the host–anion complex (**3.3b**·$H_2PO_4^-$), are interconverting under the conditions of the experiment.

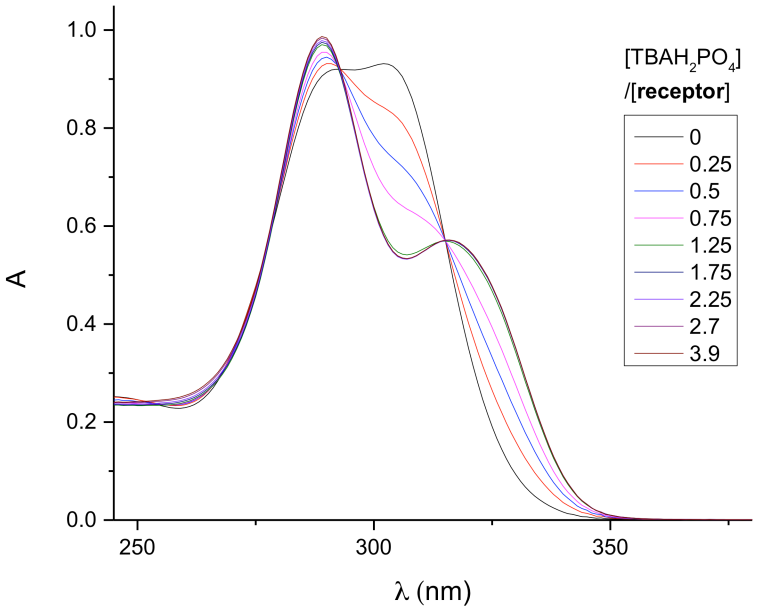

Figure 3.9: Stacked UV-Vis spectra corresponding to the titration of **3.3b** (1.2×10^{-5} M) with $TBAH_2PO_4$ (1.0×10^{-3} M) in $CHCl_3$. The molar ratio of [$TBAH_2PO_4$]/[**3.3b**] is varied from 0 to 3.9.

To provide support for the proposed 1:1 stoichiometry, a Job plot was constructed using mixtures in which total concentration of **3.3b** and $TBAH_2PO_4$ was held at 1.2×10^{-5}

M (method-1, see Experimental Section for details). Towards this end, the absorption maximum at 306 nm in the UV-Vis spectrum of **3.3b** was monitored as the ratio of $TBAH_2PO_4$ to **3.3b** was varied. Since the complex has a lower extinction coefficient than free **3.3b**, a minimum in absorbance change was expected when complex formation was greatest; this minimum in the absorbance intensity was observed when the mole fraction of the anion was equal to 0.5 (Figure 3.10). This finding is consistent with the formation of a 1:1 complex, presumably **3.3b** $\cdot H_2PO_4^-$.

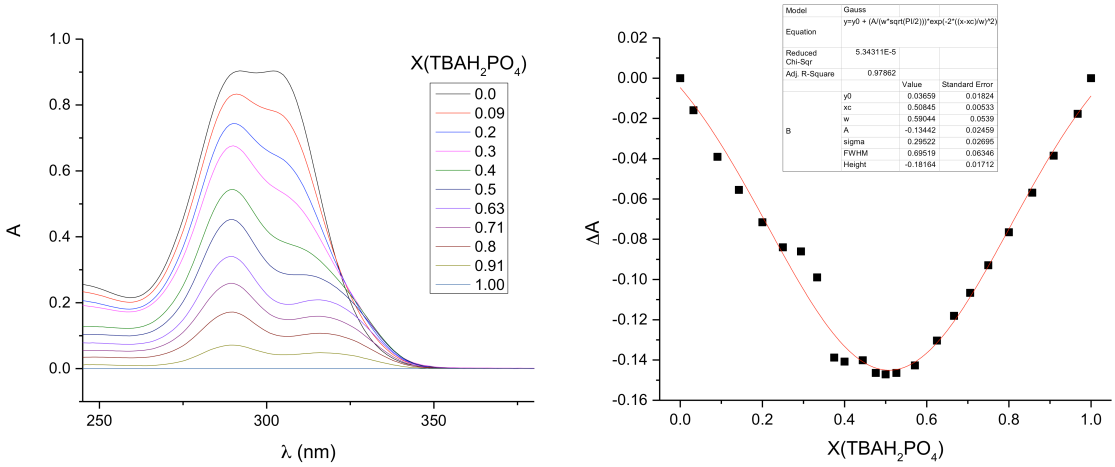

Figure 3.10: Left: UV-Vis spectra used to produce a Job plot for the interaction of **3.3b** with $TBAH_2PO_4$ in $CHCl_3$. ([**3.3b**] + [$TBAH_2PO_4$] = 1.2 x 10^{-5} M). Right: Job plot obtained from UV spectra shown in the left panel using 306 nm as the monitored wavelength.

Another method (method-2), also described in the Experimental Section (Table 3.8) was used to obtain a second Job plot (*cf.* Figure 3.11). In this method, data from titrations carried out to determine the binding affinity are used. In this system, addition of $H_2PO_4^-$ causes a decrease in the absorption of **3.3b** at 306 nm (*cf.* Figure 3.9). When this decrease is plotted against the molar fraction of $H_2PO_4^-$ added, a second Job plot may be

obtained (*cf*. Figure 3.11). Analysis of this plot leads to the same conclusion drawn from Figure 3.10, namely that a 1:1 complex is being formed.

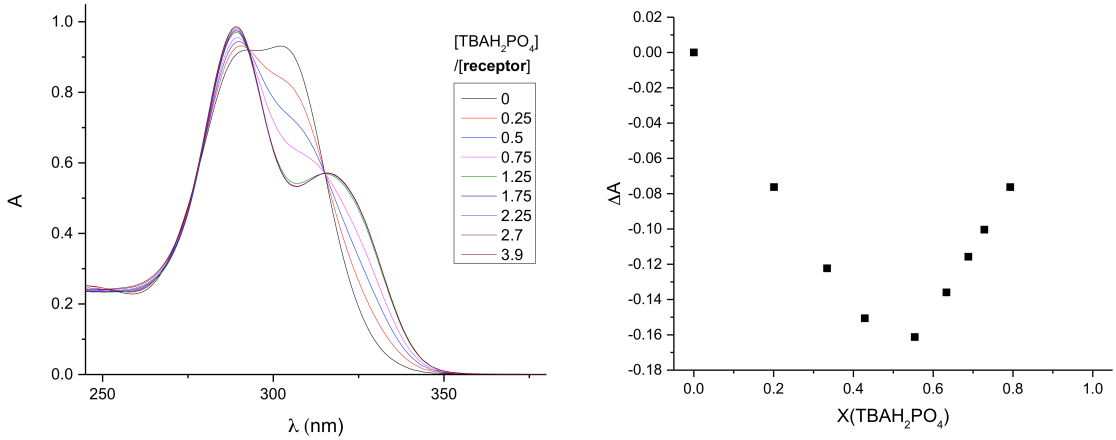

Figure 3.11: Left: UV-Vis spectra for a titration carried out with the intention of determining the binding affinity (*cf*. Figure 3.9). Right: Job plot derived from the spectra shown on the left using at 306 nm as the monitored wavelength.

After confirming *via* Job plots that the interaction between **3.3b** and $TBAH_2PO_4$ is 1:1, the data at 306 nm from Figure 3.9 was fitted to a 1:1 binding profile. The fitting curve is shown in Figure 3.12. The data (black square points) align well with the theoretical binding isotherm (red line). The theoretical curve is derived for titration conditions in which the total receptor concentration is kept constant throughout the experiment. For the specific titration of **3.3b** with $TBAH_2PO_4$, non-linear fitting gives a binding affinity of $K_a = (8 \pm 2) \times 10^6\ M^{-1}$.

Similar studies were performed for **3.3b** by titrating with $TBAH_2PO_4$, $(TBA)_3HP_2O_7$, $TBAHSO_4$, $TBAC_6H_5CO_2$, TBACl, and $TBANO_3$. The same sets of anion salts were also tested in the case of receptors **3.4b** and **3.5b**. The data were fit to a 1:1 binding isotherm using a protocol detailed on page 117. The binding affinities (K_a) obtained from these studies are collected in Table 3.2 and related spectra and binding

curve fittings are provided in the Experimental Section (starting from page 119). Based on the optical titration studies involving different anions, studied as their TBA^+ salts in $CHCl_3$, the highest affinity was observed for $H_2PO_4^-$, followed by $HP_2O_7^{3-}$ (Table 3.2).

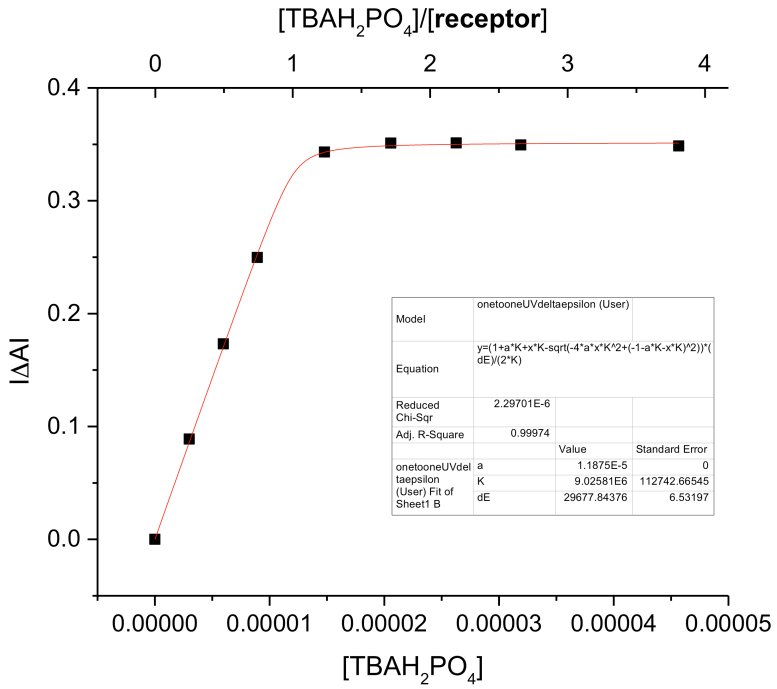

Figure 3.12: Binding curve fitting for the interaction of **3.3b** with $TBAH_2PO_4$ derived using the data in Figure 3.9 with monitoring at 306 nm. $K_a = (8 \pm 2) \times 10^6\ M^{-1}$.

In order to assess the importance of an intervening aromatic linker and its connectivity (*meta*-, *para*-) on anion binding, receptors **3.3b**, **3.4b**, and **3.5b** were compared. The positions of the two diformyl-DPM units on the aromatic ring did not appear to affect the binding affinities significantly, nor their specificities. Support for this conclusion came from the finding that the isomeric *para*- (**3.3b**) and *meta*- (**3.4b**) systems displayed similar selectivity and anion affinity trends (cf. Table 3.2). On the other hand,

the pyridine-based receptor **3.5b** was characterized by affinities that were an order of magnitude lower.

	K_a (M^{-1})		
Anion	**3.3b**	**3.4b**	**3.5b**
$H_2PO_4^-$	(8 ± 2) x 10^6	(8 ± 2) x 10^6	(4.6 ± 0.9) x 10^5
$HP_2O_7^{3-}$	(1.4 ± 0.1) x 10^5	(1.9 ± 0.3) x 10^5	(6.5 ± 0.7) x 10^4
HSO_4^-	(4.1 ± 0.2) x 10^3	(4.00 ± 0.09) x 10^3	(1.6 ± 0.1) x 10^3
$C_6H_5CO_2^-$	UD	(8 ± 1) x 10^4	(6.7 ± 0.1) x 10^3
Cl^-	NC	NC	NC
NO_3^-	NC	NC	NC

UD: could not be determined; NC: No discernible changes in the UV-Vis spectrum were observed.

Table 3.2: Calculated binding affinities (M^{-1}) for **3.3b**, **3.4b**, and **3.5b** with various TBA^+ anion salts in $CHCl_3$ as determined by UV-Vis spectroscopy.

In order to understand the electronic effects of the pyrrole on the anion binding properties of receptor **3.3b**, a series of control compounds were prepared and studied. In a first study, the $H_2PO_4^-$ binding properties of the bisDPM **3.3a** were studied with $TBAH_2PO_4$ in chloroform. BisDPM **3.3a** is the precursor to **3.3b** and has hydrogen atoms, rather than formyl, substituents at the α-positions. Unfortunately, efforts to monitor the anion binding features of **3.3a** *via* UV-Vis spectroscopy were precluded due to the fact that the $CHCl_3$ absorption in the UV portion of the spectrum overlaps with that of the pyrrole rings. Thus, for this comparison, we turned to ^{1}H NMR spectroscopy (*cf*. Section 3.3.2.5 Solution State Studies via ^{1}H NMR Spectroscopy).

A DPM control compound, **3.13**, was prepared according to the literature.[21,22] Compound **3.13** lacks the second diformyl-DPM unit present in **3.3b**. However, it is structurally more similar to **3.3b** than **3.1**. Therefore, we hypothesized that it should display a lower binding affinity. Although **3.13** is very similar to **3.3b** in terms of electronics and may be viewed as being ''half'' of the full receptor system present, no spectral change was observed in the UV-Vis spectrum when **3.13** was titrated with $TBAH_2PO_4$ in $CHCl_3$. On this basis, the substantial increase in the binding affinity seen for **3.3b** compared to **3.13** can be attributed to both the increase in number of NH hydrogen bond donors (two in **3.13**; four in **3.3b**) and the creation of what may be a better organized system.

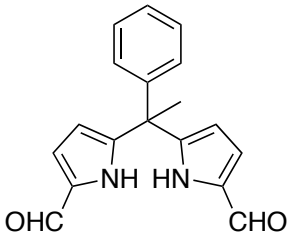

3.13

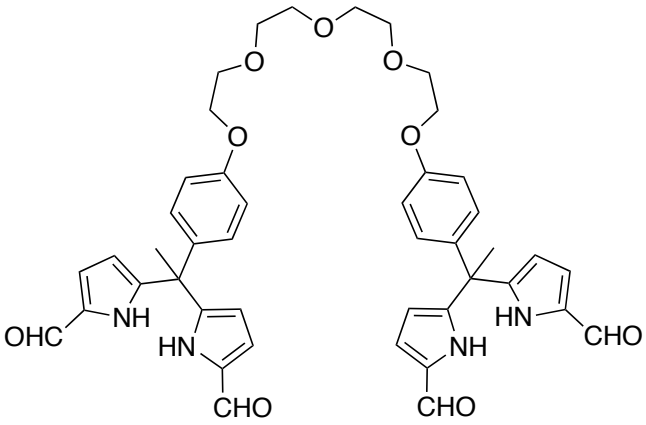

3.14

Compound **3.14** was also studied as a control. This flexible tetraethylene glycol chain linked system has the same number of α-formylpyrroles as **3.3b**; however, it lacks a similar degree of preorganization. It displays very little affinity for $H_2PO_4^-$ or the other test anions in $CHCl_3$, as inferred from the lack of observed spectral changes.

Anion	**3.3b**	**3.13**	**3.14**
$TBAH_2PO_4$	$(8 \pm 2) \times 10^6$	NC	NC
TBACl	NC	NS	NS

NC: No discernable spectral change, NS: not studied.

Table 3.3: Binding affinities as calculated from UV-Vis spectral titrations of **3.3b**, **3.13**, and **3.14** with $TBAH_2PO_4$ and TBACl in $CHCl_3$.

3.3.2.5. Solution State Studies via ^{1}H NMR Spectroscopy

Based on the visually observed solubility changes and UV-Vis spectroscopic studies discussed above, it was concluded that the formylated bisDPM receptors, **3.3b**–**3.5b**, display relatively high affinities for the $H_2PO_4^-$ anion in $CHCl_3$. Since the absorption bands of bisDPM compounds **3.3a**–**3.5a** were not observable in the solvent ($CHCl_3$) used for analysis, the $H_2PO_4^-$ binding affinities of these compounds could not be determined *via* UV-Vis spectroscopy. Therefore, ^{1}H NMR spectroscopy was used. Compounds **3.3b–3.5b** were also analyzed by ^{1}H NMR spectroscopy. This was done so that the two compound series (**3.3a**–**3.5a** and **3.3b**–**3.5b**) could be compared.

In order to find conditions under which the two series could be compared, various solvent systems were screened. Figure 3.13 displays ^{1}H NMR spectra of **3.3b** in various NMR solvents. It also became apparent that the pyrrole NH chemical shift depends on the presence and absence of residual solvent bound within the receptor (*i.e.*, DMF-free **3.3b** versus single crystal **3.3b**·2DMF). Due to these solvent dependences, which were taken as indications of receptor-solvent interactions as inferred from the crystal structure of **3.3b**·2DMF, hydrogen-bond-accepting solvents such as DMF and DMSO were deemed too competitive. Therefore, the DMF-free from of **3.3b** was used for the binding studies.

However, the solubility of **3.3b** is lower than 1.0 mM in $CHCl_3$, making the ^1H NMR spectral studies challenging.

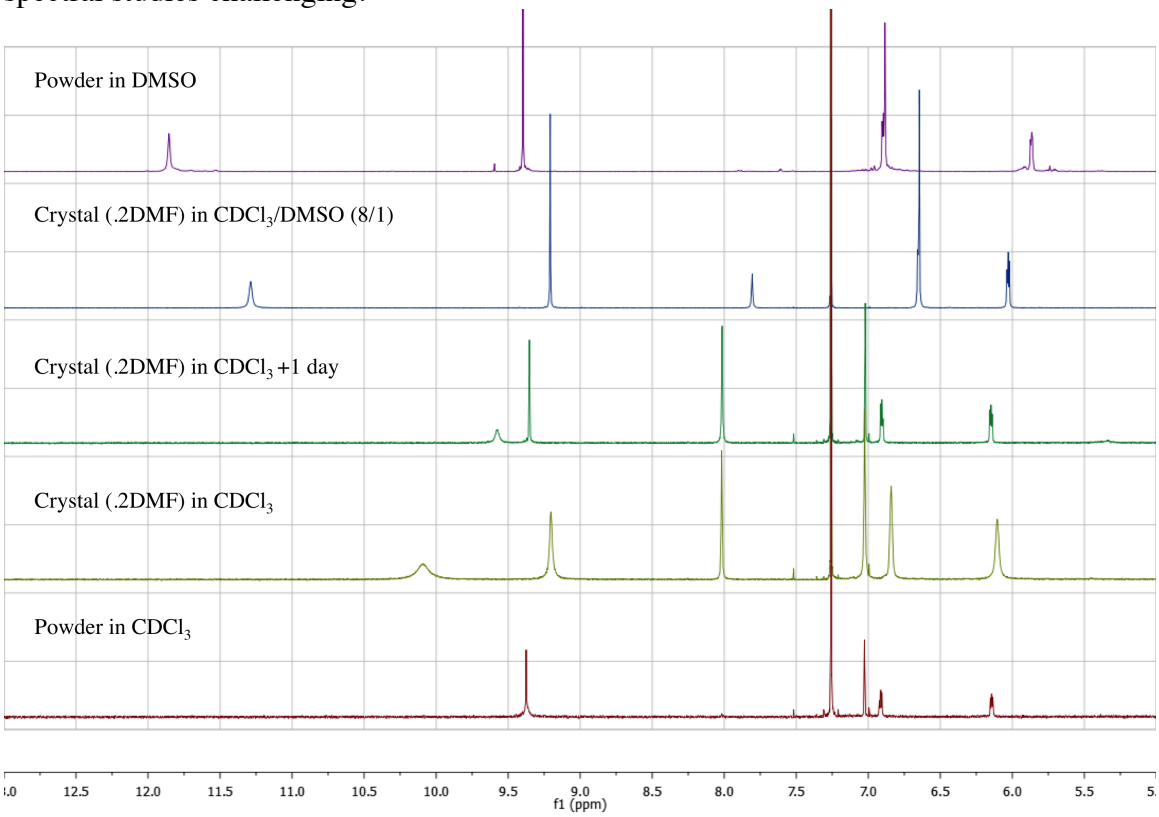

Figure 3.13: Stacked partial ^1H NMR spectra of **3.3b** (in the form of a white powder and single crystalline (**3.3b**·2DMF)) in various solvent systems.

Although solutions of **3.3b** proved turbid at concentrations ≥1.0 mM, the expected signals in the ^1H NMR spectrum could be observed in dilute solutions. Upon addition of $TBAH_2PO_4$, the solubility increases noticeably. In fact, upon the addition of one equivalent of $TBAH_2PO_4$ to a turbid 1.0 mM‡‡ mixture of **3.3b** in $CDCl_3$, the solution mixture became completely clear/soluble. Moreover, in the ^1H NMR spectrum (in $CDCl_3$)

‡‡ The 1.0 mM concentration value is given here for the purposes of convenience. It is based on the incorrect assumption that the sample of **3.3b** used was fully dissolved. The turbid nature of the mixture means that the actual solution phase concentration of **3.3b** is <1.0 mM.

an additional set of signals, other than those attributed to **3.3b**, appeared (Figure 3.14). When receptor **3.3b** (turbid 1.0 mM mixture in $CDCl_3$) was titrated with $TBAH_2PO_4$ in a stepwise manner, peaks corresponding to both the free host and the receptor-anion complex were observed in the ^1H NMR spectrum. This was taken as evidence of a strong interaction between the receptor and the anionic guest $H_2PO_4^-$, as well as a recognition process that involved exchange kinetics that are slow on the NMR time scale. Unfortunately, the incomplete solubility displayed by **3.3b** at the concentrations used for the titrations prior to the addition of a full molar equivalent of $TBAH_2PO_4$ precluded a quantitative estimate of the K_a corresponding to the receptor-anion interaction in $CDCl_3$.

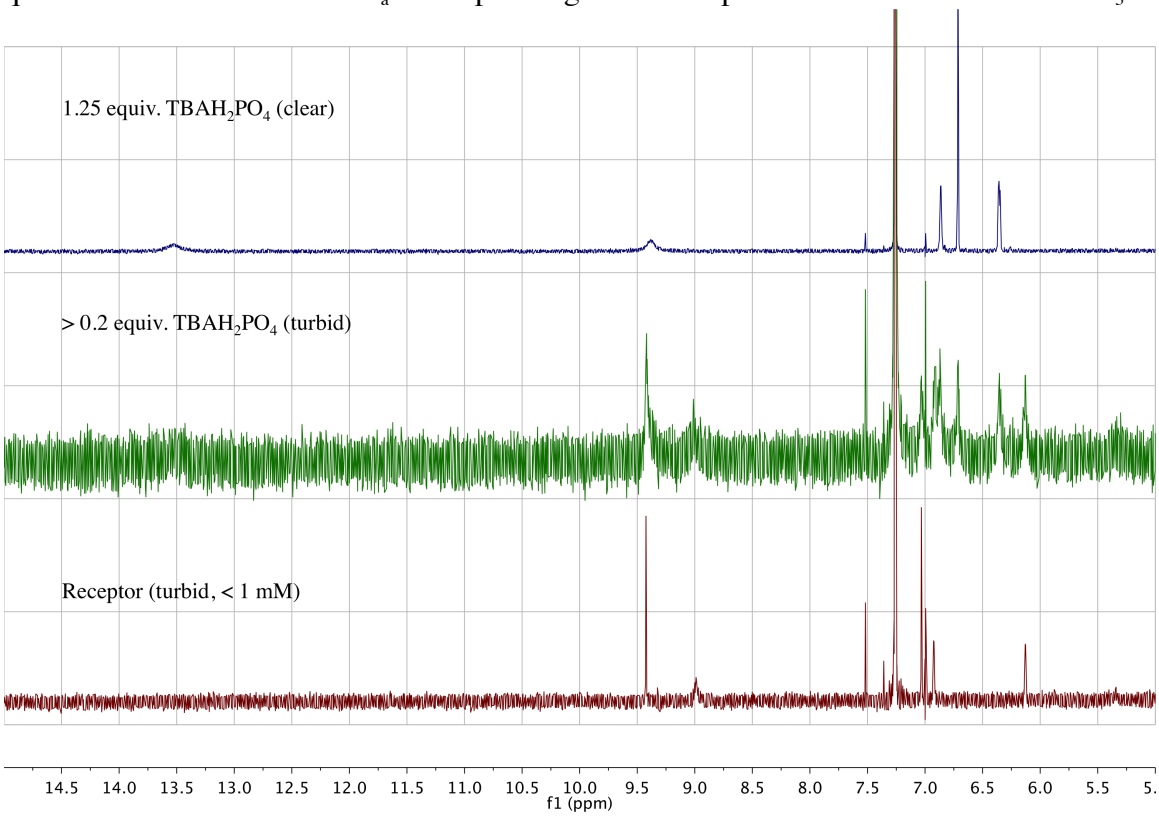

Figure 3.14: Stacked partial ^1H NMR spectra of turbid mixtures of **3.3b** without added $TBAH_2PO_4$ (red), **3.3b** with > 0.2 (but <1.0) equivalent $TBAH_2PO_4$ (green), and soluble mixture of **3.3b** and 1.25 equivalent $TBAH_2PO_4$ (blue) in $CDCl_3$.

A 1:1 binding stoichiometry was inferred from UV-Vis spectroscopic studies. The 1:1 binding isotherms were shown to fit the data obtained from titration experiments. In order to rule out other binding modes other than simple 1:1 (*e.g.* 2:2, 3:3, or n:n), diffusion ordered spectroscopy (DOSY)[23] studies were carried out. On the basis of these latter analyses, the formation of self-assembled polymeric structures is ruled out under the relatively high dilution conditions used for the spectroscopic studies (Figure 3.15).

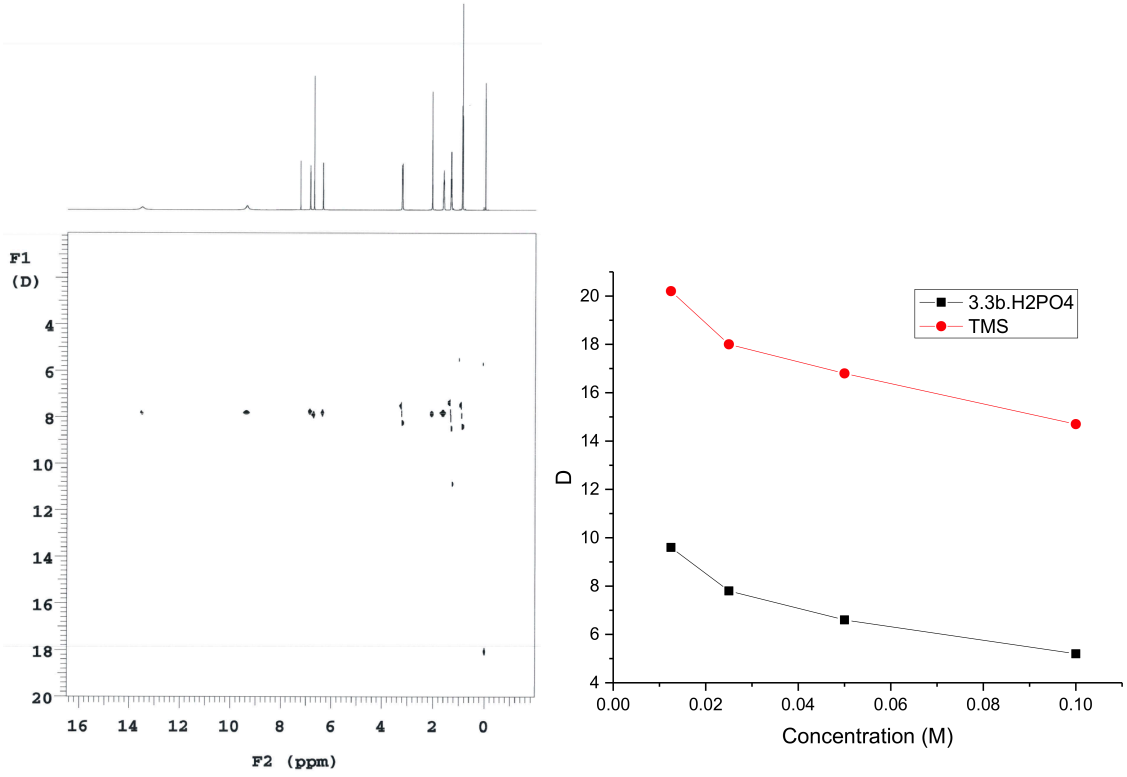

Figure 3.15: Left: A sample DOSY spectrum of **3.3b**·$TBAH_2PO_4$ recorded at a concentration of 0.025 M in $CDCl_3$. Right: Plot of DOSY spectral results for **3.3b**·$TBAH_2PO_4$ recorded at various concentrations (from 0.0125 mM to 0.10 mM) in $CDCl_3$.

In this experiment, DOSY spectrum of a stock solution of **3.3b**·$TBAH_2PO_4$ was recorded at a concentration of 0.1 M in $CDCl_3$, as well as at lower concentrations (*e.g.*, 0.05 M, 0.025 M, and 0.0125 M) (Figure 3.15). The diffusion parameter trends observed

for the **3.3b**·$TBAH_2PO_4$ and the trimethylsilane (TMS) molecule (used as an internal standard) were then recorded.

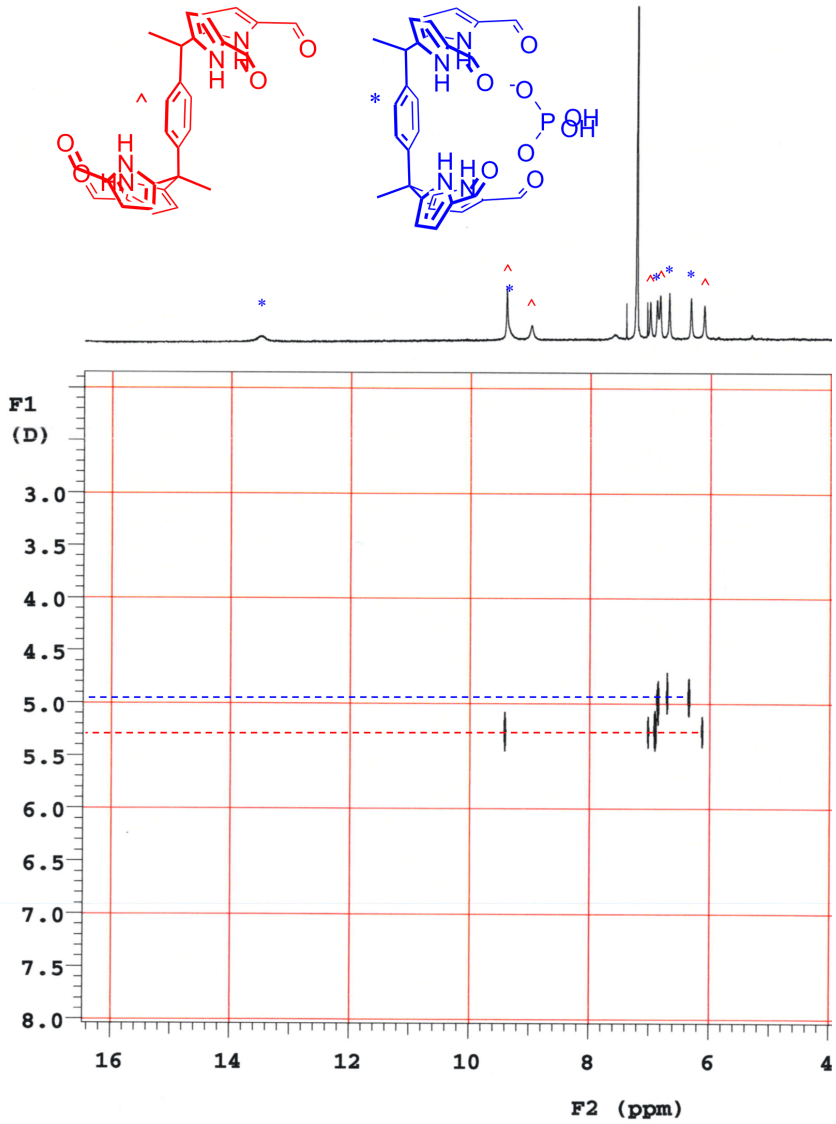

Figure 3.16: DOSY spectrum of a 1:0.5 mixture of **3.3b** and $TBAH_2PO_4$. The mixture was obtained by titrating 0.8 mM $TBAH_2PO_4$ into a turbid mixture of **3.3b** in $CDCl_3$ until the half-equivalent point was inferred from the ratio of the integration values. ^ shows free-**3.3b**; * shows **3.3b**·$H_2PO_4^-$.

In a different experiment, DOSY was used to examine the interactions between anions and receptor **3.3b**. Here, a different approach, in which both unbound and bound forms of the receptor were observed simultaneously was used. Receptor **3.3b** was chosen for these studies for two reasons. First, the low solubility of **3.3b** in $CHCl_3$ means that an equilibrium was expected to exist between species free in solution and those tied up in the solid state. Secondly, on the ^1H NMR time scale, free receptor **3.3b** and the $H_2PO_4^-$ bound complex (**3.3b**·$H_2PO_4^-$) were subject to slow-exchange (*cf*. Figure 3.14) allowing both species to be observed concurrently. Figure 3.16 shows the DOSY spectrum of a mixture of **3.3b** at the half-equivalence point obtained by titrating with $TBAH_2PO_4$ in $CDCl_3$. The one-dimensional ^1H NMR spectrum in the horizontal axis shows two sets of receptor signals; free **3.3b** and **3.3b**·$H_2PO_4^-$. These are labeled with red and blue asterisks, respectively.

After confirming the 1:1 binding stoichiometry in solution state *via* the DOSY analyses, binding affinities of **3.3a** and **3.3b** for $H_2PO_4^-$ were determined in order to understand the effect of formylation on the $H_2PO_4^-$ anion binding. The determination of K_a corresponding to the **3.3b**·$H_2PO_4^-$ anion interaction in $CDCl_3$ was precluded due to low solubility. Although **3.3a**, like **3.3b**, is poorly soluble in $CDCl_3$ and forms turbid mixtures at the mM concentrations required for NMR spectroscopic analyses, compound **3.3a** could be studied under the conditions (*i.e*., in $CDCl_3$). Specifically, the change in the pyrrole NH signals of **3.3a** were followed as $TBAH_2PO_4$ was added (Figure 3.17). Upon the addition of 7.0 molar equivalents of $TBAH_2PO_4$, a shift in the NH signal from 7.8 ppm to 10.9 ppm was observed. No appreciable changes were seen as further equivalents were added. When the pyrrole NH resonance change is plotted against the concentration of $H_2PO_4^-$ added, the binding isotherm shown in Figure 3.18 was obtained. This isotherm was fitted to a 1:1 binding profile as explained in the Experimental Section to yield K_a =

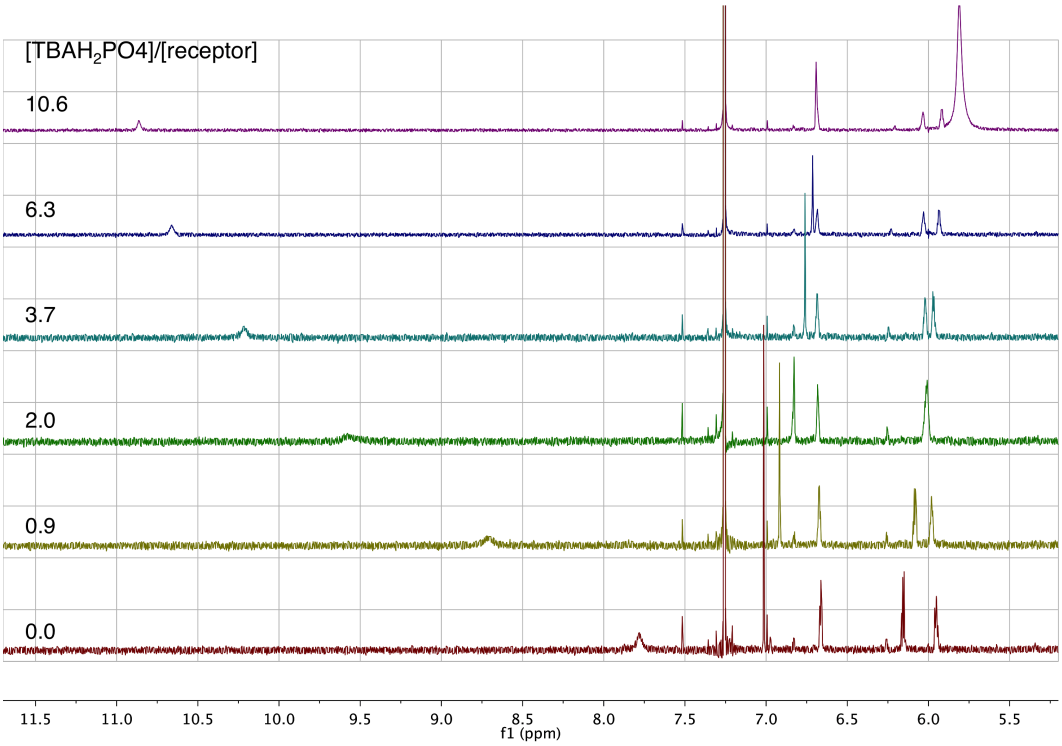

Figure 3.17: Stacked partial ^{1}H NMR spectra corresponding to the titration of **3.3a** (0.6 mM) with $TBAH_2PO_4$ (2.2 mM) in $CDCl_3$.

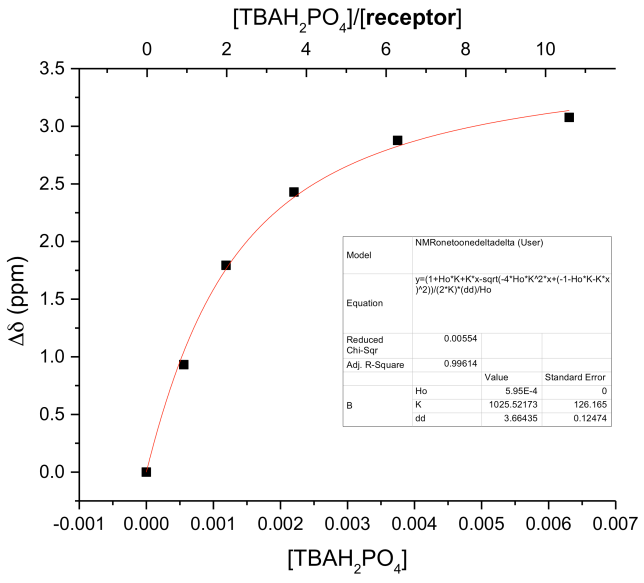

Figure 3.18: Pyrrole NH chemical shift change plotted against $[TBAH_2PO_4]$. The data were fit to a 1:1 binding curve giving $K_a = (1 \pm 0.1) \times 10^3\ M^{-1}$.

(1 ± 0.1) x10^3 M^{-1}. A discussion of the ^{1}H NMR spectra and the curve fittings for related studies are provided in Section 3.5.3.

Greater changes were observed in the case of **3.3b**; here, the NH signal is seen to undergo a change from 9 ppm to 13.6 ppm upon the addition of only one equivalent of $TBAH_2PO_4$ (Figure 3.14). From this disparate behavior we conclude that the affinity of **3.3b** for $H_2PO_4^-$ is greater than that seen for the control system **3.3a** (Table 3.4).

	3.3a[a,b]	**3.5a**[a]	**3.3b**[a,b]	**1.10**[c]
NH δ shift	7.8–10.9[a]	8.2–10.4	9.0–13.6[a]	7.0–NR
	9.0–10.9[b]		11.3–13.3[b]	
Saturation	~7 equiv.[a]	>5 equiv.	~1 equiv.	NR
K_a (M^{-1})	(1 ± 0.1) x10^3[a,d]	40.8 ± 0.6	>10^5[a,e]	97 ± 4
	184 ± 5[b]		3200 ± 900[b]	

[a] Study performed in $CDCl_3$, [b] Study performed in $CDCl_3$/DMSO-d_6 (8/1). [c] Study performed in CD_2Cl_2 ref-2. [d] Approximate value based on an analysis of what was initially a turbid mixture. [e] The value is beyond the range that may be determined accurately by ^{1}H NMR spectroscopy. NR: not reported.

Table 3.4: Summary of ^{1}H NMR spectral changes seen for **3.3a**, **3.5a**, **3.3b**, and **1.10** upon addition of $TBAH_2PO_4$.

To determine a reliable K_a value for $H_2PO_4^-$ in the case of receptor **3.3b**, a solvent mixture in which **3.3b** is soluble, $CDCl_3$/DMSO-d_6 (8/1), was required. The K_a for receptor **3.3b** proved x17 higher than that recorded for **3.3a** in $CDCl_3$/DMSO-d_6 (8/1) mixture (*cf.* Table 3.4). Control compound **3.3a** displayed a x10 higher $H_2PO_4^-$ affinity in $CDCl_3$ than did C[4]P **1.10** in CD_2Cl_2 (*cf.* Table 3.4). While a direct comparison between **3.3b** and **1.10** cannot be made due to the differing conditions of analysis, overall, the K_a

value increases on passing from **1.10** to **3.3a** and then on to **3.3b**. This benefit in binding is ascribed to a combination of structural and electronic effects.

Solvent	**3.3a**	**3.3b**	**1.10**[a]
$CDCl_3$	$(1.0 \pm 0.1) \times 10^3$	ud	$(9.7 \pm 4) \times 10^1$
$CDCl_3$/DMSO-d_6 (8/1)	$(1.84 \pm 0.05) \times 10^2$	$(3.2 \pm 0.9) \times 10^3$	-

[a] in CD_2Cl_2 from reference[2] ud: unable to determine (slow exchange)

Table 3.5: $H_2PO_4^-$ binding affinities as calculated from ^{1}H NMR spectral titrations of **3.3a**, **3.3b**, and **1.10** with $TBAH_2PO_4$ in two solvent systems as indicated in this table.

These structure-related changes appear to modulate not just the affinity, but also the inherent selectivity. Specifically, receptor **3.3b** exhibits an inversion in selectivity compared to C[4]P. It displays a higher affinity for $TBAH_2PO_4$ (subject to the solvent-related caveat noted above). However, it possesses a ~3 fold lower affinity for TBACl in similar halogenated solvents (*i.e.* $CDCl_3$ and CD_2Cl_2; *cf.* Table 3).

	3.3b[a]	**1.10**[b]
$TBAH_2PO_4$	3200 ± 900[c]	97 ± 4
TBACl	121 ± 7	350 ± 6

[a] in $CDCl_3$ and [b] in CD_2Cl_2 (Reference-2) [c] in $CDCl_3$/DMSO-d_6 (8/1)

Table 3.6: Binding affinities calculated from ^{1}H NMR spectral titrations of **3.3b** and **1.10** with $TBAH_2PO_4$ and TBACl in various solvent systems as indicated in this table.

As a part of solution state studies, we performed a 2D-NMR study involving rotating frame nuclear Overhauser effect spectroscopy (ROESY). In $CDCl_3$, no

correlation between the counter cation TBA^+ and the receptor **3.3b** was observed (red boxed area of Figure 3.19). Based on the crystal structure of **3.4b**·$H_2PO_4^-$, a heteronuclear cross-coupling between ^{31}P of the bound $H_2PO_4^-$ and ^1H of the pyrrole NH of the receptor **3.4b** was expected *via* heteronuclear Overhauser effect spectroscopy (HOESY). However, in $CDCl_3$, no correlation signal was seen.

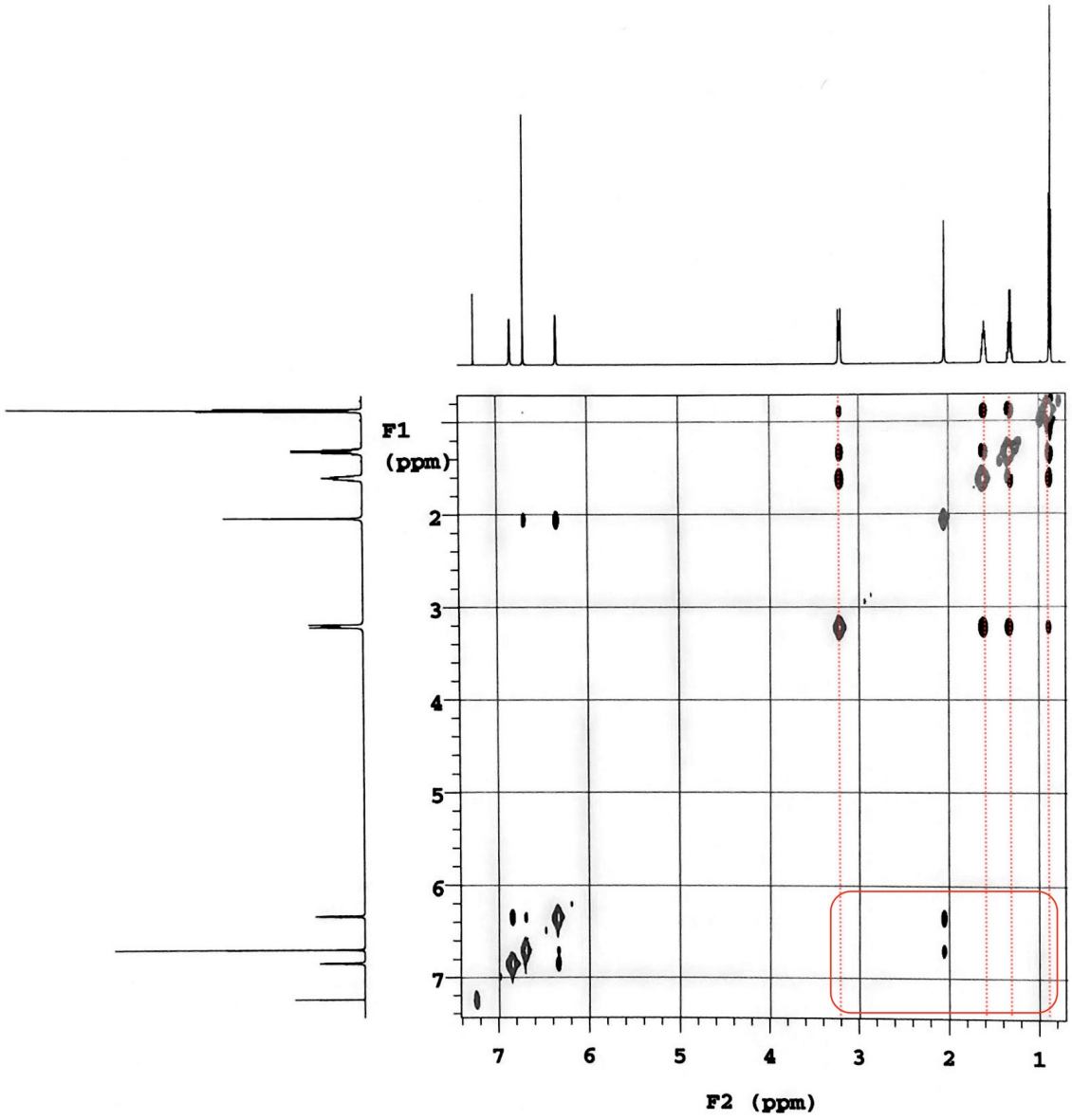

Figure 3.19: ROESY spectrum of a solution of **3.3b**:$TBAH_2PO_4$ (1:1) in $CDCl_3$.

Based on the binding mode observed in the solid state, we considered it likely that anion-π interactions, as well as pyrrole NH-anion hydrogen bonding interactions contribute to anion binding. To explore this possibility, the effect of adding $TBAH_2PO_4$ to the most soluble receptor of the present series, namely the *meta*-derivative **3.4b**, was investigated using ^{1}H NMR spectroscopy (Figure 3.20).

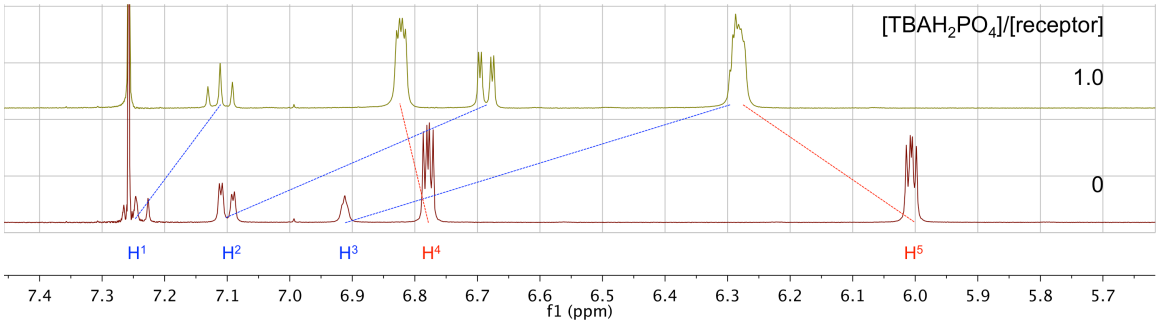

Figure 3.20: Partial ^{1}H NMR spectra of receptor **3.4b** before (bottom) and after (top) addition of one molar equivalent of $TBAH_2PO_4$ in $CDCl_3$. Dashed lines show the changes in the chemical shifts of selected proton signals ascribable to receptor **3.4b**. Hydrogens marked in blue (H^1, H^2, and H^3) are signals for the aromatic hydrogens on the benzene ring. Red signals (H^4 and H^5) correspond to pyrrole β-hydrogens. Hydrogen assignments are given in Table 3.7.

Upon addition of one molar equivalent of $TBAH_2PO_4$ to a $CDCl_3$ solution of **3.4b**, discernible shifts in the proton resonances of **3.4b** were observed (*cf.* Table 3.7). Of particular note were the 0.6 ppm upfield shifts seen for the proton signals of the intervening benzene ring. Such shifts are consistent with the presence of anion-π interactions, as inferred from previous studies of $\alpha,\alpha,\alpha,\alpha$-*meso*-tetraaryl-C[4]P derivatives reported by Ballester and co-workers.[24]

	δ (ppm)			
H-type	**3.4b**	**3.4b**·$H_2PO_4^-$	Δδ (ppm)	
H^1	7.25	7.10	- 0.15	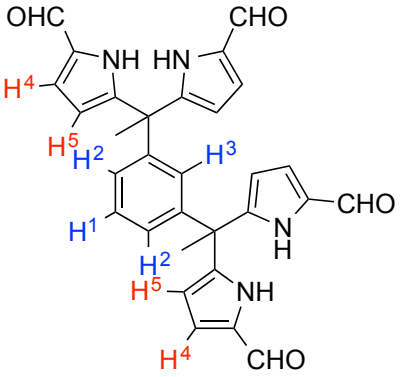
H^2	7.10	6.70	- 0.40	
H^3	6.90	6.30	- 0.60	
H^4	6.80	6.85	+ 0.05	
H^5	6.00	6.30	+ 0.30	

Table 3.7: Summary of chemical shift changes of some of the hydrogen signals of receptor **3.4b** after addition of about one molar equivalent of $H_2PO_4^-$.

3.4. CONCLUSION

On the basis of the results and discussions presented, we conclude that the macrocyclic structure of C[4]P present in **1.10** is not required for effective anion recognition. In fact, the new tetrakis(1*H*-pyrrole-2-carbaldehyde) receptors (**3.3b**–**3.5b**) bind the $H_2PO_4^-$ anion more strongly than C[4]P **1.10** in typical organic solvents. The higher affinity is attributed to a combination of factors, including the presence of better hydrogen-bond donor groups (*i.e.*, the α-formyl pyrrole units present in receptor **3.3b**–**3.5b**) and a rigid aromatic linker between the individual DPM subunits that permits conformational flexibility and, presumably, accommodation of the bound anion, including stabilizing anion-π interactions. Conformational switching from *trans*-like conformations (as seen in the free receptors **3b** and **4b**) to the corresponding *cis*-like

conformations, dominating in the presence of a bound phosphate derivatives was revealed by X-ray diffraction analyses in the solid state (Figure 3.21).

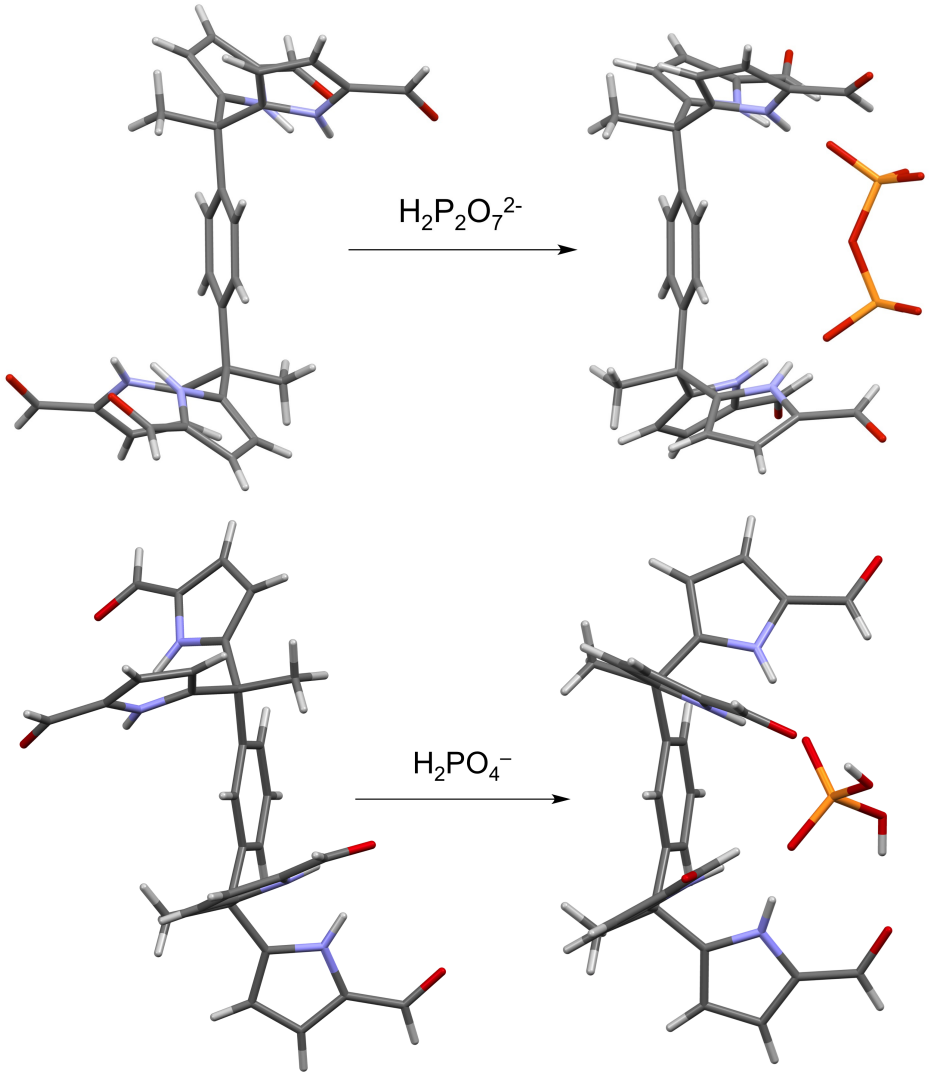

Figure 3.21: Views of the single crystal structures of **3.3b** (top) and **3.4b** (bottom) in the absence and presence of bound phosphate derivatives.

3.5. EXPERIMENTAL

All solvents and chemicals were purchased from Aldrich, TCI, and Acros. Pyrrole was distilled at 80 °C under reduced pressure (100 mbar) prior to use. Other solvents and reagents were used without further purification.

3.5.1. Synthetic Procedures

Procedure-A: BisDPM synthesis

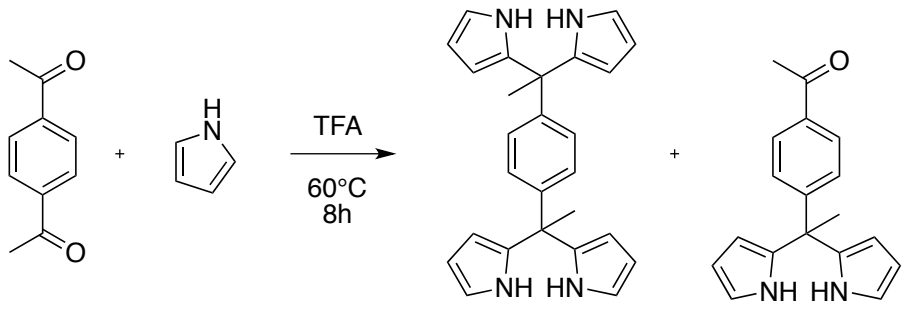

3.3c **3.3a** 70% **3.3a'** 4%

1,4-Bis(1,1-di(1*H*-pyrrol-2-yl)ethyl)benzene **(3.3a)**: 1,4-Diacetylbenzene (**3.3c)** (1.45 g, 9.0 mmol) was dissolved in pyrrole (5.0 g, 75 mmol). A catalytic amount of TFA (5 drops) was then added. The mixture was stirred in an oil bath at 60 °C for 8 h. The solution was allowed to cool to room temperature. The desired product was precipitated by addition of methanol (*ca*. 10 ml). The resulting pale green mixture was filtered. The precipitate obtained was washed further with methanol (10 ml) and was dried *in vacuo* to afford bisDPM (**3.3a**) as a white solid (2.45 g, 70%). Based on ^{1}H NMR spectral analysis, the monoDPM (**3.3a'**) was present as a 4% impurity. ^{1}H NMR (400 MHz, DMSO-d_6) δ 10.28 (bs, 4H), 6.83 (s, 4H), 6.61 (m, 4H), 5.86 (m, 4H), 5.52 (m, 4H), 1.91 (s, 6H) ppm. ^{13}C NMR (100 MHz, DMSO-d_6) δ 146.3, 137.7, 126.4, 117.1, 106.2, 105.9, 43.9, 27.9 ppm. HRMS (ESI+) *m/z* for $C_{26}H_{26}N_4$ $[M+H]^+$ calcd 395.22302, found 395.22355.

Procedure-B: Vilsmeier–Haack formylation. This is a modified version of a procedure first reported by Love and coworkers.[22]

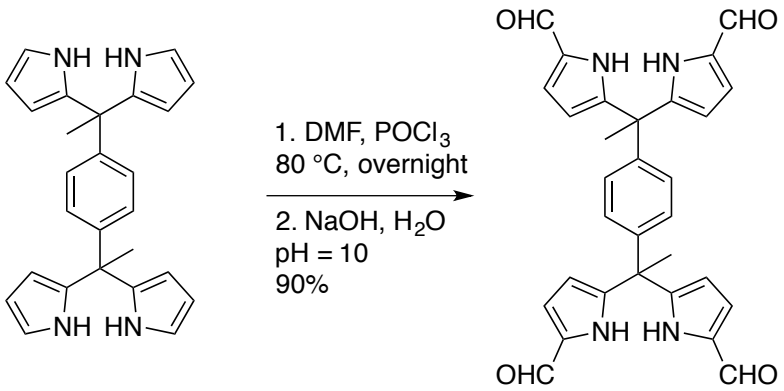

3.3a **3.3b**

5,5',5'',5'''-(1,4-Phenylenebis(ethane-1,1,1-triyl))tetrakis(1H-pyrrole-2-carbaldehyde) (**3.3b**): To a solution of **3.3a** (3.8 g, 9.6 mmol) in DMF (25 ml), $POCl_3$ (6.5 ml, 69.5 mmol) was added slowly with the vessel held in a water bath. The dark red-colored reaction mixture was allowed to stir for an hour at room temperature and then overnight at 80 °C. The mixture then was added to 100 ml water to quench the excess $POCl_3$. Aqueous NaOH (1-2 M) was added to the reaction mixture portion-wise until a pH of 10 was reached. The product precipitated out to give a solid containing an average of 2 DMF molecules per equivalent of **3.3b** (5.58 g, 90% yield), as inferred from an integration of the ^{1}H NMR spectrum and from single crystal X-ray analysis. The precipitate obtained in this way was dissolved in DMF at 80 °C and allowed to cool. This gave **3.3b**·2DMF for which the solvation was fully defined by *inter alia* a single crystal X-ray diffraction analysis (*vide infra*). The DMF present in this solid material was extracted out by sonicating the crystals in chloroform. The product (**3.3b**) was collected as white powder from the surface of the $CHCl_3$ mixture after centrifugation. ^{1}H NMR

(400 MHz, DMSO-d_6) δ 11.87 (bt, J = 2.2 Hz, 4H), 9.41 (s, 4H), 6.91 (dd, J = 3.8 Hz, J = 2.2 Hz, 4H), 6.90 (s, 4H), 5.89 (dd, J = 3.8 Hz, J = 2.3 Hz, 4H), 2.08 (s, 6H) ppm. ^{13}C NMR (100 MHz, DMSO-d_6) δ 179.5, 146.4, 145.0, 133.7, 127.2, 110.8, 45.43, 27.6 ppm. HRMS (ESI$^+$) m/z for $C_{30}H_{26}N_4O_4$ $[M+H]^+$ calcd 529.18460, found 529.18300.

Procedure-C: An alternative bisDPM synthesis

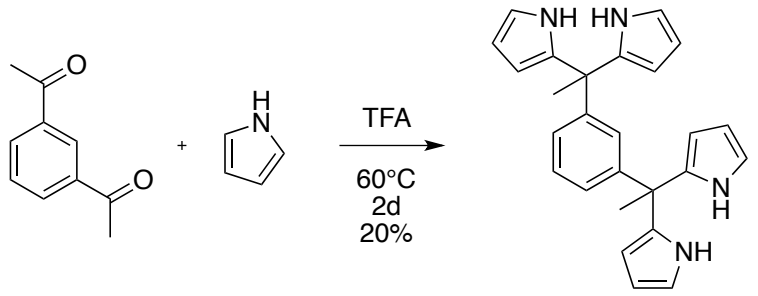

3.4c **3.4a**

1,3-Bis(1,1-di(1H-pyrrol-2-yl)ethyl)benzene (**3.4a**): 1,3-Diacetylbenzene, **3.4c**, (650 mg, 4 mmol) was dissolved in freshly distilled pyrrole (1.5 g, 20 mmol). A catalytic amount of TFA (5 drops) was then added. The mixture was stirred at 60 °C for 2 days. To the resulting mixture, 0.2 ml of TEA was added and the resulting dark green solution was heated to distill off non-reacted pyrrole. The oily crude product obtained in this way was purified by column chromatography (silica gel/dichloromethane, R_f = 0.4). Product **3.4a** was obtained in 20% yield as colorless oil. ^{1}H NMR (400 MHz, $CDCl_3$) δ 7.75 (bs, 4H), 7.19 (t, J = 7.9 Hz, 1H), 7.09 (t, J = 7.9 Hz, 1H), 6.96 (dd, J = 7.9 Hz, 2H), 6.63 (m, 4H), 6.15 (m, 4H), 5.92 (m, 4H), 2.00 (s, 6H) ppm. ^{13}C NMR (100 MHz, $CDCl_3$) δ 147.0, 137.3, 127.8, 126.8, 125.5, 116.9, 108.1, 106.2, 44.7, 28.6 ppm. HRMS (ESI$^+$) m/z for $C_{26}H_{26}N_4$ $[M+H]^+$ calcd 395.22302, found 395.22355.

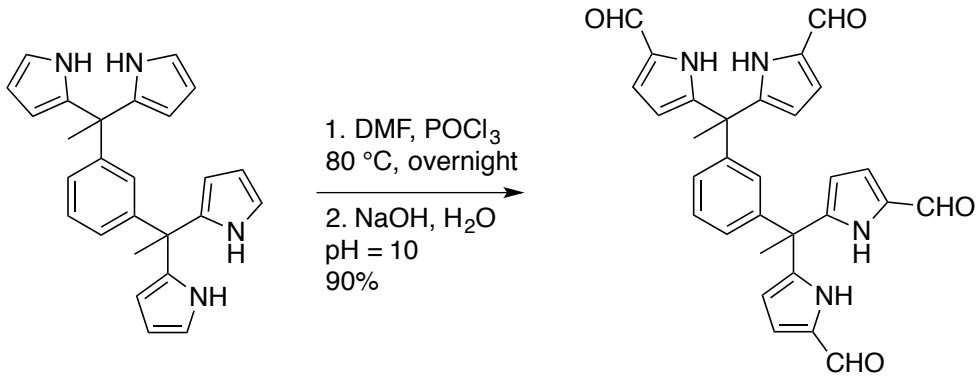

3.4a **3.4b**

5,5',5'',5'''-(1,3-Phenylenebis(ethane-1,1,1-triyl))tetrakis(1*H*-pyrrole-2-carbaldehyde) (**3.4b**): To a solution of **3.4a** (400 mg, 1 mmol) in 5 ml DMF, $POCl_3$ (0.8 ml, 8 mmol) was added slowly. Procedure-B was employed. The precipitated product was found to contain an average of 2 DMF molecules (5.58 g, 89% yield), as inferred from an integration of the ^{1}H NMR spectrum and from single crystal X-ray analysis. The precipitate was dissolved in DMF at 80 °C and allowed to cool to provide **3.4b**·2DMF as a solid. The DMF was extracted out by sonicating the crystals in diethyl ether. The resulting product was collected in the form of an off-white crystalline solid. ^{1}H NMR (400 MHz, $CDCl_3$) δ 10.48 (bs, 4H), 9.09 (s, 4H), 7.20 (t, *J* = 7.8 Hz, 1H), 7.07 (dd, *J* = 7.8 Hz, *J*=1.9 Hz, 2H), 6.98 (t, *J* = 1.9 Hz, 1H), 6.77 (dd, *J* = 4.0 Hz, *J* = 2.4 Hz, 4H), 6.01 (dd, *J* = 4.0 Hz, *J* = 2.4 Hz, 4H), 2.03 (s, 6H) ppm. ^{13}C NMR (100 MHz, $CDCl_3$) δ 179.1, 146.0, 145.0, 132.5, 128.6, 127.1, 125.5, 122.0, 110.5, 45.5, 28.0 ppm. HRMS (ESI^+) *m/z* for $C_{30}H_{26}N_4O_4$ $[M+Na]^+$ calcd 529.18460, found 529.18480.

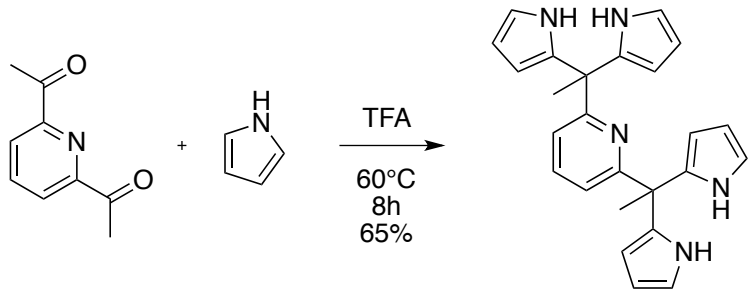

3.5c **3.5a**

2,6-Bis(1,1-di(1*H*-pyrrol-2-yl)ethyl)pyridine (**3.5a**): 2,6-Diacetylpyridine, **3.5c**, (1.0 g, 2.5 mmol) was dissolved in freshly distilled pyrrole (16.7 g, 250 mmol). A catalytic amount of TFA (10 drops) was then added. The mixture was stirred at room temperature (for one day) or at 60 °C for 8 h. Precipitation occurred. To complete precipitation, about 50 ml of methanol were added to the pale green reaction mixture. The solid obtained in this way was washed with methanol to yield 1.55 g of **3.5a** as a white solid, 65%. ^{1}H NMR (400 MHz, $CDCl_3$) δ 8.26 (bs, 4H), 7.70 (t, *J* = 7.9 Hz, 1H), 7.33 (d, *J* = 7.9 Hz, 2H), 6.57 (m, 4H), 6.14 (m, 4H), 5.89 (m, 4H), 2.11 (s, 6H) ppm. ^{13}C NMR (100 MHz, $CDCl_3$) δ 164.4, 138.4, 136.8, 117.2, 117.1, 107.9, 105.0, 45.4, 25.6 ppm. HRMS (ESI$^+$) *m/z* for $C_{25}H_{25}N_5$ $[M+Na]^+$ calcd 418.20020, found 418.20050.

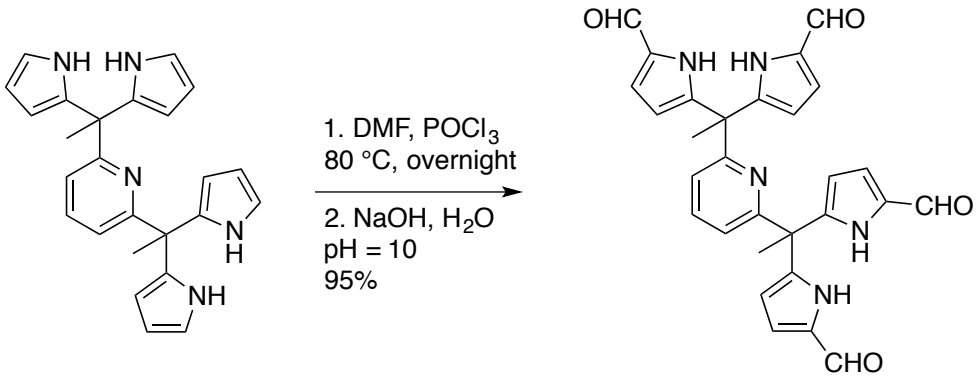

3.5a **3.5b**

5,5',5'',5'''-(Pyridine-2,6-diylbis(ethane-1,1,1-triyl))tetrakis(1*H*-pyrrole-2-carbaldehyde) (**3.5b**): To a solution of **3.5a** (370 mg, 0.94 mmol) in 5 ml DMF, $POCl_3$ (0.5 ml, 5.3 mmol) was added slowly in accord with procedure-B. The compound **3.5b** precipitates as off white/yellow solid (450 mg, 0.89 mmol). After purification by column chromatography (silica gel/EtOAc), product **3.5b** was obtained as a yellow powder by treating the appropriate fractions with diethyl ether. The yield was 95% yield. ^{1}H NMR (400 MHz, $CDCl_3$) δ 10.09 (bs, 4H), 9.29 (s, 4H), 7.68 (t, *J* = 7.9 Hz, 1H), 7.20 (d, *J* = 7.9 Hz, 2H), 6.85 (dd, *J* = 3.9 Hz, *J* = 2.5 Hz, 4H), 6.09 (d, *J* = 3.9 Hz, *J* = 2.5 Hz, 4H), 2.16 (s, 6H) ppm. ^{13}C NMR (100 MHz, $CDCl_3$) δ 179.1, 161.9, 144.8, 138.3, 132.6, 121.7, 120.2, 110.2, 47.4, 27.1 ppm. HRMS (ESI$^+$) *m/z* for $C_{29}H_{25}N_5O_4$ $[M+Na]^+$ calcd 530.17990, found 530.18010.

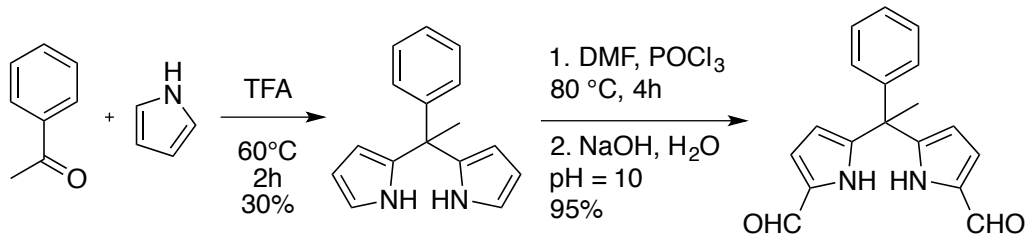

3.13c **3.13a** **3.13**

5,5'-(1-Phenylethane-1,1-diyl)bis(1*H*-pyrrole-2-carbaldehyde) (**3.13**): Acetophenone, **3.13c**, (1.5 g, 12.5 mmol) was dissolved in pyrrole (18 g, 270 mmol). Procedure-C was used. The product was characterized and the analytical data were found to match the literature.[21] DPM **3.13a** was passed through silica gel using dichloromethane as the eluent and dried *in vacuo* to afford yellow oil, **3.13a.** This was used to obtain **3.13** *via* procedure-B. The precipitated product, **3.13**, was collected and purified by column chromatography (silica gel/EtOAc). After removal of the volatiles, product **3.13** was

obtained as white solid. The recorded ^{1}H NMR spectrum was in agreement with that reported in the literature.[22]

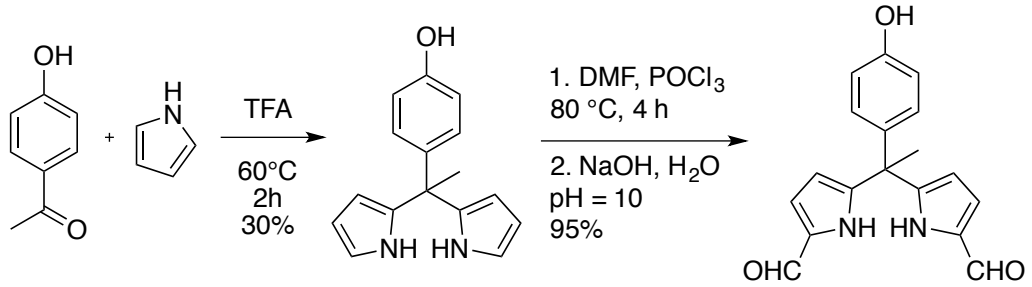

2.7b **2.8b** **2.9b**

5,5'-(1-(4-hydroxyphenyl)ethane-1,1-diyl)bis(1*H*-pyrrole-2-carbaldehyde) (**2.9b)**: Compound **2.9b** was prepared similarly. It was further described in Chapter-2. ^{1}H NMR (300 MHz, CD_3OD residual solvent peak set to 3.31 ppm) δ 9.33 (s, 2H), 6.94 (d, J = 4.0 Hz, 2H), 6.88 (m, 2H), 6.73 (m, 2H), 6.01 (d, J = 4.0 Hz, 2H), 2.09 (s, 3H) ppm. ^{13}C NMR (75 MHz, CD_3OD solvent peak set to 49.0 ppm) δ 180.6, 157.4, 148.4, 137.5, 134.2, 129.4, 116.0, 111.7, 46.2, 28.3 ppm. HRMS (ESI) calcd for $C_{18}H_{16}N_2O_3$ $(M+H)^+$ 309.12387, found 309.12337.

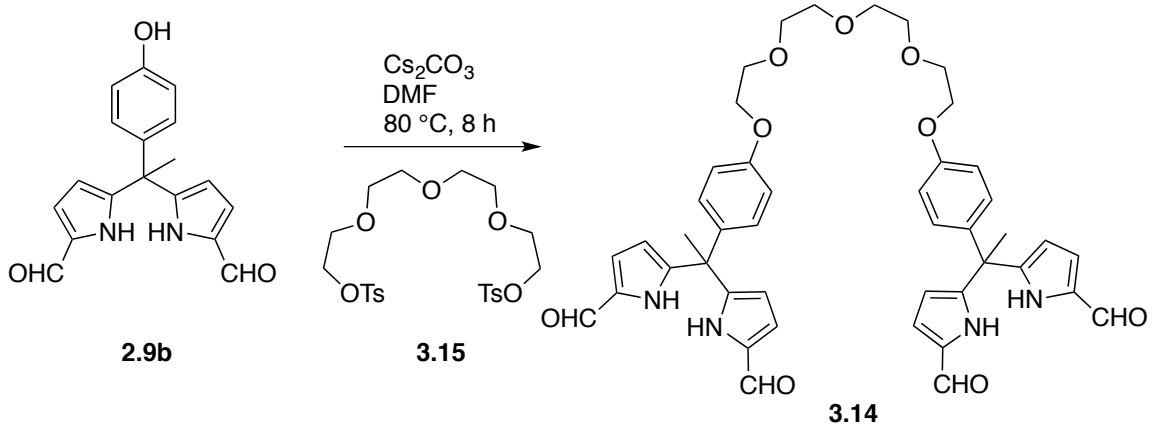

2.9b **3.15** **3.14**

5,5',5",5"'-((((((Oxybis(ethane-2,1-diyl))bis(oxy))bis(ethane-2,1-diyl))bis(oxy))bis(4,1-phenylene))bis(ethane-1,1,1-triyl))tetrakis(1H-pyrrole-2-carbaldehyde) (**3.14**): Compound **2.9b** (310 mg, 1 mmol) and Cs_2CO_3 (390 mg; 1.2

mmol, 1.2 equiv) were dissolved in DMF (5 ml). The mixture was stirred for an hour. To this solution, one half of a molar equivalent of tetraethyleneglycol ditosylate, **3.15**, (250 mg, 0.5 mmol) was added. The resulting mixture was stirred overnight at 80 °C. Excess DMF was then removed under reduced pressure. The resulting oily crude product was purified by column chromatography (silica gel/EtOAc, R_f = 0.7) to give a yellow oil. Treatment with diethyl ether then gave **3.14** as a yellow powder in 85% yield. ^{1}H NMR (400 MHz, $CDCl_3$) δ 10.07 (bs, 4 H), 9.33 (s, 4 H), 6.92 (d, *J* = 8.9 Hz, 4 H), 6.89 (dd, J = 3.9 Hz, J = 2.4 Hz, 4H), 6.80 (d, J = 8.9 Hz, 4 H), 6.17 (dd, J = 3.9 Hz, J = 2.4 Hz, 4 H), 4.09 (dd, J = 5.2 Hz, J = 4.6 Hz, 4H), 3.87 (dd, J = 5.2 Hz, J = 4.6 Hz, 4 H), 3.68 (m, 8 H), 2.06 (s, 6 H) ppm. ^{13}C NMR (100 MHz, $CDCl_3$) δ 178.9, 157.4, 146.1, 137.0, 132.6, 128.2, 121.2, 114.5, 110.3, 70.8, 70.7, 69.7, 67.4, 44.9, 28.6 ppm. HRMS (ESI^+) *m/z* for $C_{44}H_{46}O_9$ $[M+Na]^+$ calcd 797.31570, found 797.31670.

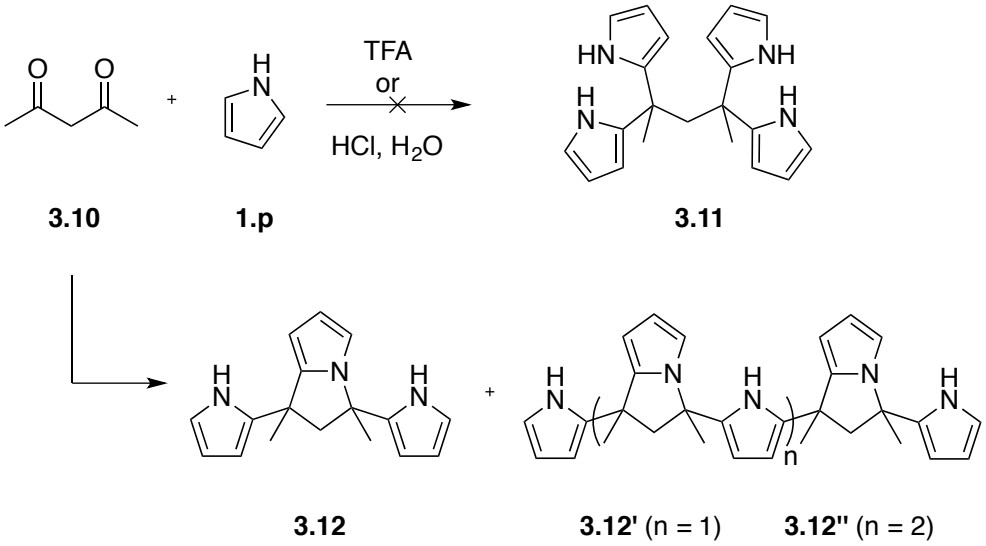

Compound **3.12** was isolated from the reaction of **3.10** in accord with procedure-C. ^{1}H NMR (400 MHz, $CDCl_3$) δ 7.94 (bs, 1H), 7.30 (bs, 1H), 6.55 (m, 2H), 6.36 (m, 1H), 6.31 (t, *J* = Hz, 1H), 6.17 (q, *J* = Hz, 1H), 6.09 (m, 1H), 6.06 (m, 1H), 6.01 (q, *J* =

Hz, 1H), 5.97 (dd, *J* = Hz, *J* = Hz, 1H), ^{13}C NMR (100 MHz, $CDCl_3$) δ 140.6, 138.3, 135.7, 117.8, 116.2, 113.1, 111.7, 109.1, 107.6, 104.8, 103.7, 98.4, 60.9, 60.8, 41.6, 30.3, 28.6 ppm. HRMS (ESI$^+$) *m*/*z* calcd. for $C_{17}H_{19}N_3$ $[M+H]^+$ 266.16520, found 266.16510. For **3.12'** HRMS (ESI$^+$) *m*/*z* calcd. for $C_{30}H_{33}N_5$ $[M+H]^+$ 464.28090, found 464.28100.

3.5.2. Studies by UV-Vis spectroscopy

All binding studies reported in Table 3.2 were carried out in commercially available Fisher Scientific $CHCl_3$ containing approximately 0.75% ethanol as a preservative. To observe better the absorbance changes, various initial receptor concentrations were chosen to obtain an A_{max} (maximum absorption) for each individual receptor (**3.3b**–**3.5b**) of 0.9. All anions were studied in the form of their commercially available tetra-*n*-butylammonium salts.

A match to a theoretical binding curve may be obtained for titration experiments wherein;

$[receptor]_o = [receptor] + [receptor\text{-}guest]$

The following equation was derived and used to determine the binding affinities:

$$\Delta A = \frac{1 + aK + xK - \sqrt{-4axK^2 + (-1 - aK - xK)^2}}{2K} \Delta\varepsilon$$

where,

ΔA (measured change in absorbance relative to the initial solution) is the y variable;

x is concentration of guest (TBA^+ anion salt) added;

a is the initial concentration of receptor (remains constant over the course of titration);

$\Delta\varepsilon$ is the extinction coefficient difference between free receptor and receptor-guest complex ($\Delta\varepsilon = \varepsilon_{complex} - \varepsilon_{receptor}$);

K is the binding affinity (K_a) of the receptor under analysis for the guest in question.

OriginPro 9.0 was used to fit data in a non-linear fashion in accord with the above equation. Iterations (choosing a fixed a value and changing $\Delta\varepsilon$ and K) were performed until an acceptable level of convergence was reached (chi-square tolerance value, $1x10^{-9}$).

The stoichiometry of binding was determined by the Job plot method.

Job plot method-1:

$[receptor]_{stock} = [guest]_{stock}$

The total concentration of the receptor and the salt of interest was kept constant by varying the fraction of receptor from 0 to 1. (under these conditions, all mixtures obtained by mixing receptor and guest stock solutions have the same numerical concentration value)

[receptor] + [guest] = constant

Job plot method-2:

Data from titrations carried out to determine the binding affinities were used. Experimentally,

[receptor] = constant

Conversion of the data so that

[receptor] + [guest] = constant

This conversion is formulized in the Excel formula sheet (*cf*. Table 3.8).

	A	B	C	D	E	F	G	H
1	$[receptor]_o$	1.19E-05				if Ct	if Ct	if Ct
2				at λ_{max}	at λ_{max}	=$B$1	=$B$1	=$B$1
3	$[anion]_o$	Ct	X_{anion}	A	ΔA	A_{total}	$A_{receptor}$	ΔA
4	0	=$B$1+A4	=A4/B4	0.91	=D5/$D$5	=D4*$F$2/B4	=$D$4*(1-C4)	=F4-G4

Table 3.8: Job plot method-2: Excel formula sheet to obtain a Job plot using data obtained from titrations carried out to determine the binding affinities.

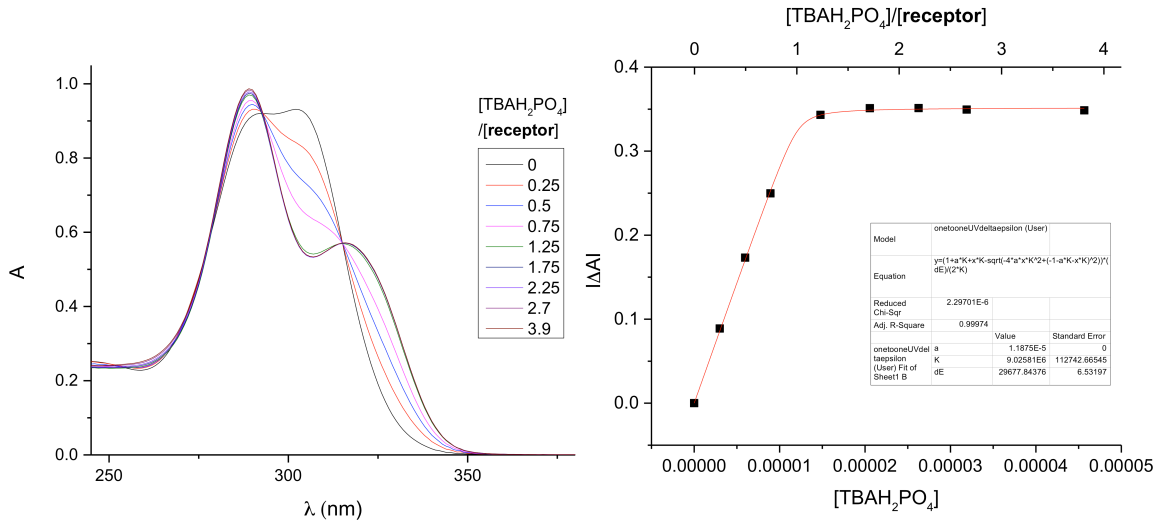

Figure 3.22: Left) Stacked UV-Vis spectra corresponding to the titration of **3.3b** (1.2 x 10^{-5} M) with $TBAH_2PO_4$ (1.0 x 10^{-3} M) in $CHCl_3$. Right) Binding curve and fit plotted using data from plot (on the left) monitored at 306 nm. K_a = (8 ± 2) x 10^6 M^{-1}.

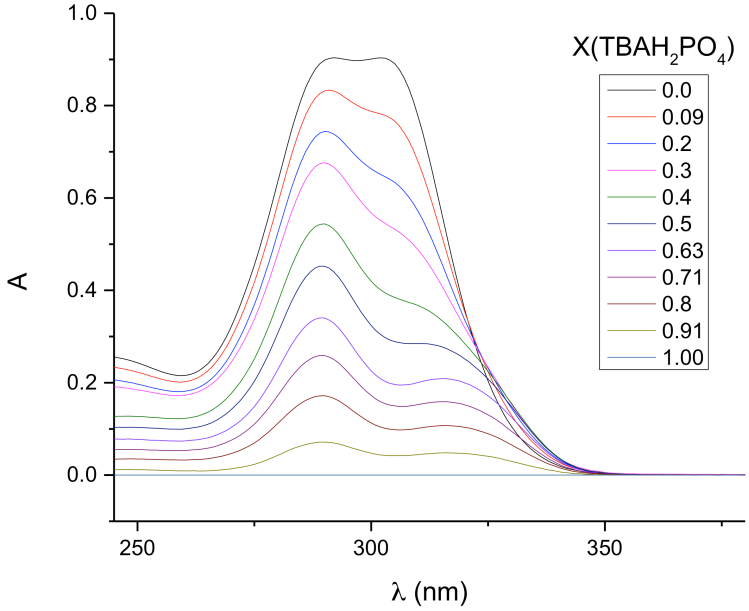

a)

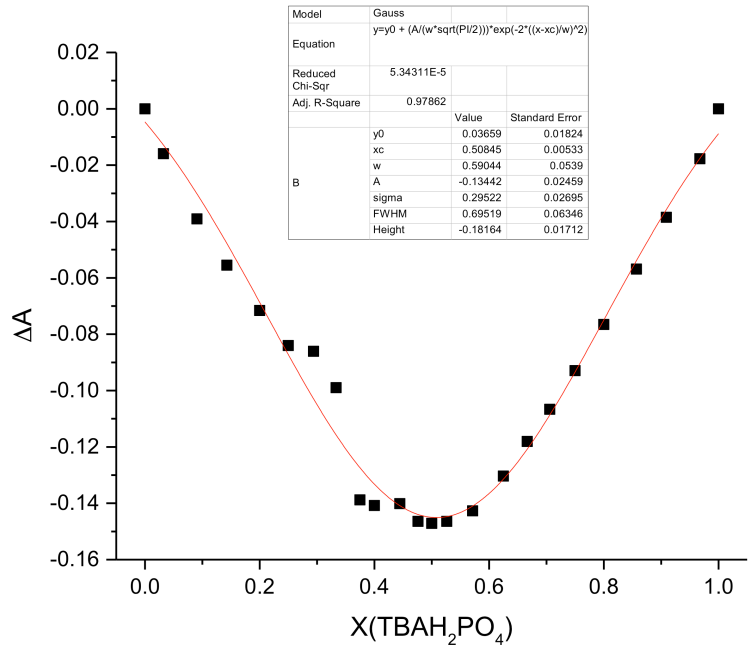

b)

Figure 3.23: a) UV-Vis spectra used to construct a Job plot of the interaction of **3.3b** with $TBAH_2PO_4$ in $CHCl_3$. ([**3.3b**] + [$TBAH_2PO_4$] = 1.2 x 10^{-5} M). b) Job plot from the data (a) monitored at 306 nm.

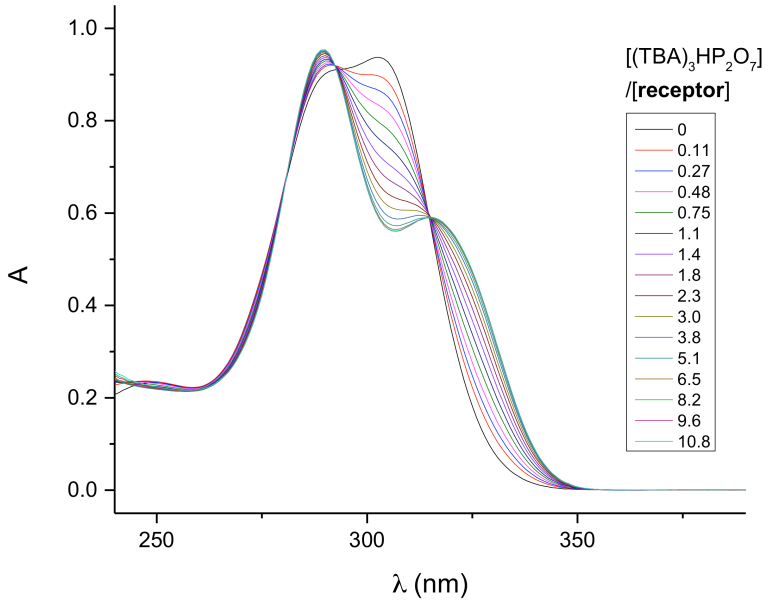

a)

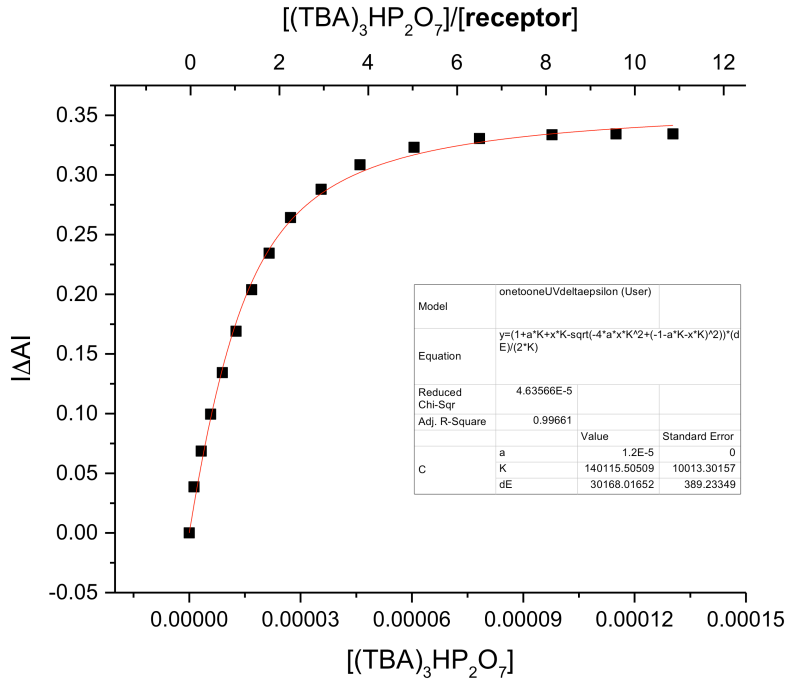

b)

Figure 3.24: a) Stacked UV-Vis spectra corresponding to the titration of **3.3b** (1.2×10^{-5} M) with $(TBA)_3HP_2O_7$ (3.9×10^{-4} M) in $CHCl_3$. b) Binding curve and fit plotted using data from (a) monitored at 306 nm. $K_a = (1.4 \pm 0.1) \times 10^5$ M^{-1}.

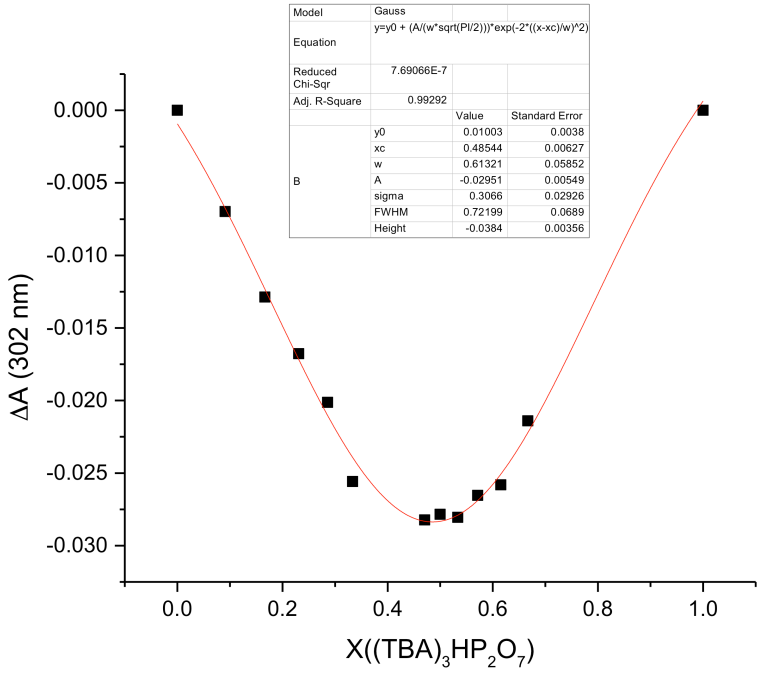

Figure 3.25: Job plot of the interaction of **3.3b** with $(TBA)_3HP_2O_7$ in $CHCl_3$, monitored at 306 nm. ([**3.3b**] + [$(TBA)_3HP_2O_7$] = 1.2 x10^{-5} M).

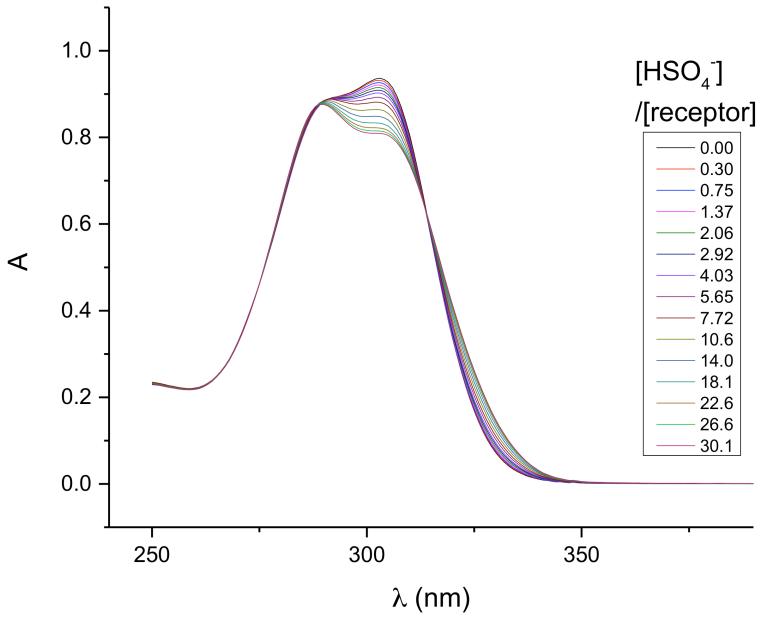

a)

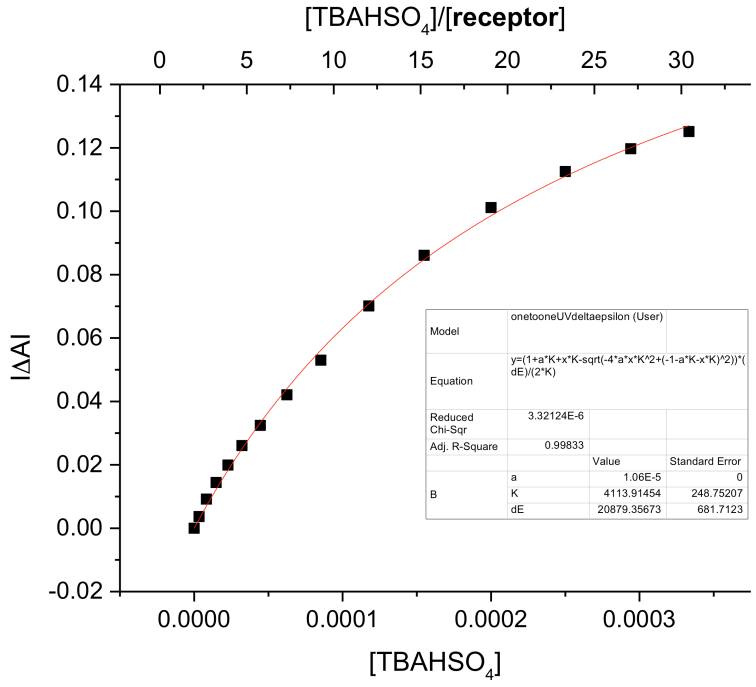

b)

Figure 3.26: a) Stacked UV-Vis spectra corresponding to the titration of **3.3b** (1.2×10^{-5} M) with $TBAHSO_4$ in $CHCl_3$. b) Binding curve and fit plotted using data from (a). $K_a = (4.1 \pm 0.2) \times 10^3\ M^{-1}$.

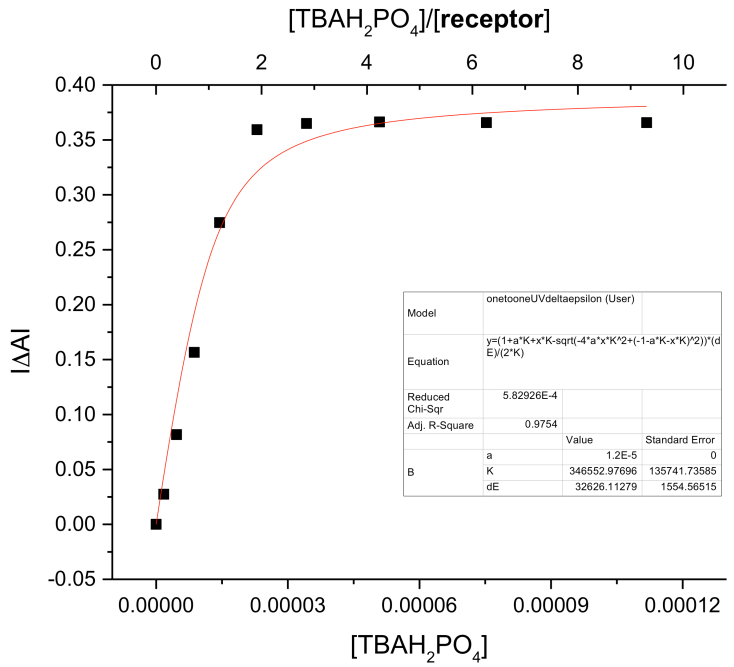

a)

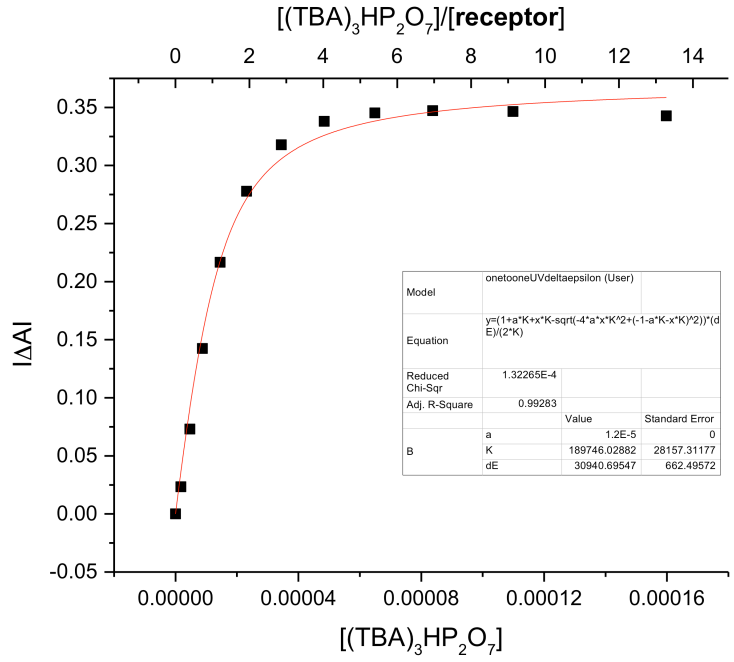

b)

Figure 3.27: a) Binding curve and fit corresponding to the titration of **3.4b** with $TBAH_2PO_4$ ($K_a = (8 \pm 2) \times 10^6\ M^{-1}$). b) Binding curve and fit corresponding to the titration of **3.4b** with $(TBA)_3HP_2O_7$ ($K_a = (1.9 \pm 0.3) \times 10^5\ M^{-1}$).

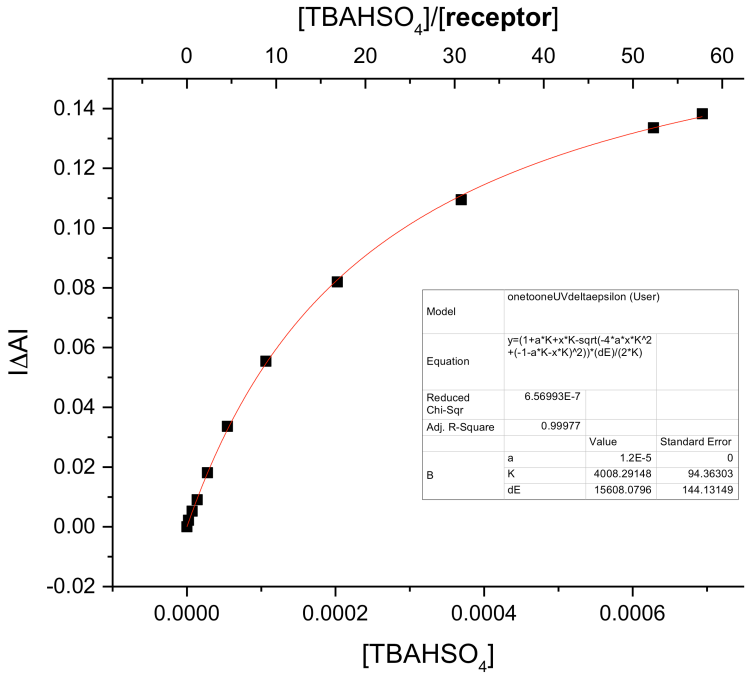

a)

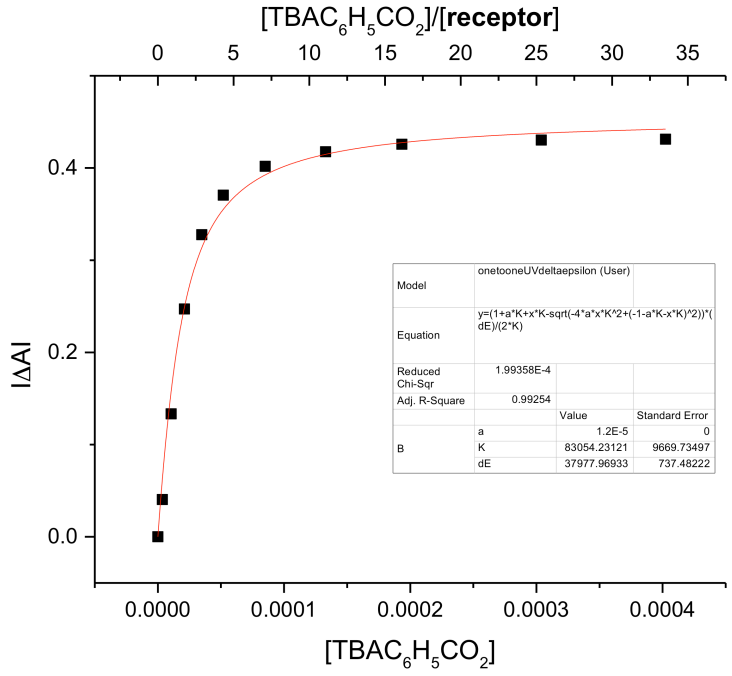

b)

Figure 3.28: a) Binding curve and fit corresponding to the titration of **3.4b** with $TBAHSO_4$ (K_a = (4.00 ± 0.09) x10^3 M^{-1}). b) Binding curve and fit corresponding to the titration of **3.4b** with $TBAC_6H_5CO_2$ (K_a = (8 ± 1) x10^4 M^{-1}).

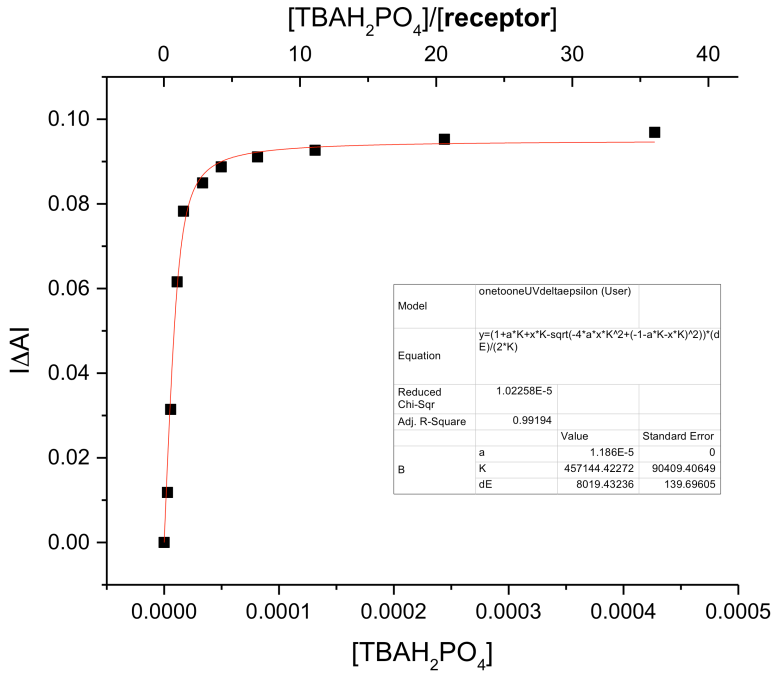

a)

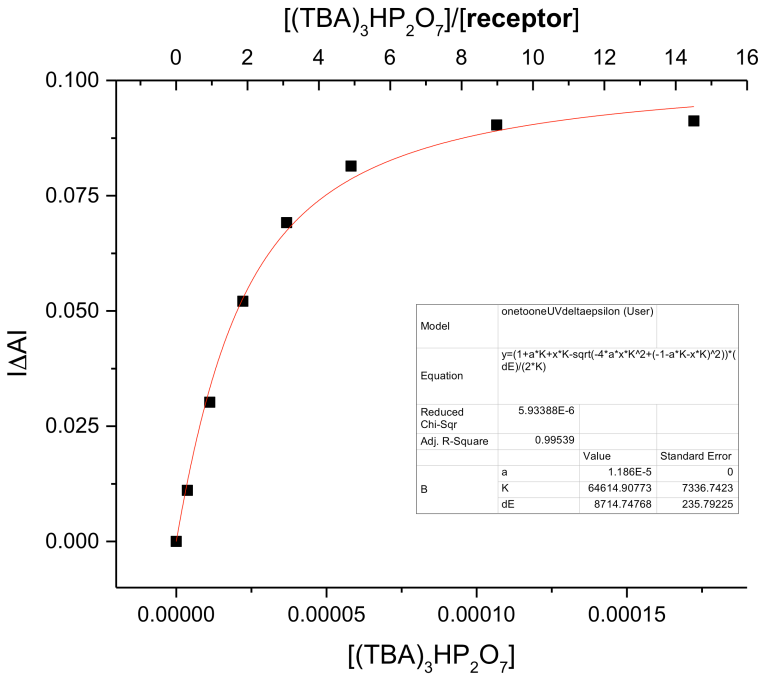

b)

Figure 3.29: a) Binding curve and fit corresponding to the titration of **3.5b** with $TBAH_2PO_4$ ($K_a = (4.6 \pm 0.9) \times 10^5\ M^{-1}$). b) Binding curve and fit corresponding to the titration of **3.5b** with $(TBA)_3HP_2O_7$ ($K_a = (6.5 \pm 0.7) \times 10^4\ M^{-1}$).

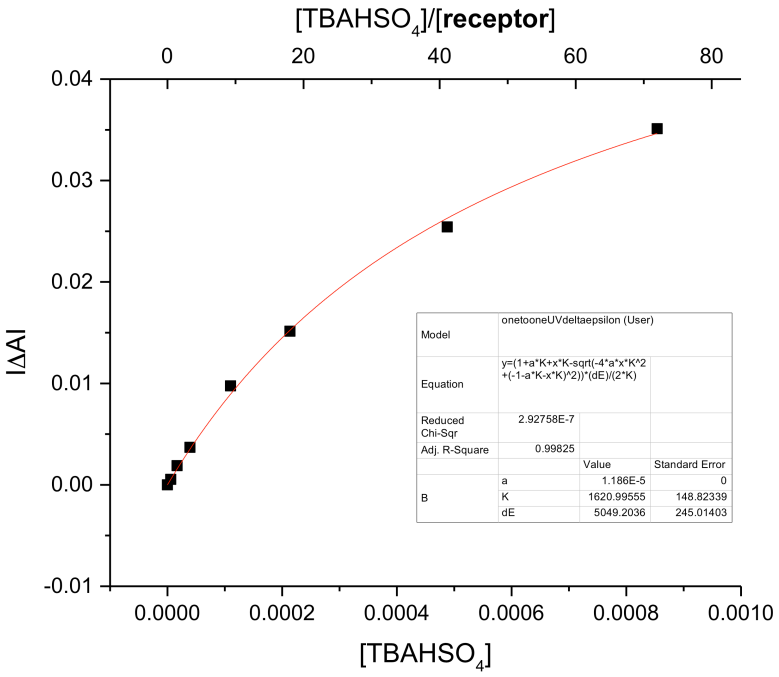

a)

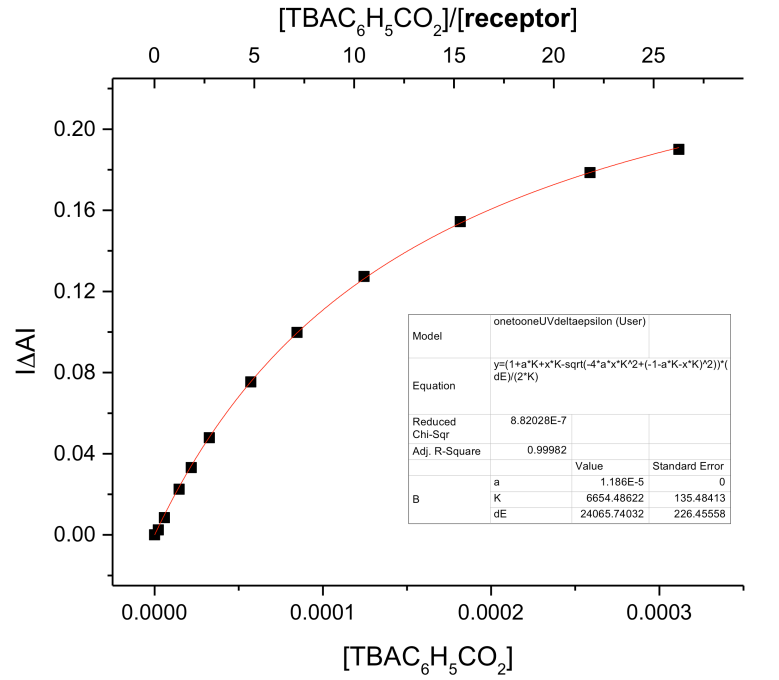

b)

Figure 3.30: a) Binding curve and fit corresponding to the titration of **3.5b** with $TBAHSO_4$ (K_a = (1.6 ± 0.1) x 10^3 M^{-1}). b) Binding curve and fit corresponding to the titration of **3.5b** with $TBAC_6H_5CO_2$ (K_a =(6.7 ± 0.1) x 10^3 M^{-1}).

3.5.3. Studies by ^{1}H NMR spectroscopy

All binding affinities reported in Table 3.4 and Table 3.5 were carried out in commercially available Cambridge Isotope Laboratories, Inc. $CDCl_3$ (D, 99.8%) and DMSO-d_6 (D, 99.9%). All spectra were recorded at 400 MHz using Varian or Agilent instruments. Various initial receptor concentrations were chosen based on their solubilities *i.e.*, 1.0 mM in $CDCl_3$ or 10 mM in $CDCl_3$/DMSO-d_6 (8/1). All anions were studied in the form of their commercially available TBA^+ salts. In the case of titrations carried out with the intention of determining binding affinities, the receptor concentration was kept constant throughout the titration study. This was done by preparing the TBA^+ anion salt solutions within these study-stock solutions of the receptor solution and using these solutions for the titrations. The following equation was used to determine the binding affinities

$$\Delta\delta = \frac{1 + aK + xK - \sqrt{-4axK^2 + (-1 - aK - xK)^2}}{2aK} (\delta_{complex} - \delta_{host})$$

where,

$\Delta\delta$ (measured change in the chemical shift of the hydrogen signal of interest relative to the chemical shift of the same signal in receptor) is the y variable;

x is concentration of guest (TBA^+ salt) added;

a is the initial concentration of receptor (remains constant over the course of titration);

$\delta_{complex}$ is the chemical shift of the hydrogen of interest in receptor-guest complex (*e.g.* **3.3b**·$H_2PO_4^-$) and

δ_{host} is the chemical shift of the same hydrogen of interest in receptor;

K is the binding affinity (K_a) of receptor for the guest in question.

OriginPro 9.0 was used to fit data in a non-linear fashion in accord with the above equation. Iterations (choosing a fixed a value and changing $\delta_{complex}$-δ_{host} and K) were performed until an acceptable level of convergence was reached (chi-square tolerance value, $1x10^{-9}$).

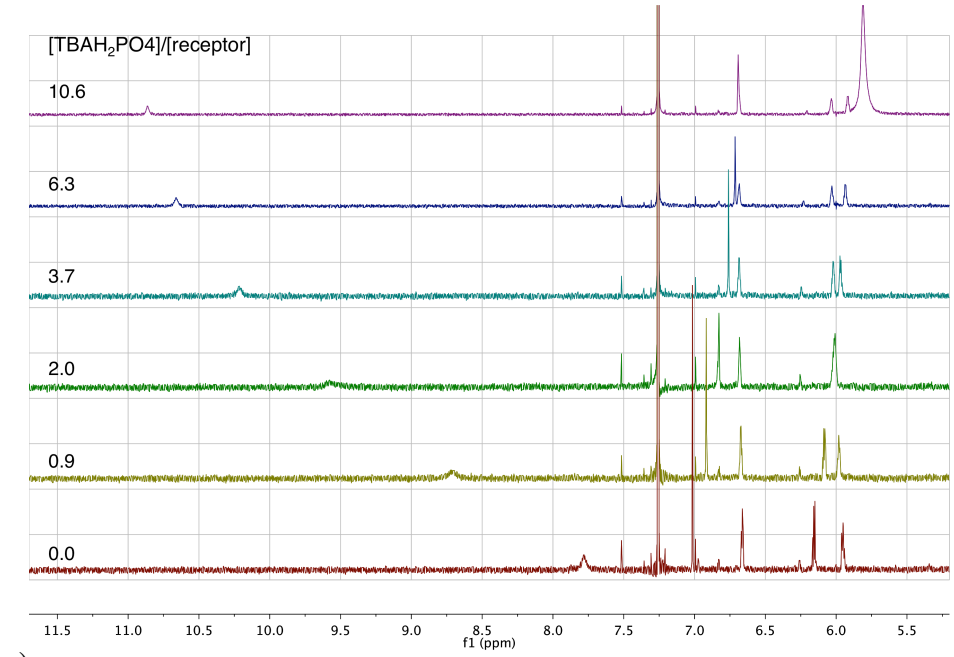

a)

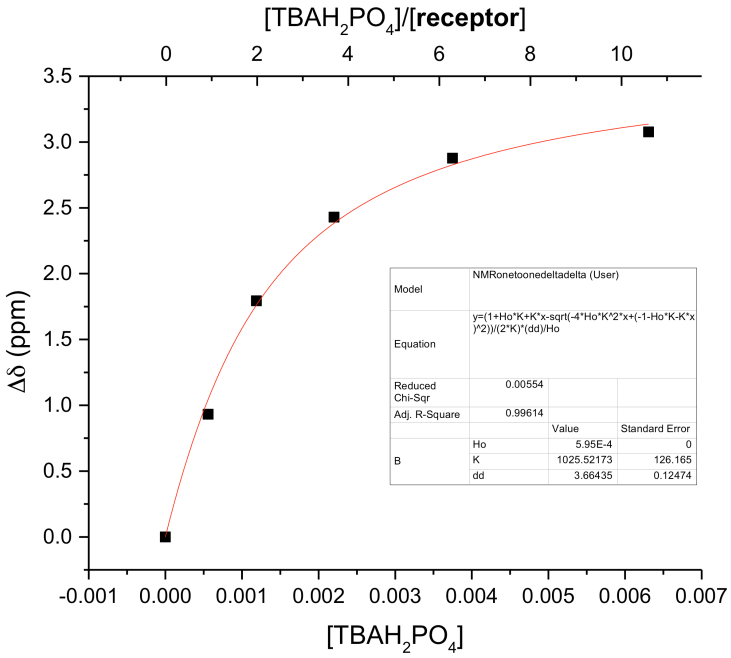

b)

Figure 3.31: a) Stacked ^{1}H NMR spectra corresponding to the titration of **3.3a** (0.6 mM) with $TBAH_2PO_4$ (2.2 mM) in $CDCl_3$. b) Binding curve obtained by fitting the chemical shift change of the pyrrole NH signal against [$TBAH_2PO_4$]. K_a = 1026 ± 126 M^{-1}.

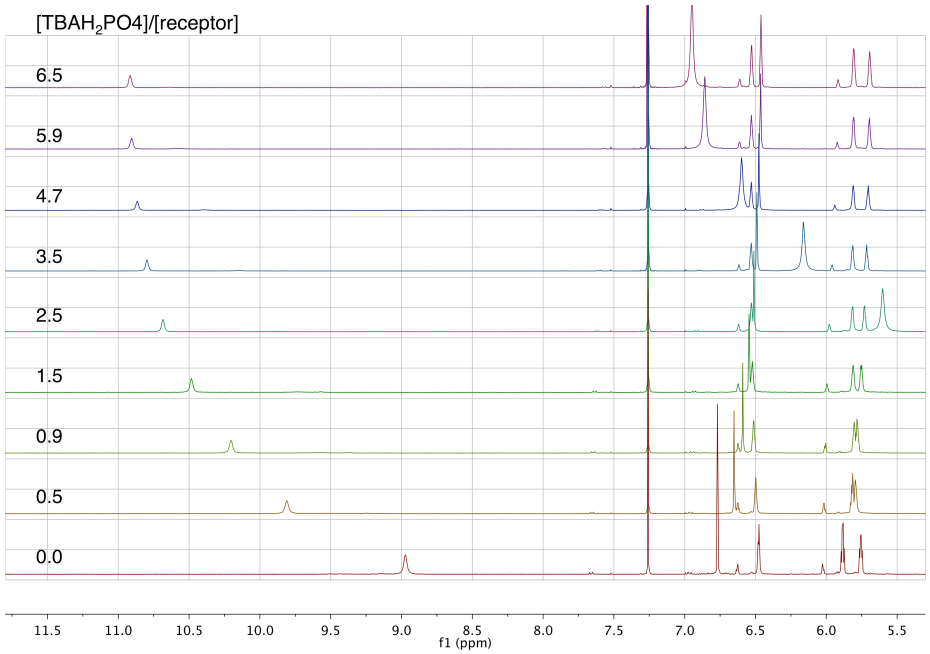

a)

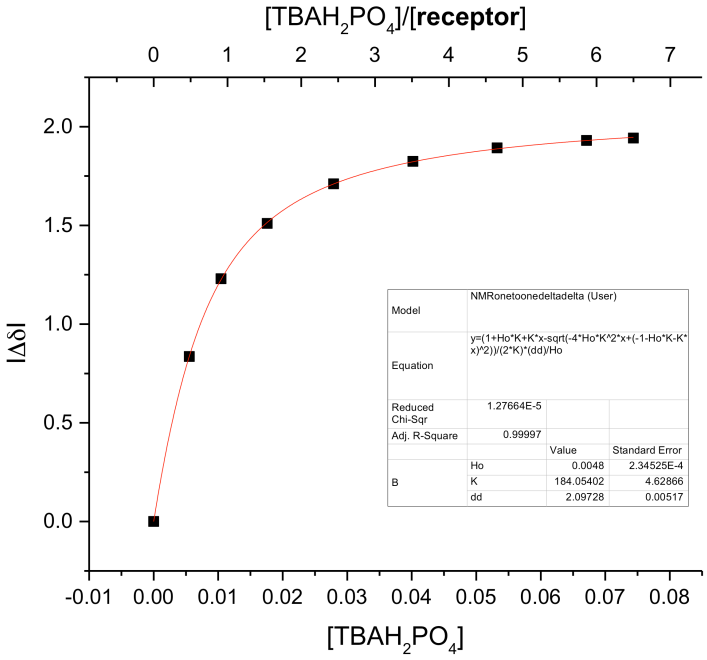

b)

Figure 3.32: a) Stacked ^{1}H NMR spectra corresponding to the titration of **3.3a** (11.4 mM) with $TBAH_2PO_4$ (97.6 mM) in $CDCl_3$/DMSO-d_6 (8:1). b) Binding curve obtained by fitting the chemical shift change of the pyrrole NH signal against [$TBAH_2PO_4$]. K_a = 184 ± 5 M^{-1}.

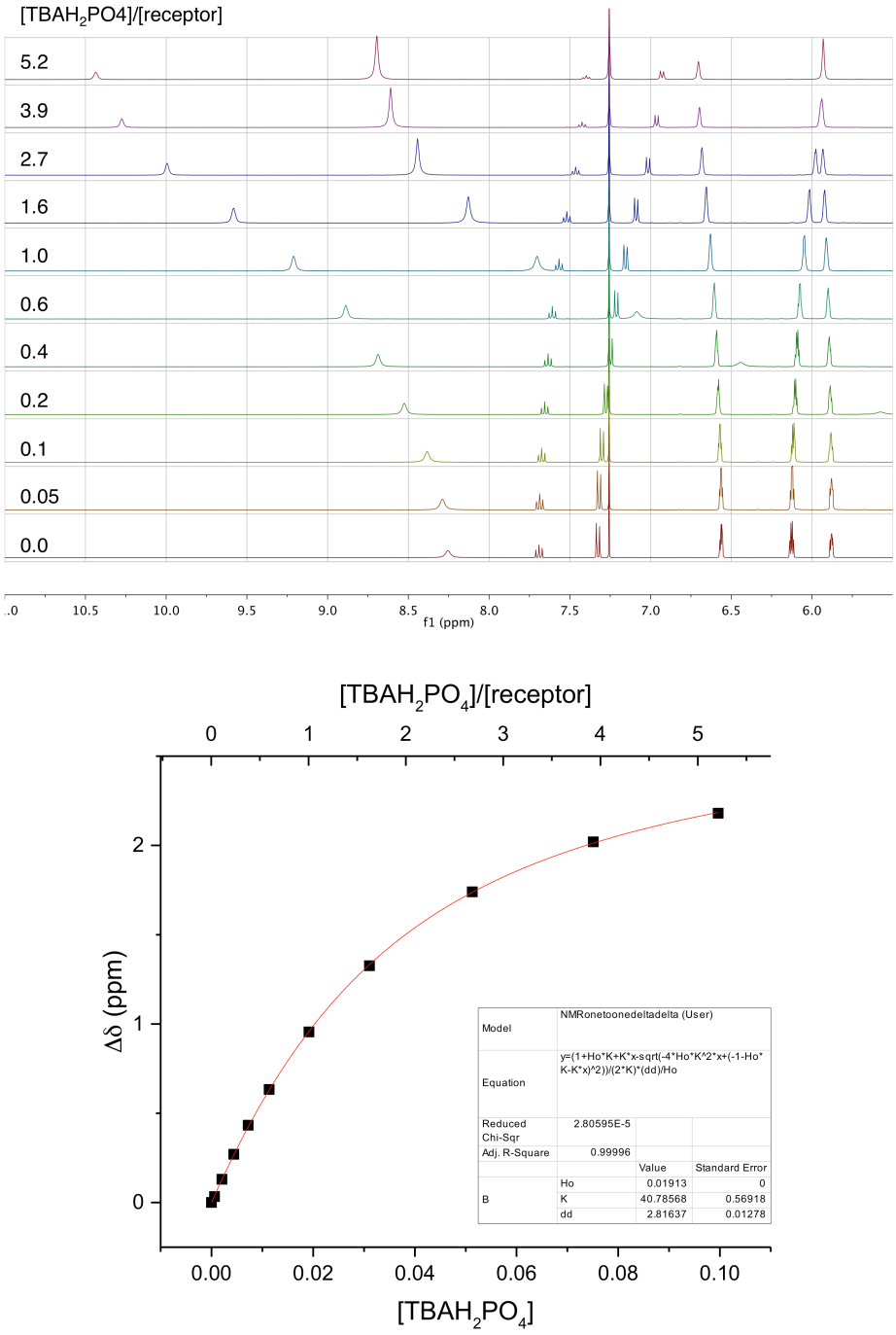

Figure 3.33: Stacked ^{1}H NMR spectra corresponding to the titration of **3.5a** (19.1 mM) with $TBAH_2PO_4$ (0.235 M) in $CDCl_3$. Binding curve obtained by fitting the chemical shift change of the pyrrole NH signal against [$TBAH_2PO_4$]. K_a = 40.8 ± 0.6 M^{-1}.

3.6. REFERENCES

1. Baeyer, A. Ueber Ein Condensationsproduct von Pyrrol Mit Aceton. *Berichte der Dtsch. Chem. Gesellschaft* **1886**, *19* (2), 2184–2185.
2. Gale, P. A.; Sessler, J. L.; Kral, V.; Lynch, V. Calix[4]pyrroles: Old yet New Anion-Binding Agents. *J. Am. Chem. Soc.* **1996**, *118* (21), 5140–5141.
3. Custelcean, R.; Delmau, L. H.; Moyer, B. A.; Sessler, J. L.; Cho, W.-S.; Gross, D.; Bates, G. W.; Brooks, S. J.; Light, M. E.; Gale, P. A. Calix[4]pyrrole: An Old yet New Ion-Pair Receptor. *Angew. Chem. Int. Ed.* **2005**, *44* (17), 2537–2542.
4. Gross, D. E.; Schmidtchen, F. P.; Antonius, W.; Gale, P. A.; Lynch, V. M.; Sessler, J. L. Cooperative Binding of calix[4]pyrrole-Anion Complexes and Alkylammonium Cations in Halogenated Solvents. *Chem. Eur. J.* **2008**, *14*, 7822–7827.
5. Cho, W.-S. Oligopyrrole-Based Anion Receptors, The University of Texas at Austin, 2005.
6. Sessler, J. L.; Cho, W.-S.; Dudek, S. P.; Hicks, L.; Lynch, V. M.; Huggins, M. T. Synthesis and Study of a Calixpyrrole-Texaphyrin Chimera: A New Oligopyrrolic Chloride Anion Receptor. *J. Porphyr. Phthalocyanines* **2003**, *07* (02), 97–104.
7. Sessler, J. L.; Camiolo, S.; Gale, P. A. Pyrrolic and Polypyrrolic Anion Binding Agents. *Coord. Chem. Rev.* **2003**, *240* (1–2), 17–55.
8. Deliomeroglu, M.; Lynch, V.; Sessler, J. Conformationally Switchable Non-Cyclic Tetrapyrrole Receptors: Synthesis of tetrakis(1*H*-Pyrrole-2-Carbaldehyde) Derivatives and Their Anion Binding Properties. *Chem. Commun.* **2014**, *50* (80), 11863–11866.
9. Lee, C.-H.; S. Lindsey, J. One-Flask Synthesis of Meso-Substituted Dipyrromethanes and Their Application in the Synthesis of Trans-Substituted Porphyrin Building Blocks. *Tetrahedron* **1994**, *50* (39), 11427–11440.
10. Zhao, H.; Liao, J.; Ning, J.; Xie, Y.; Cao, Y.; Chen, L.; Yang, D.; Wang, B. Efficient Synthesis of Novel Bis(dipyrromethanes) with Versatile Linkers via Indium(III) Chloride-Catalyzed Condensation of Pyrrole and Dialdehydes. *Adv. Synth. Catal.* **2010**, *352* (17), 3083–3088.
11. Anand, V. G.; Saito, S.; Shimizu, S.; Osuka, A. Internally 1,4-Phenylene-Bridgedmeso Aryl-Substituted Expanded Porphyrins: The Decaphyrin and Octaphyrin Cases. *Angew. Chem. Int. Ed.* **2005**, *44* (44), 7244–7248.
12. Arumugam, N.; Chung, W.-Y.; Lee, S.-W.; Lee, C.-H. Synthesis and Structure of 1,4-Bis((α,α'-Dipyrrylmethyl)cyclohexane. *Bull. Korean Chem. Soc.* **2001**, *22* (8), 932–934.

13. Mahanta, S. P.; Kumar, B. S.; Panda, P. K. Meso-Diacylated Calix[4]pyrrole: Structural Diversities and Enhanced Binding towards Dihydrogenphosphate Ion. *Chem. Commun.* **2011**, *47* (15), 4496–4498.

14. Mahanta, S. P.; Panda, P. K. Unusual Ring Annulation during Condensation of Acetylacetone with Pyrrole. *Tetrahedron Lett.* **2009**, *50* (8), 890–892.

15. Mahanta, S. P.; Panda, P. K. Interesting Reactivity of Diketones with Pyrrole under Acidic Condition. *J. Chem. Sci.* **2011**, *123* (5), 593–599.

16. McEwen, C. N.; Larsen, B. S. Ionization Mechanisms Related to Negative Ion APPI, APCI, and DART. *J. Am. Soc. Mass Spectrom.* **2009**, *20* (8), 1518–1521.

17. Custelcean, R. Anions in Crystal Engineering. *Chem. Soc. Rev.* **2010**, *39* (10), 3675–3685.

18. Bill, N. L.; Kim, D.-S.; Kim, S. K.; Park, J. S.; Lynch, V. M.; Young, N. J.; Hay, B. P.; Yang, Y.; Anslyn, E. V.; Sessler, J. L. Oxoanion Recognition by Benzene-Based Tripodal Pyrrolic Receptors. *Supramol. Chem.* **2012**, *24* (1), 72–76.

19. Cai, J.; Hay, B. P.; Young, N. J.; Yang, X.; Sessler, J. L. A Pyrrole-Based Triazolium-Phane with NH and Cationic CH Donor Groups as a Receptor for Tetrahedral Oxyanions That Functions in Polar Media. *Chem. Sci.* **2013**, *4* (4), 1560–1567.

20. Král, V.; Furuta, H.; Shreder, K.; Lynch, V.; Sessler, J. L. Protonated Sapphyrins. Highly Effective Phosphate Receptors. *J. Am. Chem. Soc.* **1996**, *118* (7), 1595–1607.

21. Laha, J. K.; Dhanalekshmi, S.; Taniguchi, M.; Ambroise, A.; Lindsey, J. S. A Scalable Synthesis of Meso-Substituted Dipyrromethanes. *Org. Process Res. Dev.* **2003**, *7* (6), 799–812.

22. Love, J. B.; Blake, A. J.; Wilson, C.; Reid, S. D.; Novak, A.; Hitchcock, P. B. The Syntheses and Structures of Group 1 Expanded Dipyrrolides: The Formation of a 12-Rung Amidolithium Circular Ladder. *Chem. Commun.* **2003**, (14), 1682–1683.

23. Neufeld, R.; Stalke, D. Accurate Molecular Weight Determination of Small Molecules via DOSY-NMR by Using External Calibration Curves with Normalized Diffusion Coefficients. *Chem. Sci.* **2015**, *6* (6), 3354–3364.

24. Gil-Ramírez, G.; Escudero-Adán, E. C.; Benet-Buchholz, J.; Ballester, P. Quantitative Evaluation of Anion-π Interactions in Solution. *Angew. Chem. Int. Ed.* **2008**, *47* (22), 4114–4118.

4. An Electroactive and a Binding-site Enriched Formylated-dipyrromethane Receptors

In Chapter 3, evidence was put forward that the bisDPM **3.3a** was a better receptor for $H_2PO_4^-$ than octamethylcalix[4]pyrrole **1.10** (K_a = 10^3 vs 10^2 M^{-1} in $CHCl_3$ and CH_2Cl_2, respectively).[1,2] Moreover, particularly high $H_2PO_4^-$ anion affinities were recorded for the four-fold formylated derivative of **3.3a**, receptor **3.3b** (K_a = (8 ± 2) x 10^6 M^{-1} in $CHCl_3$).[1] Presumably, this increased $H_2PO_4^-$ affinity reflects the favorable electronic changes induced as a result of formylation of **3.3a**. To exploit the binding characteristics of the diformyl-DPM receptors from Chapter 3, an electro-active analogue of the tetrakis(1*H*-pyrrole-2-carbaldehyde) bearing a ferrocene spacer, **4.1b** was prepared as well as was the hexakis(1*H*-pyrrole-2-carbaldehyde) receptor, **4.2b**. The latter was expected to be even more effective as a phosphate receptor than **3.3b** for reasons

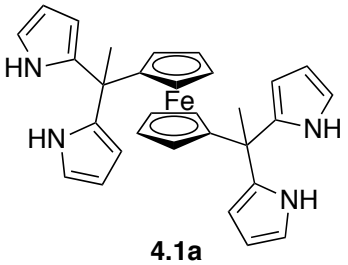

4.1a

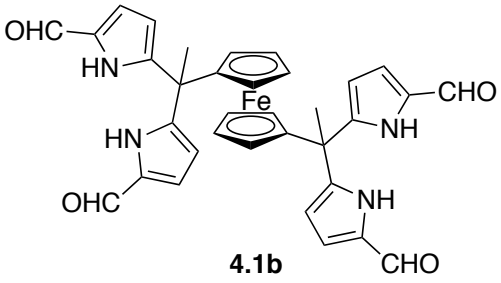

4.1b

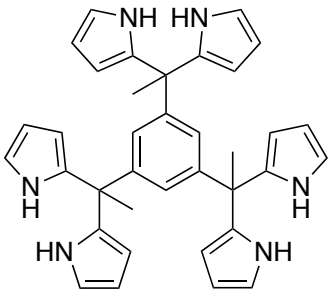

4.2a

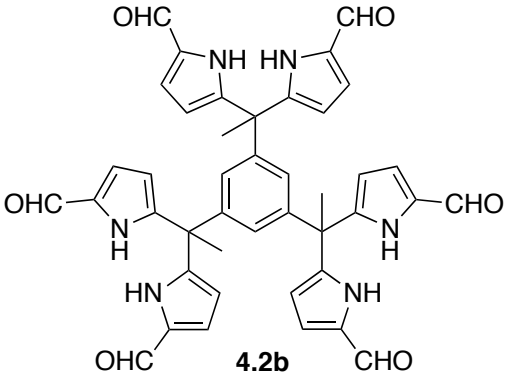

4.2b

explained in detail below.

Compound **4.1b** was designed to exploit the binding sites present in a four-fold formylated bisDPM as well as the electrostatic interactions that may emerge upon oxidation of the electroactive intervening ferrocene. On the other hand, receptor **4.2b** was prepared to determine whether the presence of a third formylated-DPM might serve to increase the $H_2PO_4^-$ binding affinity. Here, it was thought that the presence of a third formylated-DPM would serve to pre-organize the receptor such that two formylated-DPM subunits are in *cis*-like conformation. The *cis*-like conformation is the one that interacts best with the anion of interest, $H_2PO_4^-$ in the case of the bisDPM analogue **3.3b**, as concluded in Chapter 3.

4.1. Results and Discussion

4.1.1. Synthesis and Characterization

The new derivatives, **4.1b** and **4.2b**, were obtained in moderate overall yields. The synthetic routes to obtain **4.1b** and **4.2b** are shown in Scheme 4.1 and Scheme 4.2, respectively. In the first steps, commercially available diacetyl (**4.1c**) and triacetyl (**4.2c**) starting materials were converted into bisDPM **4.1a** and trisdipyrromethane (trisDPM) **4.2a**, respectively, albeit in low yields (5–15%). The low yields stand in contrast to the high yields observed for **3.3a** and **3.5a**, which precipitate from the reaction mixture and constitute the dominant reaction products. The bisDPM (**4.1a**) and trisDPM (**4.2a**) were then subjected to Vilsmeier–Haack formylation to produce tetraformyl **4.1b** and hexaformyl **4.2b** in relatively high yields (*ca*. 80%). Purification of **4.1b** was carried out by recrystallization from DMF at 80°C, whereas **4.2b** was purified by column chromatography over silica gel. The molecular structures were characterized by ^{1}H and ^{13}C NMR spectroscopy, HRMS, and single crystal X-ray diffraction analyses.

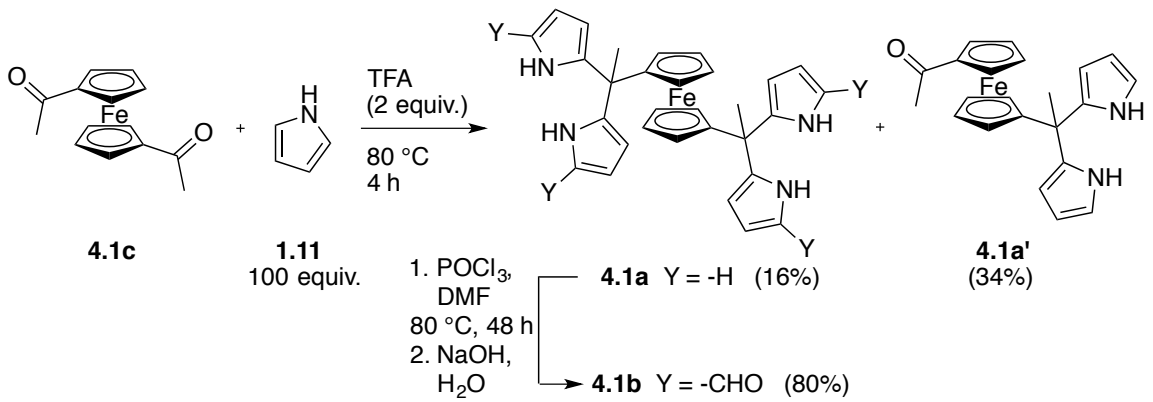

Scheme 4.1: Synthesis of receptor **4.1b**.

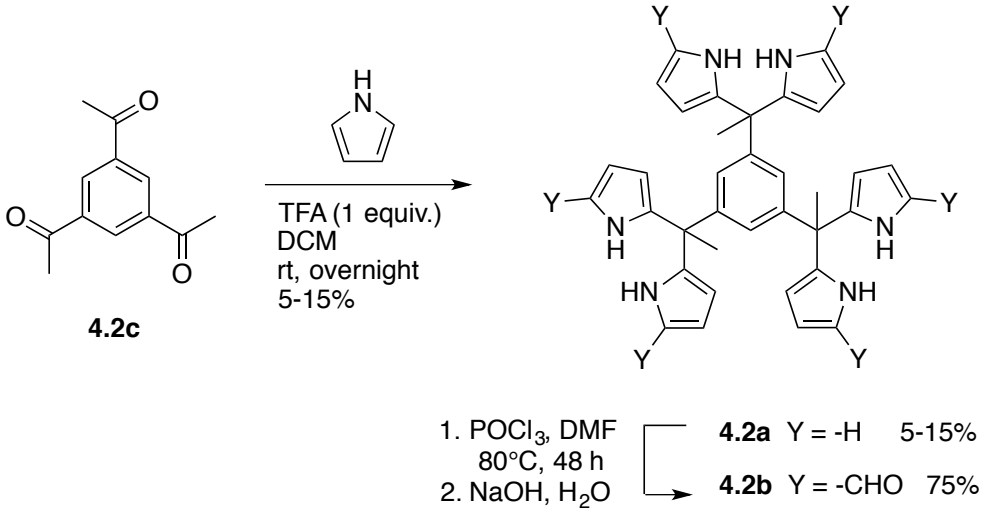

Scheme 4.2: Synthesis of receptor **4.2b**.

Receptor **4.1b** co-crystallized with two solvent molecules of DMF. The single crystal structure revealed that the two diformyl-DPM units residing on opposite cyclopentadienyl (Cp) rings of the ferrocene were locked at about 90° from one another. This conformational restriction leads to the presence of a racemic mixture of atropisomers within the single crystal. One of these isomers is shown in Figure 4.1.

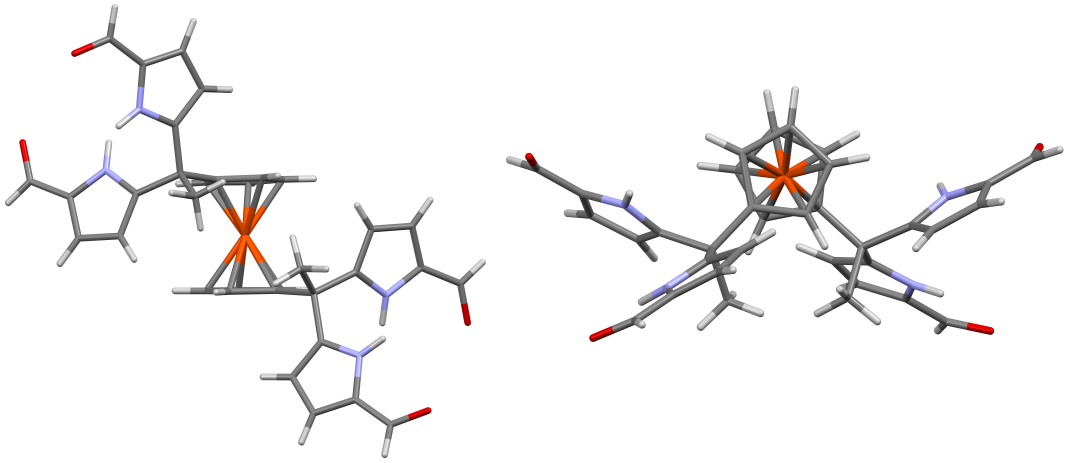

Figure 4.1: Two views of the same single crystal structure of **4.1b**. Note that only one atropisomer is shown. Two DMF solvent molecules are omitted for clarity (CCDC number 1444557).

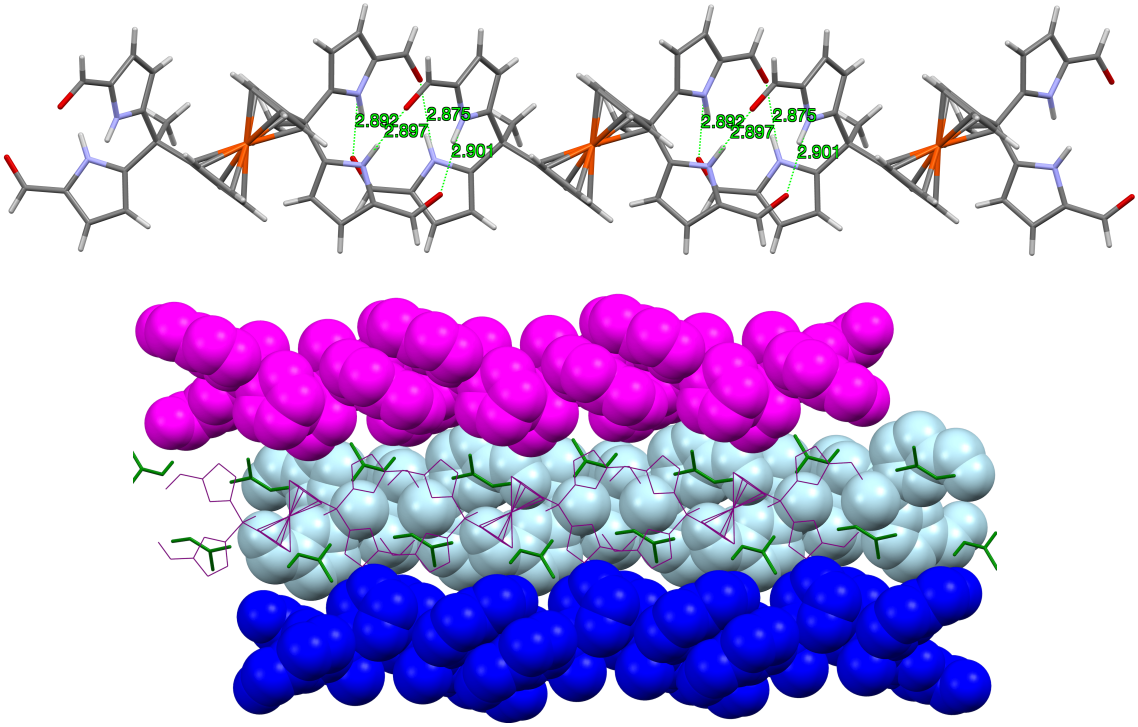

Figure 4.2: Top: Linear assembly formed by one of the atropisomers of **4.1b**. The N-H···O hydrogen bonding distances range from 2.875 to 2.901 Å. Bottom: Packing of the linear ensembles shown in the top portion of this figure.

Compound **4.1b** crystallizes as a one-dimensional hydrogen bond interlocked ensemble, even in the presence of DMF. The formation of these assemblies can be rationalized on a geometric basis. The bridging ferrocene adopts a conformation such that the two constituent Cp rings, each bearing a DPM substituent, are offset from one another by 90°. This allows for the formation of four intermolecular hydrogen bonds between the two diformyl-DPM subunits, as can be seen from an inspection of Figure 4.2.

Receptor **4.2b**, on the other hand, co-crystallized with $CHCl_3$. Each of the three diformyl-DPM subunits on the bridging benzene is oriented in a different direction (*cf.* Figure 4.3). One of the three DPM subunits was found to resemble what is seen in the case of **3.3b**,[1] wherein two diformyl-DPM units are seen to orient towards opposite π-faces of the intervening benzene ring. On the other hand, two of the diformyl-DPM units present in **4.2b** adopt conformations in which pyrrole NH groups point away from one another.

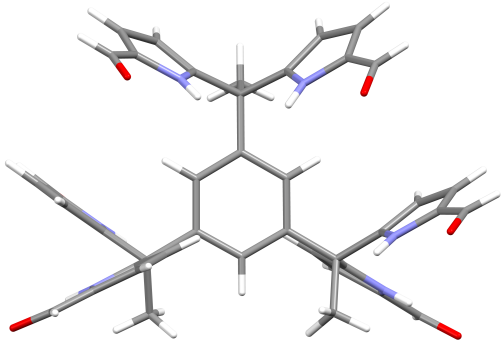

Figure 4.3: Single crystal structure of **4.2b**. Solvent molecules ($CHCl_3$) are omitted for clarity (CCDC number 1444558).

As a result, **4.2b** forms dimers stabilized by four hydrogen bonds that extend to create two-dimensional layers (Figure 4.4). The assemblies formed by **4.1b** and **4.2b** may be viewed as being examples of Gale and co-worker's "narcissistic dimer"[3] that are

extended into one and two-dimensional space, respectively. The hydrogen bond interlocked aggregates seen in the solid state structures of **4.1b** and **4.2b** may account for the low solubility of these species in many solvents.

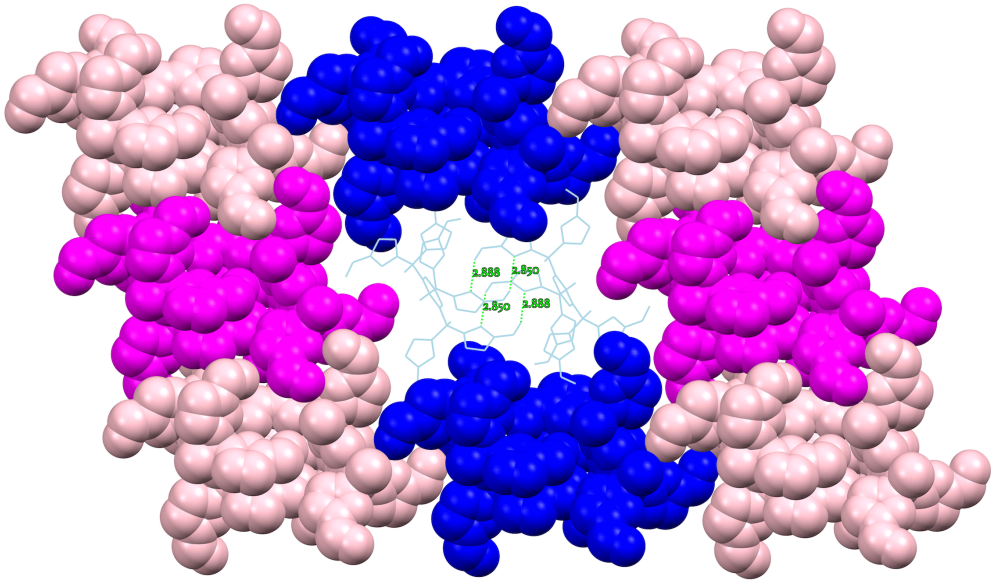

Figure 4.4: Hydrogen bond linked dimers of **4.2b** and their further self-assembly into layers. Each color indicates one dimer made up from **4.2b**. The N-H···O distances for the dimer are 2.850 and 2.888 Å. The dimer in the center is drawn in a wireframe representation. The space between the layers is filled with $CHCl_3$.

4.1.2. Anion Binding Studies

4.1.2.1. Solubility Changes monitored by Electrochemistry

To exploit the binding characteristics of the diformyl-DPM receptors (**3.3b**–**3.5b**) presented in Chapter 3 for the purposes of anion sensing, analogue **4.1b** was prepared. It incorporates a ferrocene spacer and was designed to perform as an electro-active analogue of the tetrakis(1*H*-pyrrole-2-carbaldehyde) receptor series, **3.3b**–**3.5b**. This new derivative, **4.1b**, displayed low solubility in typical organic solvents used for electrochemical studies (*e.g.*, CH_3CN, DMF, CH_2Cl_2). However, as found true for **3.3b**

(*cf*. Chapter 3), an increase in its solubility was observed upon the addition of $TBAH_2PO_4$. This was realized as a "useful property"[4] that could be exploited to obtain insights into the $H_2PO_4^-$ binding events under conditions of electrochemical analysis. It was found, for instance, that initial turbid mixtures of free receptor **4.1b** in CH_3CN containing 10% (v/v) DMF give rise to a quasi-reversible cyclic voltammogram (CV) (black line in Figure 4.5). The oxidation wave for **4.1b** becomes increasingly irreversible

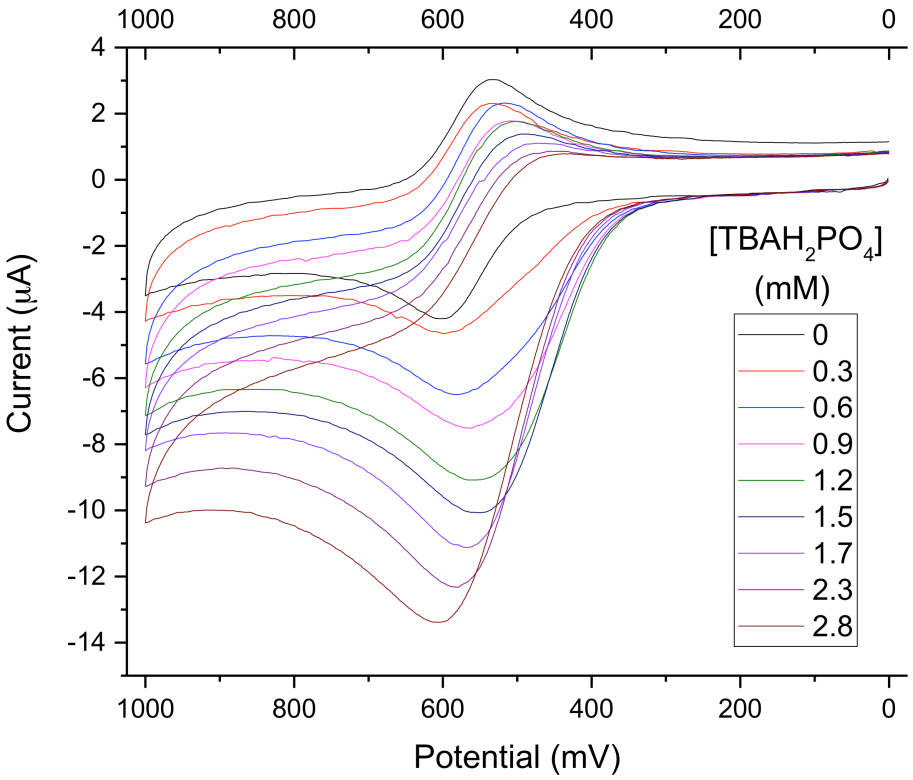

Figure 4.5: Stacked cyclic voltammogram of **4.1b** in CH_3CN containing 10% (v/v) DMF. The initial turbid mixture of **4.1b** contained a quantity of material sufficient to produce a 1.0 mM solution once completely dissolved. This mixture was titrated with $TBAH_2PO_4$ until the $TBAH_2PO_4$ concentration reached 2.8 mM. $TBAPF_6$ (0.1 M) was used as the supporting electrolyte. Glassy carbon was used as the working electrode, a Pt wire as the counter electrode, and a Ag/AgCl couple as the reference electrode.

as the relative concentration of $TBAH_2PO_4$ increases. Eventually, the CV becomes characterized by a relatively intense anodic peak and a near-absence of a corresponding cathodic feature.

The observed enhancement in the anodic peak current is ascribed to the increase in the concentration of **4.1b** (both free and anion-complexed) during the course of the titration. Since **4.1b** is not completely soluble in the solvent mixture in the absence of $H_2PO_4^-$, the concentration of free **4.1b** in the titration mixture should be constant up until the point where all traces of solid **4.1b** are dissolved. Therefore, the increase in **4.1b** concentration is presumably due to the formation of the corresponding dihydrogenphosphate complex, **4.1b**·$H_2PO_4^-$. To the extent such a supposition is correct, it would account for the observed increase in the peak current, which could be attributed directly to the formation of the readily oxidizable species, **4.1b**·$H_2PO_4^-$. When the increase in the anodic peak current is plotted against the added $H_2PO_4^-$ concentration, a binding isotherm could be obtained (*cf*. Figure 4.6) from which an approximate $H_2PO_4^-$ affinity, $(1.0 \pm 0.1) \times 10^3\ M^{-1}$, could be calculated (*cf*. experimental section, Table 4.2). The loss in reduction signal intensity is believed to reflect a strong interaction between the oxidized ferrocenium receptor (**4.1b**$^+$) and $H_2PO_4^-$.

A control experiment was performed using ferrocene under the same experimental conditions used to study **4.1b**. In the control experiment, no anodic peak current increase was observed. This was presumably because ferrocene in the initial solution was completely soluble. However, upon addition of $TBAH_2PO_4$, a new reduction signal at 280 mV appeared in the cyclic voltammogram (*cf*. Figure 4.7).

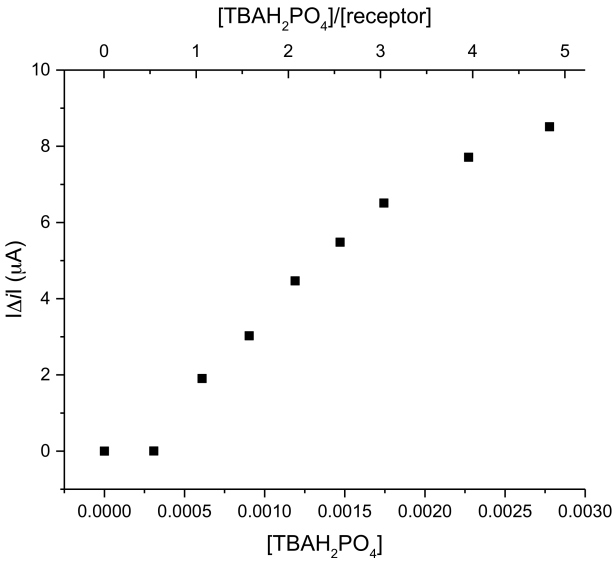

Figure 4.6: The change in anodic peak current at around 600 mV is plotted against concentration of $TBAH_2PO_4$ added. Titration voltammograms are presented in Figure 4.5.

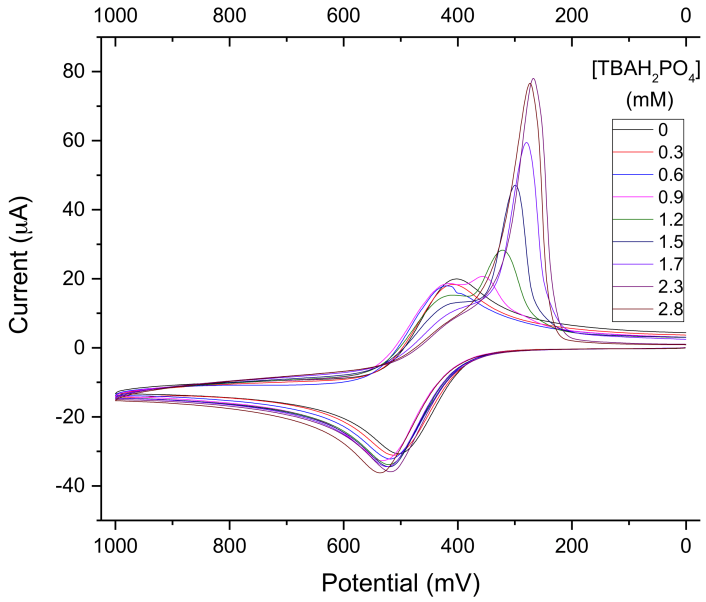

Figure 4.7: Stacked cyclic voltammogram of a 1.0 mM solution of ferrocene in CH_3CN containing 10% (v/v) DMF (black line). This solution was titrated with $TBAH_2PO_4$ until the $TBAH_2PO_4^-$concentration reached 2.8 mM. $TBAPF_6$ (0.1 M) was used as the supporting electrolyte. Glassy carbon was used as the working electrode, a Pt wire as the counter electrode, and a Ag/AgCl couple as the reference electrode.

4.1.2.2. Solid State Studies via X-ray Diffraction Analysis

Single crystals of complex **4.2b**·$H_2PO_4^-$ were obtained by using $TBAH_2PO_4$ to solubilize receptor **4.2b** in $CHCl_3$ (by conversion to the corresponding $H_2PO_4^-$ complex) and then layering with *n*-pentane. The resulting crystal structure is shown in Figure 4.8. The structure of **4.2b**·$H_2PO_4^-$ resembles to that of **3.4b**·$H_2PO_4^-$ discussed in Chapter 3, particularly in terms of the (diformyl-DPM)-$H_2PO_4^-$ interactions. However, in **4.2b**·$H_2PO_4^-$, the third diformyl-DPM of **4.2b** is too distant to interact well with the bound $H_2PO_4^-$ anion. It thus interacts in an intermolecular sense with a $H_2PO_4^-$ anion bound to a second receptor. The result is a dimeric complex with overall 2:2 stoichiometry. The four pyrrole NH-to-deprotonated phosphate oxygen N-H···O distances range from 2.730 to 2.827 Å. The intermolecular hydrogen bond that is presumed to play a role in stabilizing the 2:2 complex is characterized by an O-H···O distance of 2.598 Å.

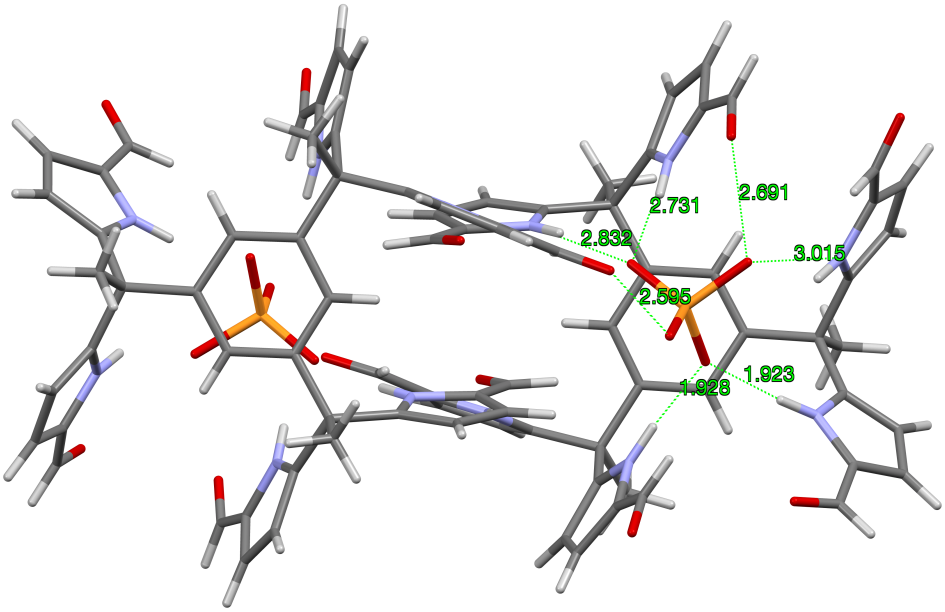

Figure 4.8: Single crystal structure of the 2:2 complex [**4.2b**·$H_2PO_4^-$]$_2$. One TBA^+ counter cation per $H_2PO_4^-$ and 1.5 molecules of $CHCl_3$ per **4.2b** have been omitted for clarity. The CCDC number is 1444561.

Bill *et al*., reported two tripodal receptors[5] (**1.29** and **1.30**) that show structural similarity to receptor, **4.2b**. Receptors **1.29** and **1.30** were based on pyrrole- and DPM-functionalized derivatives of a sterically geared precursor, 1,3,5-tris(aminomethyl)-2,4,6-triethylbenzene (Figure 4.9). These systems displayed high affinity and selectivity for tetrahedral anionic guests as inferred from solution studies involving ITC analyses carried out in CH_3CN and solid state single crystal X-ray diffraction analyses. Both receptors (**1.29** and **1.30**) were constructed from a well known tripodal core that confers preorganization on the receptors.[5] Single crystal structures of co-crystals **4.2b**·$TBAH_2PO_4$ and **1.29**·$TBAH_2PO_4$ were compared. The shortest distance between the phosphrous (P) of the $H_2PO_4^-$ anion and the intervening benzene ring of **4.2b** is 3.92 Å in the single crystal structure of [**4.2b**·$H_2PO_4^-$]$_2$. On the other hand, this distance is 4.7 Å in the crystal structure of **1.29**·$TBAH_2PO_4$.[5] Based on the crystal structures, it was concluded that the $H_2PO_4^-$ resides closer to the aromatic π-surface in **4.2b**.

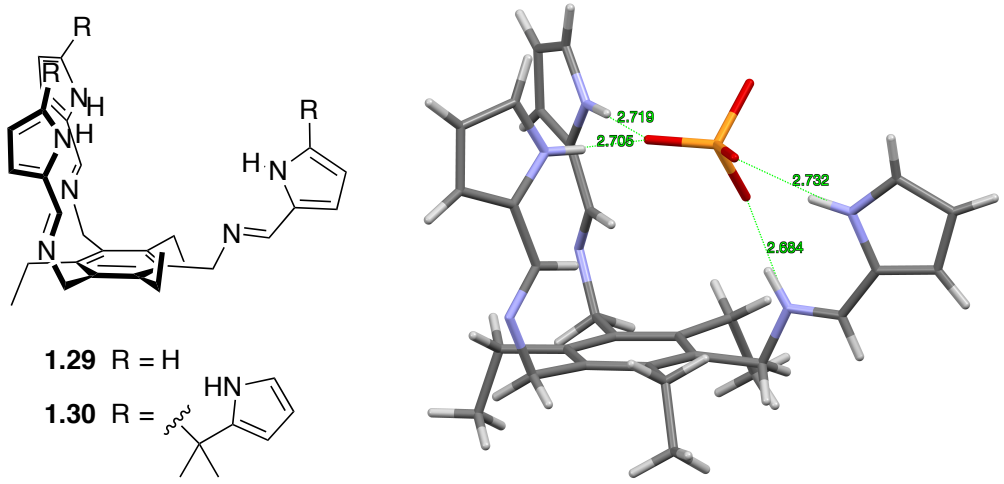

Figure 4.9: Left: Structures of **1.29** and **1.30**. These compounds were presented in Chapter 1. Right: Single crystal structure of **1.29** and $H_2PO_4^-$anion complex. The TBA^+ counter cation has been omitted for clarity. This structure was originally reported by Bill *et al*.[5] and was redrawn using data from the CCDC (number 833333).

4.1.2.3. Solution State Studies Involving ^{1}H NMR Spectroscopy

An ^{1}H NMR spectroscopic study of **4.2b** carried out in a competitive solvent mixture, $CDCl_3$:DMSO-d_6 (8:1), revealed an upfield shift in the intervening benzene resonance (*cf*. Figure 4.10). Such a shift is consistent with the presence of anion-π interactions, as inferred from previous studies of $\alpha,\alpha,\alpha,\alpha$-*meso*-tetraaryl-C[4]P derivatives reported by Ballester and co-workers.[5]

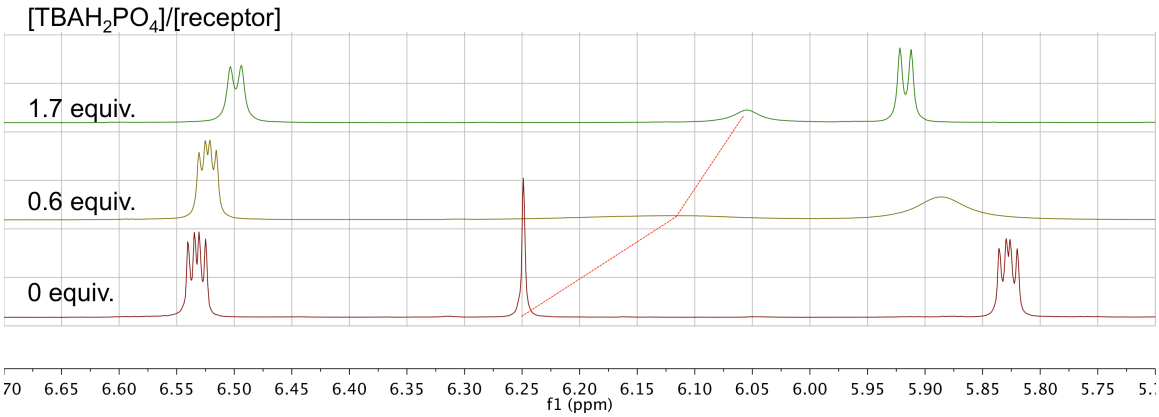

Figure 4.10: Stacked partial ^{1}H NMR spectra of receptor **4.2b** (15.6 mM) with varying quantities of $H_2PO_4^-$recorded in $CDCl_3$:DMSO-d_6 (8:1). Dashed lines show changes in the chemical shifts for the aromatic hydrogen atoms of the benzene ring of receptor **4.2b** ($\Delta\delta$ = -0.19 ppm).

The signal for the aromatic hydrogen atoms of **4.2b** is subject to peak broadening when $TBAH_2PO_4$ is added (Figure 4.10). On the other hand, the H^3 signal ascribed to **3.4b**, remained sharp after the addition of $TBAH_2PO_4$ (*cf*. Chapter 3). Based on the crystal structure of **3.4b**·$TBAH_2PO_4$, the $H_2PO_4^-$anion is thought to reside very close to H^3. In the case of receptor **4.2b**, there are three equivalent aromatic hydrogen atoms in the free form of the receptor. Upon binding $H_2PO_4^-$, the chemical environment of one of the three aromatic hydrogen atoms is altered more due to the asymmetry of the complex, **4.2b**·$TBAH_2PO_4$ (Figure 4.8). A fast exchange between the free from of **4.2b** and the

4.2b·$H_2PO_4^-$in NMR time scale is thought to be the reason for the signal broadening observed for the aromatic hydrogen signals in the case of **4.2b**.

4.1.2.4. Solution State Studies Involving UV-Vis Spectroscopy

Receptor **4.2b** proved even less soluble in neat, non-hydrogen bonding solvents, such as $CHCl_3$, than its congeners **3.3b–3.5b**. This made it impossible to carry out binding studies that were directly comparable to **3.3b–3.5b**. However, in analogy to what was seen in the case of these other receptors (**3.3b–3.5b**), it was found that the solubility of **4.2b** increased upon the addition of $TBAH_2PO_4$. Dilute solutions of **4.2b**·$H_2PO_4^-$ in $CHCl_3$ could thus be prepared by mixing single crystals of **4.2b** with *ca*. 2.75 molar equivalents of $TBAH_2PO_4$. The UV-Vis spectrum of this solution was characterized by features similar to those seen in the reported spectrum of **3.3b**·$H_2PO_4^-$ at analogous concentrations. Thus, the observed spectral features were ascribed to the complex **4.2b**·$H_2PO_4^-$. When the $CHCl_3$ solution made up from **4.2b** and $TBAH_2PO_4$ was titrated with CH_3OH, spectral changes and isosbestic behavior were observed. On this basis, we conclude that the $H_2PO_4^-$ affinity of **4.2b** decreases in the presence of increasing quantities of CH_3OH (Figure 4.11).

However, it was also apparent that large quantities of CH_3OH were required to disrupt the complex completely. It was thus decided that a solution of 3% (v/v) CH_3OH in $CHCl_3$ would provide a good balance between solubility and binding affinity and allow for quantitative analyses. In a first set of experiments, an 11 μM solution of **4.2b** in 3% (v/v) CH_3OH in $CHCl_3$ was prepared and then subjected to titration with $TBAH_2PO_4$ (*cf*. Figure 4.12).

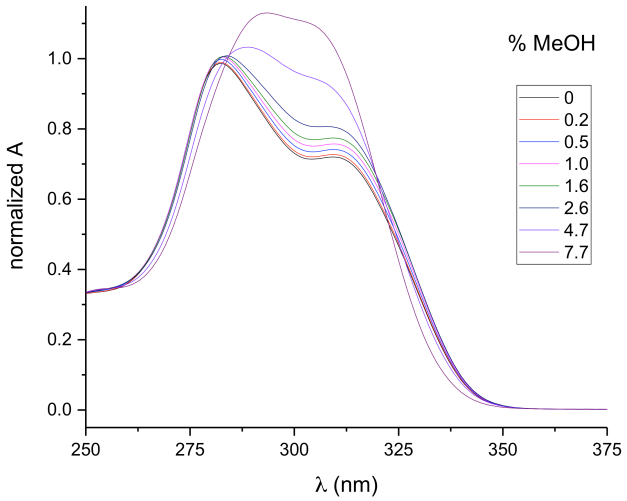

Figure 4.11: Stacked UV-Vis spectra of **4.2b** (solubilized by adding 2.75 molar equivalents of $TBAH_2PO_4$ in neat $CHCl_3$; 0% added CH_3OH) and increasing percentages of added CH_3OH. Spectra are normalized to eliminate the effect of dilution.

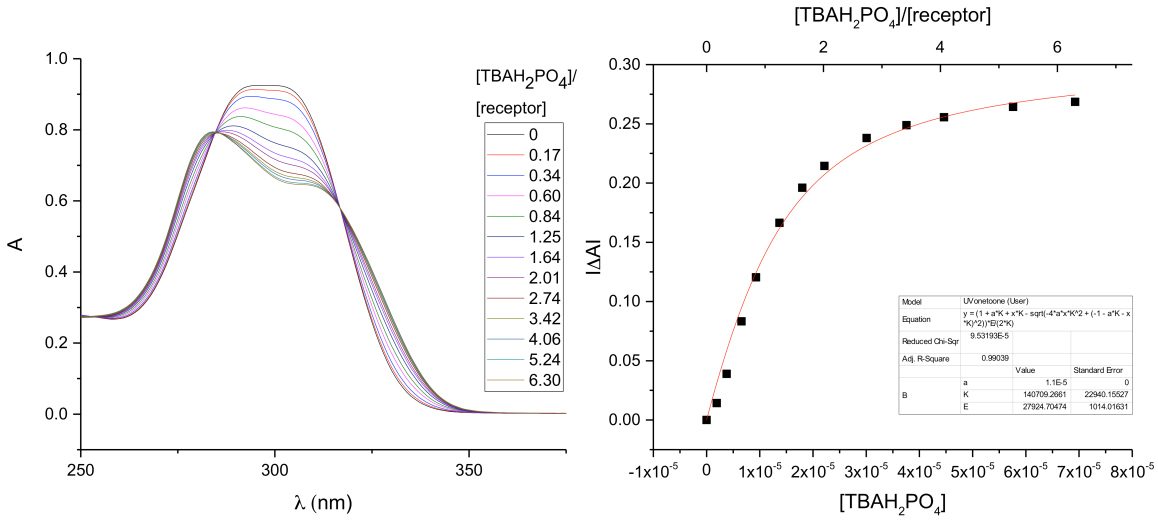

Figure 4.12: Left: Stacked UV-Vis spectra corresponding to the titration of **4.2b** (1.1 x 10^{-5} M) with $TBAH_2PO_4$ (2.9 x 10^{-4} M) in $CHCl_3$ containing 3% (v/v) CH_3OH. Right: Binding curve and fit generated from the titration data obtained by monitoring the absorbance changes at 302 nm. K_a = (1.4 ± 0.2) x 10^5 M^{-1}.

The induced spectral changes were then fit to a 1:1 binding profile and used to calculate the binding constant corresponding to $H_2PO_4^-$ binding (Figure 4.12) in accord with the methods described previously (see experimental section of Chapter 3). Similar UV-Vis titrations were carried out with a series of anions in the form of their respective TBA salts. It was found that titration with either the $H_2PO_4^-$ or $HP_2O_7^{3-}$ anions gave rise to significant spectral changes with saturation behavior being observed in the presence of fewer than ten molar equivalents of these two anions. On the other hand, no discernable spectral changes were seen upon titration with HSO_4^-, Cl^-, or NO_3^-.

In the initial studies of **3.3b–3.5b**, $CHCl_3$ was used as the solvent. To allow for a comparison between the original tetrakis(1*H*-pyrrole-2-carbaldehyde) anion receptors and the newer hexakis analogue **4.2b**, compound **3.3b** was subject to titration with $H_2PO_4^-$ in 3% (v/v) CH_3OH-$CHCl_3$. The results from this comparison are summarized in Table 4.1.

Anions[a]	**3.3b**[b]	**3.3b**[c]	**4.2b**[c]
$H_2PO_4^-$	$(8 \pm 2) \times 10^6$	$(2.1 \pm 0.3) \times 10^3$	$(1.4 \pm 0.2) \times 10^5$
$HP_2O_7^{3-}$	$(1.4 \pm 0.1) \times 10^5$	$(3.8 \pm 0.6) \times 10^3$	$(3.6 \pm 0.2) \times 10^4$
HSO_4^-	$(4.1 \pm 0.2) \times 10^3$	nd	nd
NO_3^-	nd	nd	nd
Cl^-	nd	nd	nd

nd: No discernable spectral change. [a] The anions were studied as their TBA^+ salts. [b] In $CHCl_3$ [c] In $CHCl_3$ containing 3% (v/v) CH_3OH.

Table 4.1: Summary of calculated binding affinities, K_a (M^{-1}) as determined by UV-Vis spectroscopy in two separate solvent systems.

Briefly, **4.2b** is characterized by a *ca*. 2 orders of magnitude higher $H_2PO_4^-$ anion affinity. This increase agrees with the design expectations underlying **4.2b**, namely that the presence of a third DPM subunit would force this system to adopt a preorganized conformation in a way that is not possible for **3.3b**.

4.2. CONCLUSIONS

The tetrakis (1*H*-pyrrole-2-carbaldehyde) receptor family was extended by including a new electroactive derivative, **4.1b**, incorporating a ferrocene linker and a binding-site enriched hexaformyl trisDPM derivative, **4.2b**. The anion binding properties of these new systems were studied by monitoring the increase in solubility electrochemically, *via* single crystal X-ray diffraction analyses, as well as by means of ^{1}H NMR and UV-Vis spectroscopic titrations. Conformational switching from *trans*-like conformations as seen in the free receptors **3.3b** and **3.4b** to the corresponding *cis*-like conformations upon interacting with phosphate derivatives was revealed by X-ray diffraction analyses in the solid state for the hexakis-(1*H*-pyrrole-2-carbaldehyde) receptor (**4.2b**) (Figure 4.13).

In mixed CH_3OH-$CHCl_3$ solution, the new hexakis -carbaldehyde derivative **4.2b** was found to exhibit an affinity for $H_2PO_4^-$ that is roughly 100x higher than that displayed by the tetrakis analogue **3.3b**. This increase in binding affinity is rationalized in terms of a receptor design that overcomes in part the conformational penalty that needs to be paid in order to achieve substrate binding. As such, the present findings provide experimental insights that might prove useful in the design of anion receptors based on rather simple binding motifs, such as pyrroles and dipyrromethane subunits.

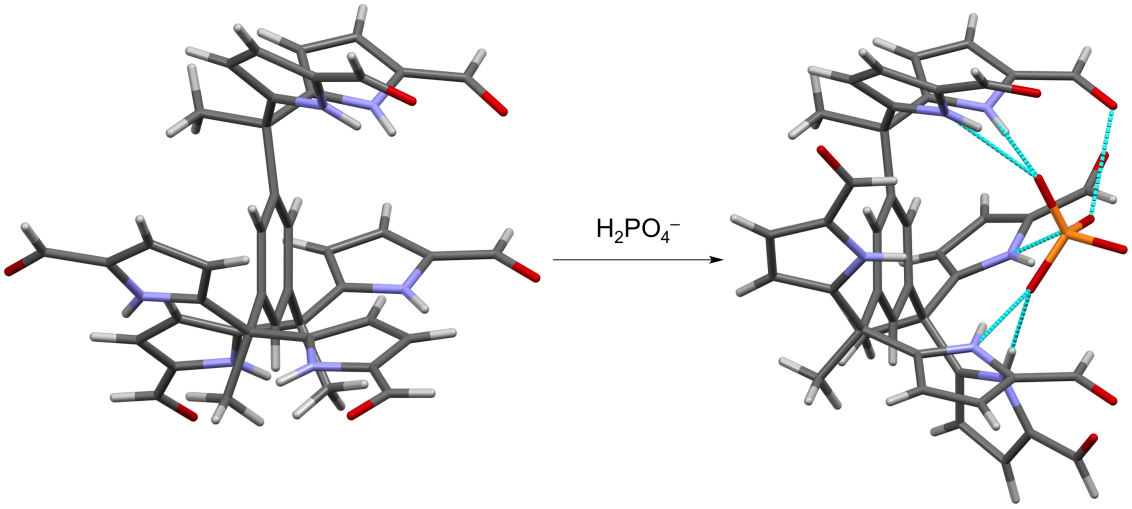

Figure 4.13: Views of the single crystal structures of **4.2b** without (left) and with (right) a bound $H_2PO_4^-$ anion.

4.3. EXPERIMENTAL

1,1'-Diacetylferrocene was obtained from Ark Pharm, Inc. All other solvents and chemicals were purchased from Aldrich, TCI, and Acros. Pyrrole was distilled at 80 °C under reduced pressure (100 mbar) prior to use. Other solvents and reagents were used without further purification.

4.3.1. Synthetic Procedures

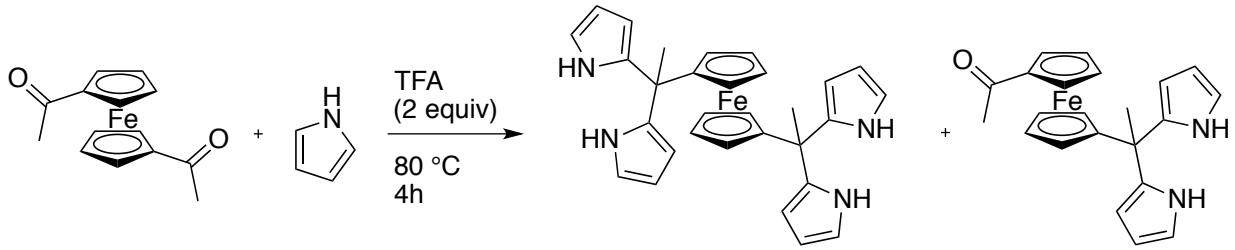

4.1c **1.11** (100 equiv) **4.1a** 16% **4.1a'** 34%

1,1'-Bis(1,1-di(1*H*-pyrrol-2-yl)ethyl)ferrocene (**4.1a**):

1,1'-Diacetylferrocene (500 mg, 1.85 mmol) was dissolved in pyrrole (12 mL, 185 mmol). Dry nitrogen gas was bubbled through this solution for 10 min. TFA (0.3 mL, 3.9 mmol) was added to the mixture and the mixture was heated to 80°C for 4 hours while bubbling with N_2.[§§] The reaction mixture was then cooled to room temperature and dissolved in dichloromethane (DCM). The organic solution was extracted with 0.5 M NaOH to remove the TFA. The organic layer was dried over anhydrous $MgSO_4$ and the solvent was removed. Unreacted pyrrole was recycled from this crude product mixture by distillation at 80 °C and 100 mbar. Column chromatography (silica gel) was performed using 15:1 DCM:EtOAc as the eluent. The yellow fraction (R_f = 0.95) was collected and gave yellowish green oil upon evaporation (150 mg, 16%). The oil was solidified in 1 ml of CH_3OH. ^{1}H NMR (400 MHz, $CDCl_3$) δ 7.78 (bs, 4H), 6.59 (m, 4H), 6.11 (m, 4H), 5.93 (m, 4H), 4.08 (t, *J* = 1.9 Hz, 4H), 3.96 (t, *J* = 1.9 Hz, 4H), 1.95 (s, 6H) ppm. ^{13}C NMR (100 MHz, $CDCl_3$) δ 138.32, 116.51, 107.97, 105.48, 98.08, 68.97, 67.90, 39.48, 28.64 ppm. HRMS (CI^+) *m/z* for $C_{30}H_{30}FeN_4$ $[M]^+$ calcd 502.1820, found 502.1826.

1-Acetyl-1'-(1,1-di(1H-pyrrol-2-yl)ethyl)ferrocene (**4.1a'**):

This product was obtained as a side product from the above product mixture. The product is a red solid (240 mg, 34%) that elutes from the column after **4.1a** (for **4.1a'** R_f = 0.5). ^{1}H NMR (400 MHz, $CDCl_3$) δ 7.99 (bs, 2H), 6.66 (m, 2H), 6.12 (m, 2H), 5.91 (m, 2H), 4.73 (t, *J* = 2.0 Hz, 2H), 4.46 (t, *J* = 2.0 Hz, 2H), 4.22 (t, *J* = 1.9 Hz, 2H), 4.00 (t, *J* = 1.9 Hz, 2H), 2.31 (s, 3H), 2.00 (s, 3H) ppm. ^{13}C NMR (100 MHz, $CDCl_3$) δ 203.05,

[§§] Proper ventilation is required since TFA is a corrosive and low boiling substance.

137.60, 117.02, 107.87, 105.76, 100.32, 79.47, 75.53, 70.62, 69.53, 68.86, 39.40,29.00, 27.62 ppm. HR-MS-CI$^+$ *m/z* for $C_{22}H_{22}FeN_2O$ $[M]^+$ calcd 386.1082, found 386.1072.

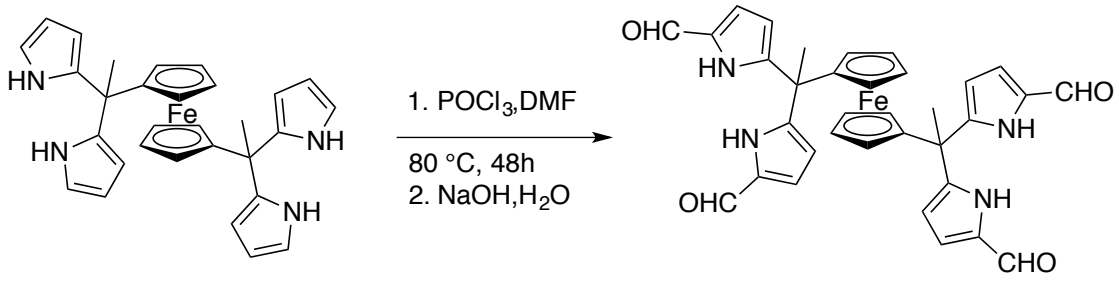

4.1a **4.1b** 80%

5,5',5'',5'''-(1,1'-Ferrocenylenebis(ethane-1,1,1-triyl))tetrakis(1*H*-pyrrole-2-carbaldehyde) (**4.1b**):

A Vilsmeier–Haack formylation procedure identical to that reported in Chapter 3 (Procedure-B) was used, albeit starting with **4.1a**. The product, **4.1b**, was obtained in 80% yield. ^{1}H NMR (400 MHz, DMSO-d_6) δ 11.63 (bs, 4H), 9.41 (s, 4H), 6.83 (m, 4H), 5.67 (m, 4H), 4.07 (m, 4H), 3.87 (m, 4H), 2.02 (s, 6H) ppm. ^{13}C NMR (100 MHz, DMSO-d_6) δ 178.7, 146.9, 132.3, 109.7, 95.7, 68.1, 67.9, 55.3, 25.0 ppm. ^{13}C NMR (100 MHz, DMF-d_7) δ 179.3, 147.7, 133.6, 110.5, 96.8, 69.1, 68.9, 41.0, 26.0 ppm. HRMS (ESI$^+$) *m/z* for $C_{34}H_{30}FeN_4O_4$ $[M+H]^+$ calcd 615.16900, found 615.16930.

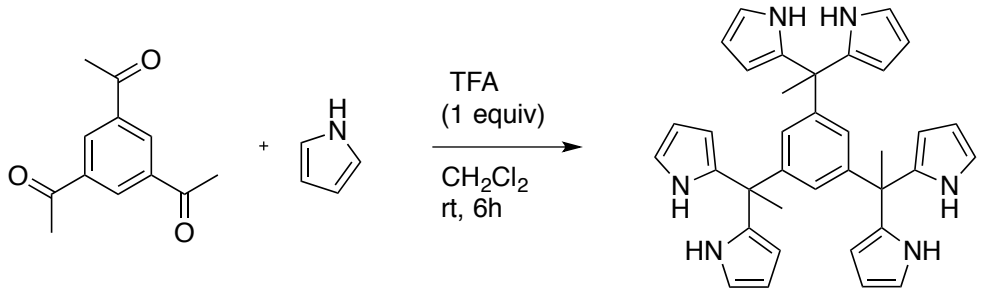

4.2c **1.11** (100 equiv) **4.2a** 5–15%

1,3,5-Tris(1,1-di(1*H*-pyrrol-2-yl)ethyl)benzene (**4.2a**):

A modification of the published dipyrromethane-forming procedure was employed starting with 1,3,5-teiacetylbenene and using CH_2Cl_2 as a co-solvent and carrying out the reaction at room temperature. A co-solvent is used to reduce the formation of insoluble side products. The desired product **4.2a** was obtained as a colorless oil in 15% yield. ^{1}H NMR (400 MHz, $CDCl_3$) δ 7.65 (bs, 6H), 6.90 (s, 3H), 6.54 (m, 6H), 6.13 (m, 6H), 5.89 (m, 6H), 1.95 (s, 9H) ppm. ^{13}C NMR (100 MHz, $CDCl_3$) δ 146.5, 137.4, 124.8, 117.1, 108.0, 106.3, 44.7, 28.5 ppm. HRMS (ESI$^+$) *m/z* for $C_{36}H_{36}N_6$ $[M+H]^+$ calcd 553.30740, found 553.30730.

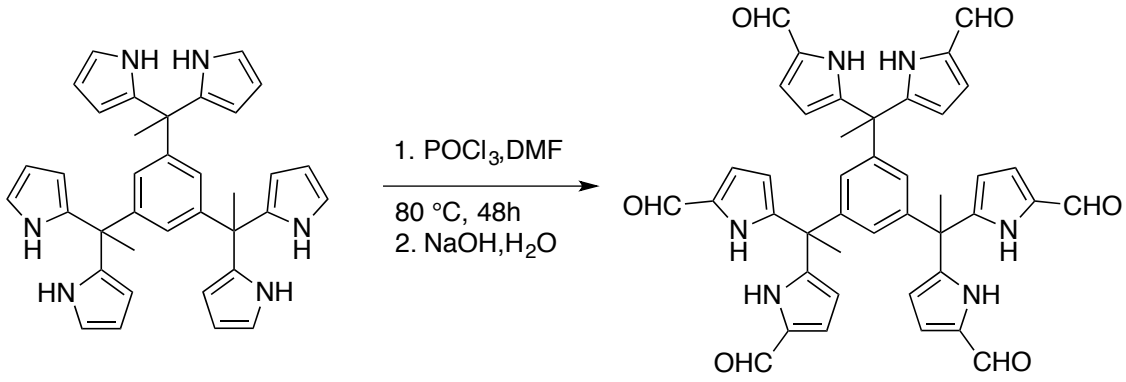

4.2a **4.2b** 80%

5,5',5'',5''',5'''',5'''''-(Benzene-1,3,5-triyltris(ethane-1,1,1-triyl))hexakis(1*H*-pyrrole-2-carbaldehyde) (**4.2b**):

The Vilsmeier–Haack formylation procedure identical to that reported in Chapter 3 (Procedure-B) was used, albeit starting with **4.2a**. Product **4.2b** was obtained in 80% yield. ^{1}H NMR (400 MHz, DMSO-d_6) δ 11.68 (s, 6H), 9.34 (s, 6H), 6,75 (m, 6H), 6.42 (s, 3H), 5.74 (m, 6H), 1.91 (s, 9H) ppm. ^{13}C NMR (100 MHz, DMSO-d_6) δ 178.87,

145.67, 145.26, 133.03, 124.63, 110.43, 109.59, 45.38, 26.95 ppm. HRMS (ESI^+) *m/z* for $C_{42}H_{36}N_6O_6$ $[M+Na]^+$ calcd 743.25890, found 743.25920.

4.3.2. Electrochemical Studies

For the titration of **4.1b** with $TBAH_2PO_4$ in CH_3CN containing 10% (v/v) DMF, two chemical equilibria can be written as follows.

$$\textbf{4.1b}\ (s) \quad \rightleftharpoons \quad \textbf{4.1b}\ (org) \qquad K_{sp}$$

$$\textbf{4.1b}\ (org) + H_2PO_4^-(org) \quad \rightleftharpoons \quad \textbf{4.1b}\cdot H_2PO_4^-(org) \qquad K_a$$

The concentration of **4.1b** is expected to be constant during the titration as long as **4.1b** is present in the solid form. This approximation is especially valid for the earlier data points.

$$K_{sp} = [\textbf{4.1b}]$$

The peak current (i_p) is a function of concentration as defined by the following equation:

$$i_p = 2.69x10^5\, n^{3/2} v^{1/2} ADC$$

$$i_p = \kappa C$$

Where n is the number of electrons transferred, v is the scan rate, A is the electrode surface area, C is the concentration and D is the diffusion coefficient. In the simplified equation, κ is a derived parameter that is held constant.

$$i_{p,o} = \kappa_{\textbf{4.1b}}.[\textbf{4.1b}]$$

$$i_p = \kappa_{\textbf{4.1b}}.[\textbf{4.1b}] + \kappa_{complex.}[\textbf{4.1b}\cdot H_2PO_4^-]$$

$\Delta i_p = \kappa_{\text{complex}}.[\mathbf{4.1b}\cdot TBAH_2PO_4^-]$

$$K_a = \frac{[\mathbf{6b}\cdot H_2PO_4^-]}{[\mathbf{6b}].[H_2PO_4^-]}$$

$$K_a = \frac{\Delta i_p/\kappa_{complex}}{\left(\frac{i_{p,o}}{\kappa_{\mathbf{6b}}}\right).[H_2PO_4^-]}$$

$[\mathbf{4.1b}\cdot H_2PO_4^-]_{max}$ = 1 mM

$i_{p,max} = \kappa_{complex}\ [\mathbf{4.1b}\cdot H_2PO_4^-]_{max}$

It is assumed that all of the initial sample of **4.1b** is solubilized upon formation of complex ($\mathbf{4.1b}\cdot H_2PO_4^-$) and $\kappa_{complex} = \kappa_{\mathbf{4.1b}}$

For the calculations,

$[\mathbf{4.1b}]_{sat} = i_{p,max}/[\mathbf{4.1b}]_{max}$

$[\mathbf{4.1b}\cdot H_2PO_4^-] = \Delta i_p\ ([\mathbf{4.1b}\cdot H_2PO_4^-]/\ i_{p,max})$

$[H_2PO_4^-] = [H_2PO_4^-]_o - [\mathbf{4.1b}\cdot H_2PO_4^-]$

A plot of Δi_p against added $H_2PO_4^-$($[H_2PO_4^-]_o$) is shown in Figure 4.6 and the calculated equilibrium composition is presented in Table 4.2.

Experimental conditions		Unit		Calculated		Unit	
$[\mathbf{4.1b}]_{max}$	1.0E-03	M		$[\mathbf{4.1b}]_{sat}$	3.50E-04	M	
$i_{p,max}$	13.1	uA					
Experimental	Calculated						
$[H_2PO_4^-]_o$	I*i*I (μA)	Δi	$[\mathbf{4.1b}{\cdot}H_2PO_4^-]$	$[\mathbf{4.1b}]$	$[\mathbf{4.1b}]_t$	$[H_2PO_4^-]$	K_a
0.00E+00	4.589	0.00E+00	0.00E+00	3.50E-04	3.50E-04	0.00E+00	n/a
3.09E-04	4.592	3.00E-03	2.29E-07	3.50E-04	3.51E-04	3.08E-04	outlier
6.10E-04	6.495	1.91E+00	1.45E-04	3.50E-04	4.96E-04	4.64E-04	8.95E+02
9.04E-04	7.615	3.03E+00	2.31E-04	3.50E-04	5.81E-04	6.73E-04	9.80E+02
1.19E-03	9.057	4.47E+00	3.41E-04	3.50E-04	6.91E-04	8.49E-04	1.15E+03
1.47E-03	10.07	5.48E+00	4.18E-04	3.50E-04	7.69E-04	1.05E-03	1.14E+03
1.74E-03	11.1	6.51E+00	4.97E-04	3.50E-04	8.47E-04	1.25E-03	1.14E+03
2.27E-03	12.3	7.71E+00	5.89E-04	3.50E-04	1.00E-03	1.68E-03	9.98E+02
2.78E-03	13.1	8.51E+00	6.50E-04	3.50E-04	1.00E-03	2.13E-03	8.72E+02
						$K_{a,av}$	1.02E+03
						STD	1.17E+02
						%std	1.15E-01
Note: $i_{p,max}$ input in the Excel sheet has an influence on calculated K_a value for $\mathbf{4.1b}{\cdot}H_2PO_4^-$ complex formation.							

Table 4.2: Excel formula sheet used to calculate the *K* value corresponding to the formation of $\mathbf{4.1b}{\cdot}H_2PO_4^-$.

4.3.3. UV-Vis Spectroscopic Studies

For the determination of binding affinities (K_a), titration experiments are carried out as described in Chapter 3. The spectra of these titrations are presented here.

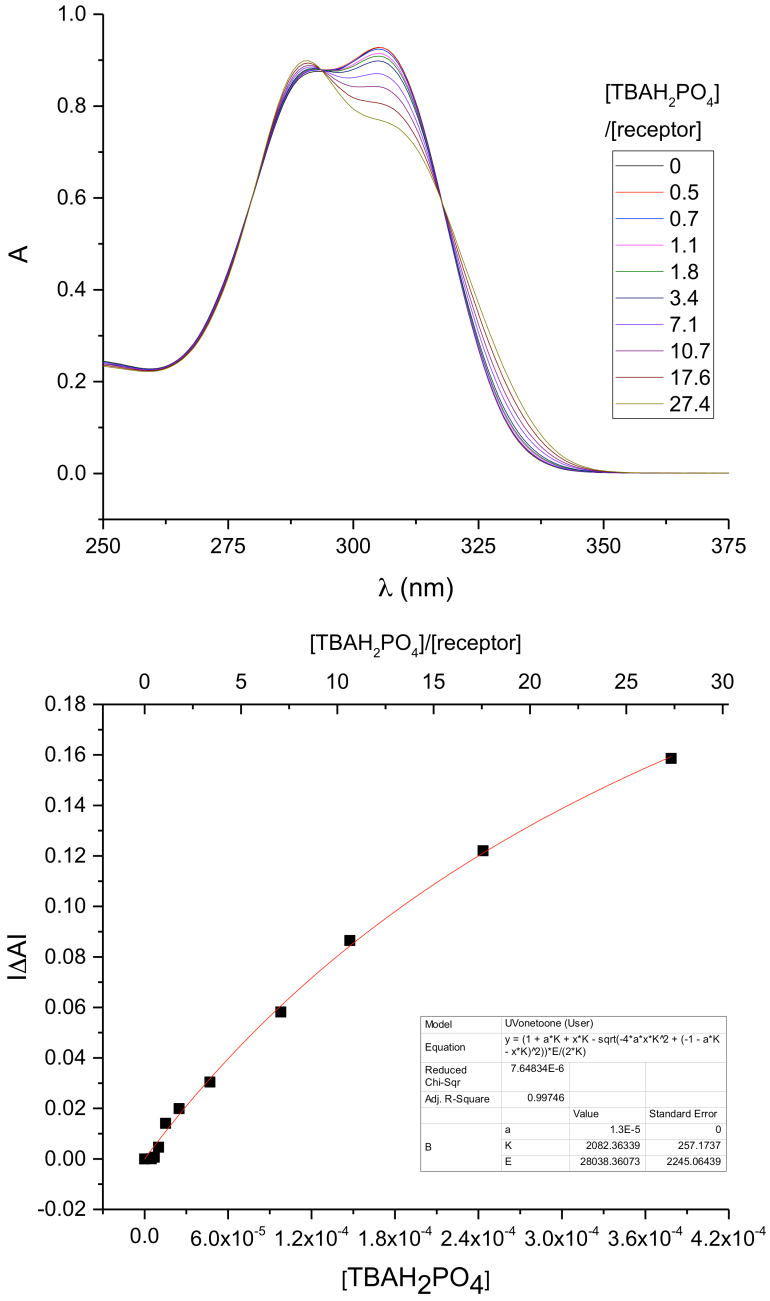

Figure 4.14: Top: Stacked UV-Vis spectra corresponding to the titration of **3.3b** (1.3 x 10^{-5} M) with $TBAH_2PO_4$ (4.1 x 10^{-3} M) in $CHCl_3$ containing 3% (v/v) CH_3OH. Bottom: Binding curve and fit generated from the titration data obtained by monitoring the absorbance changes at 305 nm. K_a = (2.1 ± 0.3) x 10^3 M^{-1}.

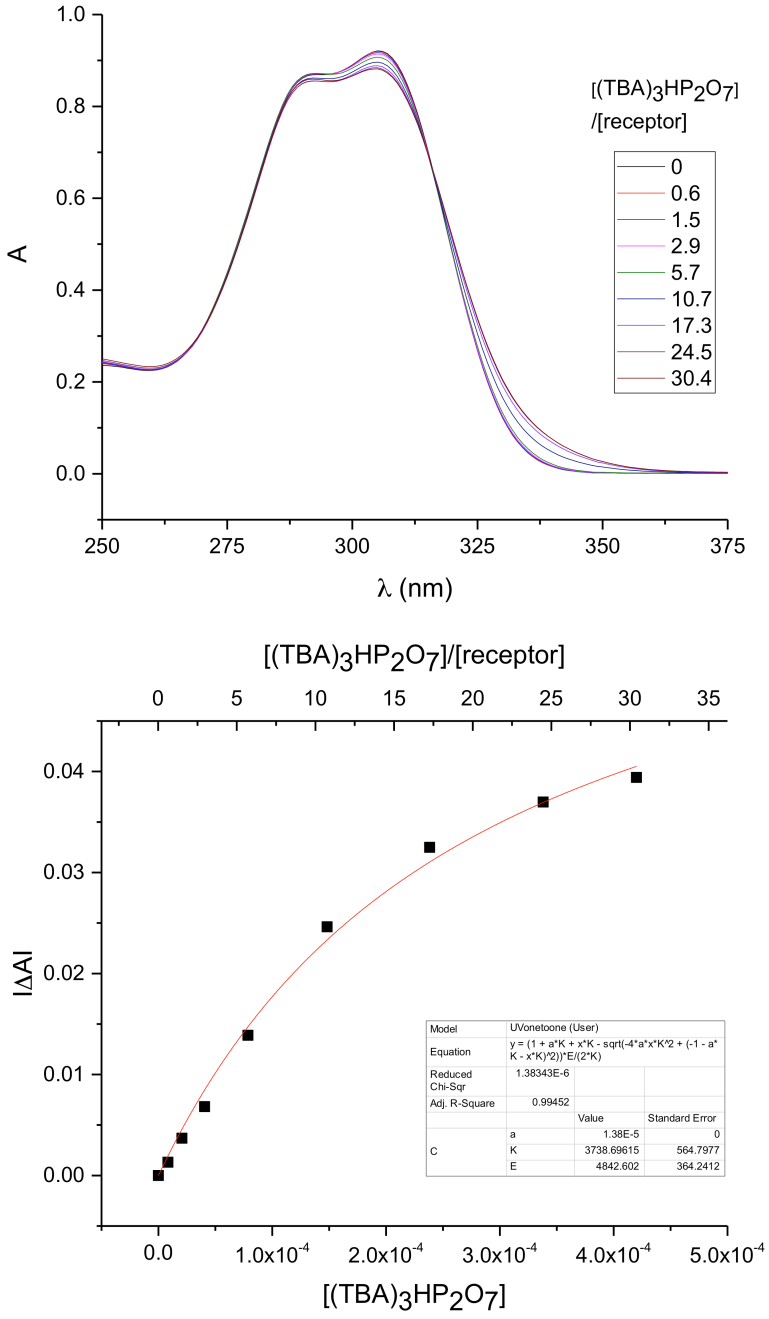

Figure 4.15: Top: Stacked UV-Vis spectra corresponding to the titration of **3.3b** (1.3 x 10^{-5} M) with $(TBA)_3HP_2O_7$ (1.3 x 10^{-3} M) in $CHCl_3$ containing 3% (v/v) CH_3OH. Bottom: Binding curve and fit generated from the titration data obtained by monitoring the absorbance changes at 305 nm. K_a = (3.8 ± 0.6) x 10^3 M^{-1}.

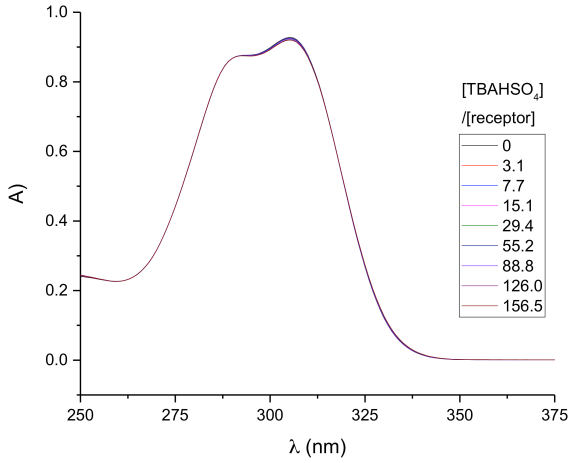

Figure 4.16: Stacked UV-Vis spectra corresponding to the titration of **3.3b** (1.3 x 10^{-5} M) with $TBAHSO_4$ (6.5 x 10^{-3} M) in $CHCl_3$ containing 3% (v/v) CH_3OH.

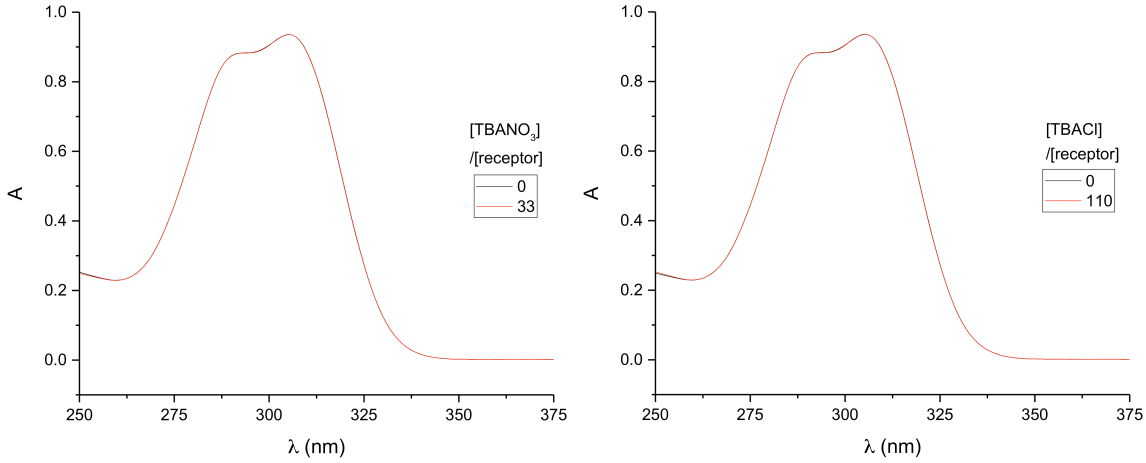

Figure 4.17: Left: Stacked UV-Vis spectra of **3.3b** (1.3 x 10^{-5} M) recorded in the presence and absence of $TBANO_3$ (4.6 x 10^{-4} M) in $CHCl_3$ containing 3% (v/v) CH_3OH. Right: Stacked UV-Vis spectra of **3.3b** (1.3 x 10^{-5} M) recorded in the presence and absence of TBACl (1.5 x 10^{-3} M) in $CHCl_3$ containing 3% (v/v) CH_3OH.

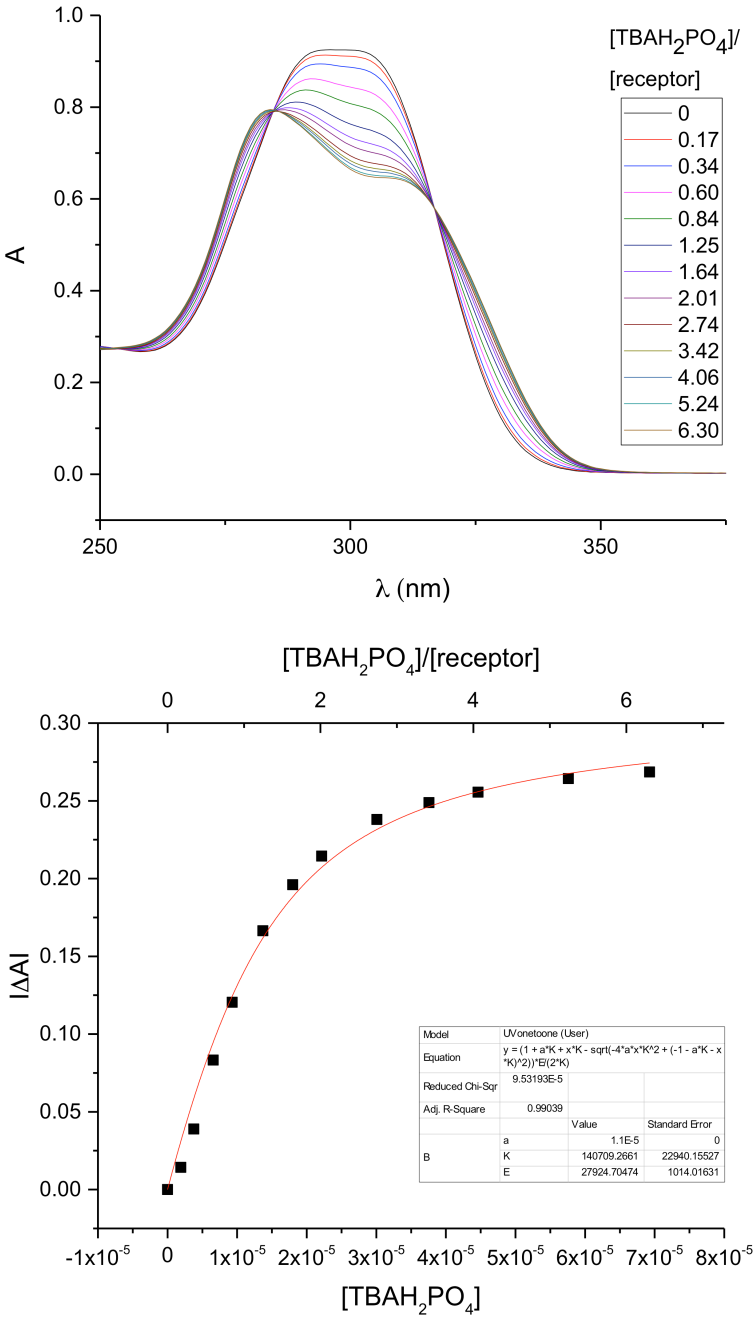

Figure 4.18: Top: Stacked UV-Vis spectra corresponding to the titration of **4.2b** (1.1 x 10^{-5} M) with $TBAH_2PO_4$ (2.9 x 10^{-4} M) in $CHCl_3$ containing 3% (v/v) CH_3OH. Bottom: Binding curve and fit generated from the titration data obtained by monitoring the absorbance changes at 302 nm. K_a = (1.4 ± 0.2) x 10^5 M^{-1}.

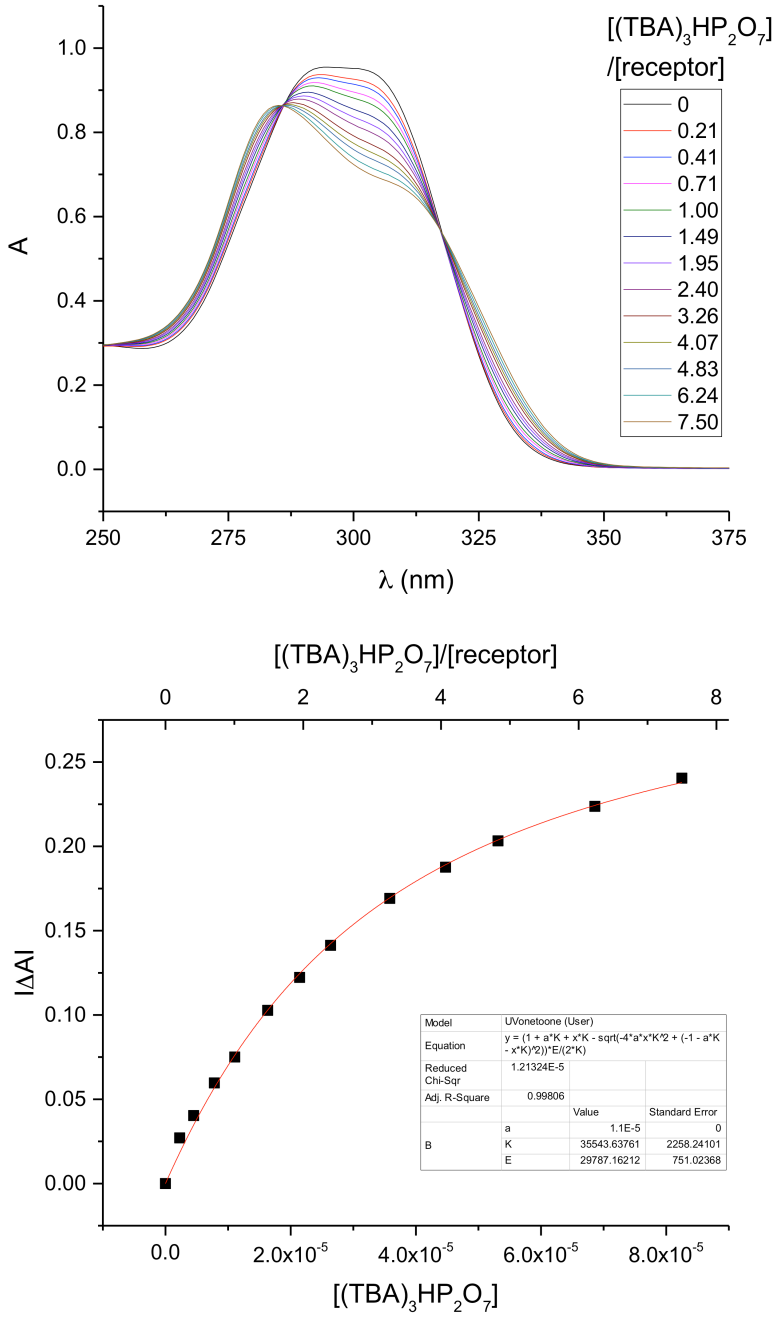

Figure 4.19: Top: Stacked UV-Vis spectra corresponding to the titration of **4.2b** (1.1 x 10^{-5} M) with $(TBA)_3HP_2O_7$ (2.9 x 10^{-4} M) in $CHCl_3$ containing 3% (v/v) CH_3OH. Bottom: Binding curve and fit generated from the titration data obtained by monitoring the absorbance changes at 302 nm. K_a = (3.6 ± 0.2) x 10^4 M^{-1}.

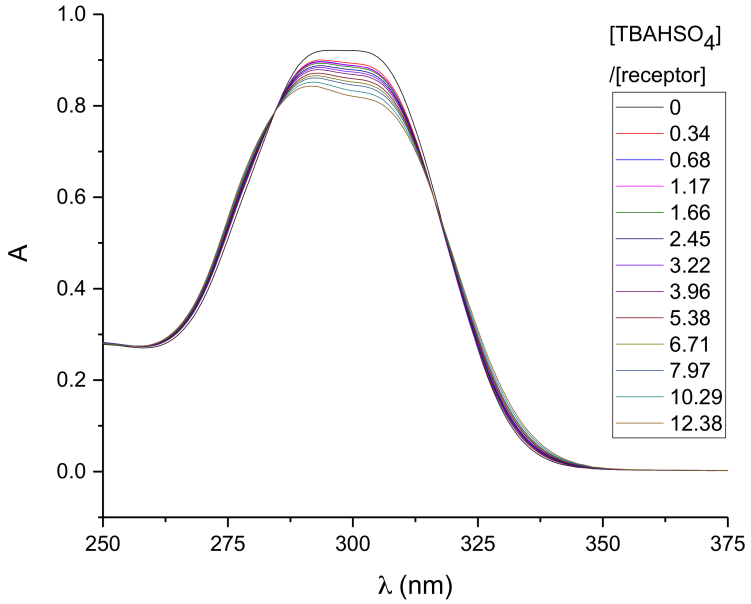

Figure 4.20: Stacked UV-Vis spectra corresponding to the titration of **4.2b** (1.1 x 10^{-5} M) with $TBAHSO_4$ (5.7 x 10^{-4} M) in $CHCl_3$ containing 3% (v/v) CH_3OH. No saturation behavior is observed.

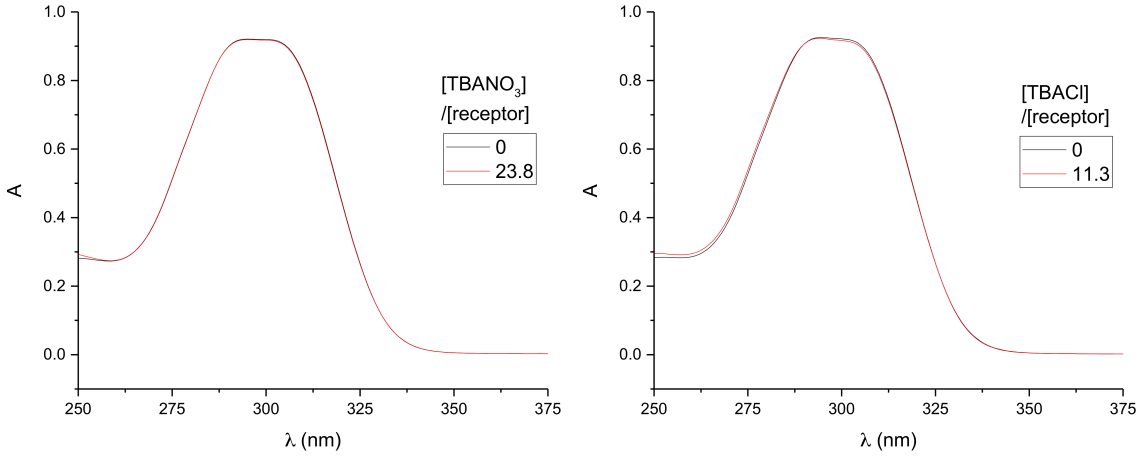

Figure 4.21 Left: Stacked UV-Vis spectra of **4.2b** (1.1 x 10^{-5} M) recorded in the presence and absence of $TBANO_3$ (2.4 x 10^{-4} M) in $CHCl_3$ containing 3% (v/v) CH_3OH. Right: Stacked UV-Vis spectra of **4.2b** (1.1 x 10^{-5} M) recorded in the presence and absence of TBACl (1.2 x 10^{-4} M) in $CHCl_3$ containing 3% (v/v) CH_3OH.

4.4. REFERENCES

1. Deliomeroglu, M.; Lynch, V.; Sessler, J. Conformationally Switchable Non-Cyclic Tetrapyrrole Receptors: Synthesis of tetrakis(1*H*-Pyrrole-2-Carbaldehyde) Derivatives and Their Anion Binding Properties. *Chem. Commun.* **2014**, *50* (80), 11863–11866.
2. Gale, P. A.; Sessler, J. L.; Kral, V.; Lynch, V. Calix[4]pyrroles: Old yet New Anion-Binding Agents. *J. Am. Chem. Soc.* **1996**, *118* (21), 5140–5141.
3. Camiolo, S.; Gale, P. A.; Hursthouse, M. B.; Light, M. E.; Shi, A. J. Solution and Solid-State Studies of 3,4-Dichloro-2,5-Diamidopyrroles: Formation of an Unusual Anionic Narcissistic Dimer. *Chem. Commun.* **2002**, *3* (7), 758–759.
4. Connors, K. A. *Binding Constants: The Measurement of Molecular Complex Stability*; John Wiley & Sons: New York, 1987.
5. Bill, N. L.; Kim, D.-S.; Kim, S. K.; Park, J. S.; Lynch, V. M.; Young, N. J.; Hay, B. P.; Yang, Y.; Anslyn, E. V.; Sessler, J. L. Oxoanion Recognition by Benzene-Based Tripodal Pyrrolic Receptors. *Supramol. Chem.* **2012**, *24* (1), 72–76.
6. Gil-Ramírez, G.; Escudero-Adán, E. C.; Benet-Buchholz, J.; Ballester, P. Quantitative Evaluation of Anion-π Interactions in Solution. *Angew. Chem. Int. Ed.* **2008**, *47* (22), 4114–4118.

5. Future Directions

The common subunit among the receptors presented in Chapters 2, 3, and 4 is a formylated-DPM, which contains an aryl group in its *meso*-position. In Chapter 2 and 3, it was shown that the intervening aromatic linker of bis and trisDPM receptors plays a role in anion-π interactions. The relative contribution of these interactions to the overall anion binding event can be investigated by creating electronically altered derivatives of receptor **3.4b**. Several possible candidates are compounds **5.1**–**5.3**.

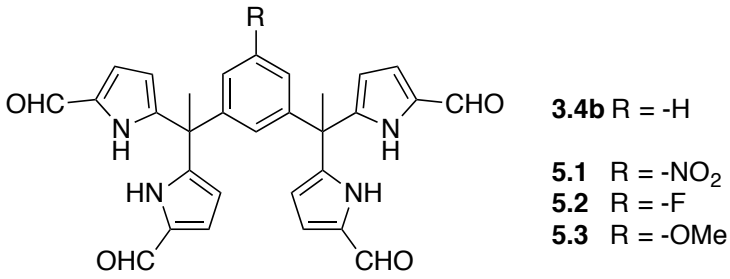

In Chapter 4, hydrogen bound polymeric assemblies were observed for receptors **4.1b** and **4.2b**. The fact that there were an equal number of hydrogen bond donating and accepting groups makes these receptors self-complementary. This feature was thought to play role in the formation of hydrogen bound assemblies.

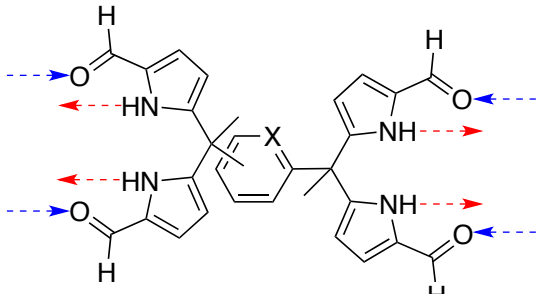

Receptors **3.3b–3.5b** can be tested for their ability to cross-link polymeric materials bearing formylated-DPM pendants, which can be in principle prepared employing synthetic methods used in Chapter 2 and in former groups members research.[1] Such cross-linking is proposed based on the self-complementary nature of formylated-DPM moiety. In addition to displaying anion binding features, these polymer should be susceptible to when exposed to the ditopic systems such as **3.3b**, discussed in Chapter 3. This proposed cross-linking chemistry will most likely need to be studied in a non-hydrogen-bonding solvent such as $CHCl_3$. However, might show responsive behavior, such as deformations or disaggregation, may be seen in the presence of other solvents or if the anion content of the media is varied.

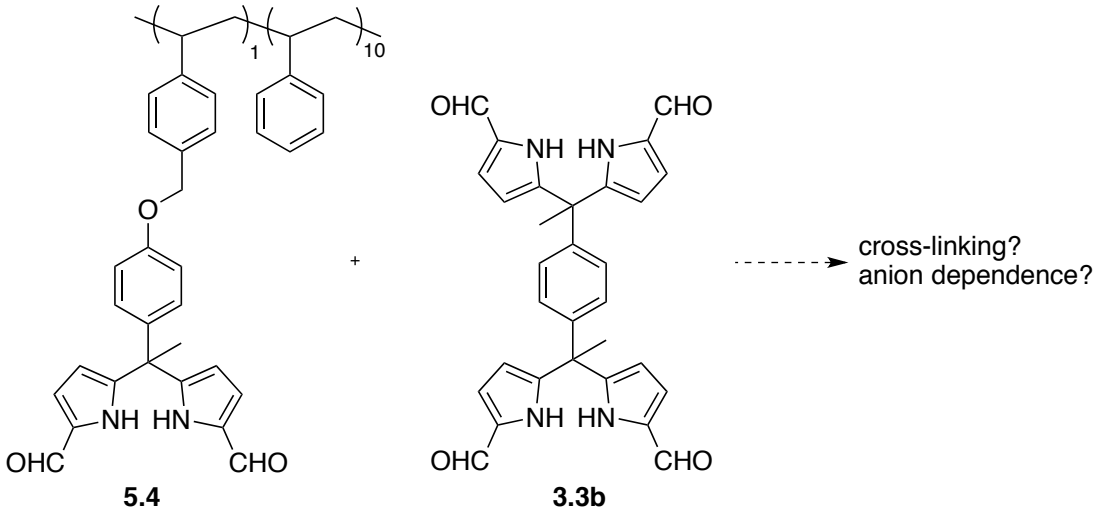

Scheme 5.1: Possible scheme for supramolecular cross-linking of polymer **5.4** illustrated with **3.3b** as the cross-linker.

The polymeric system can be studied *via* UV-Vis spectroscopy. By measuring the viscosity[2] of the polymer solutions, cross-linking behavior may be monitored in the presence and absence of a potential cross-linking bisDPM.

Four-fold formylated bisDPMs **3.3b** and **3.4b** and six-fold formylated trisDPM **4.2b** were individually shown to adopt *cis*-like conformations when a phosphate derivative is bound. The achiral nature of **3.4b** and *trans*-like conformation seen in **3.3b** and **3.4b** point to the possibility that the rotation needed for interconversion of conformations is not restricted. The use of steric gearing to fix the *cis*-like conformation may lead to higher $H_2PO_4^-$ affinities. One approach to achieving this goal is shown in Scheme 5.2 and discussed briefly below.

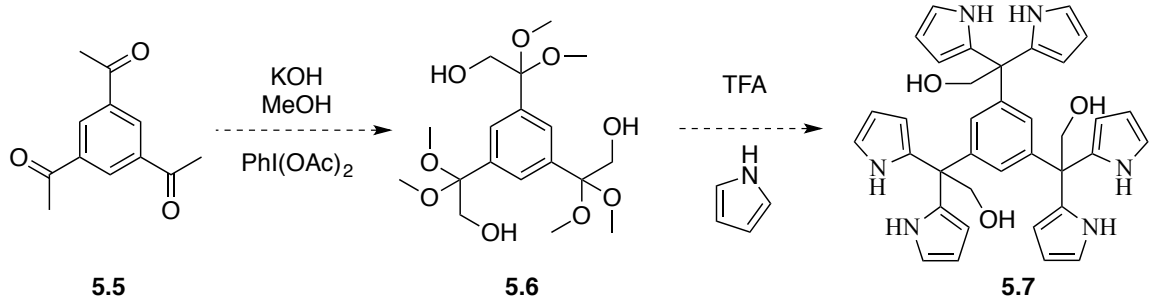

Scheme 5.2: Synthetic route for a functionalized trisDPM **5.7**.

The α-hydroxylation of acetophenone derivatives using organohypervalent iodine reagents was developed by Moriarty.[3,4] The reported conditions[3] can be used to oxidize regioselectively **5.5** in all three α-positions to yield **5.6**. Compound **5.6** could be used as a precursor to prepare novel trisDPM systems (*e.g.*, **5.7**). Covalent modifications of **5.7** at the –OH functional groups might then allow the synthesis of pre-organized *cis*-like systems. Such systems should display higher $H_2PO_4^-$ anion affinities, while also possessing more favorable solubility characteristics.

Given the research directions outlined above, it is the opinion of the author that considerable benefit could accrue from the further study of formylated-DPM derivatives. Further transformations involving the carbonyl (*e.g.*, imine formation) would also be of interest. There thus remains much to to building off the present work.

5.1. REFERENCES

1. Silver, E. S.; Rambo, B. M.; Bielawski, C. W.; Sessler, J. L. Reversible Anion-Induced Cross-Linking of Well-Defined Calix[4]pyrrole-Containing Copolymers. *J. Am. Chem. Soc.* **2014**, *136* (6), 2252–2255.
2. Sijbesma, R. P. Reversible Polymers Formed from Self-Complementary Monomers Using Quadruple Hydrogen Bonding. *Science* **1997**, *278* (5343), 1601–1604.
3. Moriarty, M.; Hu, H.; Gupta, S. C. Direct α-Hydroxylation of Ketones Using Iodosobenzene. *Tetrahedron Lett.* **1981**, *22* (14), 1283–1286.
4. Moriarty, R. M. Organohypervalent Iodine: Development, Applications, and Future Directions. *J. Org. Chem.* **2005**, *70* (8), 2893–2903.

6. ^{1}H & ^{13}C NMR Spectra

6.1. General

All nuclear magnetic resonance (NMR) spectra were recorded at the University of Texas at Austin Department of Chemistry NMR Facility. Instruments used include:

Varian Unity 300 (300 MHz),

Agilent MR 400 MHz,

Varian MR 400 MHz,

Varian Inova 500 MHz,

and Bruker AC 300 MHz spectrometer.

Chemical shifts (δ) are reported in ppm and referenced to the solvent. All deuterated NMR solvents were purchased from Cambridge Isotope Laboratories and used as received. Solvent reference chemical shifts were set for values reported in the literature.[1] Diffusion-Ordered NMR (DOSY) spectra (presented in Chapter 3) were recorded on Varian DirectDrive 600 (600 MHz).

6.2. Spectra

^{1}H and ^{13}C NMR spectra for the compounds presented in Chapters 2, 3, and 4 are presented here.

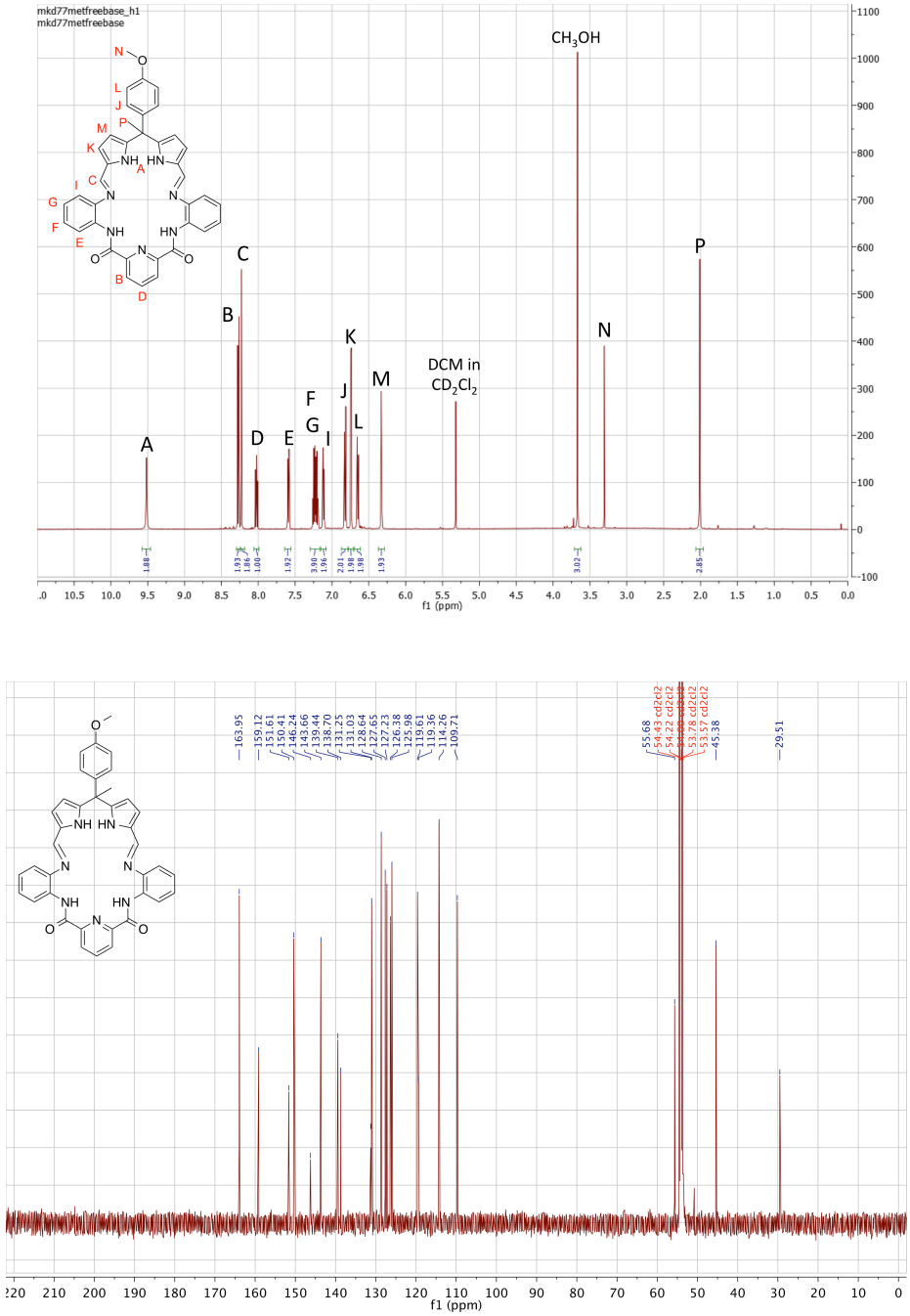

Figure 6.1: Top: ^{1}H NMR (500 MHz), Bottom: ^{13}C NMR (126 MHz) spectra of **2.15a** in CD_2Cl_2.

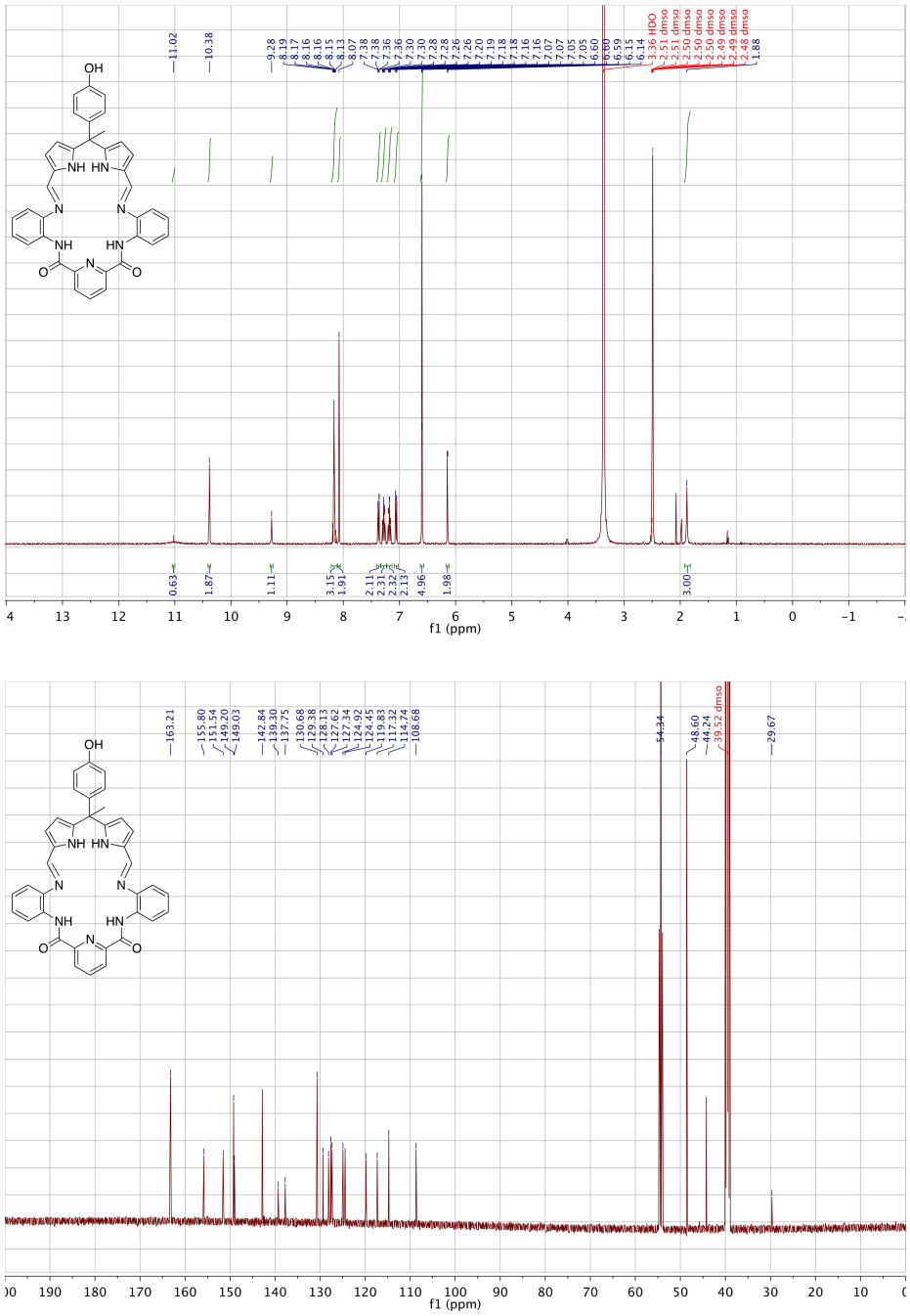

Figure 6.2: Top: ^{1}H NMR (400 MHz), Bottom: ^{13}C NMR (150 MHz) spectra of **2.15b** in DMSO-d_6.

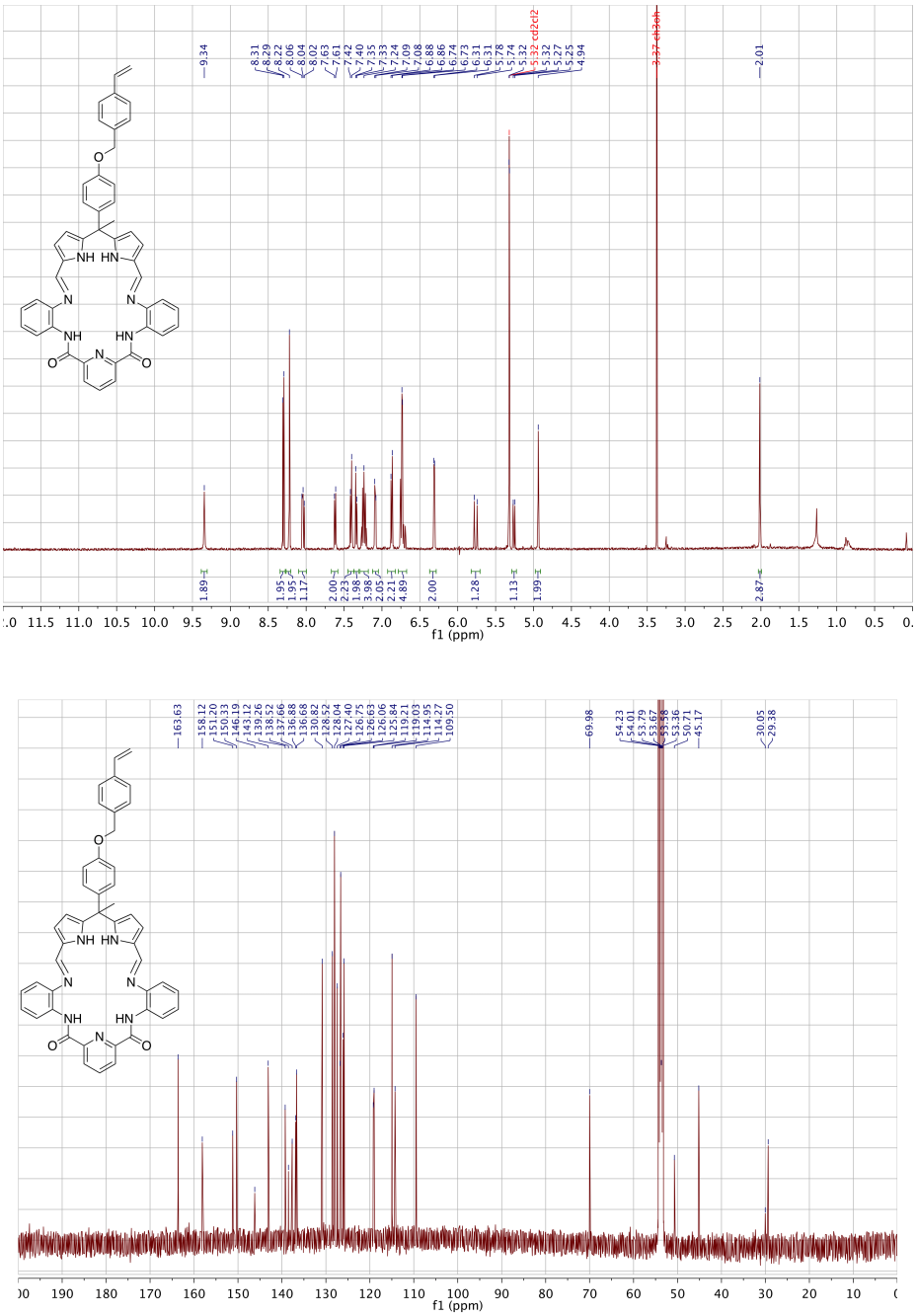

Figure 6.3: Top: ^{1}H NMR (500 MHz), Bottom: ^{13}C NMR (126 MHz) spectra of **2.15c** in CD_2Cl_2.

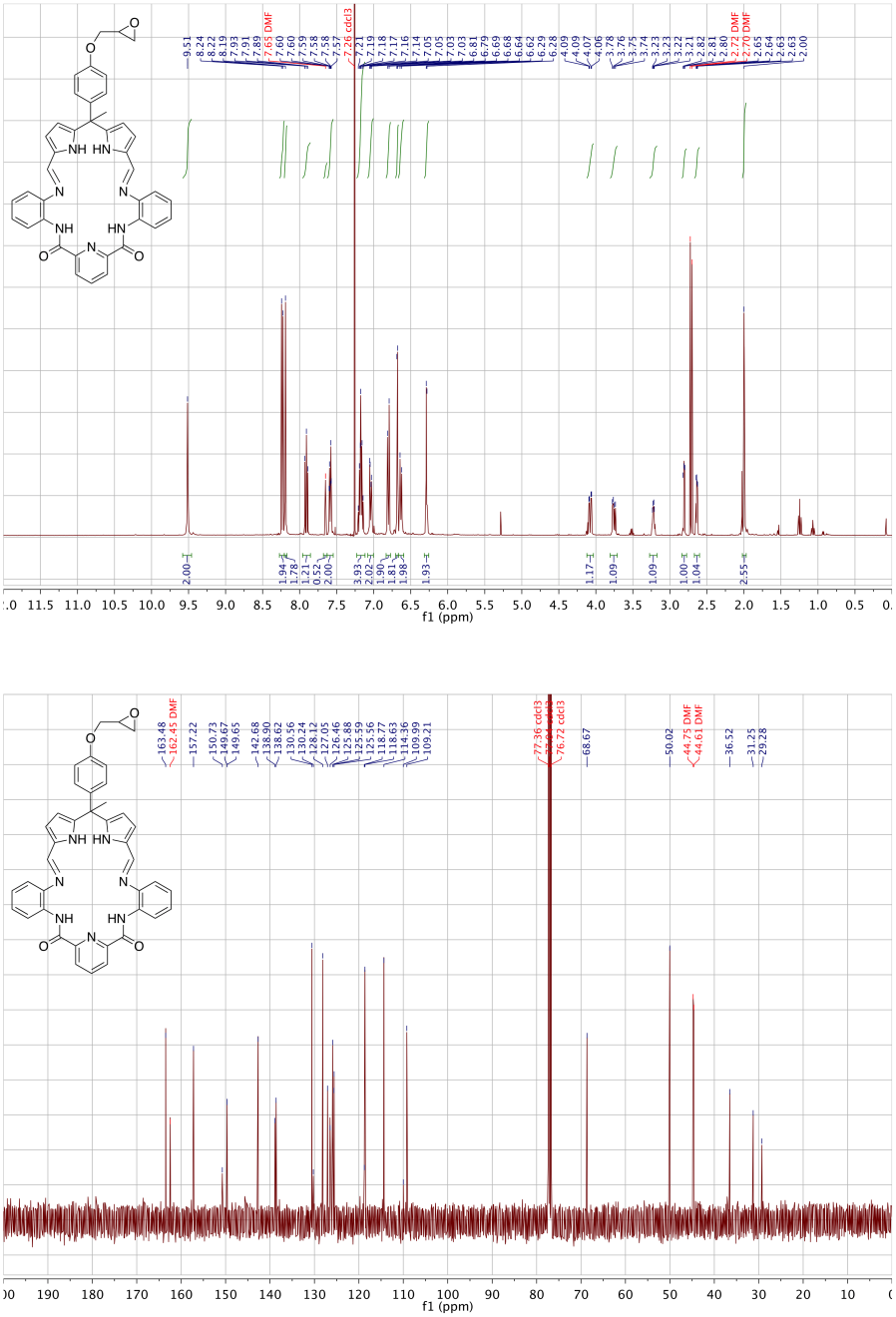

Figure 6.4: Top: ^{1}H NMR (400 MHz), Bottom: ^{13}C NMR (100 MHz) spectra of **2.15e** in $CDCl_3$.

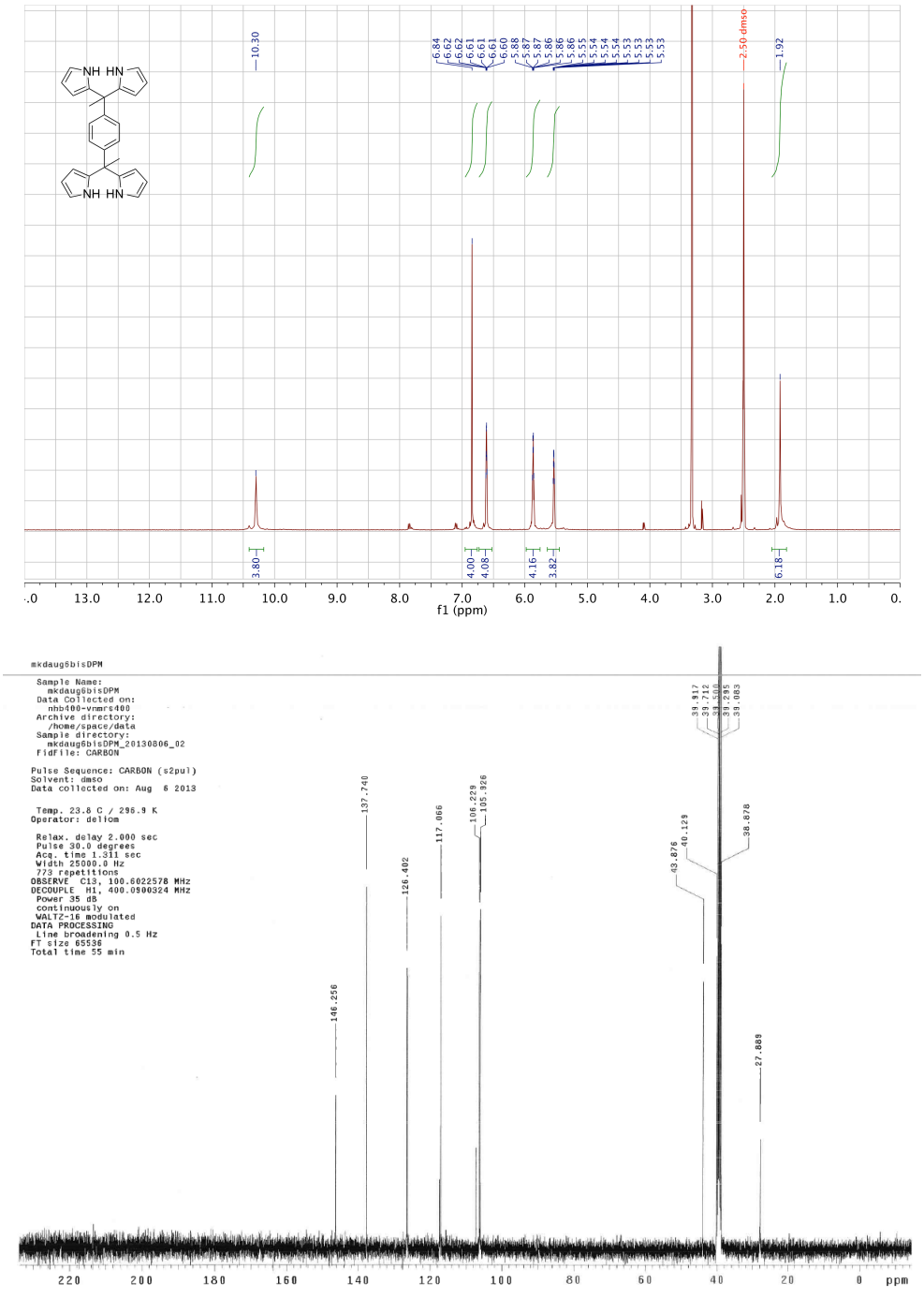

Figure 6.5: Top: ^{1}H NMR (400 MHz) Bottom:^{13}C NMR (100 MHz) spectra of **3.3a** in DMSO-d_6.

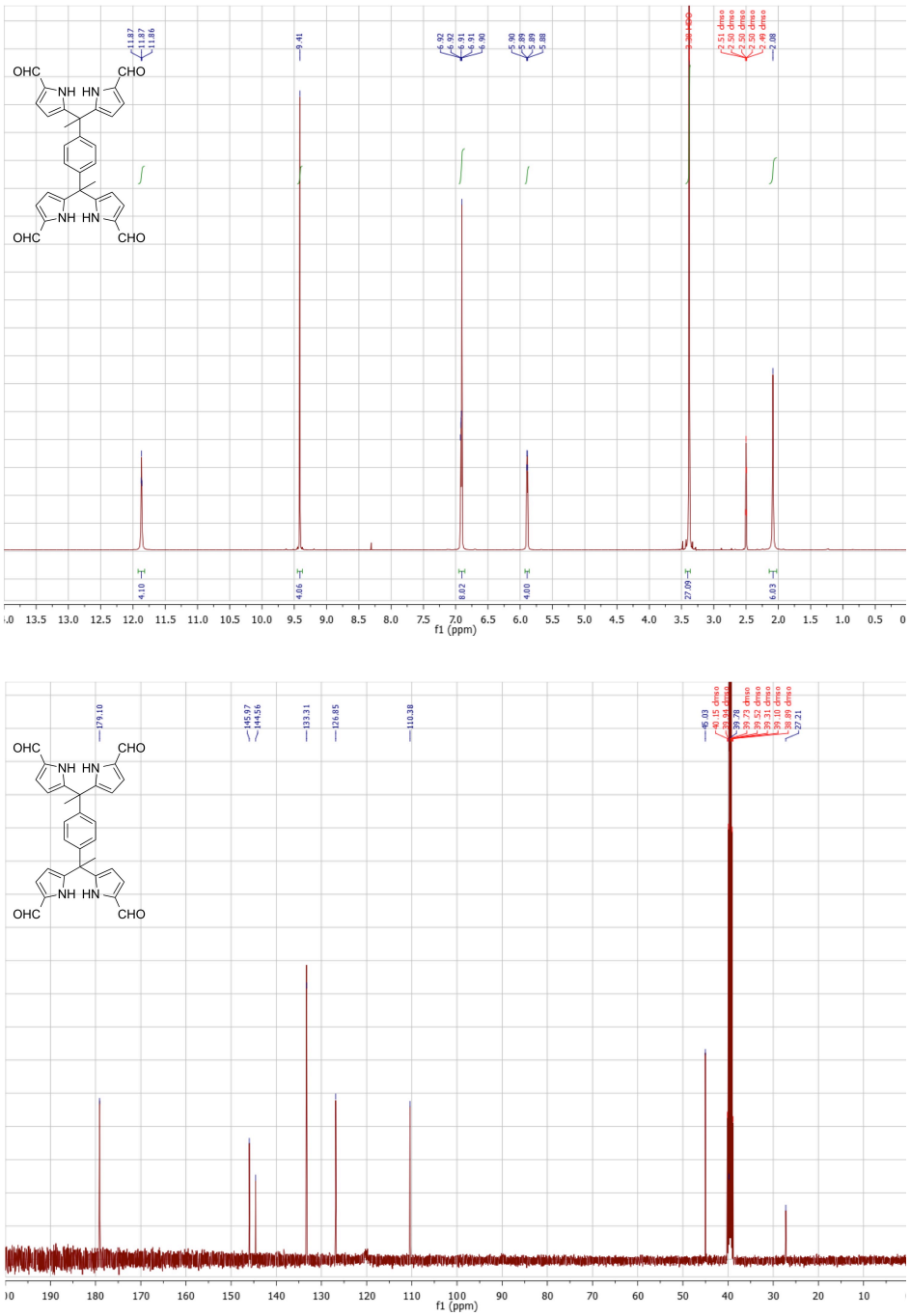

Figure 6.6: Top: ^{1}H NMR (400 MHz) Bottom: ^{13}C NMR (100 MHz) spectra of **3.3b** in DMSO-d_6.

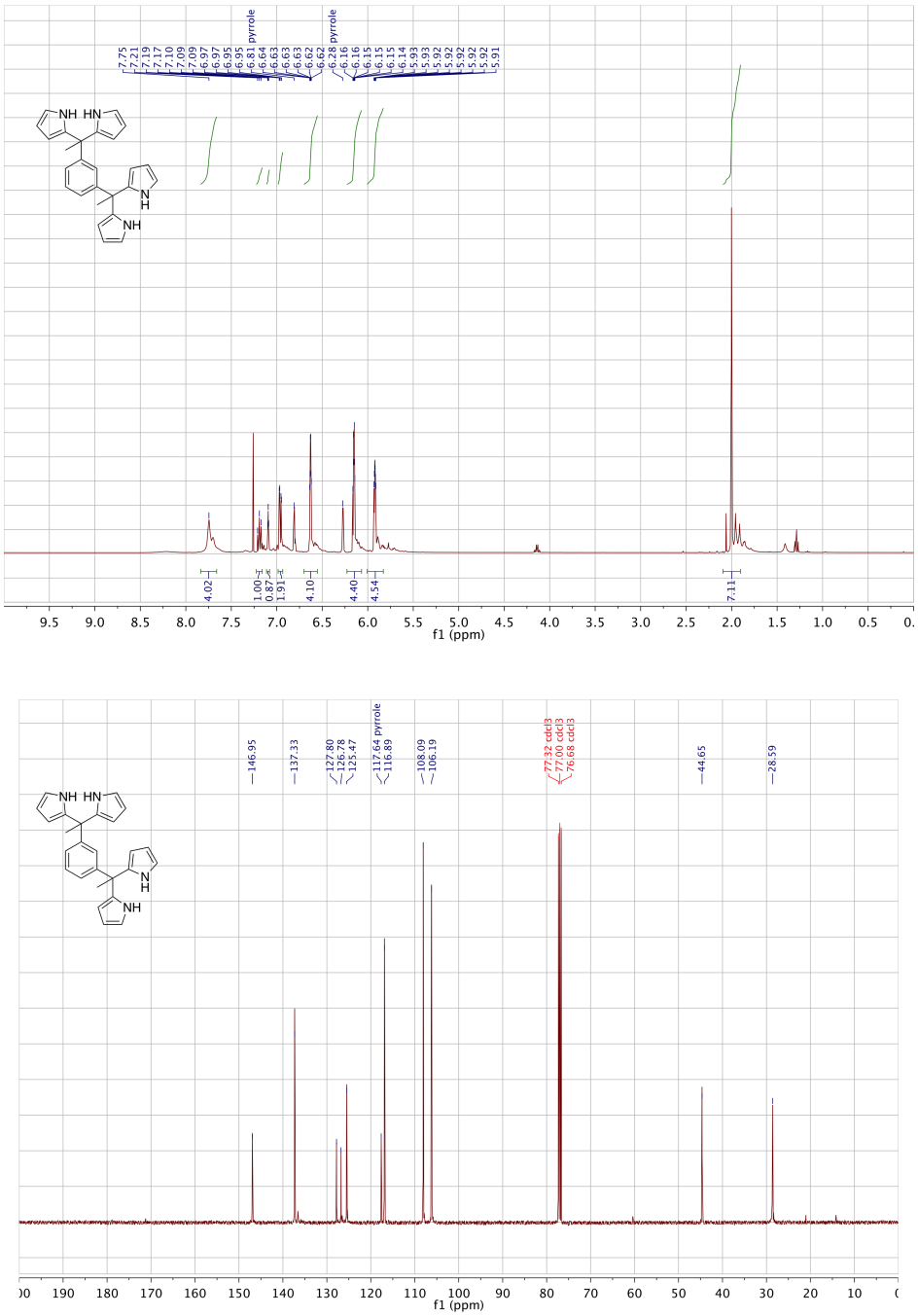

Figure 6.7: Top: ^{1}H NMR (400 MHz) Bottom:^{13}C NMR (100 MHz) spectra of **3.4a** in $CDCl_3$.

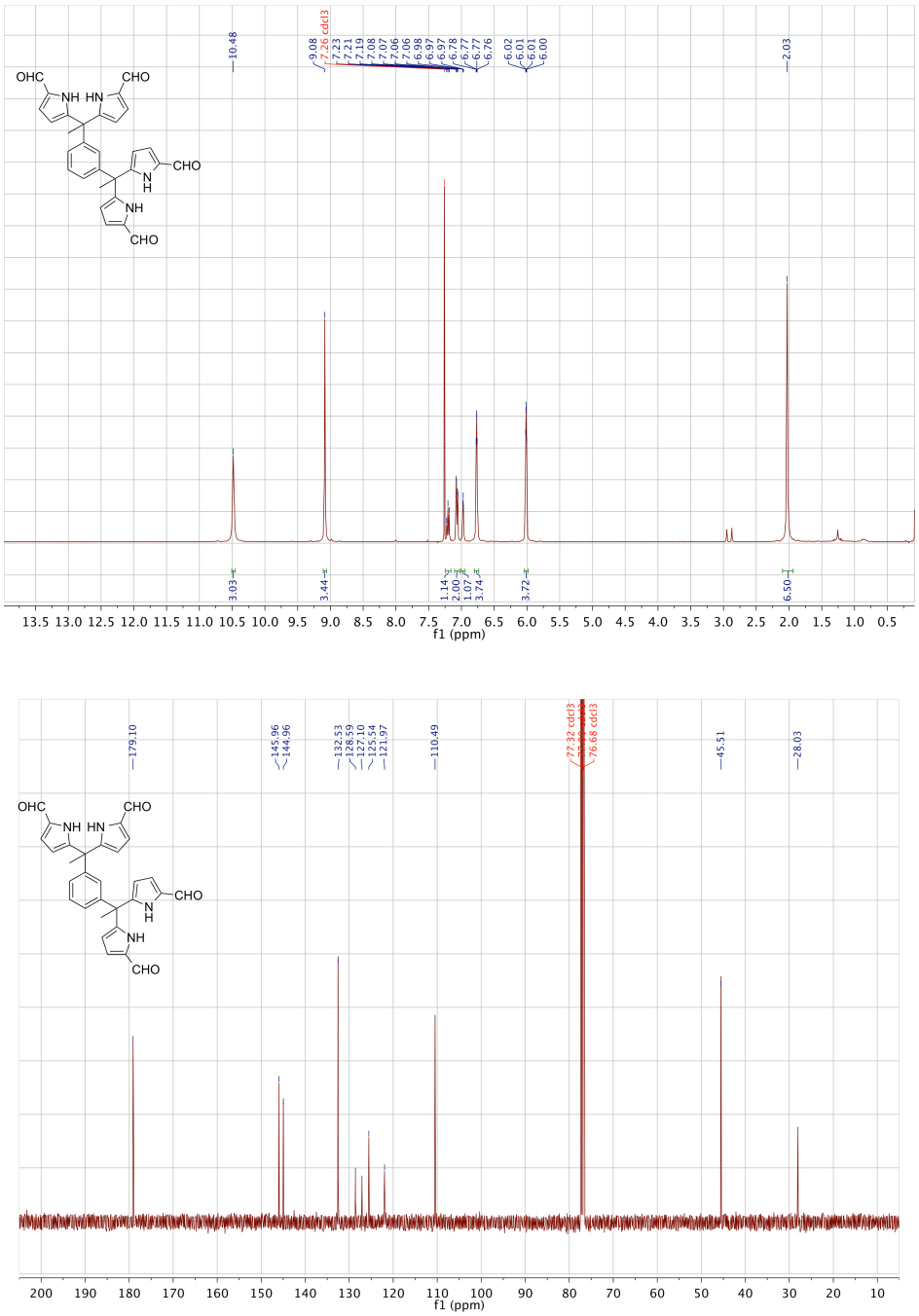

Figure 6.8: Top: ^{1}H NMR (400 MHz) Bottom:^{13}C NMR (100 MHz) spectra of **3.4b** in $CDCl_3$.

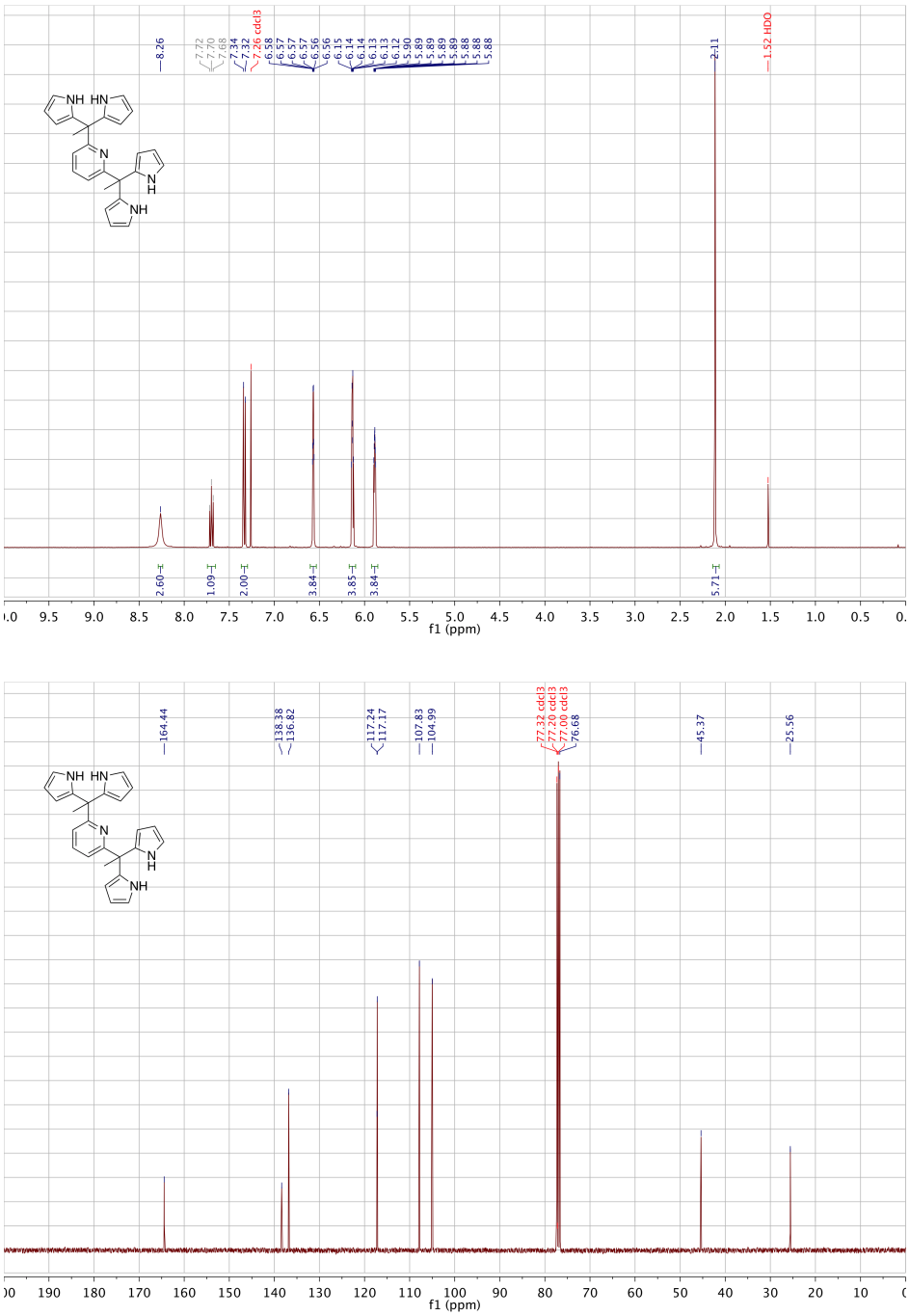

Figure 6.9: Top: ^{1}H NMR (400 MHz) Bottom:^{13}C NMR (100 MHz) spectra of **3.5a** in $CDCl_3$.

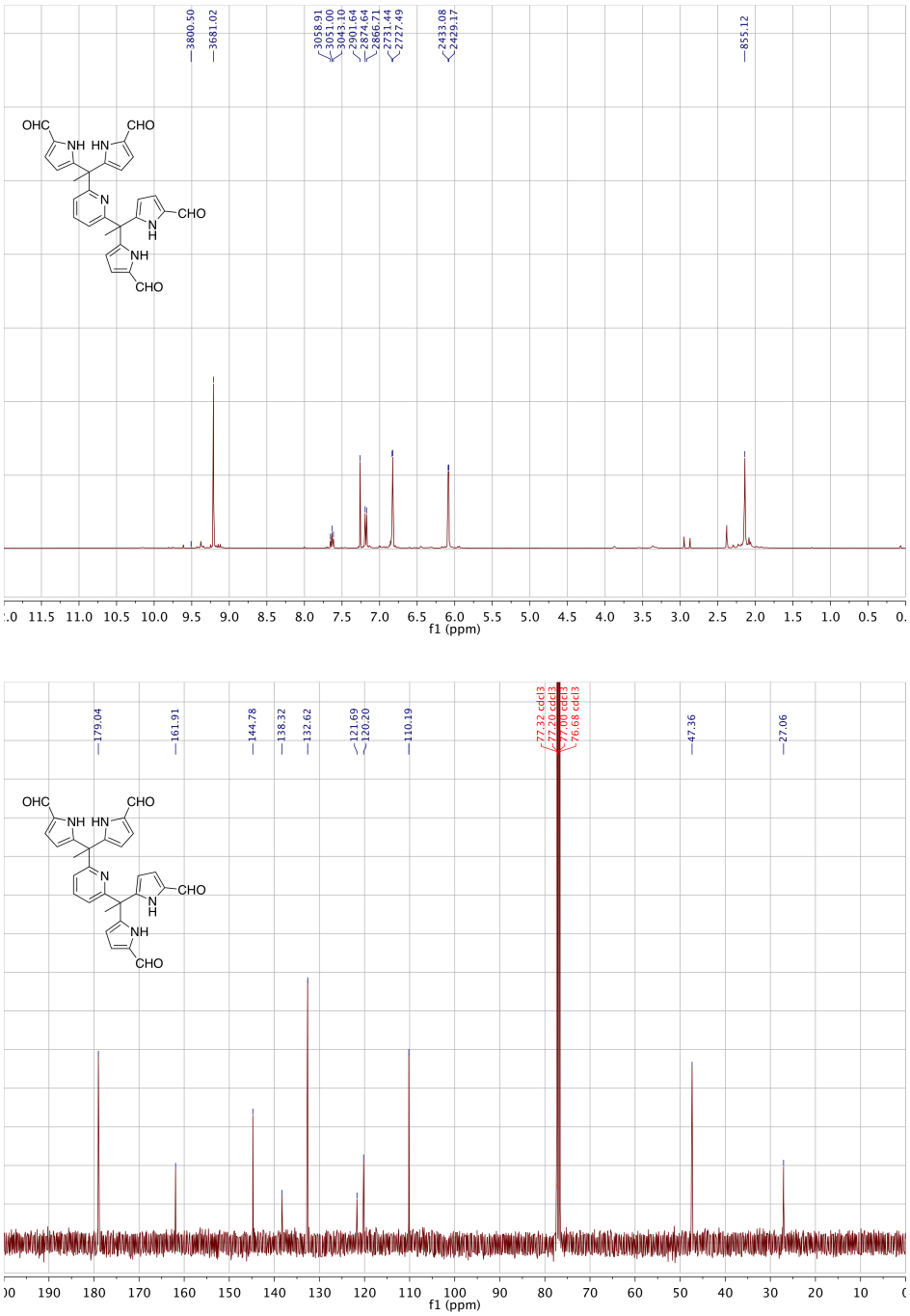

Figure 6.10: Top: ^{1}H NMR (400 MHz) Bottom: ^{13}C NMR (100 MHz) spectra of **3.5b** in $CDCl_3$.

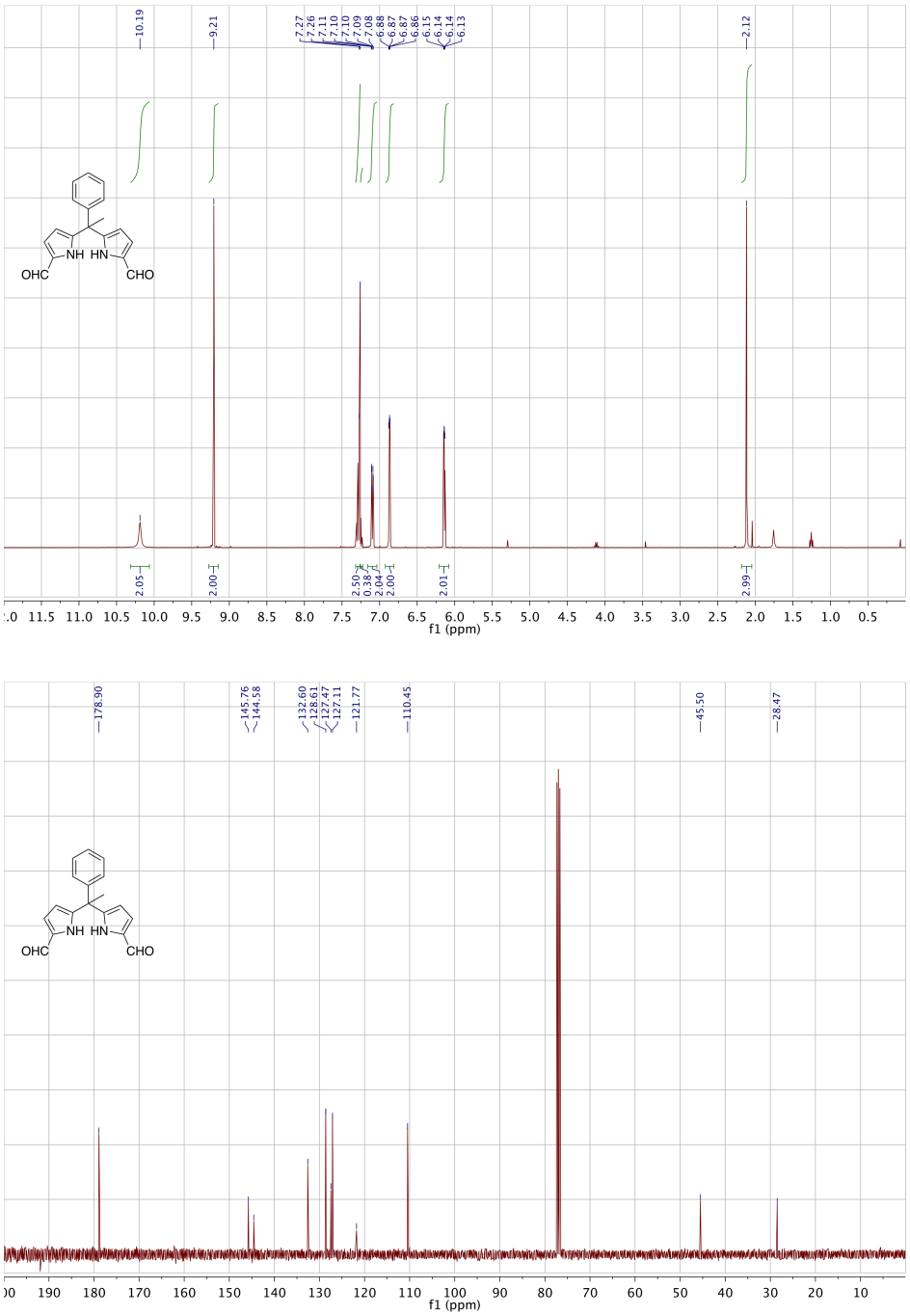

Figure 6.11: Top: ^{1}H NMR (400 MHz) Bottom: ^{13}C NMR (100 MHz) spectra of **3.13** in $CDCl_3$.

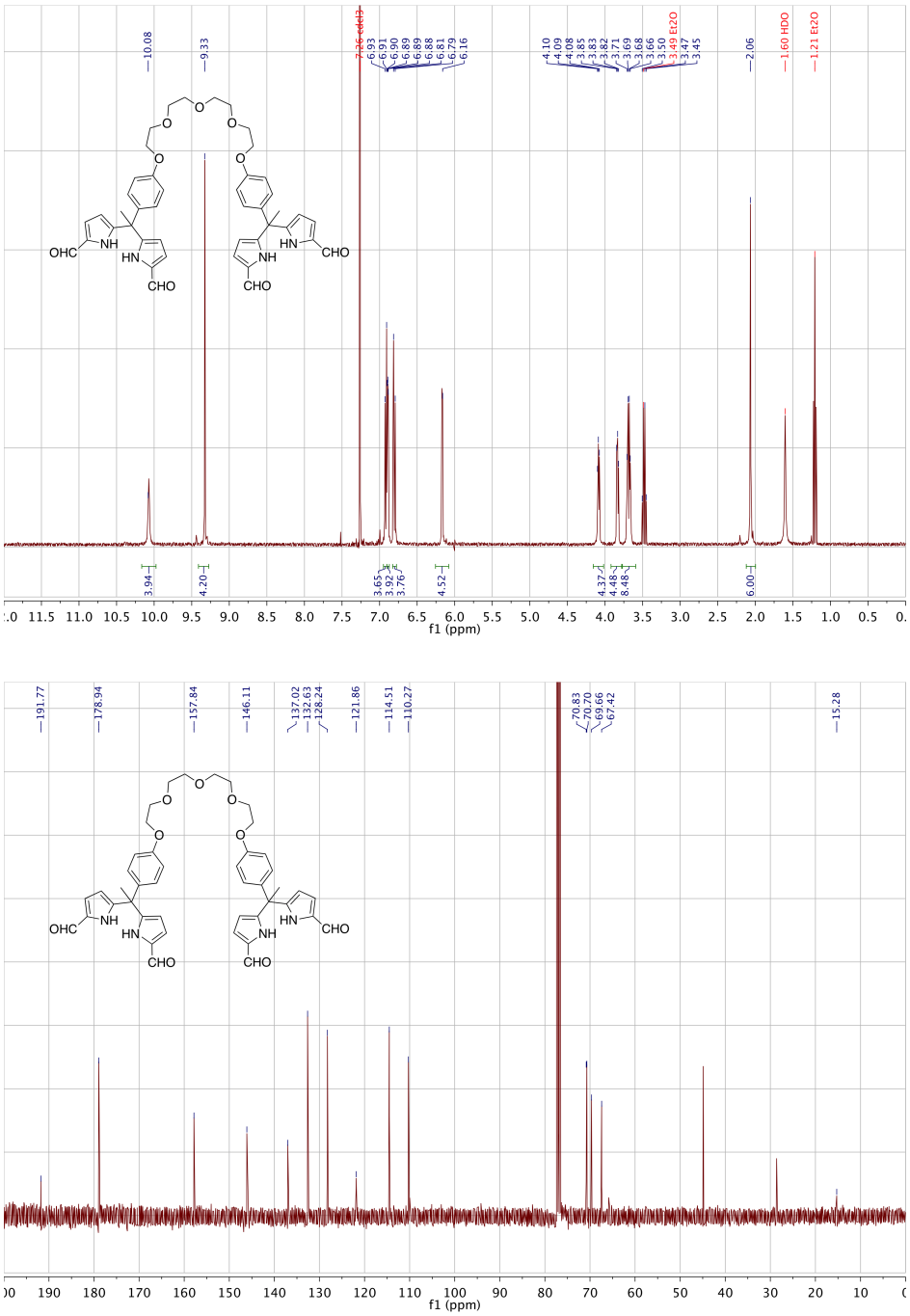

Figure 6.12: Top: ^{1}H NMR (400 MHz) Bottom: ^{13}C NMR (100 MHz) spectra of **3.14** in $CDCl_3$.

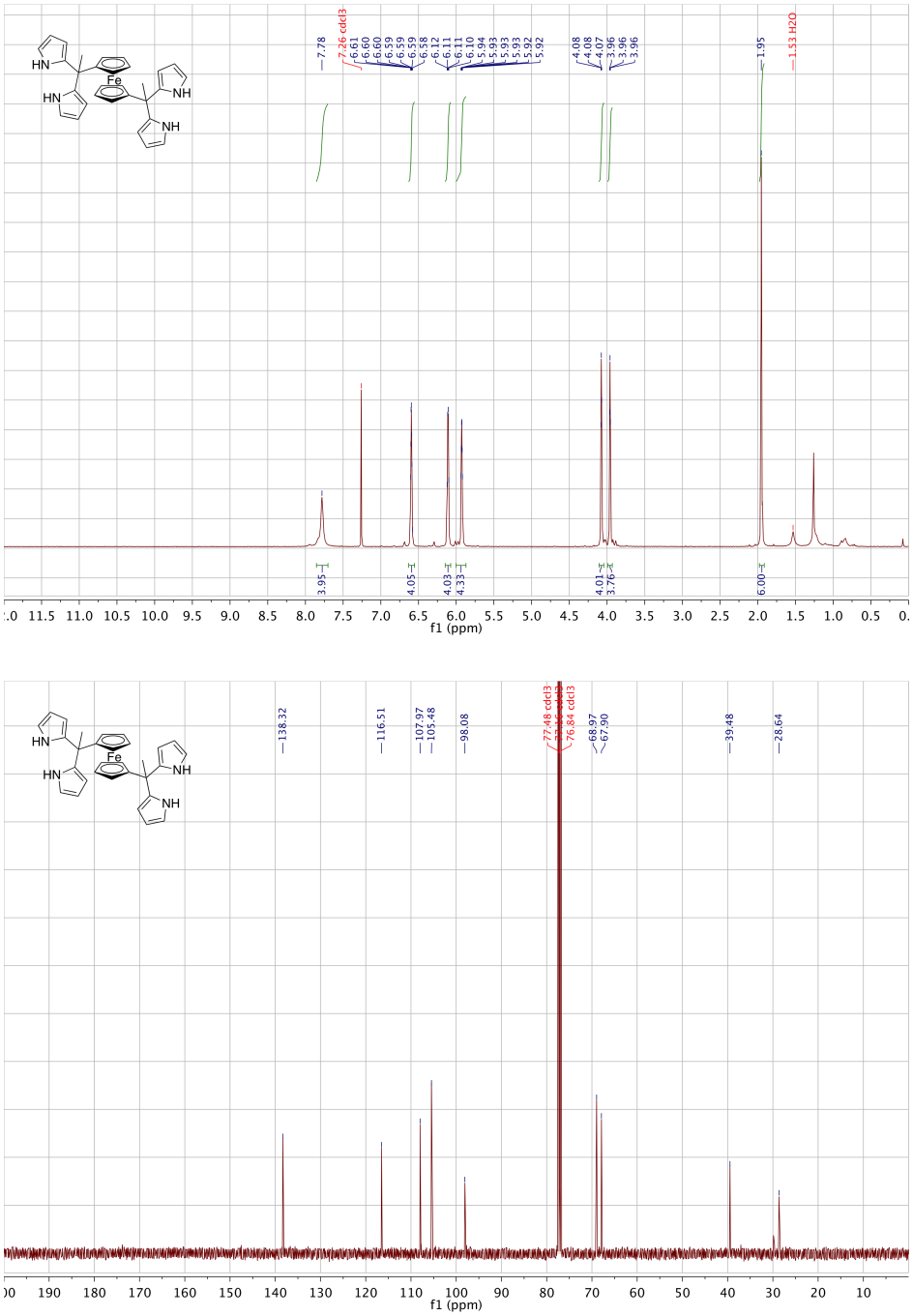

Figure 6.13: Top: ^{1}H NMR (400 MHz) Bottom: ^{13}C NMR (100 MHz) spectra of **4.1a** in $CDCl_3$.

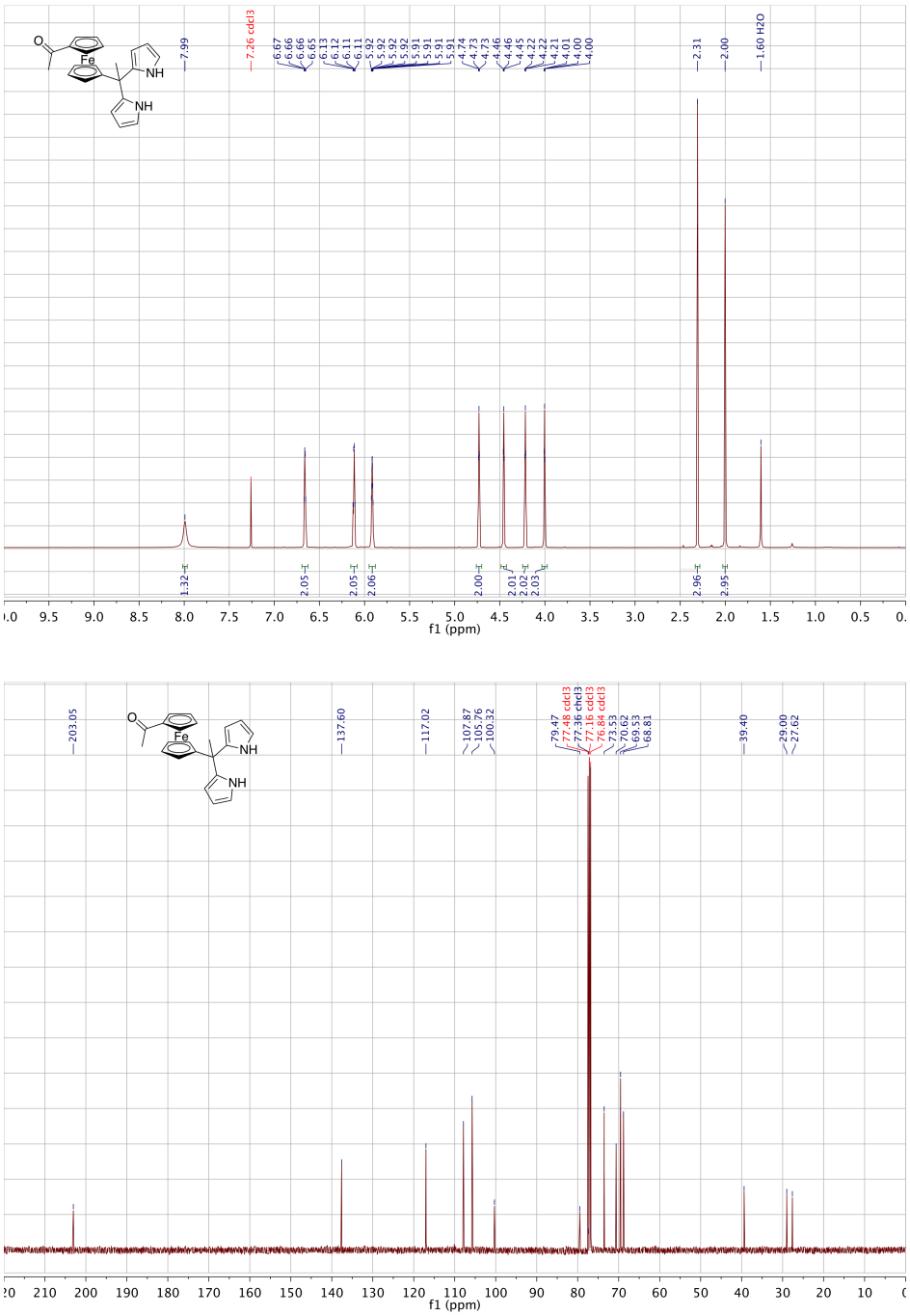

Figure 6.14: Top: ^{1}H NMR (400 MHz) Bottom: ^{13}C NMR (100 MHz) spectra of **4.1a'** in $CDCl_3$.

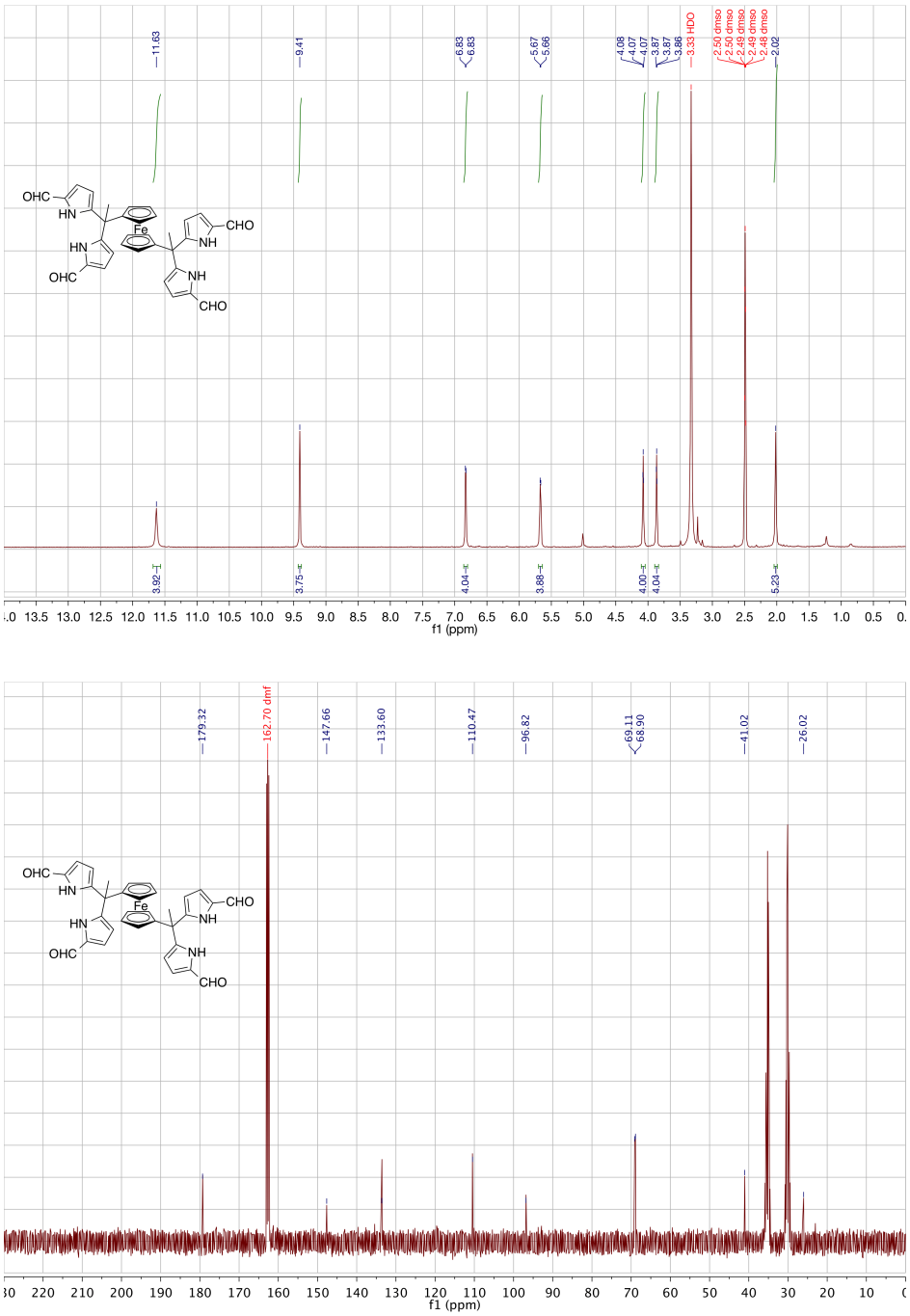

Figure 6.15: Top: ^{1}H NMR (400 MHz) spectrum of **4.1b** in DMSO-d_6. Bottom: ^{13}C NMR (100 MHz) spectrum of **4.1b** in DMF-d_7.

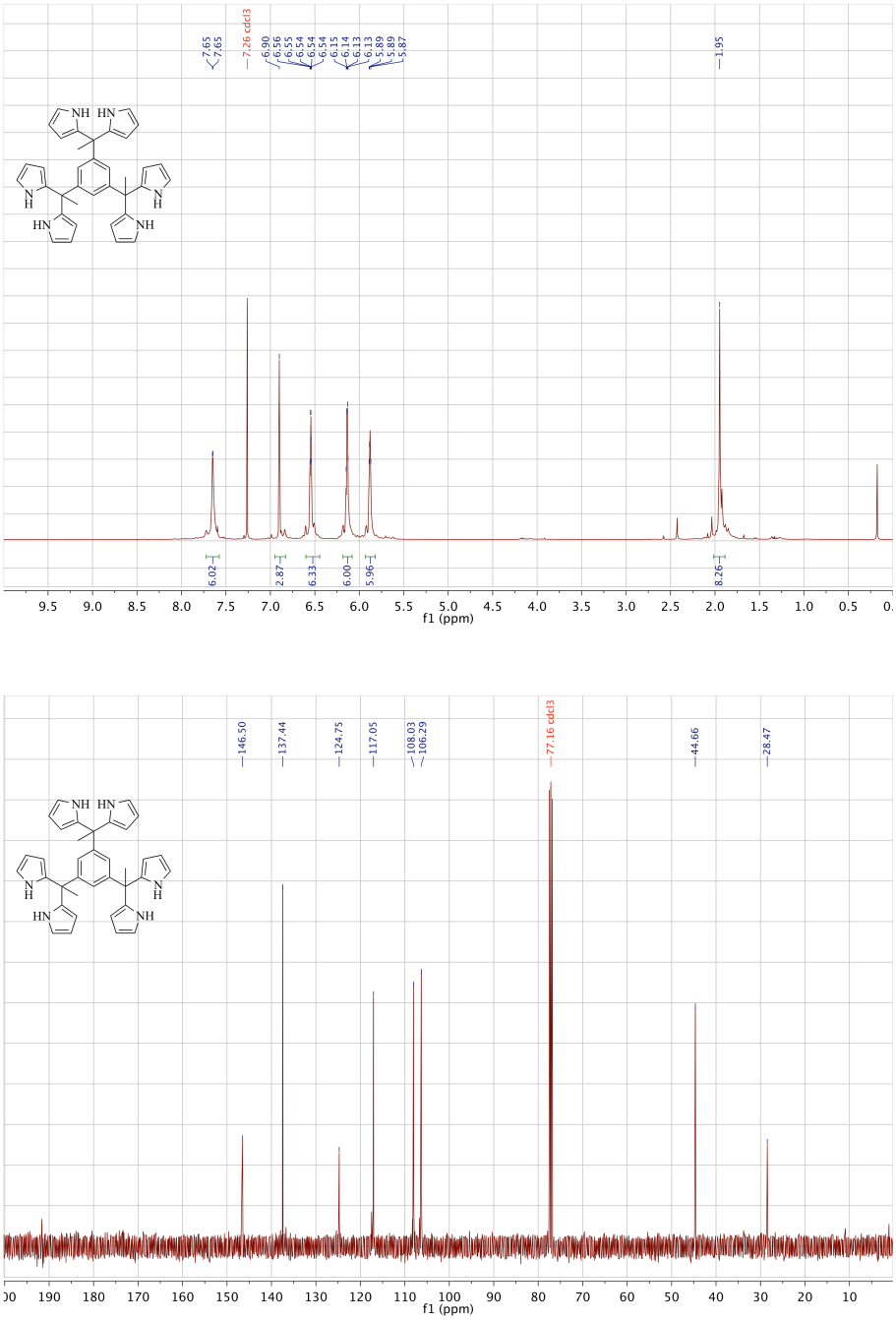

Figure 6.16: Top: ^{1}H NMR (400 MHz) Bottom: ^{13}C NMR (100 MHz) spectra of **4.2a** in $CDCl_3$.

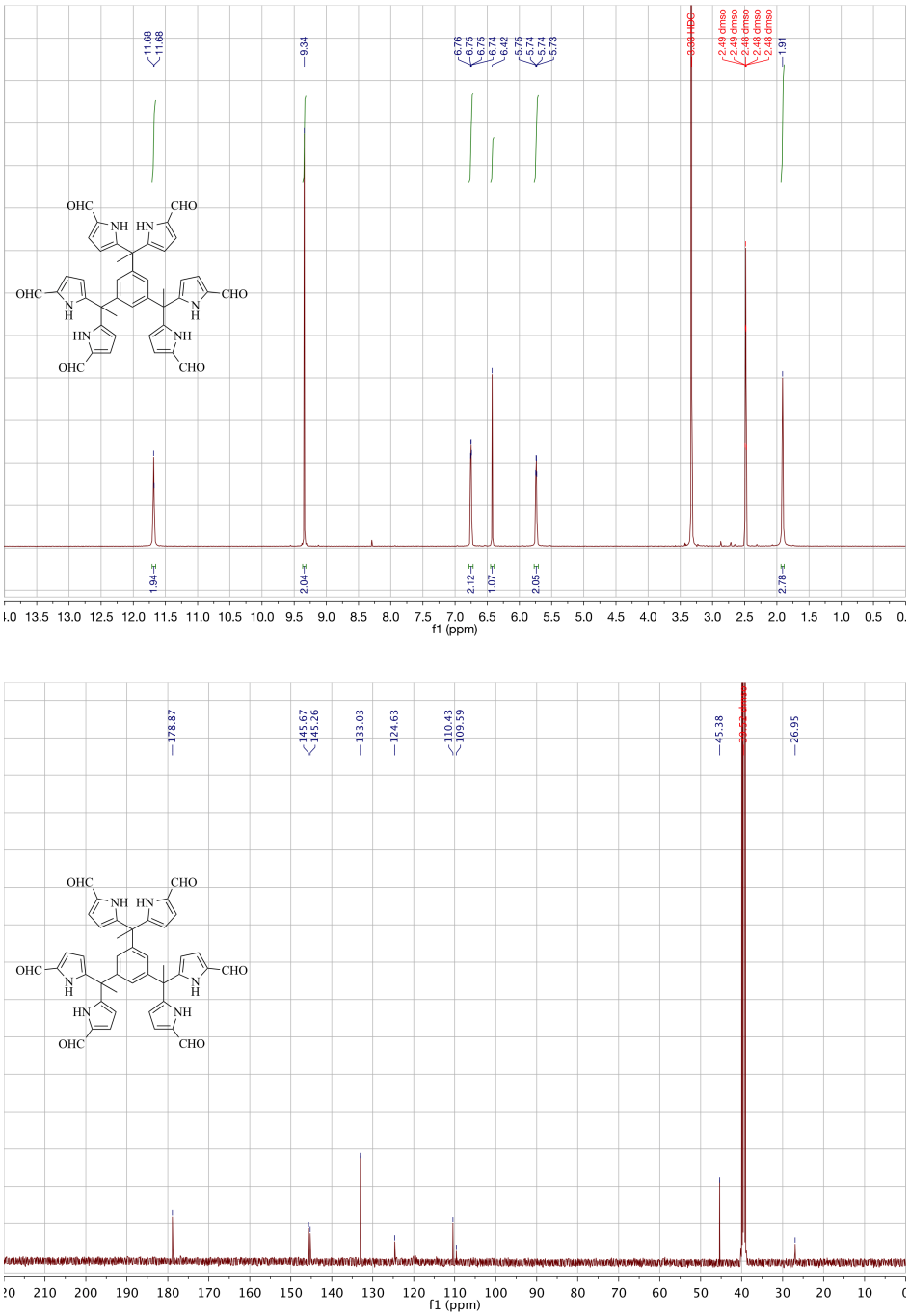

Figure 6.17: Top: ^{1}H NMR (400 MHz) Bottom: ^{13}C NMR (100 MHz) spectra of **4.2b** in DMSO-d_6.

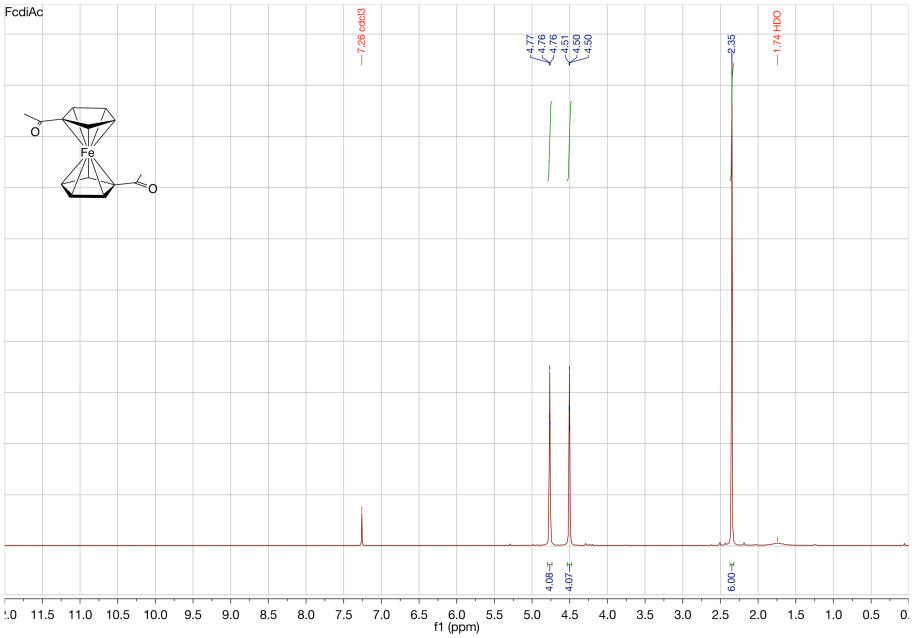

Figure 6.18: ^{1}H NMR (400 MHz) spectrum of starting material **4.1c** in $CDCl_3$.

6.3. REFERENCES

1. Gottlieb, H. E.; Kotlyar, V.; Nudelman, A. NMR Chemical Shifts of Common Laboratory Solvents as Trace Impurities. *J. Org. Chem.* **1997**, *62* (3), 7512–7515.

7. X-ray Diffraction Data

The X-ray diffraction data collections and refinements for crystal structures of **2.9b**, **2.14**, **2.15a**, **2.15b**, **3.3b**, **3.4b**, **4.1b**, and **4.2b** were performed by Dr. Vincent M. Lynch of the X-ray Diffraction Laboratory, Department of Chemistry and Biochemistry, University of Texas at Austin. Relevant data tables for all the refinements are included.

7.1. Crystallographic Experimental Methods

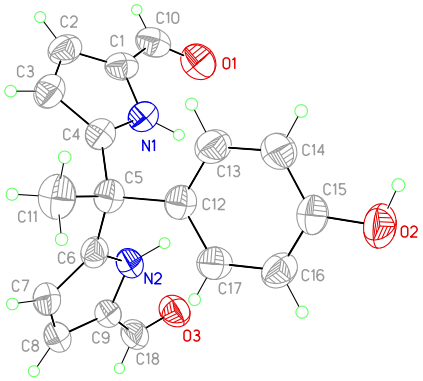

X-ray experimental for **2.9b** ($C_{18}H_{16}N_2O_3$): Crystals grew as clusters of large, colorless prisms by slow evaporation from methanol. The data crystal was cut from a larger crystal and had approximate dimensions; 0.48 x 0.32 x 0.11 mm. The data were collected at room temperature on a Rigaku SCX-Mini diffractometer with a Mercury 2 CCD using a graphite monochromator with MoKα radiation (λ = 0.71073Å). A total of 311 frames of data were collected using ω-scans with a scan range of 1° and a counting time of 35 seconds per frame. Details of crystal data, data collection and structure refinement are listed in Table 7.1. Data reduction were performed using the Rigaku

Americas Corporation's Crystal Clear version 1.40.[1] The structure was solved by direct methods using SIR2004[2] and refined by full-matrix least-squares on F^2 with anisotropic displacement parameters for the non-H atoms using SHELXL-2014/7.[3] Structure analysis was aided by use of the programs PLATON98[4] and WinGX.[5] The hydrogen atoms on carbon were calculated in ideal positions with isotropic displacement parameters set to 1.2xUeq of the attached atom (1.5xUeq for methyl hydrogen atoms). The H atoms bond to the pyrrole nitrogen atoms and to the hydroxyl oxygen atom were located in a ΔF map and refined with isotropic displacement parameters.

The function, $\Sigma w(|F_o|^2 - |F_c|^2)^2$, was minimized, where $w = 1/[(\sigma(F_o))^2 + (0.0558*P)^2 + (0.2999*P)]$ and $P = (|F_o|^2 + 2|F_c|^2)/3$. $R_w(F^2)$ refined to 0.121, with R(F) equal to 0.0447 and a goodness of fit, S, = 1.02. Definitions used for calculating R(F), $R_w(F^2)$ and the goodness of fit, S, are given below.[6] The data were checked for secondary extinction but no correction was necessary. Neutral atom scattering factors and values used to calculate the linear absorption coefficient are from the International Tables for X-ray Crystallography (1992).[7] All figures were generated using SHELXTL/PC.[8] Tables of positional and thermal parameters, bond lengths and angles, torsion angles and figures are not published.

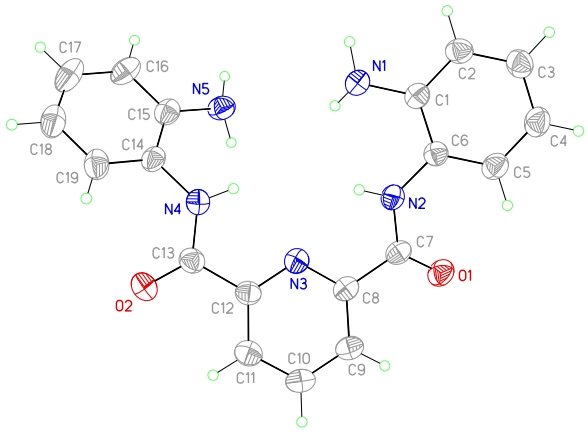

X-ray experimental for **2.14** ($C_{19}H_{17}N_5O_2$): Crystals grew as yellow prisms by slow evaporation from $CHCl_3$. The data crystal was cut from a larger crystal and had approximate dimensions; 0.30 x 0.20 x 0.10 mm. The data were collected on a Rigaku R-Axis Spider diffractometer with an image plate detector using a graphite monochromator with CuKα radiation (λ = 1.5418Å). A total of 180 images of data were collected using ω-scans with a scan range of 5° and a counting time of 240 seconds per image. The data were collected at 100 K using a Rigaku XStream low temperature device. Details of crystal data, data collection and structure refinement are listed in Table 7.2. Data reduction was performed using the Rigaku Americas Corporation's Crystal Clear version 1.40.[1] The structure was solved by direct methods using SIR97[9] and refined by full-matrix least-squares on F^2 with anisotropic displacement parameters for the non-H atoms using SHELXL-97.[10] Structure analysis was aided by use of the programs PLATON98[4] and WinGX.[5] The hydrogen atoms on carbon were calculated in ideal positions with isotropic displacement parameters set to 1.2xUeq of the attached atom. The hydrogen

atoms bound to nitrogen were observed in a ΔF map and refined with isotropic displacement parameters.

The function, $\Sigma w(|F_o|^2 - |F_c|^2)^2$, was minimized, where $w = 1/[(\sigma(F_o))^2 + (0.054*P)^2]$ and $P = (|F_o|^2 + 2|F_c|^2)/3$. $R_w(F^2)$ refined to 0.130, with R(F) equal to 0.0477 and a goodness of fit, S, = 1.29. Definitions used for calculating R(F), $R_w(F^2)$ and the goodness of fit, S, are given below.[6] The data were checked for secondary extinction effects but no correction was necessary. Neutral atom scattering factors and values used to calculate the linear absorption coefficient are from the International Tables for X-ray Crystallography (1992).[7] All figures were generated using SHELXTL/PC.[8] Tables of positional and thermal parameters, bond lengths and angles, torsion angles and figures are not yet published.

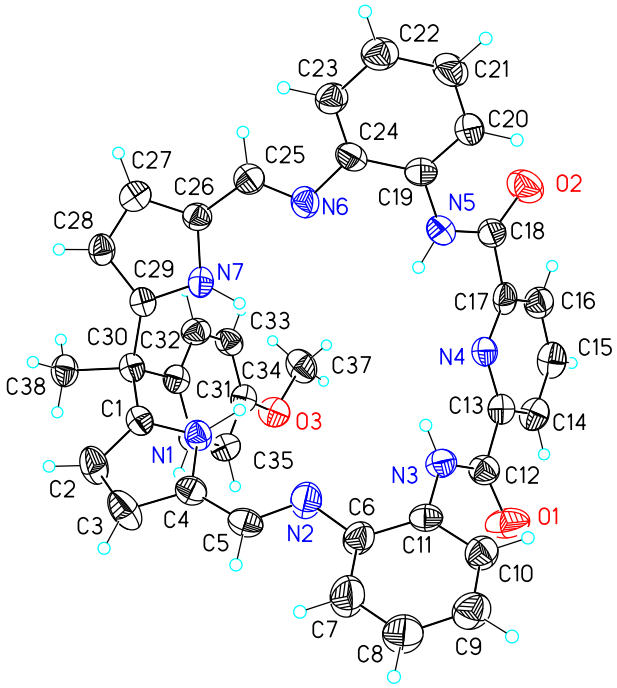

X-ray Experimental for **2.15a** ($C_{38}H_{31}N_7O_3$ – 2.5 CH_3OH): Crystals grew as long, yellow laths by slow evaporation from methanol. The data crystal had approximate

dimensions; 0.30 x 0.15 x 0.08 mm. The data were collected on a Nonius Kappa CCD diffractometer using a graphite monochromator with MoKα radiation (λ = 0.71073Å). A total of 356 frames of data were collected using ω-scans with a scan range of 0.8° and a counting time of 174 seconds per frame. The data were collected at 153 K using an Oxford Cryostream low temperature device. Details of crystal data, data collection and structure refinement are listed in Table 7.3. Data reduction were performed using DENZO-SMN.[11] The structure was solved by direct methods using SIR97[9] and refined by full-matrix least-squares on F^2 with anisotropic displacement parameters for the non-H atoms using SHELXL-97.[10] The hydrogen atoms were calculated in ideal positions with isotropic displacement parameters set to 1.2xUeq of the attached atom (1.5xUeq for methyl hydrogen atoms).

One molecule of methanol was disordered about a crystallographic inversion center at 0, 0, ½. It was assigned an occupancy of ½ because of the low electron density associated with this molecule. No H atoms for this molecule were included in the refinement model. One of the methanol molecules H-bound to the macrocycle appeared to have a disordered hydroxyl group H atom. This molecule composed of atoms O1b and C1b, was H-bound via the Schiff base amines, N3 and N5. The hydroxyl hydrogen appeared to be H-bound to the imine nitrogen atoms, N2 and N6, resulting in the disordered hydroxyl hydrogen bound to O1b.

The function, $\Sigma w(|F_o|^2 - |F_c|^2)^2$, was minimized, where $w = 1/[(\sigma(F_o))^2 + (0.0399*P)^2 + (1.2999*P)]$ and $P = (|F_o|^2 + 2|F_c|^2)/3$. $R_w(F^2)$ refined to 0.169, with R(F) equal to 0.0794 and a goodness of fit, S, = 1.07. Definitions used for calculating R(F),$R_w(F^2)$ and the goodness of fit, S, are given below.[6] The data were checked for secondary extinction effects but no correction was needed. Neutral atom scattering factors and values used to calculate the linear absorption coefficient are from the

International Tables for X-ray Crystallography (1992).[7] All figures were generated using SHELXTL/PC.[8] Tables of positional and thermal parameters, bond lengths and angles, torsion angles, H-bonding interactions and figures are not yet published.

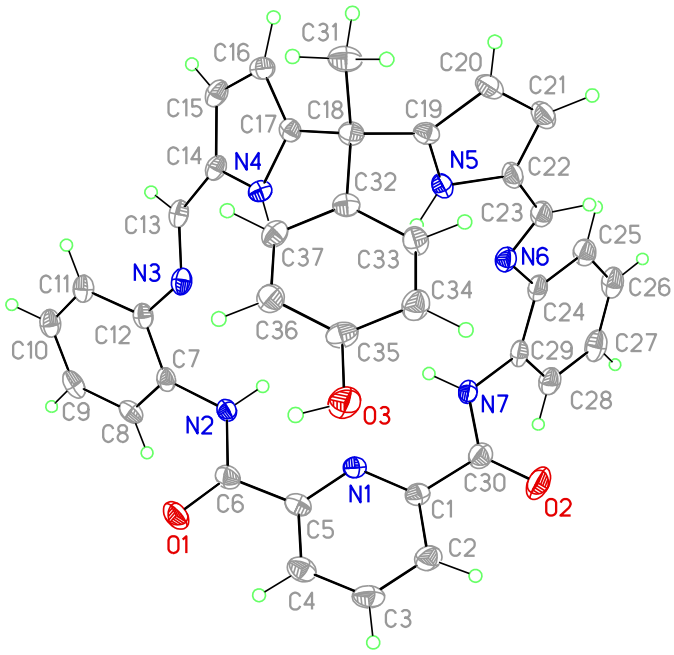

X-ray experimental for **2.15b** ($C_{37}H_{36}N_7O_3$ – 4 C_3H_7NO): Crystals grew as yellow plates by slow evaporation from N,N-dimethylformamide. The data crystal was cut from a larger crystal and had approximate dimensions; 0.34 x 0.24 x 0.09 mm. The data were collected on a Rigaku SCX-Mini diffractometer with a Mercury 2 CCD using a graphite monochromator with MoKα radiation (λ = 0.71075Å). A total of 1440 frames of data were collected using ω-scans with a scan range of 0.5° and a counting time of 21 seconds per frame. The data were collected at 100 K using a Rigaku XStream low temperature device. Details of crystal data, data collection and structure refinement are listed in Table 7.4. Data reduction was performed using the Rigaku Americas Corporation's Crystal Clear version 1.40.[1] The structure was solved by direct methods

using SIR97[9] and refined by full-matrix least-squares on F^2 with anisotropic displacement parameters for the non-H atoms using SHELXL-97.[10] Structure analysis was aided by use of the programs PLATON98[4] and WinGX.[5] The hydrogen atoms on carbon were calculated in ideal positions with isotropic displacement parameters set to 1.2xUeq of the attached atom (1.5xUeq for methyl hydrogen atoms). The hydrogen atoms on nitrogen and oxygen were observed in a ΔF map and refined with isotropic displacement parameters.

The function, $\Sigma w(|F_o|^2 - |F_c|^2)^2$, was minimized, where $w = 1/[(\sigma(F_o))^2 + (0.0484*P)^2 + (4.0684*P)]$ and $P = (|F_o|^2 + 2|F_c|^2)/3$. $R_w(F^2)$ refined to 0.154, with R(F) equal to 0.0642 and a goodness of fit, S, = 1.06. Definitions used for calculating R(F), $R_w(F^2)$ and the goodness of fit, S, are given below.[6] The data were checked for secondary extinction but no correction was necessary. Neutral atom scattering factors and values used to calculate the linear absorption coefficient are from the International Tables for X-ray Crystallography (1992).[7] All figures were generated using SHELXTL/PC.[8] Tables of positional and thermal parameters, bond lengths and angles, torsion angles and figures are not yet published.

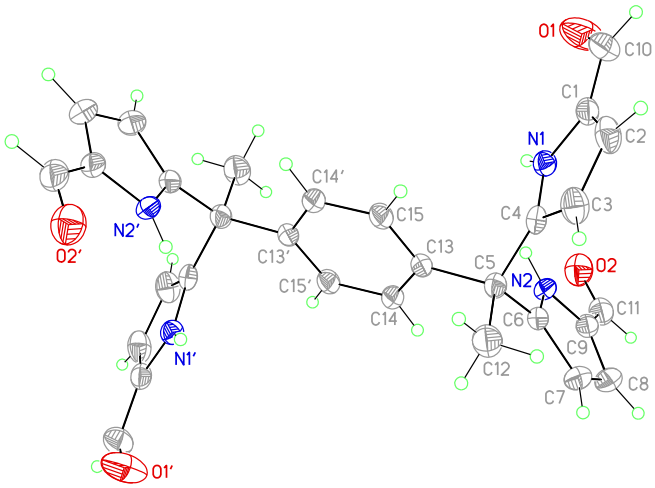

X-ray experimental for **3.3b**·2DMF ($C_{30}H_{36}N_4O_4$ – 2 C_3H_7NO): Crystals grew as orange prisms by slow evaporation from DMF. The data crystal was cut from a larger crystal and had approximate dimensions; 0.32 x 0.30 x 0.25 mm. The data were collected at -120 °C on a Nonius Kappa CCD diffractometer using a Bruker AXS Apex II detector and a graphite monochromator with MoKα radiation (λ = 0.71075Å). Reduced temperatures were maintained by use of an Oxford Cryosystems 600 low-temperature device. A total of 403 frames of data were collected using ω and ϕ-scans with a scan range of 2° and a counting time of 40 seconds per frame. Details of crystal data, data collection and structure refinement are listed in Table 7.5. Data reduction was performed using SAINT V8.27B.[12] The structure was solved by direct methods using SIR97[9] and refined by full-matrix least-squares on F^2 with anisotropic displacement parameters for the non-H atoms using SHELXL-2013.[13] Structure analysis was aided by use of the programs PLATON98[4] and WinGX.[5] The hydrogen atoms on C14 and C15 were observed in a ΔF map and refined with isotropic displacement parameters. The remaining

H atoms were calculated in idealized positions with Uiso set to 1.2xUeq of the attached atom (1.5xUeq for the methyl groups).

The DMF solvate molecule was disordered. The disorder was modeled by assigning the variable x to the site occupancy factors for one component of the disorder, while (1-x) was assigned to the site occupancy factors for the alternate component. The geometry of the two components was restrained to be equivalent throughout the refinement process. A common isotropic displacement parameter was refined while refining x. In this way, the major component of the disordered solvate molecule had a site occupancy of 80(2)%.

The function, $\Sigma w(|F_o|^2 - |F_c|^2)^2$, was minimized, where $w = 1/[(\sigma(F_o))^2 + (0.0425*P)^2 + (0.8566*P)]$ and $P = (|F_o|^2 + 2|F_c|^2)/3$. $R_w(F^2)$ refined to 0.116, with R(F) equal to 0.0437 and a goodness of fit, S, = 1.03. Definitions used for calculating R(F),$R_w(F^2)$ and the goodness of fit, S, are given below.[6] The data were checked for secondary extinction but no correction was necessary. Neutral atom scattering factors and values used to calculate the linear absorption coefficient are from the International Tables for X-ray Crystallography (1992).[7] All figures were generated using SHELXTL/PC.[8] Tables of positional and thermal parameters, bond lengths and angles, torsion angles and figures may be obtained from the CCDC by referencing CCDC number 1012700.

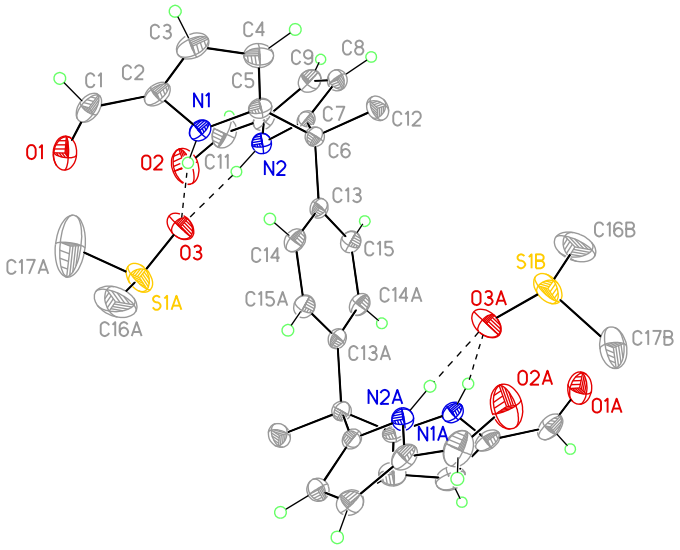

X-ray experimental for **3.3b**·2DMSO ($C_{30}H_{26}N_4O_4$ – 2 C_2H_6SO): Crystals grew as large, pale yellow plates by slow evaporation from DMSO. The data crystal was cut from a larger crystal and had approximate dimensions; 0.22 x 0.20 x 0.14 mm. The data were collected at -120 °C on a Nonius Kappa CCD diffractometer using a Bruker AXS Apex II detector and a graphite monochromator with MoKα radiation (λ = 0.71075Å). Reduced temperatures were maintained by use of an Oxford Cryosystems 600 low-temperature device. A total of 1342 frames of data were collected using ω and ϕ-scans with a scan range of 1.1° and a counting time of 39 seconds per frame. Details of crystal data, data collection and structure refinement are listed in Table 7.6. Data reduction were performed using SAINT V8.27B.[12] The structure was solved by direct methods using SIR97[9] and refined by full-matrix least-squares on F^2 with anisotropic displacement parameters for the non-H atoms using SHELXL-97.[10] Structure analysis was aided by use of the programs PLATON98[4] and WinGX.[5] Most of the hydrogen atoms on carbon were calculated in idealized positions with Uiso set to 1.2xUeq of the attached atom (1.5xUeq

for methyl groups). The hydrogen atoms bound to N1, N2, C14 and C15 were observed in a ΔF map and refined with isotropic displacement parameters.

The complex sits around a crystallographic inversion center at ¼, ¼, ½. The DMSO molecule is disordered. The disorder involves the sulfur atom and the two methyl groups. The disorder was modeled by assigning the variable x to the site occupancy factors for one component of the disorder. The variable (1-x) was assigned to the site occupancy factors of the alternate component. The geometry of the two components was restrained to be equivalent throughout the refinement process. A common isotropic displacement parameter was refined for the S atoms and a second isotropic displacement parameter was refined for the C atoms while refining the variable x. In this way, the site occupancy for the major component refined to 58(2)%.

The function, $\Sigma w(|F_o|^2 - |F_c|^2)^2$, was minimized, where $w = 1/[(\sigma(F_o))^2 + (0.0478*P)^2 + (3.1524*P)]$ and $P = (|F_o|^2 + 2|F_c|^2)/3$. $R_w(F^2)$ refined to 0.107, with R(F) equal to 0.0391 and a goodness of fit, S, = 1.05. Definitions used for calculating R(F),$R_w(F^2)$ and the goodness of fit, S, are given below.[6] The data were checked for secondary extinction but no correction was necessary. Neutral atom scattering factors and values used to calculate the linear absorption coefficient are from the International Tables for X-ray Crystallography (1992).[7] All figures were generated using SHELXTL/PC.[8] Tables of positional and thermal parameters, bond lengths and angles, torsion angles and figures may be obtained from the CCDC by referencing CCDC number 1012698.

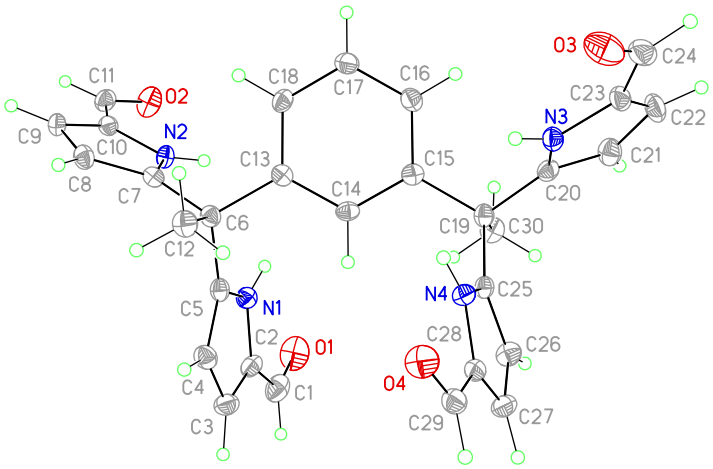

X-ray experimental for **3.4b**·2DMF ($C_{30}H_{26}N_4O_4$ - 2 C_3H_7NO): Crystals grew as clusters of octahedral shaped colorless prisms by slow evaporation from N,N-dimethylformamide. The data crystal had approximate dimensions; 0.20 x 0.11 x 0.10 mm. The data were collected on a Rigaku AFC12 diffractometer with a Saturn 724+ CCD using a graphite monochromator with MoKα radiation (λ = 0.71073Å). A total of 1104 frames of data were collected using ω-scans with a scan range of 0.5° and a counting time of 45 seconds per frame. The data were collected at 153 K using an Oxford Cryostream low temperature device. Details of crystal data, data collection and structure refinement are listed in Table 7.7. Data reduction were performed using the Rigaku Americas Corporation's Crystal Clear version 1.40.1 The structure was solved by direct methods using SIR97[9] and refined by full-matrix least-squares on F^2 with anisotropic displacement parameters for the non-H atoms using SHELXL-97.[10] Structure analysis was aided by use of the programs PLATON98[4] and WinGX.[5] The hydrogen atoms on

carbon were calculated in ideal positions with isotropic displacement parameters set to 1.2xUeq of the attached atom (1.5xUeq for methyl hydrogen atoms). The hydrogen atoms bound to nitrogen were located in a ΔF map and refined with isotropic displacement parameters.

The function, $\Sigma w(|F_o|^2 - |F_c|^2)^2$, was minimized, where $w = 1/[(\sigma(F_o))^2 + (0.0326*P)^2 + (4.3345*P)]$ and $P = (|F_o|^2 + 2|F_c|^2)/3$. $R_w(F^2)$ refined to 0.123, with R(F) equal to 0.0676 and a goodness of fit, S, = 1.13. Definitions used for calculating R(F), $R_w(F^2)$ and the goodness of fit, S, are given below.[6] The data were checked for secondary extinction effects but no correction was necessary. Neutral atom scattering factors and values used to calculate the linear absorption coefficient are from the International Tables for X-ray Crystallography (1992).[7] All figures were generated using SHELXTL/PC.[8] Tables of positional and thermal parameters, bond lengths and angles, torsion angles and figures may be obtained from the CCDC by referencing CCDC number 1012699.

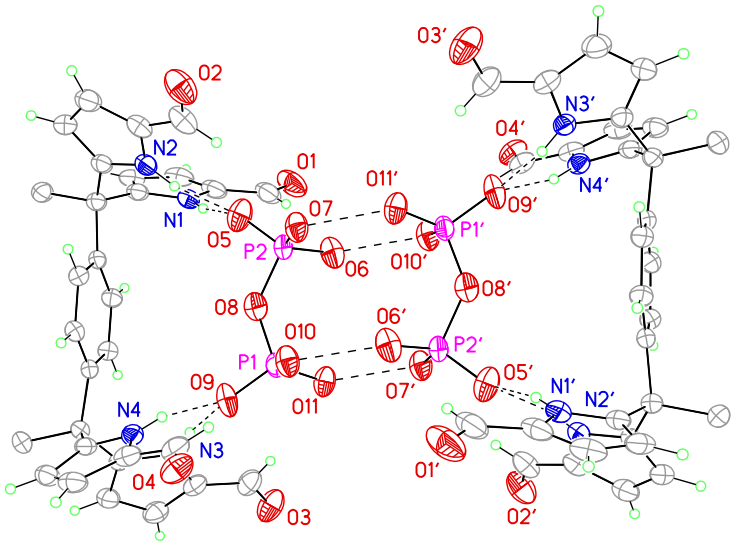

X-ray Experimental for **3.3b**·$(TBA)_2H_2P_2O_7$ $C_{30}H_{26}N_4O_4$ - 2 $C_{16}H_{36}N^{1+}$ $H_2P_2O_7^{2-}$ ½ CH_2Cl_2: Crystals grew as thin, colourless prisms by layering a solution of **3.3b**·$(TBA)_3HP_2O_7$ in CH_2Cl_2 with *n*-pentane. The data crystal had approximate dimensions; 0.16 x 0.11 x 0.06 mm. The data were collected on an Agilent Technologies SuperNova Dual Source diffractometer using a μ-focus Cu Kα radiation source (λ = 1.5418Å) with collimating mirror monochromators. A total of 850 frames of data were collected using ω-scans with a scan range of 0.5° and a counting time of 7 seconds per frame using a detector offset of +/- 41.1° and a counting time of 25 seconds per frame using a detector offset of +/- 108.3°. The data were collected at 100 K using an Oxford Cryostream low temperature device. Details of crystal data, data collection and structure refinement are listed in Table 7.8. Data collection, unit cell refinement and data reduction were performed using Agilent Technologies CrysAlisPro V 1.171.37.31.[14] The structure was solved by direct methods using SIR97[9] and refined by full-matrix least-squares on F^2 with anisotropic displacement parameters for the non-H atoms using SHELXL-2013.[13] Structure analysis was aided by use of the programs PLATON98[4] and WinGX.[5] The hydrogen atoms were calculated in ideal positions with isotropic displacement parameters set to 1.2xUeq of the attached atom (1.5xUeq for methyl hydrogen atoms.

Compound **3.3b** and the pyrophosphate form H-bound dimers across a crystallographic inversion centre located at ½, ½, ½. The pyrophosphate dianion was H-bound to itself across this centre. Reliable coordinates for the hydrogen atoms bound to the pyrophosphate could not be located in a difference electron density map. These hydrogen atoms were not included in the final refinement model.

A molecule of dichloromethane was found to be badly disordered around a crystallographic inversion centre at 0, ½, ½. Attempts to model the disorder were unsatisfactory. The contributions to the scattering factors due to this solvent molecule

were removed by use of the utility SQUEEZE in PLATON98. PLATON98 was used as incorporated in WinGX.

The function, $\Sigma w(|F_o|^2 - |F_c|^2)^2$, was minimized, where $w = 1/[(\sigma(F_o))^2 + (0.0827*P)^2 + (5.3705*P)]$ and $P = (|F_o|^2 + 2|F_c|^2)/3$. $R_w(F^2)$ refined to 0.171, with R(F) equal to 0.0603 and a goodness of fit, S, = 1.03. Definitions used for calculating R(F), $R_w(F^2)$ and the goodness of fit, S, are given below.[6] The data were checked for secondary extinction effects but no correction was necessary. Neutral atom scattering factors and values used to calculate the linear absorption coefficient are from the International Tables for X-ray Crystallography (1992).[7] All figures were generated using SHELXTL/PC.[8] Tables of positional and thermal parameters, bond lengths and angles, torsion angles and figures may be obtained from the CCDC by referencing CCDC number 1444559.

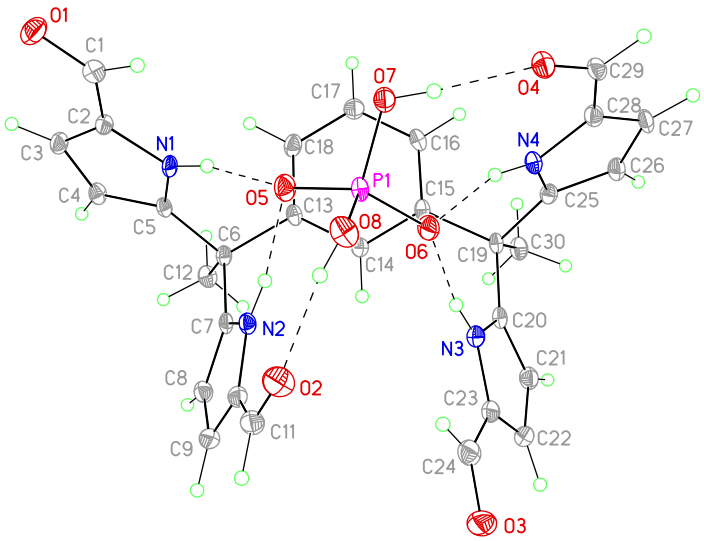

X-ray Experimental for complex **3.4b**·$TBAH_2PO_4$ $(C_{30}H_{26}N_4O_4)(C_{16}H_{36}N)^{1+}$ $O_2P(OH)_2^{1-}$ -1/2 $CHCl_3$: Crystals grew as yellow plates by layering a solution of **3.4b**·$TBAH_2PO_4$ in $CHCl_3$ with *n*-pentane.The data crystal had approximate dimensions; 0.18 x 0.07 x 0.05 mm. The data were collected on an Agilent Technologies SuperNova Dual Source diffractometer using a μ-focus Cu Kα radiation source (λ = 1.5418Å) with collimating mirror monochromators. A total of 1659 frames of data were collected using ω-scans with a scan range of 1° and a counting time of 9 seconds per frame with a detector offset of +/- 40.8° and 20 seconds per frame with a detector offset of +/- 108.3°. The data were collected at 100 K using an Oxford Cryostream low temperature device. Details of crystal data, data collection and structure refinement are listed in Table 7.9. Data collection, unit cell refinement and data reduction were performed using Agilent Technologies CrysAlisPro V 1.171.37.31.[14] The structure was solved by direct methods using SuperFlip[15] and refined by full-matrix least-squares on F^2 with anisotropic displacement parameters for the non-H atoms using SHELXL-2013.[13] Structure analysis was aided by use of the programs PLATON98[4] and WinGX.[5] The hydrogen atoms bound to carbon atoms were calculated in ideal positions with isotropic displacement parameters set to 1.2xUeq of the attached atom (1.5xUeq for methyl hydrogen atoms). The hydrogen atoms bound to the pyrrole nitrogen atoms and the hydroxyl atoms of the phosphate ion were observed in a ΔF map and refined with isotropic displacement parameters.

The function, $\Sigma w(|F_o|^2 - |F_c|^2)^2$, was minimized, where $w = 1/[(\sigma(F_o))^2 + (0.0516*P)^2 + (2.5503*P)]$ and $P = (|F_o|^2 + 2|F_c|^2)/3$. $R_w(F^2)$ refined to 0.124, with R(F) equal to 0.0500 and a goodness of fit, S, = 1.05. Definitions used for calculating R(F), $R_w(F^2)$ and the goodness of fit, S, are given below.[6] The data were checked for secondary extinction effects but no correction was necessary. Neutral atom scattering factors and values used to calculate the linear absorption coefficient are from the International Tables

for X-ray Crystallography (1992).[7] All figures were generated using SHELXTL/PC.[8] Tables of positional and thermal parameters, bond lengths and angles, torsion angles and figures may be obtained from the CCDC by referencing CCDC number 1444560.

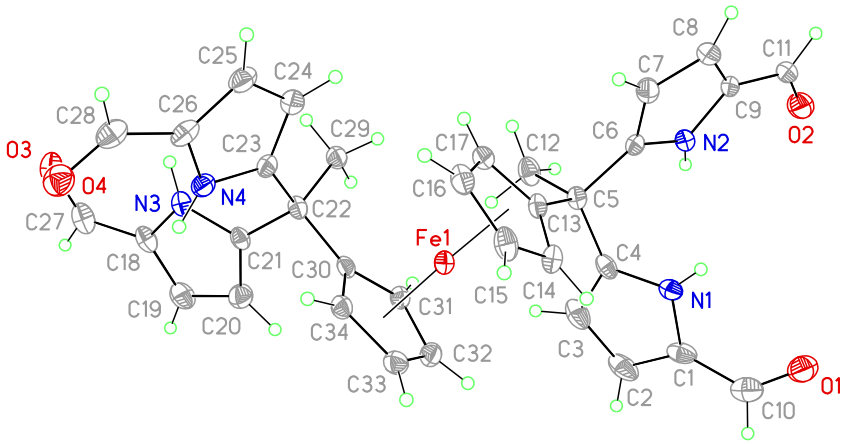

X-ray Experimental for **4.1b** $(C_{17}H_{15}N_2O)_2Fe$ – 2 C_3H_7NO: Crystals grew as clear, yellow prisms by slow evaporation from dimethylformamide with a small amount of dichloromethane. The data crystal had approximate dimensions; 0.27 x 0.20 x 0.09 mm. The data were collected at -140 °C on a Nonius Kappa CCD diffractometer using a Bruker AXS Apex II detector and a graphite monochromator with MoKα radiation (λ = 0.71073 Å). Reduced temperatures were maintained by use of an Oxford Cryosystems 600 low-temperature device. A total of 1110 frames of data were collected using ω and ϕ-scans with a scan range of 1.1° and a counting time of 43 seconds per frame. Details of

crystal data, data collection and structure refinement are listed in Table 7.10. Data reduction was performed using SAINT V8.27B.[12] The structure was solved by direct methods using SUPERFLIP[15] and refined by full-matrix least-squares on F^2 with anisotropic displacement parameters for the non-H atoms using SHELXL-2013.[13] Structure analysis was aided by use of the programs PLATON98[4] and WinGX.[5] The hydrogen atoms bound to carbon atoms were calculated in idealized positions. The hydrogen atoms on the pyrrole nitrogen atoms were observed in a ΔF map and refined with isotropic displacement parameters.

The function, $\Sigma w(|F_o|^2 - |F_c|^2)^2$, was minimized, where $w = 1/[(\sigma(F_o))^2 + (0.0331*P)^2 + (2.7996*P)]$ and $P = (|F_o|^2 + 2|F_c|^2)/3$. $R_w(F^2)$ refined to 0.111, with R(F) equal to 0.0471 and a goodness of fit, S, = 1.01. Definitions used for calculating R(F),$R_w(F^2)$ and the goodness of fit, S, are given below.[6] The data were checked for secondary extinction but no correction was necessary. Neutral atom scattering factors and values used to calculate the linear absorption coefficient are from the International Tables for X-ray Crystallography (1992).[7] All figures were generated using SHELXTL/PC.[8] Tables of positional and thermal parameters, bond lengths and angles, torsion angles and figures may be obtained from the CCDC by referencing CCDC number 1444557.

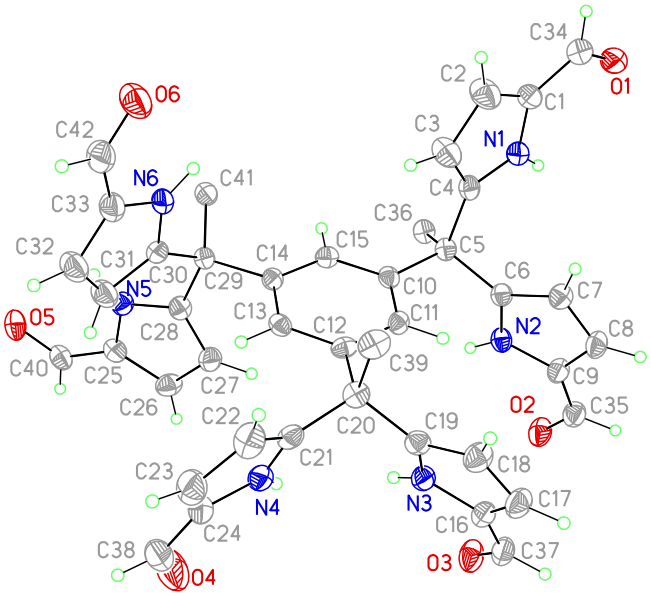

X-ray Experimental for **4.2b** $C_{42}H_{36}N_6O_6$ - 2 $CHCl_3$: Crystals grew as clusters of yellow prisms by slow evaporation from chloroform, methanol and dimethylformamide. The data crystal was cut from a larger crystal and had approximate dimensions; 0.30 x 0.23 x 0.15 mm. The data were collected on a Rigaku SCX-Mini diffractometer with a Mercury 2+ CCD using a graphite monochromator with MoKα radiation (λ = 0.71073 Å). A total of 1080 frames of data were collected using ω-scans with a scan range of 0.5° and a counting time of 25 seconds per frame. The data were collected at 100 K using a Rigaku XStream low temperature device. Details of crystal data, data collection and structure refinement are listed in Table 7.11. Data reduction was performed using the Rigaku Americas Corporation's Crystal Clear version 1.40.[1] The structure was solved by direct methods using SIR2004[2] and refined by full-matrix least-squares on F^2 with anisotropic displacement parameters for the non-H atoms using SHELXL-2013.[13] Structure analysis was aided by use of the programs PLATON98[4] and WinGX.[5] The

hydrogen atoms were calculated in ideal positions with isotropic displacement parameters set to 1.2xUeq of the attached atom (1.5xUeq for methyl hydrogen atoms).

A molecule of chloroform was disordered. The disorder resulted in two principal conformations. The disorder was modelled by assigning the variable x to the site occupancy for one component and (1-x) to the site occupancy of the alternate component. The variable x was refined while restraining the geometry of the two components to be equivalent. A common isotropic displacement parameter was refined while refining x. In this way, the major component of the disordered solvent molecule consisting of atoms, Cl4, Cl5, Cl6 and C1b refined to a site occupancy of 53(1)%. The non-H atoms of both components were ultimately refined anisotropically with their displacement parameters restrained to be approximately isotropic.

The function, $\Sigma w(|F_o|^2 - |F_c|^2)^2$, was minimized, where $w = 1/[(\sigma(F_o))^2 + (0.086*P)^2 + (3.5129*P)]$ and $P = (|F_o|^2 + 2|F_c|^2)/3$. $R_w(F^2)$ refined to 0.2593, with R(F) equal to 0.0937 and a goodness of fit, S, = 1.16. Definitions used for calculating R(F), $R_w(F^2)$ and the goodness of fit, S, are given below.[6] The data were checked for secondary extinction effects but no correction was necessary. Neutral atom scattering factors and values used to calculate the linear absorption coefficient are from the International Tables for X-ray Crystallography (1992).[7] All figures were generated using SHELXTL/PC.[8] Tables of positional and thermal parameters, bond lengths and angles, torsion angles and figures may be obtained from the CCDC by referencing CCDC number 1444558.

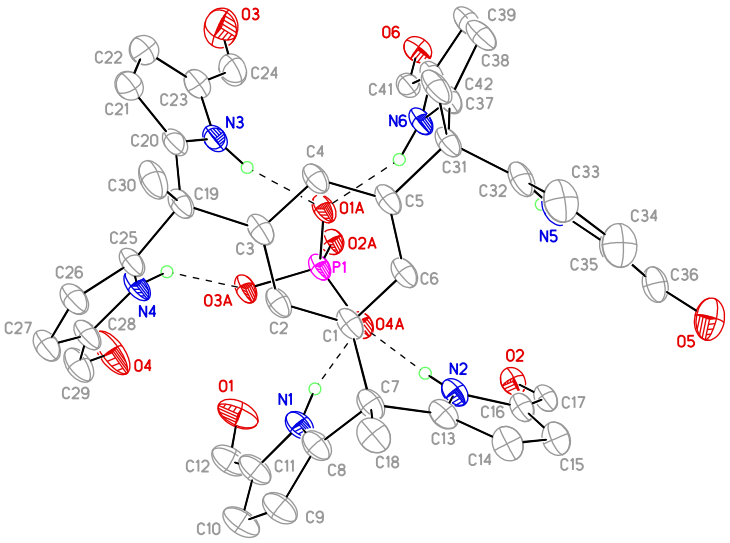

X-ray Experimental for **4.2b**·TBAH$_2$PO$_4$ (2 $C_{42}H_{36}N_6O_6$ - 2 $C_{16}H_{36}N^{1+}$ $H_2PO_4^{1-}$ - 3 $CHCl_3$): Crystals grew as thin, yellow plates by layering a solution of **7b**·TBAH$_2$PO$_4$ in $CHCl_3$ with *n*-pentane. The data crystal had approximate dimensions; 0.27 x 0.16 x 0.08 mm. The data were collected on an Agilent Technologies SuperNova Dual Source diffractometer using a μ-focus Cu Kα radiation source (λ = 1.5418Å) with collimating mirror monochromators. A total of 1035 frames of data were collected using ω-scans with a scan range of 0.5° and a counting time of 14 seconds per frame using a detector offset of +/- 41.1° and a counting time of 38 seconds per frame using a detector offset of +/- 108.3°. The data were collected at 100 K using an Oxford Cryostream low temperature device. Details of crystal data, data collection and structure refinement are listed in Table 7.12. Data collection, unit cell refinement and data reduction were performed using Agilent Technologies CrysAlisPro V 1.171.37.31.[14] The structure was solved by direct methods using SIR97[9] and refined by full-matrix least-squares on F^2

with anisotropic displacement parameters for the non-H atoms using SHELXL-2013.[13] Structure analysis was aided by use of the programs PLATON98[4] and WinGX.[5] The hydrogen atoms were calculated in ideal positions with isotropic displacement parameters set to 1.2xUeq of the attached atom (1.5xUeq for methyl hydrogen atoms.

The two tetra-n-butyl ammonium ions had highly anisotropic displacement parameters. One of the ions was refined with a disorder model. The disorder was modelled by assigning the variable x to the site occupancy for one component of the disorder and (1-x) to the site occupancy for the alternate component. The geometry of the two components was restrained by the extensive use of SADI instructions to maintain the C-C bonds and C-C-C angles to be equivalent. A common isotropic displacement parameter was assigned to the nitrogen atoms and the methylene carbon atoms while refining the variable x. A separate isotropic displacement parameter was refined for the methyl carbon atoms.

There are several regions of unidentified disordered solvent. The solvent was badly disordered and could not be reliably identified but was probably a mixture of the solvents used for crystallization, chloroform and n-hexane. The quantity and identity of the solvent in these voids was in doubt. The squeezed out solvent was not included in the UNIT card. The contributions to the scattering factors due to this solvent molecule were removed by use of the utility SQUEEZE[6] in PLATON98. PLATON98 was used as incorporated in WinGX.

The function, $\Sigma w(|F_o|^2 - |F_c|^2)^2$, was minimized, where $w = 1/[(\sigma(F_o))^2 + (0.1*P)^2]$ and $P = (|F_o|^2 + 2|F_c|^2)/3$. $R_w(F^2)$ refined to 0.345, with R(F) equal to 0.126 and a goodness of fit, S, = 1.61. Definitions used for calculating R(F), $R_w(F^2)$ and the goodness of fit, S, are given below.[6] The data were checked for secondary extinction effects but no correction was necessary. Neutral atom scattering factors and values used

to calculate the linear absorption coefficient are from the International Tables for X-ray Crystallography (1992).[7] All figures were generated using SHELXTL/PC.[8] Tables of positional and thermal parameters, bond lengths and angles, torsion angles and figures may be obtained from the CCDC by referencing CCDC number 1444561.

7.2. STURCTURE REFINEMENT PARAMETERS

Table 7.1: Crystal data and structure refinement parameters for **2.9b**.

Empirical formula	C18 H16 N2 O3	
Formula weight	308.33	
Temperature	298(2) K	
Wavelength	0.71073 Å	
Crystal system	monoclinic	
Space group	P 21/n	
Unit cell dimensions	a = 8.9152(10) Å	α= 90°.
	b = 16.056(2) Å	β= 107.031(3)°.
	c = 11.6016(15) Å	γ = 90°.
Volume	1587.9(3) $Å^3$	
Z	4	
Density (calculated)	1.290 Mg/m^3	
Absorption coefficient	0.089 mm^{-1}	
F(000)	648	
Crystal size	0.480 x 0.320 x 0.110 mm^3	
Theta range for data collection	3.132 to 27.480°.	
Index ranges	-11<=h<=11, -20<=k<=20, -15<=l<=10	
Reflections collected	9559	
Independent reflections	3600 [R(int) = 0.0263]	
Completeness to theta = 25.242°	99.8 %	
Absorption correction	Semi-empirical from equivalents	
Max. and min. transmission	1.00 and 0.717	
Refinement method	Full-matrix least-squares on F^2	
Data / restraints / parameters	3600 / 0 / 221	
Goodness-of-fit on F^2	1.024	
Final R indices [I>2sigma(I)]	R1 = 0.0447, wR2 = 0.1099	
R indices (all data)	R1 = 0.0595, wR2 = 0.1206	
Extinction coefficient	n/a	
Largest diff. peak and hole	0.163 and -0.212 $e.Å^{-3}$	

Table 7.2: Crystal data and structure refinement parameters for **2.14**.

Empirical formula	C19 H17 N5 O2	
Formula weight	347.38	
Temperature	100(2) K	
Wavelength	1.54180 Å	
Crystal system	Monoclinic	
Space group	P21/n	
Unit cell dimensions	a = 15.9252(14) Å	α= 90°.
	b = 13.253(2) Å	β= 116.594(9)°.
	c = 17.3380(15) Å	γ = 90°.
Volume	3272.1(6) $Å^3$	
Z	8	
Density (calculated)	1.410 Mg/m^3	
Absorption coefficient	0.780 mm^{-1}	
F(000)	1456	
Crystal size	0.30 x 0.20 x 0.10 mm	
Theta range for data collection	6.62 to 66.58°.	
Index ranges	-18<=h<=16, -15<=k<=15, -19<=l<=20	
Reflections collected	37427	
Independent reflections	5740 [R(int) = 0.0431]	
Completeness to theta = 66.58°	99.5 %	
Absorption correction	Semi-empirical from equivalents	
Max. and min. transmission	0.930 and 0.786	
Refinement method	Full-matrix least-squares on F^2	
Data / restraints / parameters	5740 / 0 / 517	
Goodness-of-fit on F^2	1.290	
Final R indices [I>2sigma(I)]	R1 = 0.0477, wR2 = 0.1133	
R indices (all data)	R1 = 0.0677, wR2 = 0.1298	
Largest diff. peak and hole	0.211 and -0.290 $e.Å^{-3}$	

Table 7.3: Crystal data and structure refinement parameters for **2.15a**.

Empirical formula	C40.50 H41 N7 O5.50	
Formula weight	713.80	
Temperature	153(2) K	
Wavelength	0.71070 Å	
Crystal system	Triclinic	
Space group	P-1	
Unit cell dimensions	a = 10.5529(4) Å	α= 93.079(3)°.
	b = 11.5600(5) Å	β= 98.706(2)°.
	c = 16.4194(9) Å	γ = 113.756(2)°.
Volume	1797.57(14) $Å^3$	
Z	2	
Density (calculated)	1.319 Mg/m^3	
Absorption coefficient	0.090 mm^{-1}	
F(000)	754	
Crystal size	0.30 x 0.15 x 0.08 mm	
Theta range for data collection	1.94 to 25.00°.	
Index ranges	-12<=h<=11, -13<=k<=13, -18<=l<=19	
Reflections collected	10189	
Independent reflections	6195 [R(int) = 0.0633]	
Completeness to theta = 25.00°	97.7 %	
Absorption correction	None	
Refinement method	Full-matrix least-squares on F^2	
Data / restraints / parameters	6195 / 16 / 516	
Goodness-of-fit on F^2	1.073	
Final R indices [I>2sigma(I)]	R1 = 0.0794, wR2 = 0.1351	
R indices (all data)	R1 = 0.1768, wR2 = 0.1686	
Largest diff. peak and hole	0.378 and -0.266 $e.Å^{-3}$	

Table 7.4: Crystal data and structure refinement parameters for **2.15b**.

Empirical formula	C49 H57 N11 O7	
Formula weight	912.06	
Temperature	100(2) K	
Wavelength	0.71073 Å	
Crystal system	Monoclinic	
Space group	P21/c	
Unit cell dimensions	a = 21.787(3) Å	α= 90°.
	b = 10.6512(15) Å	β= 114.832(3)°.
	c = 22.247(3) Å	γ = 90°.
Volume	4685.3(12) $Å^3$	
Z	4	
Density (calculated)	1.293 Mg/m^3	
Absorption coefficient	0.089 mm^{-1}	
F(000)	1936	
Crystal size	0.34 x 0.24 x 0.09 mm^3	
Theta range for data collection	3.09 to 27.48°.	
Index ranges	-28<=h<=28, -13<=k<=13, -28<=l<=28	
Reflections collected	62241	
Independent reflections	10735 [R(int) = 0.0999]	
Completeness to theta = 27.48°	99.8 %	
Absorption correction	Semi-empirical from equivalents	
Max. and min. transmission	1.00 and 0.335	
Refinement method	Full-matrix least-squares on F^2	
Data / restraints / parameters	10735 / 0 / 633	
Goodness-of-fit on F^2	1.058	
Final R indices [I>2sigma(I)]	R1 = 0.0642, wR2 = 0.1345	
R indices (all data)	R1 = 0.1078, wR2 = 0.1541	
Largest diff. peak and hole	0.529 and -0.299 e. $Å^{-3}$	

Table 7.5: Crystal data and structure refinement parameters for **3.3b**·2DMF.

CCDC number	1012700	
Empirical formula	C36 H40 N6 O6	
Formula weight	652.74	
Temperature	153(2) K	
Wavelength	0.71073 Å	
Crystal system	monoclinic	
Space group	P 21/c	
Unit cell dimensions	a = 8.3870(4) Å	α= 90°.
	b = 14.2432(5) Å	β= 104.354(2)°.
	c = 14.6816(7) Å	γ = 90°.
Volume	1699.08(13) $Å^3$	
Z	2	
Density (calculated)	1.276 Mg/m^3	
Absorption coefficient	0.088 mm^{-1}	
F(000)	692	
Crystal size	0.320 x 0.300 x 0.250 mm	
Theta range for data collection	2.860 to 27.494°.	
Index ranges	-10<=h<=10, -18<=k<=18, -19<=l<=19	
Reflections collected	29051	
Independent reflections	3904 [R(int) = 0.0546]	
Completeness to theta = 25.242°	99.9 %	
Absorption correction	Semi-empirical from equivalents	
Max. and min. transmission	1.00 and 0.873	
Refinement method	Full-matrix least-squares on F^2	
Data / restraints / parameters	3904 / 38 / 247	
Goodness-of-fit on F^2	1.027	
Final R indices [I>2sigma(I)]	R1 = 0.0437, wR2 = 0.0989	
R indices (all data)	R1 = 0.0696, wR2 = 0.1163	
Extinction coefficient	n/a	
Largest diff. peak and hole	0.256 and -0.394 $e.Å^{-3}$	

Table 7.6: Crystal data and structure refinement parameters for **3.3b**·2DMSO.

CCDC number	1012698	
Empirical formula	C34 H38 N4 O6 S2	
Formula weight	662.80	
Temperature	153(2) K	
Wavelength	0.71073 Å	
Crystal system	Monoclinic	
Space group	C2/c	
Unit cell dimensions	a = 22.6373(7) Å	α= 90°.
	b = 9.5570(3) Å	β= 105.708(2)°.
	c = 16.0764(5) Å	γ = 90°.
Volume	3348.15(18) $Å^3$	
Z	4	
Density (calculated)	1.315 Mg/m^3	
Absorption coefficient	0.209 mm^{-1}	
F(000)	1400	
Crystal size	0.22 x 0.20 x 0.14 mm	
Theta range for data collection	1.87 to 27.50°.	
Index ranges	-29<=h<=29, -12<=k<=12, -20<=l<=20	
Reflections collected	52202	
Independent reflections	3843 [R(int) = 0.0505]	
Completeness to theta = 27.50°	99.9 %	
Absorption correction	Semi-empirical from equivalents	
Max. and min. transmission	1.00 and 0.857	
Refinement method	Full-matrix least-squares on F^2	
Data / restraints / parameters	3843 / 3 / 259	
Goodness-of-fit on F^2	1.046	
Final R indices [I>2sigma(I)]	R1 = 0.0391, wR2 = 0.0975	
R indices (all data)	R1 = 0.0512, wR2 = 0.1070	
Largest diff. peak and hole	0.324 and -0.252 $e.Å^{-3}$	

Table 7.7: Crystal data and structure refinement parameters for **3.4b**·2DMF.

CCDC number	1012699	
Empirical formula	C36 H40 N6 O6	
Formula weight	652.74	
Temperature	100(2) K	
Wavelength	0.71073 Å	
Crystal system	orthorhombic	
Space group	P b c a	
Unit cell dimensions	a = 15.1665(12) Å	α= 90°.
	b = 17.7506(16) Å	β= 90°.
	c = 24.997(2) Å	γ = 90°.
Volume	6729.5(10) $Å^3$	
Z	8	
Density (calculated)	1.289 Mg/m^3	
Absorption coefficient	0.089 mm^{-1}	
F(000)	2768	
Crystal size	0.200 x 0.110 x 0.100 mm	
Theta range for data collection	3.016 to 27.481°.	
Index ranges	-19<=h<=19, -23<=k<=23, -31<=l<=32	
Reflections collected	81471	
Independent reflections	7708 [R(int) = 0.0981]	
Completeness to theta = 25.242°	99.8 %	
Absorption correction	Semi-empirical from equivalents	
Max. and min. transmission	1.00 and 0.774	
Refinement method	Full-matrix least-squares on F^2	
Data / restraints / parameters	7708 / 0 / 455	
Goodness-of-fit on F^2	1.134	
Final R indices [I>2sigma(I)]	R1 = 0.0676, wR2 = 0.1114	
R indices (all data)	R1 = 0.1068, wR2 = 0.1226	
Extinction coefficient	n/a	
Largest diff. peak and hole	0.253 and -0.266 $e.Å^{-3}$	

Table 7.8: Crystal data and structure refinement parameters for **3.3b·**$(TBA)_2H_2P_2O_7$.

CCDC number	1444559	
Empirical formula	C62.50 H99 Cl N6 O11 P2	
Formula weight	1207.86	
Temperature	100(2) K	
Wavelength	1.54184 Å	
Crystal system	monoclinic	
Space group	P 21/n	
Unit cell dimensions	a = 19.5077(3) Å	α= 90°.
	b = 15.3419(3) Å	β= 95.4010(10)°.
	c = 22.1726(3) Å	γ = 90°.
Volume	6606.47(19) $Å^3$	
Z	4	
Density (calculated)	1.214 Mg/m^3	
Absorption coefficient	1.457 mm^{-1}	
F(000)	2604	
Crystal size	0.160 x 0.110 x 0.060 mm^3	
Theta range for data collection	2.886 to 74.239°.	
Index ranges	-23<=h<=24, -17<=k<=18, -26<=l<=27	
Reflections collected	35854	
Independent reflections	13076 [R(int) = 0.0339]	
Completeness to theta = 67.684°	99.8 %	
Absorption correction	Semi-empirical from equivalents	
Max. and min. transmission	1.00 and 0.961	
Refinement method	Full-matrix least-squares on F^2	
Data / restraints / parameters	13076 / 535 / 761	
Goodness-of-fit on F^2	1.029	
Final R indices [I>2sigma(I)]	R1 = 0.0603, wR2 = 0.1574	
R indices (all data)	R1 = 0.0777, wR2 = 0.1710	
Extinction coefficient	n/a	
Largest diff. peak and hole	1.034 and -0.466 e.$Å^{-3}$	

Table 7.9: Crystal data and structure refinement parameters for **3.4b**·$TBAH_2PO_4$.

CCDC number	1444560	
Empirical formula	C46.50 H64.50 Cl1.50 N5 O8 P	
Formula weight	905.67	
Temperature	100(2) K	
Wavelength	1.54184 Å	
Crystal system	triclinic	
Space group	P -1	
Unit cell dimensions	a = 9.9599(4) Å	α= 81.050(3)°.
	b = 14.6932(6) Å	β= 75.273(3)°.
	c = 16.4802(5) Å	γ = 88.017(3)°.
Volume	2304.10(15) $Å^3$	
Z	2	
Density (calculated)	1.305 Mg/m^3	
Absorption coefficient	1.802 mm^{-1}	
F(000)	966	
Crystal size	0.170 x 0.070 x 0.050 mm^3	
Theta range for data collection	2.805 to 74.533°.	
Index ranges	-12<=h<=12, -16<=k<=18, -20<=l<=19	
Reflections collected	24272	
Independent reflections	9074 [R(int) = 0.0371]	
Completeness to theta = 67.684°	99.5 %	
Absorption correction	Semi-empirical from equivalents	
Max. and min. transmission	1.00 and 0.863	
Refinement method	Full-matrix least-squares on F^2	
Data / restraints / parameters	9074 / 6 / 607	
Goodness-of-fit on F^2	1.047	
Final R indices [I>2sigma(I)]	R1 = 0.0500, wR2 = 0.1188	
R indices (all data)	R1 = 0.0641, wR2 = 0.1237	
Extinction coefficient	n/a	
Largest diff. peak and hole	0.749 and -0.617 $e.Å^{-3}$	

Table 7.10: Crystal data and structure refinement for **4.1b**·2DMF.

CCDC number	1444557	
Empirical formula	C40 H44 Fe N6 O6	
Formula weight	760.66	
Temperature	133(2) K	
Wavelength	0.71073 Å	
Crystal system	monoclinic	
Space group	P 21/c	
Unit cell dimensions	a = 12.5879(6) Å	α= 90°.
	b = 20.8699(10) Å	β= 93.531(4)°.
	c = 13.6448(8) Å	γ = 90°.
Volume	3577.8(3) $Å^3$	
Z	4	
Density (calculated)	1.412 Mg/m^3	
Absorption coefficient	0.480 mm^{-1}	
F(000)	1600	
Crystal size	0.27 x 0.20 x 0.09 mm	
Theta range for data collection	1.621 to 27.595°.	
Index ranges	-16<=h<=16, -27<=k<=27, -17<=l<=17	
Reflections collected	87367	
Independent reflections	8232 [R(int) = 0.1341]	
Completeness to theta = 25.242°	99.8 %	
Absorption correction	Semi-empirical from equivalents	
Max. and min. transmission	1.00 and 0.867	
Refinement method	Full-matrix least-squares on F^2	
Data / restraints / parameters	8232 / 0 / 500	
Goodness-of-fit on F^2	1.013	
Final R indices [I>2sigma(I)]	R1 = 0.0471, wR2 = 0.0897	
R indices (all data)	R1 = 0.1007, wR2 = 0.1109	
Extinction coefficient	n/a	
Largest diff. peak and hole	0.382 and -0.331 $e.Å^{-3}$	

Table 7.11: Crystal data and structure refinement parameters for **4.2b**·2$CHCl_3$.

CCDC number	1444558	
Empirical formula	C44 H38 Cl6 N6 O6	
Formula weight	959.50	
Temperature	100(2) K	
Wavelength	0.71073 Å	
Crystal system	triclinic	
Space group	P -1	
Unit cell dimensions	a = 10.1932(19) Å	α= 72.773(4)°.
	b = 12.318(2) Å	β= 77.793(4)°.
	c = 19.654(4) Å	γ = 81.490(4)°.
Volume	2294.1(7) $Å^3$	
Z	2	
Density (calculated)	1.389 Mg/m^3	
Absorption coefficient	0.428 mm^{-1}	
F(000)	988	
Crystal size	0.300 x 0.230 x 0.150 mm	
Theta range for data collection	3.059 to 27.483°.	
Index ranges	-13<=h<=13, -15<=k<=15, -25<=l<=25	
Reflections collected	23595	
Independent reflections	10438 [R(int) = 0.0717]	
Completeness to theta = 25.242°	99.8 %	
Absorption correction	Semi-empirical from equivalents	
Max. and min. transmission	1.00 and 0.654	
Refinement method	Full-matrix least-squares on F^2	
Data / restraints / parameters	10438 / 81 / 600	
Goodness-of-fit on F^2	1.140	
Final R indices [I>2sigma(I)]	R1 = 0.0937, wR2 = 0.2330	
R indices (all data)	R1 = 0.1450, wR2 = 0.2589	
Extinction coefficient	n/a	
Largest diff. peak and hole	0.945 and -1.034 e.$Å^{-3}$	

Table 7.12: Crystal data and structure refinement parameters for [**4.2b**·$TBAH_2PO_4$]$_2$.

CCDC number	1444561	
Empirical formula	C119 H151 Cl9 N14 O20 P2	
Formula weight	2478.52	
Temperature	100(2) K	
Wavelength	1.54184 Å	
Crystal system	triclinic	
Space group	P -1	
Unit cell dimensions	a = 16.0755(7) Å	α= 93.415(2)°.
	b = 18.9299(7) Å	β= 96.103(3)°.
	c = 24.4976(6) Å	γ = 111.261(4)°.
Volume	6869.2(5) Å^3	
Z	2	
Density (calculated)	1.198 Mg/m^3	
Absorption coefficient	2.423 mm^{-1}	
F(000)	2612	
Crystal size	0.270 x 0.160 x 0.080 mm^3	
Theta range for data collection	2.950 to 74.200°.	
Index ranges	-13<=h<=19, -23<=k<=22, -27<=l<=30	
Reflections collected	40560	
Independent reflections	26292 [R(int) = 0.0646]	
Completeness to theta = 67.684°	98.1 %	
Absorption correction	Semi-empirical from equivalents	
Max. and min. transmission	1.00 and 0.560	
Refinement method	Full-matrix least-squares on F^2	
Data / restraints / parameters	26292 / 3337 / 1638	
Goodness-of-fit on F^2	1.544	
Final R indices [I>2sigma(I)]	R1 = 0.1255, wR2 = 0.3052	
R indices (all data)	R1 = 0.1811, wR2 = 0.3446	
Extinction coefficient	n/a	
Largest diff. peak and hole	1.140 and -1.260 e.Å^{-3}	

7.3. REFERENCES

1. Rigaku Americas Corporation, CrystalClear 1.40, The Woodlands, TX, 2008.
2. Altomare A.; Burla M.C.; Camalli M.; Cascarano G.L.; Giacovazzo C.; Guagliardi A.; Moliterni A.G.G.; Polidori G.; Spagna R. SIR2004, A program for crystal structure solution, *J. Appl. Crystallogr.* **2005**, (38), 381–388.
3. Sheldrick, G. M. SHELXL-2014/7. Program for the Refinement of Crystal Structures. *Acta Cryst.* **2015**, C71, 9-18.
4. Spek, A. L.,*PLATON, A Multipurpose Crystallographic Tool*, Utrecht University, The Netherlands, 1998.
5. Farrugia, L. J. WinGX 1.64. An Integrated System of Windows Programs for the Solution, Refinement and Analysis of Single Crystal X-ray Diffraction Data. *J. Appl. Cryst.* **1999**, (32). 837-838.
6. $R_w(F^2) = \{\Sigma w(|F_o|^2 - |F_c|^2)^2/\Sigma w(|F_o|)^4\}^{1/2}$ where w is the weight given each reflection.

   $R(F) = \Sigma(|F_o| - |F_c|)/\Sigma|F_o|\}$ for reflections with $F_o > 4(\sigma(F_o))$.

   $S = [\Sigma w(|F_o|^2 - |F_c|^2)^2/(n - p)]^{1/2}$, where n is the number of reflections and p is the number of refined parameters.
7. Wilson, A. J. C. (editor), *International Tables for X-ray Crystallography. Vol. C, Tables 4.2.6.8 and 6.1.1.4*, Boston: Kluwer Academic Press, 1992.
8. Sheldrick, G. M. *SHELXTL/PC (Version 5.03)*, Siemens Analytical X-ray Instruments, Inc., Madison, Wisconsin, USA, 1994.
9. Altomare, A.; Burla, M. C.; Camalli, M.; Cascarano, G. L.; Giacovazzo, C.; Guagliardi, A.; Moliterni, A. G.; Polidori, G.; Spagna, R. SIR97: A New Tool for Crystal Structure Determination and Refinement. *J. Appl. Crystallogr.* **1999**, (32), 115–119.
10. Sheldrick, G. SHELX-97: Programs for Crystal Structure Analysis. *Göttingen, Ger.* 1997.
11. a) Otwinowski, Z.; Minor, W. DENZO-SMN. Methods in Enzymology, *Macromolecular Crystallography, part A*, (276), 307–326. b) Carter, Jr. C. W.; Sweets, R. M. Editors, Academic Press, 1997.
12. Bruker AXS Inc, SAINT V8.27B Madison, WI, 2012.
13. Sheldrick, G. M. SHELXL-2013 (Program for the Refinement of Crystal Structures), *Acta Cryst.*, **2008**, (A64), 112–122.
14. Agilent Technologies, CrysAlisPro. Agilent Technologies UK Ltd., Oxford, UK, SuperNova CCD System, CrysAlicPro Software System, 1.171.37.31, 2013.

15. Palatinus, L.; Chapuis, G. SUPERFLIP - A Computer Program for the Solution of Crystal Structures by Charge Flipping in Arbitrary Dimensions. *J. Appl. Crystallogr.* **2007**, *40* (4), 786–790.

16. Sluis, P. V. D.; Spek, A. L. SQUEEZE. *Acta Cryst.*, **1990**, (A46), 194–201.

8. Comprehensive Bibliography

Adriaenssens, L.; Estarellas, C.; Vargas Jentzsch, A.; Martinez Belmonte, M.; Matile, S.; Ballester, P. Quantification of Nitrate-Pi Interactions and Selective Transport of Nitrate Using calix[4]pyrroles with Two Aromatic Walls. *J. Am. Chem. Soc.* **2013**, *135* (22), 8324–8330.

Agilent Technologies, CrysAlisPro. Agilent Technologies UK Ltd., Oxford, UK, SuperNova CCD System, CrysAlicPro Software System, 1.171.37.31, 2013.

Allen, W. E.; Gale, P. A.; Brown, C. T.; Lynch, V. M.; Sessler, J. L. Binding of Neutral Substrates by Calix[4]pyrroles. *J. Am. Chem. Soc.* **1996**, *118* (49), 12471–12472.

Altomare, A.; Burla, M. C.; Camalli, M.; Cascarano, G. L.; Giacovazzo, C.; Guagliardi, A.; Moliterni, A. G.; Polidori, G.; Spagna, R. SIR97: A New Tool for Crystal Structure Determination and Refinement. *J. Appl. Crystallogr.* **1999**, (32), 115–119.

Altomare A.; Burla M.C.; Camalli M.; Cascarano G.L.; Giacovazzo C.; Guagliardi A.; Moliterni A.G.G.; Polidori G.; Spagna R. SIR2004, A program for crystal structure solution, *J. Appl. Crystallogr.* **2005**, (38), 381–388.

Anand, V. G.; Saito, S.; Shimizu, S.; Osuka, A. Internally 1,4-Phenylene-Bridgedmeso Aryl-Substituted Expanded Porphyrins: The Decaphyrin and Octaphyrin Cases. *Angew. Chem. Int. Ed.* **2005**, *44* (44), 7244–7248.

Arumugam, N.; Chung, W.-Y.; Lee, S.-W.; Lee, C.-H. Synthesis and Structure of 1,4-Bis((a,a'-Dipyrrylmethyl)cyclohexane. *Bull. Korean Chem. Soc.* **2001**, *22* (8), 932–934.

Arumugaperumal, R.; Srinivasadesikan, V.; Ramakrishnam Raju, M. V.; Lin, M.-C.; Shukla, T.; Singh, R.; Lin, H.-C. Acid/Base and H2PO4– Controllable High-Contrast Optical Molecular Switches with a Novel BODIPY Functionalized [2]Rotaxane. *ACS Appl. Mater. Interfaces* **2015**, *7* (48), 26491–26503.

Aydogan, A.; Coady, D. J.; Lynch, V. M.; Akar, A.; Marquez, M.; Bielawski, C. W.; Sessler, J. L. Poly(methyl Methacrylate)s with Pendant Calixpyrroles: Polymeric Extractants for Halide Anion Salts. *Chem. Commun.* **2008**, (12), 1455–1457.

Aydogan, A.; Coady, D. J.; Kim, S. K.; Akar, A.; Bielawski, C. W.; Marquez, M.; Sessler, J. L. Poly(methyl Methacrylate)s with Pendant Calixpyrroles and Crown Ethers: Polymeric Extractants for Potassium Halides. *Angew. Chem. Int. Ed.* **2008**, *47* (50), 9648–9652.

Ayus, J. C.; Achinger, S. G.; Mizani, M. R.; Chertow, G. M.; Furmaga, W.; Lee, S.; Rodriguez, F. Phosphorus Balance and Mineral Metabolism with 3 H Daily Hemodialysis. *Kidney Int.* **2007**, *71* (4), 336–342.

Baeyer, A. Ueber Ein Condensationsproduct von Pyrrol Mit Aceton. *Berichte der Dtsch. Chem. Gesellschaft* **1886**, *19* (2), 2184–2185.

Ballester, P. Anion Binding in Covalent and Self-Assembled Molecular Capsules. *Chem. Soc. Rev.* **2010**, *39* (10), 3810–3830.

Barnard, J. L. Biological Nutrient Removal without the Addition of Chemicals. *Water Res.* **1975**, *9* (5-6), 485–490.

Bazzicalupi, C.; Bencini, A.; Lippolis, V. Tailoring Cyclic Polyamines for Inorganic/organic Phosphate Binding. *Chem. Soc. Rev.* **2010**, *39* (10), 3709–3728.

Bill, N. L.; Kim, D.-S.; Kim, S. K.; Park, J. S.; Lynch, V. M.; Young, N. J.; Hay, B. P.; Yang, Y.; Anslyn, E. V.; Sessler, J. L. Oxoanion Recognition by Benzene-Based Tripodal Pyrrolic Receptors. *Supramol. Chem.* **2012**, *24* (1), 72–76.

Bisson, A. P.; Lynch, V. M.; Monahan, M.-K. C.; Anslyn, E. V. Recognition of Anions through NH-Pi Hydrogen Bonds in a Bicyclic Cyclophane- Selectivity for Nitrate. *Angew. Chem. Int. Ed. English* **1997**, *36* (21), 2340–2342.

Bjerrum, J. *Stability Constants of Metal-Ion Complexes, with Solubility Products of Inorganic Substances: Inorganic Ligands*; Special publication; Chemical Society: London, 1958.

Bowman-James, K.; Bianchi, A.; Garcia-Espana, E. *Anion Coordination Chemistry*; Wiley-VCH Verlag & Co. KGaA: Weinheim, 2012.

Bruker AXS Inc, SAINT V8.27B Madison, WI, 2012.

Cai, J.; Hay, B. P.; Young, N. J.; Yang, X.; Sessler, J. L. A Pyrrole-Based Triazolium-Phane with NH and Cationic CH Donor Groups as a Receptor for Tetrahedral Oxyanions That Functions in Polar Media. *Chem. Sci.* **2013**, *4* (4), 1560–1567.

Camiolo, S.; Gale, P. A.; Hursthouse, M. B.; Light, M. E.; Shi, A. J. Solution and Solid-State Studies of 3,4-Dichloro-2,5-Diamidopyrroles: Formation of an Unusual Anionic Narcissistic Dimer. *Chem. Commun.* **2002**, *3* (7), 758–759.

Carpenter, S. R.; Caraco, N. F.; Correll, D. L.; Howarth, R. W.; Sharpley, A. N.; Smith, V. H. Nonpoint Pollution of Surfaces Waters with Phosphorus and Nitrogen. *Ecol. Appl.* **1991**, *8* (3), 559–568.

Carter, Jr. C. W.; Sweets, R. M. Editors, Academic Press, 1997.

Cavallo, G.; Metrangolo, P.; Pilati, T.; Resnati, G.; Sansotera, M.; Terraneo, G. Halogen Bonding: A General Route in Anion Recognition and Coordination. *Chem. Soc. Rev.* **2010**, *39* (10), 3772–3783.

Chiu, C. W.; Gabbaï, F. P. Fluoride Ion Capture from Water with a Cationic Borane. *J. Am. Chem. Soc.* **2006**, *128* (44), 14248–14249.

Cho, W.-S. Oligopyrrole-Based Anion Receptors, The University of Texas at Austin, 2005.

Coles, S. J.; Gale, P. A.; Hursthouse, M. B. The First Example of an Anion-Pyrrole Complex. *CrystEngComm* **2001**, *3* (53), 259–261.

Connors, K. A. *Binding Constants: The Measurement of Molecular Complex Stability*; John Wiley & Sons: New York, 1987.

Cram, D. J.; Cram, J. M. Host-Guest Chemistry. *Science* **1974**, *183* (4127), 803–809.

Custelcean, R.; Delmau, L. H.; Moyer, B. A.; Sessler, J. L.; Cho, W.-S.; Gross, D.; Bates, G. W.; Brooks, S. J.; Light, M. E.; Gale, P. A. Calix[4]pyrrole: An Old yet New Ion-Pair Receptor. *Angew. Chem. Int. Ed.* **2005**, *44* (17), 2537–2542.

Custelcean, R. Anions in Crystal Engineering. *Chem. Soc. Rev.* **2010**, *39* (10), 3675–3685.

Deliomeroglu, M.; Lynch, V.; Sessler, J. Conformationally Switchable Non-Cyclic Tetrapyrrole Receptors: Synthesis of tetrakis(1H-Pyrrole-2-Carbaldehyde) Derivatives and Their Anion Binding Properties. *Chem. Commun.* **2014**, *50* (80), 11863–11866.

Dietrich, B.; Lehn, J. M.; Sauvage, J. P. Les Cryptates. *Tetrahedron Lett.* **1969**, *10* (34), 2889–2892.

Farrugia, L. J. WinGX 1.64. An Integrated System of Windows Programs for the Solution, Refinement and Analysis of Single Crystal X-ray Diffraction Data. *J. Appl. Cryst.* **1999**, (32). 837-838.

Gale, P. A.; Sessler, J. L.; Kral, V.; Lynch, V. Calix[4]pyrroles: Old yet New Anion-Binding Agents. *J. Am. Chem. Soc.* **1996**, *118* (21), 5140–5141.

Gale, P. A.; Sessler, J. L.; Král, V. Calixpyrroles. *Chem. Commun.* **1998**, (1), 1–8.

Gale, P. A. Anion and Ion-Pair Receptor Chemistry: Highlights from 2000 and 2001. *Coord. Chem. Rev.* **2003**, *240*, 191–221.

Gamez, P.; Mooibroek, T. J.; Teat, S. J.; Reedijk, J. Anion Binding Involving Pi-Acidic Heteroaromatic Rings. *Acc. Chem. Res.* **2007**, *40* (6), 435–444.

Gil-Ramírez, G.; Escudero-Adán, E. C.; Benet-Buchholz, J.; Ballester, P. Quantitative Evaluation of Anion-π Interactions in Solution. *Angew. Chem. Int. Ed.* **2008**, *47* (22), 4114–4118.

Ghosh, S. K.; Ishida, M.; Li, J.; Cha, W.-Y.; Lynch, V. M.; Kim, D.; Sessler, J. L. Synthesis and Anion Binding Studies of O-Phenylenevinylene-Bridged Tetrapyrrolic Macrocycle as an Expanded Analogue of calix[4]pyrrole. *Chem. Commun. (Camb).* **2014**, *50* (28), 3753–3756.

Gross, D. E.; Schmidtchen, F. P.; Antonius, W.; Gale, P. A.; Lynch, V. M.; Sessler, J. L. Cooperative Binding of calix[4]pyrrole-Anion Complexes and Alkylammonium Cations in Halogenated Solvents. *Chem. Eur. J.* **2008**, *14*, 7822–7827.

Goldsmith, D. R.; Scott, L. J.; Cvetkovi, R. S.; Plosker, G. L.; Bihl, G.; Kidney, W.; West, S.; Africa, S.; Bommer, J. Sevelamer Hydrochloride A Review of Its Use for Hyperphosphataemia in Patients with End-Stage Renal Disease on Haemodialysis. *Drugs* **2008**, *68* (1), 85–104.

Gottlieb, H. E.; Kotlyar, V.; Nudelman, A. NMR Chemical Shifts of Common Laboratory Solvents as Trace Impurities. *J. Org. Chem.* **1997**, *62* (3), 7512–7515.

Gutzwiller, J.-P.; Schneditz, D.; Huber, A. R.; Schindler, C.; Gutzwiller, F.; Zehnder, C. E. Estimating Phosphate Removal in Haemodialysis: An Additional Tool to Quantify Dialysis Dose. *Nephrol. Dial. Transplant.* **2002**, *17* (6), 1037–1044.

Hirai, M.; Gabbaï, F. P. Squeezing Fluoride out of Water with a Neutral Bidentate Antimony(V) Lewis Acid. *Angew. Chem. Int. Ed.* **2015**, *54* (4), 1205–1209.

Hirsch, A. K. H.; Fischer, F. R.; Diederich, F. Phosphate Recognition in Structural Biology. *Angew. Chem. Int. Ed.* **2007**, *46* (3), 338–352.

Jeffrey, G. A. *An Introduction to Hydrogen Bonding (Topics in Physical Chemistry)*, Oxford University Press, 1997.

Iverson, B. L.; Shreder, K.; Král, V.; Sessler, J. L. Phosphate Recognition by Sapphyrin. A New Approach to DNA Binding. *J. Am. Chem. Soc.* **1993**, *115* (16), 11022–11023.

Katayev, E. A.; Boev, N. V.; Khrustalev, V. N.; Ustynyuk, Y. A.; Tananaev, I. G.; Sessler, J. L. Bipyrrole- and Dipyrromethane-Based Amido-Imine Hybrid Macrocycles. New Receptors for Oxoanions. *J. Org. Chem.* **2007**, *72* (8), 2886–2896.

Kim, S. K.; Sessler, J. L.; Gross, D. E.; Lee, C.-H.; Kim, J. S.; Lynch, V. M.; Delmau, L. H.; Hay, B. P. A calix[4]arene Strapped calix[4]pyrrole: An Ion-Pair Receptor Displaying Three Different Cesium Cation Recognition Modes. *J. Am. Chem. Soc.* **2010**, *132* (16), 5827–5836.

Kim, S. K.; Sessler, J. L. Calix[4]pyrrole-Based Ion Pair Receptors. *Acc. Chem. Res.* **2014**, *47*, 2525–2536.

Kioussis, D. R.; Smith, D. F.; Kofinas, P. Ammonium Perchlorate-Binding Poly(allylamine Hydrochloride) Hydrogels for Wastewater Remediation. *J. Appl. Polym. Sci.* **2001**, *80* (11), 2073–2083.

Král, V.; Furuta, H.; Shreder, K.; Lynch, V.; Sessler, J. L. Protonated Sapphyrins. Highly Effective Phosphate Receptors. *J. Am. Chem. Soc.* **1996**, *118*, 1595–1607.

Laha, J. K.; Dhanalekshmi, S.; Taniguchi, M.; Ambroise, A.; Lindsey, J. S. A Scalable Synthesis of Meso-Substituted Dipyrromethanes. *Org. Process Res. Dev.* **2003**, *7* (6), 799–812.

Lee, C.-H.; S. Lindsey, J. One-Flask Synthesis of Meso-Substituted Dipyrromethanes and Their Application in the Synthesis of Trans-Substituted Porphyrin Building Blocks. *Tetrahedron* **1994**, *50* (39), 11427–11440.

Lee, C. H.; Na, H. K.; Yoon, D. W.; Won, D. H.; Cho, W. S.; Lynch, V. M.; Shevchuk, S. V.; Sessler, J. L. Single Side Strapping: A New Approach to Fine Tuning the Anion Recognition Properties of calix[4]pyrroles. *J. Am. Chem. Soc.* **2003**, *125* (24), 7301–7306.

Levin, G. V.; Shapiro, J. Metabolic Uptake of Phosphorus by Wastewater Organisms. *Water Environ. Fed.* **1965**, *37* (6), 800–821.

Love, J. B.; Blake, A. J.; Wilson, C.; Reid, S. D.; Novak, A.; Hitchcock, P. B. The Syntheses and Structures of Group 1 Expanded Dipyrrolides: The Formation of a 12-Rung Amidolithium Circular Ladder. *Chem. Commun.* **2003**, No. 14, 1682–1683.

Maeda, H.; Ito, Y. BF2 Complex of Fluorinated Dipyrrolyldiketone: A New Class of Efficient Receptor for Acetate Anions. *Inorg. Chem.* **2006**, *45* (20), 8205–8210.

Maeda, H.; Ito, Y.; Kusunose, Y.; Nakanishi, T. Di-Pyrrolyl-Pyrazoles: Anion Receptors in Protonated Form and Efficient Building Blocks for Organized Structures. *J. Org. Chem.* **2007**, *72* (7), 2612–2616.

Mahanta, S. P.; Panda, P. K. Unusual Ring Annulation during Condensation of Acetylacetone with Pyrrole. *Tetrahedron Lett.* **2009**, *50* (8), 890–892.

Mahanta, S. P.; Kumar, B. S.; Panda, P. K. Meso-Diacylated Calix[4]pyrrole: Structural Diversities and Enhanced Binding towards Dihydrogenphosphate Ion. *Chem. Commun.* **2011**, *47* (15), 4496–4498.

Mahanta, S. P.; Panda, P. K. Interesting Reactivity of Diketones with Pyrrole under Acidic Condition. *J. Chem. Sci.* **2011**, *123* (5), 593–599.

Marcus, Y. Thermodynamics of Solvation of Ions. *J. Chem. Soc. Faraday Trans.* **1991**, *87* (18), 2995–2999.

Mateus, P.; Delgado, R.; Brandão, P.; Félix, V. Polyaza Cryptand Receptor Selective for Dihydrogen Phosphate. *J. Org. Chem.* **2009**, *74* (22), 8638–8646.

McEwen, C. N.; Larsen, B. S. Ionization Mechanisms Related to Negative Ion APPI, APCI, and DART. *J. Am. Soc. Mass Spectrom.* **2009**, *20* (8), 1518–1521.

Mino, T.; Van Loosdrecht, M. C. M.; Heijnen, J. J. Microbiology and Biochemistry of the Enhanced Biological Phosphate Removal Process. *Water Res.* **1998**, *32* (11), 3193–3207.

Mino, T. Microbial Selection of Polyphosphate-Accumulating Bacteria in Activated Sludge Wastewater Treatment Processes for Enhanced Biological Phosphate Removal. *Biochemistry. (Mosc).* **2000**, *65* (3), 341–348.

Morokuma, K. Why Do Molecules Interact? The Origin of Electron Donor-Acceptor Complexes, Hydrogen Bonding and Proton Affinity. *Acc. Chem. Res.* **1977**, *10* (8), 294–300.

Neufeld, R.; Stalke, D. Accurate Molecular Weight Determination of Small Molecules via DOSY-NMR by Using External Calibration Curves with Normalized Diffusion Coefficients. *Chem. Sci.* **2015**, *6* (6), 3354–3364.

Ohkuma, S.; Sato, T.; Okamoto, M.; Matsuya, H.; Arai, K.; Kataoka, T.; Nagai, K.; Wasserman, H. H. Prodigiosins Uncouple Lysosomal Vacuolar-Type ATPase through Promotion of H + / Cl – Symport. *Biochem. J.* **1998**, *334* (3), 731–741.

Otwinowski, Z.; Minor, W. DENZO-SMN. Methods in Enzymology, *Macromolecular Crystallography, part A*, (276), 307–326.

Palatinus, L.; Chapuis, G. SUPERFLIP - A Computer Program for the Solution of Crystal Structures by Charge Flipping in Arbitrary Dimensions. *J. Appl. Crystallogr.* **2007**, *40* (4), 786–790.

Park, C. H.; Simmons, H. E. Macrobicyclic Amines. III. Encapsulation of Halide Ions by In,in-1,(k + 2)-Diazabicyclo[k.l.m.]alkane Ammonium Ions. *J. Am. Chem. Soc.* **1968**, *90* (9), 2431–2432.

Pedersen, C. J. Cyclic Polyethers and Their Complexes with Metal Slats. *J. Am. Chem. Soc.* **1967**, *89* (26), 7017–7036.

Quiñonero, D.; Garau, C.; Rotger, C.; Frontera, A.; Ballester, P.; Costa, A.; Deyà, P. M. Anion-π Interactions: Do They Exist? *Angew. Chem. Int. Ed.* **2002**, *41* (18), 3389–3392.

Rashin, A. a.; Honig, B. Reevaluation of the Born Model of Ion Hydration. *J. Phys. Chem.* **1985**, *89* (26), 5588–5593.

Rigaku Americas Corporation, CrystalClear 1.40, The Woodlands, TX, 2008.

Schmidtchen, F. P.; Berger, M. Artificial Organic Host Molecules for Anions. *Chem. Rev.* **1997**, *97* (5), 1609–1646.

Seidel, D.; Lynch, V.; Sessler, J. L. Cyclo[8]pyrrole: A Simple-to-Make Expanded Porphyrin with No Meso Bridges. *Angew. Chem. Int. Ed.* **2002**, *41* (8), 1422–1425.

Selman, M.; Greenhalgh, S. Eutrophication : Sources and Drivers of Nutrients Pollution. *WRI Policy Note* **2009**, No. 2, 1–8.

Sessler, J. L.; Cyr, M. J.; Lynch, V.; McGhee, E.; Ibers, J. A. Synthetic and Structural Studies of Sapphyrin, a 22-π-Electron Pentapyrrolic "Expanded Porphyrin." *J. Am. Chem. Soc.* **1990**, *112* (7), 2810–2813.

Sessler, J. L.; Weghorn, S. J.; Morishima, T.; Rosingana, M.; Lynch, V.; Lee, V. Rosarin: A New, Easily Prepared Hexapyrrolic Expanded Porphyrin. *J. Am. Chem. Soc.* **1992**, *114* (14), 8306–8307.

Sessler, J. L.; Weghorn, S. J.; Lynch, V.; Fransson, K. 5,15,25-Tris-nor-Hexapyrrin: The First Structurally Characterized Linear Hexapyrrin. *J. Chem. Soc. Chem. Commun.* **1994**, *169* (11), 1289.

Sessler, J. L.; Camiolo, S.; Gale, P. A. Pyrrolic and Polypyrrolic Anion Binding Agents. *Coord. Chem. Rev.* **2003**, *240* (1–2), 17–55.

Sessler, J. L.; Cho, W.-S.; Dudek, S. P.; Hicks, L.; Lynch, V. M.; Huggins, M. T. Synthesis and Study of a Calixpyrrole-Texaphyrin Chimera: A New Oligopyrrolic Chloride Anion Receptor. *J. Porphyr. Phthalocyanines* **2003**, *07* (02), 97–104.

Sessler, J. L.; Katayev, E.; Pantos, G. D.; Ustynyuk, Y. A. Synthesis and Study of a New Diamidodipyrromethane Macrocycle. An Anion Receptor with a High Sulfate-to-Nitrate Binding Selectivity. *Chem. Commun.* **2004**, No. 11, 1276–1277.

Sessler, J. L.; Katayev, E.; Dan Pantos, G.; Scherbakov, P.; Reshetova, M. D.; Khrustalev, V. N.; Lynch, V. M.; Ustynyuk, Y. A. Fine Tuning the Anion Binding Properties of 2,6-Diamidopyridine Dipyrromethane Hybrid Macrocycles. *J. Am. Chem. Soc.* **2005**, *127* (32), 11442–11446.

Sessler, J. L.; Gale, P. A.; Cho, W.-S. *Anion Receptor Chemistry*; The Royal Society of Chemistry: Cambridge, U.K., 2006.

Sessler, J. L.; Kim, S. K.; Gross, D. E.; Lee, C. H.; Kim, J. S.; Lynch, V. M. Crown-6-calix[4]arene-Capped calix[4]pyrrole: An Ion-Pair Receptor for Solvent-Separated CsF Ions. *J. Am. Chem. Soc.* **2008**, *130* (39), 13162–13166.

Sheldrick, G. M. *SHELXTL/PC (Version 5.03)*, Siemens Analytical X-ray Instruments, Inc., Madison, Wisconsin, USA, 1994.

Sheldrick, G. SHELX-97: Programs for Crystal Structure Analysis. *Göttingen, Ger.* 1997.

Sheldrick, G. M. SHELXL-2014/7. Program for the Refinement of Crystal Structures. *Acta Cryst.* **2015**, C71, 9-18.

Sheldrick, G. M. SHELXL-2013 (Program for the Refinement of Crystal Structures), *Acta Cryst.*, **2008**, (A64), 112–122.

Shriver, D. F.; Biallas, M. J. Observation of the Chelate Effect with a Bidentate Lewis Acid, F2BCH2CH2BF2. *J. Am. Chem. Soc.* **1967**, *89* (5), 1078–1081.

Sijbesma, R. P. Reversible Polymers Formed from Self-Complementary Monomers Using Quadruple Hydrogen Bonding. *Science* **1997**, *278* (5343), 1601–1604.

Silver, E. S.; Rambo, B. M.; Bielawski, C. W.; Sessler, J. L. Reversible Anion-Induced Cross-Linking of Well-Defined Calix[4]pyrrole-Containing Copolymers. *J. Am. Chem. Soc.* **2014**, *136* (6), 2252–2255.

Sluis, P. V. D.; Spek, A. L. SQUEEZE. *Acta Cryst.*, **1990**, (A46), 194–201.

Sokkalingam, P.; Kim, D. S.; Hwang, H.; Sessler, J. L.; Lee, C.-H. A Dicationic calix[4]pyrrole Derivative and Its Use for the Selective Recognition and Displacement-Based Sensing of Pyrophosphate. *Chem. Sci.* **2012**, *3*, 1819.

Spek, A. L.,*PLATON, A Multipurpose Crystallographic Tool*, Utrecht University, The Netherlands, 1998.

Steed, J. W.; Turner, D. R.; Wallace, K. *Core Concepts in Supramolecular Chemistry and Nanochemistry*; Wiley, Hoboken, NJ, 2007.

Tanford, C. Preparation and Properties of Serum and Plasma Proteins. XXIII. Hydrogen Ion Equilibria in Native and Modified Human Serum Albumins. *J. Am. Chem. Soc.* **1950**, *72* (1), 441–451.

Tanford, C. The Association of Acetate with Ammonium and Guanidinium Ions. *J. Am. Chem. Soc.* **1954**, *76* (3), 945.

Tobey, S. L.; Anslyn, E. V. Energetics of Phosphate Binding to Ammonium and Guanidinium Containing Metallo-Receptors in Water. *J. Am. Chem. Soc.* **2003**, *125* (48), 14807–14815.

Tobey, S. L.; Jones, B. D.; Anslyn, E. V. C3v Symmetric Receptors Show High Selectivity and High Affinity for Phosphate. *J. Am. Chem. Soc.* **2003**, *125* (14), 4026–4027.

Tobey, S. L.; Anslyn, E. V. Determination of Inorganic Phosphate in Serum and Saliva Using a Synthetic Receptor. *Org. Lett.* **2003**, *5* (12), 2029–2031.

Varghese, S.; Senanayake, T.; Murray-Stewart, T.; Doering, K.; Fraser, A.; Casero, R. A.; Woster, P. M. Polyaminohydroxamic Acids and Polyaminobenzamides as Isoform Selective Histone Deacetylase Inhibitors. *J. Med. Chem.* **2008**, *51* (8), 2447–2456.

Walker, J. Some Observations on Salts of Amidines and Related Compounds. *J. Chem. Soc.* **1949**, No. 0, 1996.

Wang, Z.; Luecke, H.; Yao, N.; Quiocho, F. A. A Low Energy Short Hydrogen Bond in Very High Resolution Structures of Protein Receptor--Phosphate Complexes. *Nat. Struct. Biol.* **1997**, *4* (7), 519–522.

Wilson A. J. C. (editor), *International Tables for X-ray Crystallography. Vol. C, Tables 4.2.6.8 and 6.1.1.4*, Boston: Kluwer Academic Press, 1992.

Yang, L.-Z.; Li, Y.; Jiang, L.; Feng, X.-L.; Lu, T.-B. Size and Temperature Dependent Encapsulation of Tetrahedral Anions by a Protonated Cryptand Host. *CrystEngComm* **2009**, *11* (11), 2375.

Zhao, H.; Liao, J.; Ning, J.; Xie, Y.; Cao, Y.; Chen, L.; Yang, D.; Wang, B. Efficient Synthesis of Novel Bis(dipyrromethanes) with Versatile Linkers via Indium(III) Chloride-Catalyzed Condensation of Pyrrole and Dialdehydes. *Adv. Synth. Catal.* **2010**, *352* (17), 3083–3088.

Zhang, Y.; Desmidt, E.; Van Looveren, A.; Pinoy, L.; Meesschaert, B.; Van Der Bruggen, B. Phosphate Separation and Recovery from Wastewater by Novel Electrodialysis. *Environ. Sci. Technol.* **2013**, *47* (11), 5888–5895.

9. Vita

Murat Kadir Deliomeroglu was born in Turkey. He started his elementary school in Tokat, Turkey in 1994 and finished in Boyabat, Sinop in 2002. He attended a private high school, Samanyolu Lisesi from 2002 to 2005. He represented Turkey in 37th international chemistry Olympiad in Taipei, Taiwan in July 2005. After spending a year in language school for English in Ankara, he attended Department of Chemistry of Middle East Technical University. He received his Bachelor of Science degree with a high honor degree in July 2010. (Ankara, Turkey). In August 2010, he entered the Graduate School for organic chemistry at the University of Texas at Austin.

E-mail: mkadird@gmail.com

This dissertation was typed by Murat Kadir Deliomeroglu.